2005-14

Final Report

Earth Pressure Behind a Retaining Wall

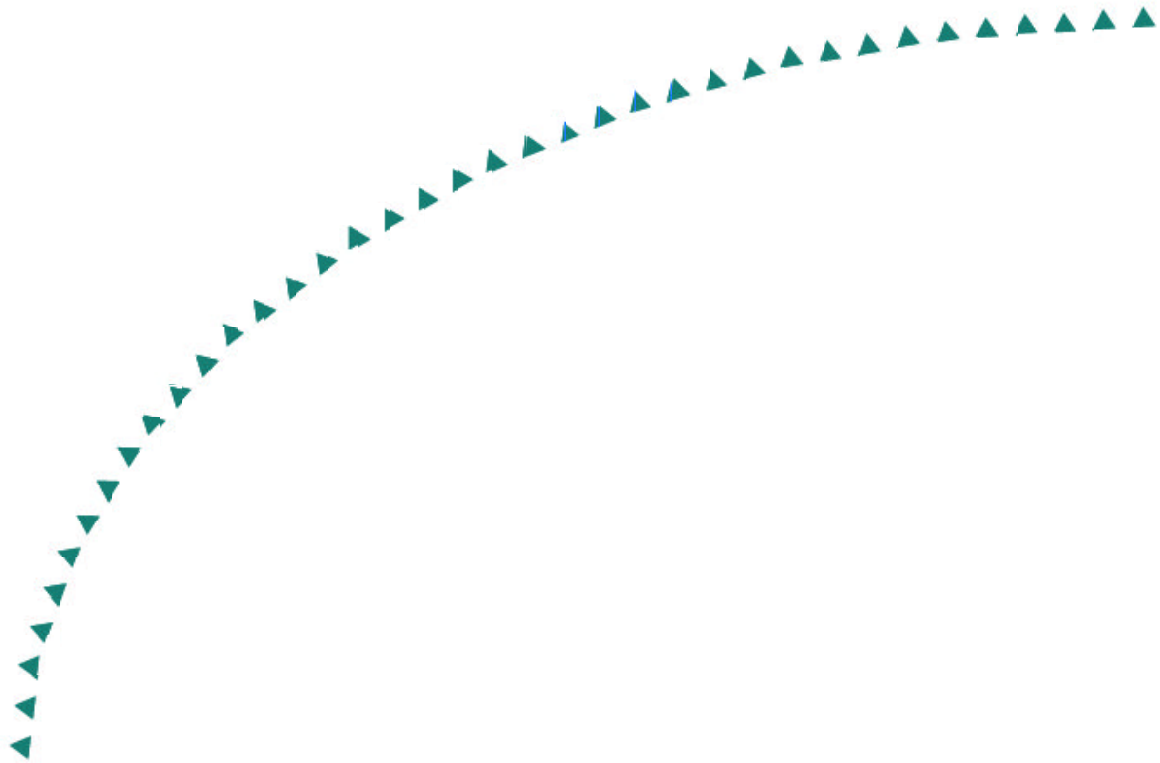

Research

Technical Report Documentation Page

1. Report No.	2.	3. Recipients Accession No.	
2005-14			
4. Title and Subtitle EARTH PRESSURE BEHIND A RETAINING WALL		5. Report Date March 2005	
		6.	
7. Author(s) Joseph G. Bentler, Joseph F. Labuz & Arturo E. Schultz		8. Performing Organization Report No.	
9. Performing Organization Name and Address Department of Civil Engineering University of Minnesota 500 Pillsbury Drive S.E. Minneapolis, Minnesota 55455-0220		10. Project/Task/Work Unit No.	
		11. Contract (C) or Grant (G) No. (c) 81655 (wo) 9	
12. Sponsoring Organization Name and Address Minnesota Department of Transportation 395 John Ireland Boulevard Mail Stop 330 St. Paul, Minnesota 55155		13. Type of Report and Period Covered Final Report	
		14. Sponsoring Agency Code	
15. Supplementary Notes http://www.lrrb.org/PDF/200514.pdf			

16. Abstract (Limit: 200 words)

Earth pressure cells, tiltmeters, strain gages, inclinometer casings, and survey reflectors were installed in fall 2002 during construction of a 26-ft (7.9-m) high Minnesota Department of Transportation (Mn/DOT) reinforced concrete cantilever retaining wall. A data acquisition system with remote access monitored some 60 sensors on a continual basis. Analyses of the data indicated the development of active earth pressure at the end of backfilling, with a resultant at about one-third of the backfill height. Translation of 0.45 in. (11 mm), or about 0.1% of the backfill height, was responsible for development of the active condition. The wall also rotated 0.03° into the backfill as a rigid body, while the top of the stem deflected 0.16 in. (4 mm) away from the backfill. Sensor readings showed the earth pressure distribution to be quite complex during the backfilling process. Evidence was found for residual lateral stresses from compaction. Translation of the wall overnight following the construction workday reduced the compaction-induced lateral stresses. Changes in earth pressure and wall deflection weeks after backfilling were attributed to changes in temperature and rainfall. The data showed that the wall design, while reasonable, could be made more efficient by removing the shear key, which was ineffective.

17. Document Analysis/Descriptors		18. Availability Statement	
Active earth pressure	Cells	No restrictions. Document available from:	
Cantilever retaining wall	Temperature	National Technical Information Services,	
Earth pressure	Rainfall	Springfield, Virginia 22161	
19. Security Class (this report)	20. Security Class (this page)	21. No. of Pages	22. Price
Unclassified	Unclassified	182	

EARTH PRESSURE BEHIND A RETAINING WALL

Final Report

Prepared by:
Joseph G. Bentler
Joseph F. Labuz
Arturo E. Schultz

Department of Civil Engineering
University of Minnesota

March 2005

Published by:
Minnesota Department of Transportation
Research Services Section, MS 330
395 John Ireland Boulevard
St. Paul, Minnesota 55155-1899

Acknowledgements

Partial support was provided by the Minnesota Department of Transportation. Special thanks are extended to (a) Mn/DOT Bridge Office, especially Jihshya Lin, Joe Louis, Gary Peterson, and Erik Wolhowe; (b) Mn/DOT Metro Construction Office, especially Steve Barrett; (c) Mn/DOT Geodetic Office, especially Don Seitz; (d) contractors Edward Kraemer and Sons, Inc. (Burnsville, MN); and Progressive Contractors, Inc. (St. Michael, MN).

Table of Contents

List of Figures

List of Tables

Executive Summary

The objective of the project was to determine the earth pressure behind a Minnesota Department of Transportation (Mn/DOT) reinforced concrete cantilever retaining wall. Based on triaxial compression tests performed on the sand backfill, a friction angle of 37° was used to predict earth pressures and stem deflections. Instrumentation consisting of about 60 individual sensors was installed on a 26-ft (7.9-m) high panel of a cantilever wall along Interstate 494 in Bloomington, Minnesota. Earth pressure cells (EPCs) and tiltmeters were monitored for 12 months with nearly continuous data acquisition and remote modem access. A total station was used to monitor the position of the wall during backfilling in fall 2002. An inclinometer probe was used to monitor two inclinometer casings during this time. Readings from strain gages installed within a second 26-ft (7.9-m) high panel were taken manually while it was backfilled in spring 2003.

The lateral earth pressure on the stem was observed to be active at the end of backfilling. The wall translated horizontally 0.45 in. (11 mm) away from the backfill and vertically downward about 0.42 in. (11 mm) as a rigid body. Translation of about 0.1% of the backfill height coincided with development of the active condition. The wall rotated 0.03° into the backfill as a rigid body, and the vertical stress was greater under the footing heel than under the footing toe. The top of the stem deflected 0.16 in. (4 mm) away from the backfill, approximately equal in magnitude and opposite in direction to the displacement from rotation of the footing. Deflections were predicted by modeling the wall as a piecewise constant cantilever beam. Measured deflections were within the range of predicted deflections. Strains measured on the reinforcing bars within a second wall panel were used to back-calculate the load on the stem. This compared very well with the theoretical active force, and a friction angle of 37.5° was determined from this back-calculated force. Triaxial tests showed the angle of internal friction to be from 35° – 39°.

Stem EPCs and tiltmeters showed evidence for residual effects from compaction. Translation of the wall overnight following the construction workday reduced both the compaction-induced lateral stresses and stem deflections. Furthermore, it allowed stresses within the soil to redistribute. Changes in lateral earth pressure weeks after backfilling were attributed to changes in temperature and rainfall events. Daily variations in air temperature apparently created a gradient in temperature through the thickness of the wall stem, resulting in small changes in shape and subsequent movements of the wall. However, there appeared to be no permanent effect from the daily changes in temperature. Air temperatures well below the freezing point coincided with readings showing no earth pressure on the top part of the stem. This was attributed to water freezing within the soil and consequently creating a temporary cohesion. In spring and summer, rainfall caused a transient increase in lateral earth pressure because the water increased the unit weight of the soil until the backfill dried.

The earth pressure cell in front of the shear key on the bottom of the footing showed no evidence for the development of passive pressure. The factor of safety against sliding was calculated using Mn/DOT's design assumptions and using a modified method that accounted for the resistance of the soil in front of the wall but disregarded the shear key. Using this modified approach, the factor of safety was calculated for walls with no shear key. For walls up to 30 ft (9.1 m) high, $FS_{sliding}$ exceeded 1.5. It is recommended that Mn/DOT's cantilever retaining wall design could be made more efficient by removing the shear key for retaining walls 30 ft (9.1 m) or less in height that are founded on granular soils and for which the toe of the footing is covered with granular soil before the wall is completely backfilled.

In addition, design values for the internal forces were evaluated according to the Mn/DOT Load Factor Design (LFD) and Load and Resistance Factor Design (LRFD) methods. The LFD and LRFD methods based on active earth pressures gave comparable results, with safety margins that were somewhat conservative in most cases, and for the largest measured soil pressures both methods maintained partial safety margins that exceeded the lower limit of 1.5. The LRFD method with at-rest earth pressures provided results that were over-conservative in most cases. Even for the most severe soil pressure profile measured, the margins of safety for this method exceeded 2.0.

Chapter 1
Introduction

Motivation

In 2000, federal regulations were proposed that would stipulate that reinforced concrete cantilever retaining walls must be designed for at-rest rather than active lateral earth pressure (but this proposal has since been rejected). The Minnesota Department of Transportation (Mn/DOT) responded by sponsoring a study to determine the earth pressure behind one of its walls, since factored design pressures and resulting moments would increase significantly with the addition of specifications that require at-rest pressures be considered. At-rest loading conditions would dictate a design pressure distribution of 50 psf/ft (7.9 kPa/m) of wall if Jaky's empirical relationship for K_0 is used [1]. However, Mn/DOT retaining walls have traditionally performed well, and they have been designed assuming an active pressure distribution of 33 psf/ft (5.2 kPa/m) of wall. Increasing the design loading was seen as costly and unnecessary; hence this study. (*English units are used throughout this report to conform to Mn/DOT's convention; SI units are included when convenient*.)

Overview

The objective of this research was to determine the earth pressure behind a reinforced concrete cantilever retaining wall. The strategy for achieving this objective was to

1. determine the strength parameters of the soil backfill,
2. develop an instrumentation plan,
3. measure earth pressures and wall movements,
4. compare observed wall response to assumed design behavior, and
5. estimate load and resistance factors for the retaining wall.

A site along Interstate 494 near West Bush Lake Road in Bloomington, Minnesota, was selected in late 2001. An instrumentation plan was developed for one 30.5-ft (9.30-m) panel of the wall with the goal of measuring earth pressure and wall movement. Redundancy of measurements was a major feature of the instrumentation plan, since field conditions are often harsh on sensitive instruments. Construction on the 0.5-mile (0.8-km) long retaining wall began in the summer of 2002, with the selected wall panel being instrumented in fall 2002. Earth pressure cells, tiltmeters, strain gages, inclinometer casings, and extensometers were installed during construction of the reinforced concrete cantilever retaining wall. A data acquisition system with remote access was set up to continually monitor approximately 60 sensors. In addition, a total station was used to measure overall movement of four survey points on the wall.

A load test was also conducted using weighted trucks to observe the response of the wall to loading beyond that from the backfill. A second panel was instrumented with ten strain gages in late spring 2003 to provide further data on the structural behavior of these walls.

The data were analyzed to determine the earth pressure on the retaining wall and how wall movements and construction activities such as compaction affected the earth pressure. The overall performance of the wall was also evaluated, since a better understanding of the design

methods, construction materials, and construction processes has the potential to decrease the cost for retaining walls, abutments, and their foundations. Data were collected for over 12 months.

A parametric study of the internal forces that are typically obtained from the structural analysis of a cantilever retaining wall and used for designing the wall is included as Appendix F. The analysis focused on the distribution and magnitude of the shear forces (V) and bending moments (M) in the stem of the wall. The influence of lateral earth pressure profile was evaluated by comparing two common theories, namely active and at-rest pressures, with pressure profiles that were measured for the instrumented retaining wall at six discrete times during the monitoring period. Design values for the internal forces were also evaluated according to the Mn/DOT Load Factor Design (LFD) and Load and Resistance Factor Design (LRFD) methods.

Two versions of the LFD procedure were considered, including the procedure as defined in the Mn/DOT standard, and a variation in which one of the load factors for the lateral earth pressure was reduced. Two versions of the LRFD procedure were also considered, one that utilized active earth pressure theory and the other that used at-rest pressure theory. The goal of these comparisons was to evaluate the safety margins in the internal forces (V and M) that are calculated according to the Mn/DOT LFD and LRFD procedures, so as to verify the adequacy of the load factors and load combinations in these two procedures.

Organization

This report explores the earth pressure behind and performance of a reinforced (RC) concrete cantilever retaining wall. It is divided into six chapters, with Chapter 1 serving as the introduction. Chapter 2 includes background on earth pressure theory and previous work, both experimental and numerical, on retaining walls. The wall design of Mn/DOT is also described. The instrumentation plan is presented in Chapter 3, with a description of the different types of instruments and their respective installation procedures. Measurements from the wall instrumentation, as well as soil properties measured in the lab, are discussed and analyzed in Chapter 4. Data are further interpreted in Chapter 5, with sections on the backfilling process, the effects of temperature and rainfall, determination of interface friction below the footing, and passive earth pressure in front of the toe and the shear key. The performance of the shear key is discussed in particular with respect to the factor of safety against sliding. Chapter 6 contains the conclusions and recommendations. The Appendices include calibration plots for the earth pressure cells, results of soil tests, a brief discussion of problems with the readings from one type of earth pressure cell, an overview of the structural analysis and computer code used to predict displacements, plots of sensor readings during and after backfilling, and a detailed analysis of load combinations in the MnDOT standards.

Chapter 2
Background

Classical Earth Pressure Theory

For uniform backfill with a constant unit weight, the theoretical distribution of earth pressure on a frictionless vertical retaining wall is linear with depth (Fig. 2.1), although the magnitude of the earth pressure is dependent upon wall movement. If the wall is stationary, the earth pressure is termed at-rest. If the wall is allowed to move a small amount away from the backfill, the earth pressure is called active. All else being equal, active earth pressure is roughly two-thirds of at-rest earth pressure for common backfill materials. This is a result of the movement of the retaining wall, which allows the soil to mobilize its strength so that the soil supports more of its own weight. Active earth pressure s_a at the bottom depth of a 26-ft high retaining wall was expected to be about 850 psf (40 kPa) for an angle of internal friction f = 35 and a unit weight g = 120 pcf:

$$s_a = gHK_a \tag{2.1}$$

where

$$K_a = \frac{1-\sin f}{1+\sin f} \tag{2.2}$$

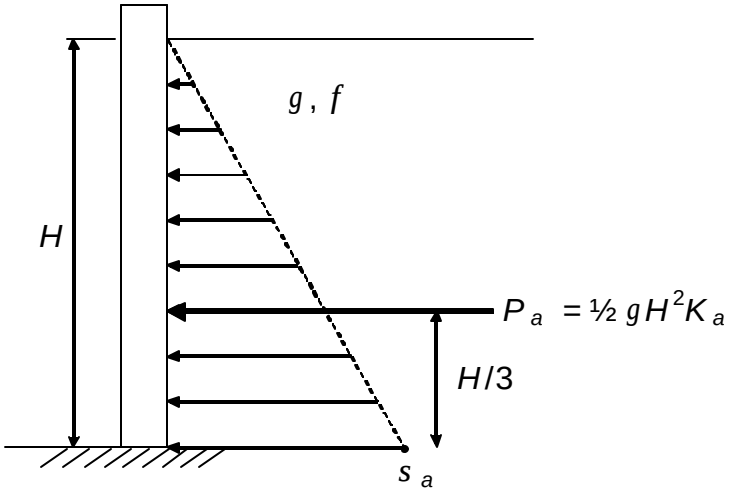

Figure 2.1. Theoretical lateral earth pressure distribution for backfill with constant unit weight.

The empirical relationship commonly used for the coefficient of earth pressure at-rest K_0 for coarse-grained soils comes from Jaky [1]:

$$K_0 = 1 - \sin f \tag{2.3}$$

This is the equation that would be used if Mn/DOT were to design for at-rest earth pressure. Though this relationship has been the subject of some debate, it is commonly accepted to sufficiently represent the at-rest condition in granular soils. This is due in part to the laboratory investigations of Bishop [2]. This expression for K_0 will also be used throughout this report for all calculations involving the at-rest earth pressure.

Morgenstern and Eisenstein [3] compared Rankine's theory, which assumes no wall friction, to several theoretical approaches that do account for wall friction and found that for the active condition, the other theories were all within about 10% of each other. Furthermore, Rankine's theory was more conservative than other theories for all values of internal friction angle up to nearly 40°. Hence using Rankine's theory for active pressure in design is justified so long as sufficient movement occurs for the active condition to develop.

Experimental Projects

In his classic experiments with a large-scale model retaining wall, Terzaghi [4] found that even for the simplest conditions (i.e. dry sand backfill, vertical wall, single mode of movement) the earth pressure conditions were quite complex. He also found evidence for relaxation of internal frictional stresses between sand grains when a strain state was maintained for a few hours. One of Terzaghi's most important findings was that only a small amount of movement (0.25% of the wall height) was required to achieve the active condition and that a relatively larger amount of movement was required to achieve the fully passive condition. He found that the ratio between the top of wall movement and the wall height needed only to reach 0.0025 before the active condition was achieved. In contrast, the ratio of wall movement to wall height had to reach about 0.01 before the passive condition was fully realized.

Coyle et al. [5] for the Texas Transportation Institute instrumented a cantilever retaining wall in an extensive manner, seeking to measure earth pressure, as well as the three modes of movement (rigid body translation, rigid body rotation, and deflection). Earth pressure cells were installed on the back face of the stem. Rigid body translation was measured relative to a reinforced concrete drilled shaft using an engineer's steel tape, and displacement of the stem from vertical was recorded by means of a plumb bob suspended from a frame attached to the top of the wall. The wall was 16-ft (4.9-m) high and rested on H-piles driven into the clay subsoil. They found that the earth pressure compared well with theoretical active pressure only for the top 7 ft (2.1 m) of the wall. Earth pressure for the bottom of the wall was between the active and at-rest values. However, 0.2 in. (5 mm) of rigid body translation had occurred when only 2 ft (0.6 m) of backfill had been placed. The authors attributed this to compaction of the soil behind the footing heel by heavy equipment. From this point forward, only 0.1 in. (2.5 mm) of wall translation occurred as the final 14 ft (4.3 m) of backfill was placed, a displacement to height ratio of 0.0006. It is conceivable that the H-piles below the footing provided restraint to lateral wall movement, thus preventing the wall from translating sufficiently for the active condition to fully develop. Similar behavior was observed during a lateral load test of a retaining wall foundation by Peck and Ireland [6]. Piles beneath the foundation elastically provided lateral resistance through beam action.

Coyle and Bartoskewitz [7] also presented the results from instrumenting a 10-ft (3-m) high, 12-ft (3.7-m) wide precast panel retaining wall uniquely designed for the measurement of forces. The footing was a reinforced concrete cap on top of 20-ft (6.1-m) deep drilled piers. Precast panels were held in place by T-shaped pilasters constructed on top of the cap. Also, horizontal timbers in front of the pilasters formed a barrier that prevented passive earth pressure from acting on the front of the wall. Earth pressure cells were installed, and wall movements were determined in a similar manner as the cantilever wall instrumented by Coyle et al. [5]. The results regarding lateral earth pressure were very similar to previous data [5] in that the earth pressure had reduced to active levels at the top of the wall, but not at the bottom. Most wall movement during backfilling was in the form of translation, but some rotation and translation away from the backfill occurred for a few months after backfilling had ended.

Numerical Analyses

Several researchers have performed finite element analyses of gravity retaining walls [8, 9]. Recognizing the complexities that real-life construction sequences and the displacements occurring during construction introduce to soil-structure interactions, they examined the behavior of the wall using increments simulating the construction sequence. Other researchers [10, 11] had previously developed methods of incremental elastic analysis for embankments. While Kulhawy [9] considered a wall founded on rock, Clough and Duncan [8] analyzed a concrete gravity retaining wall founded on sand.

Previous analyses had usually been performed using one of two limiting assumptions: (1) that the soil-structure interface was perfectly rough, i.e. no slip; or (2) that the interface was perfectly smooth, i.e. no shear stresses. Clough and Duncan [8] employed an empirical relationship determined from direct shear tests to calculate the interface shear stiffness. Using increments of loading, they simulated the construction and backfill processes. It was found that the retaining wall rotated into the backfill and translated forward from its original position. Thus, the earth pressure did decrease from at-rest values but not completely to values associated with the fully active condition. The total wall rotation was due to two effects: (1) differential settlement of the foundation soil from the weight of the backfill, and (2) the overturning moment from lateral earth pressure. The foundation soil settlement caused rotation into the backfill, while the moment from lateral loading caused somewhat less rotation away from the backfill.

Clough and Duncan [8] also performed finite element analyses exploring the relative amounts of displacements needed to achieve the active and passive conditions. They found that the ratio between the top of wall displacement and the wall height for the active condition was about 0.25%, while the ratio was 2% to achieve the fully passive condition. These results confirmed Terzaghi's experimental findings concerning the relative amounts of displacements needed to achieve the active and passive conditions.

Goh [12] performed a finite element analysis to examine the behavior of concrete cantilever retaining walls using a method very similar to that of Clough and Duncan [8], including the same empirical interface shear stiffness relationship. Again, increments of loading were used to simulate the backfill process. The backfill was granular but somewhat loose, with a unit weight of 100 lb/ft^3 (15.7 kN/m^3), or 100 pcf.

Though Goh [12] considered a cantilever wall, while Clough and Duncan [8] analyzed a gravity wall, the results were qualitatively similar. For instance, at the end of backfilling, differential

settlements between the toe and heel of the footing had caused the wall to rotate into the backfill. The wall stem had tilted forward due to elastic deflection, and the base of the wall had translated forward. Another interesting result was that during the initial stages of backfilling, the heel settlement caused the top of the stem to move into the backfill. With additional fill, however, the stem deflected away from the backfill.

Other aspects of retaining wall behavior were also investigated by Goh [12]. For instance, a rough wall resulted in smaller lateral pressures than for a smooth wall, as would be expected. The effects of wall stiffness were explored by means of a wall with a rigid stem and a wall with an effectively cracked stem. The differences in earth pressure were minor for either case, since the cracked wall stiffness was still over 60 times greater than that of the backfill soil. Even for a very stiff wall, the stem displaced sufficiently that the top part of the lateral pressure distribution was approximately active. For the bottom third of the wall stem, in particular, the lateral pressures were between active and at-rest values. Thus, Goh [12] proposed that a bilinear earth pressure distribution be used for design (Fig. 2.2).

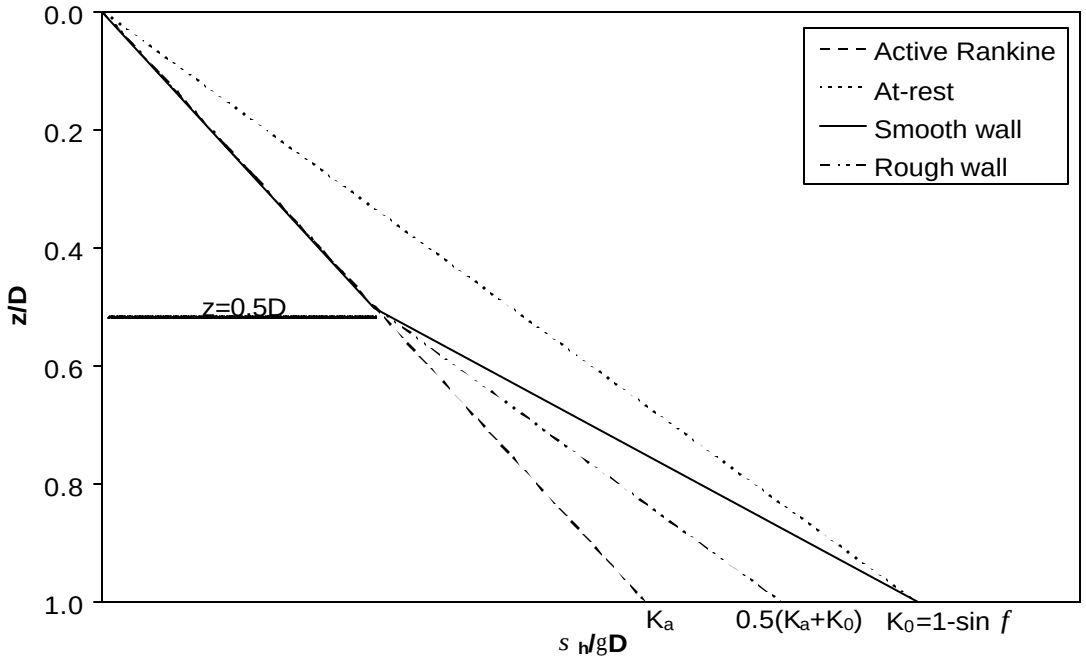

Figure 2.2. Bilinear earth pressure distribution from a numerical analysis [12].

Effect of Compaction

The effect of compaction on the lateral earth pressure behind retaining walls has been studied by several researchers [13. 14, 15, 16]. Aggour and Brown [14] developed a theoretical model to predict pressure and wall deflection produced during compaction, taking into account how compaction equipment affects tractions on the wall and stem deflections. There is a temporary increase in tractions and deflections when a compactor moves along a wall, followed by a decrease to residual values for these quantities upon removal of the equipment. The researchers

implemented an incremental finite element scheme to model the backfill process. It was determined that compaction, while necessary behind retaining walls, significantly affected the magnitude and distribution of earth pressure. The resulting earth pressure distribution was found to be non-linear, with final values as much as twice the initial values for the top half of the stem (Fig. 2.3). Deflection of the wall stem at the end of backfilling also was appreciably more for compacted backfill than uncompacted. Another intriguing finding was that a stiff wall experienced less residual deflection and less residual pressure than a flexible wall.

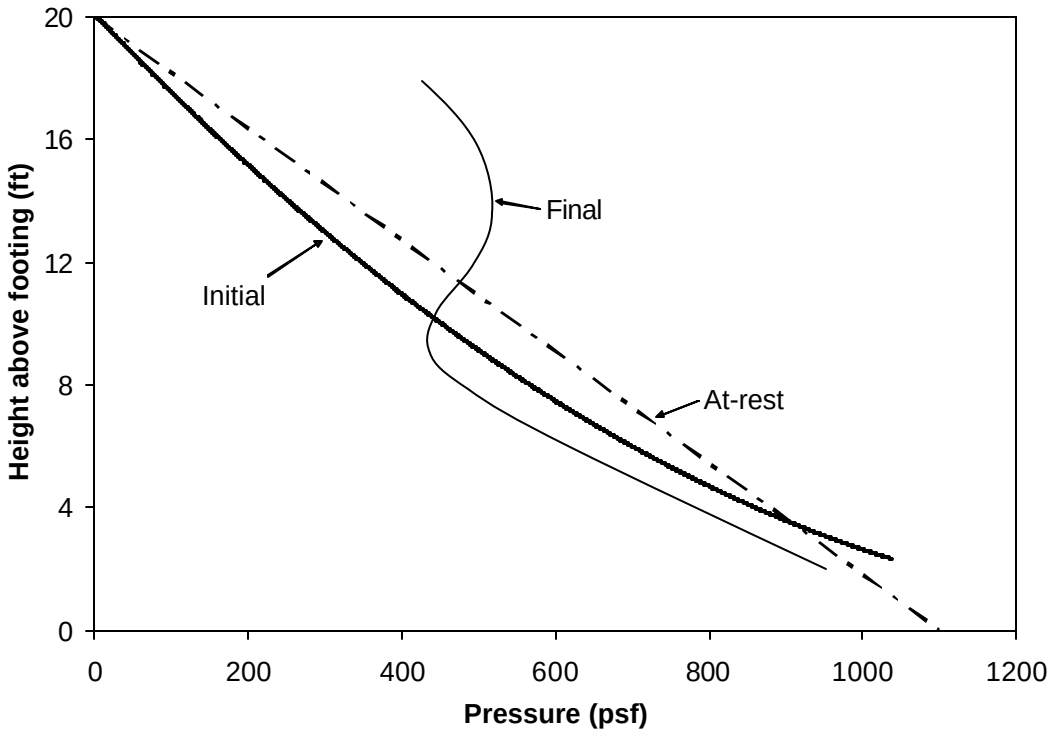

Figure 2.3. Earth pressure due to compaction, estimated from a numerical analysis [14].

Mn/DOT Design

Mn/DOT designs reinforced concrete cantilever retaining walls according to the 1992 AASHTO (American Association of State Highway and Transportation Officials) design specifications. Working stress design is used for stability calculations and foundation design, while load factor design is used for the reinforced concrete structure. The factor of safety against overturning shall be greater than 2.0, while that against sliding shall be greater than 1.5. The coefficient of sliding friction between the base of the footing and the soil beneath is taken to be 0.55 (d = 28.8°). The backfill is assumed to have a unit weight of 125 pcf (19.6 kN/m^3) and an angle of internal friction f = 35°.

Retaining wall panels over 20 ft (6.1 m) in height are designed with a 1 ft x 1 ft (0.3 m x 0.3 m) shear key to provide additional resistance to sliding. The resistance provided by soil in front of the footing toe is neglected. The shear key may be formed or unformed, depending on the

contractor's preference and the project engineer's approval. The shear key for the retaining wall in this study was formed using plywood sheets and wooden cross-bracing. A scale drawing of the 26 ft (7.92 m) high panel instrumented for this study is given in Fig. 2.4. It should be noted that the front face of the wall was vertical, whereas the back face was inclined 2.4° from the vertical. Also, a decorative "rustication" was formed 1 in. (25 mm) into the front face of the wall. The rebar for the stem is epoxy-coated, but the rebar for the footing is not. Individual panels were separated by expansion joints but were connected to one another through smooth, epoxy-coated dowels, which were spaced vertically at 1 ft (0.3 m) increments. The individual dowels were designed to transmit no torsion or tension, only shear force. The expansion joints consisted of 0.5 in. (13 mm) thick cork spacers. Drain tile covered by a silt-screening fabric was placed at the base of the heel, within granular material. Weepholes are used for drainage on some retaining walls instead of drain tile.

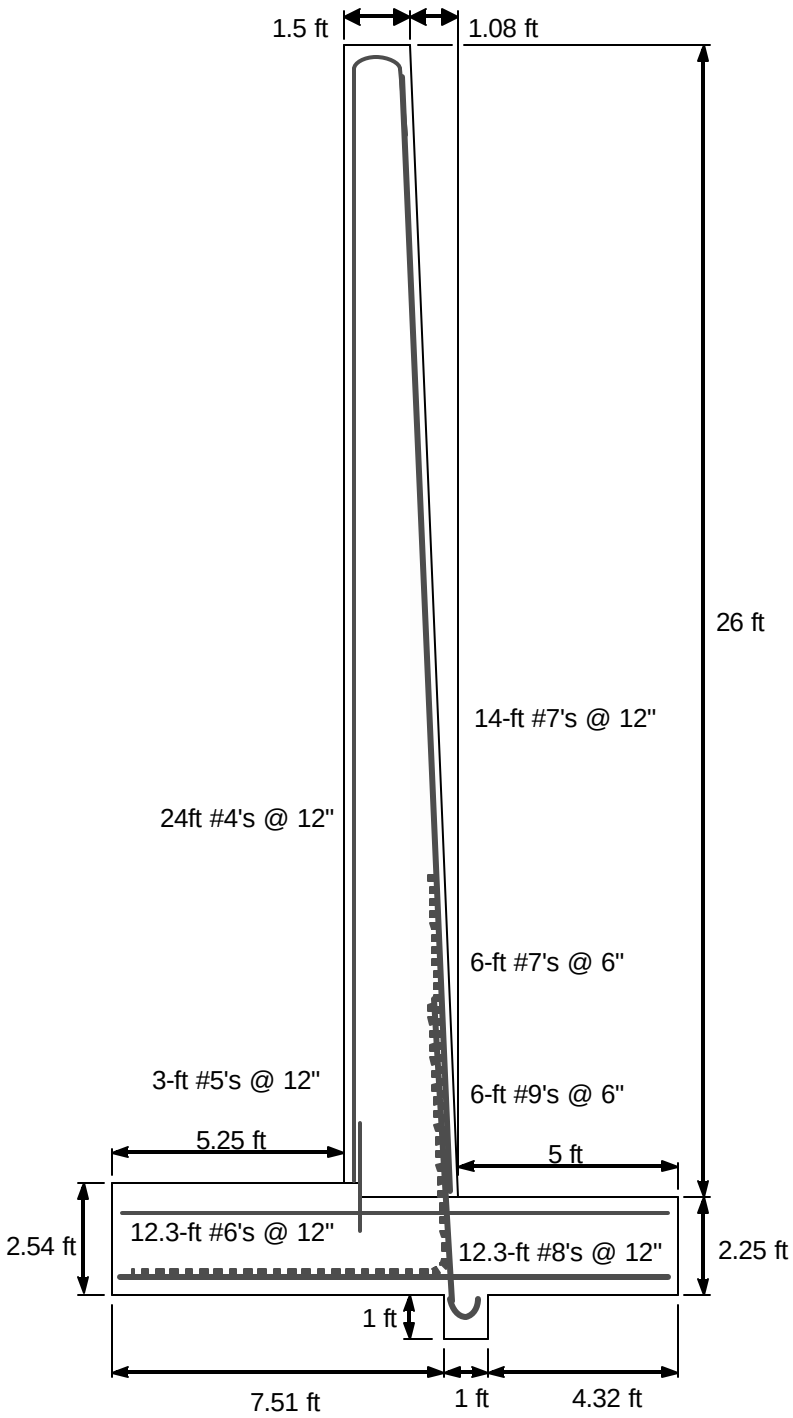

Figure 2.4. Scale drawing of retaining wall panel that was instrumented. Reinforcing bar sizes and spacings are given as total length of certain bar size spaced at X inches. (1 ft = 0.305 m).

Chapter 3
Instrumentation

Site Location

The particular retaining wall is located parallel to Interstate 494 in Bloomington, on the south side of the interstate between West Bush Lake Road and East Bush Lake Road. This wall has eighty-three 30.5 ft (9.30 m) panels, designated A thru CE, with stem heights ranging from 13 ft to 26 ft (4.0 m to 7.9 m). A major factor in the choice of this site was timing with regard to construction. The wall at this site was also seen as typical of other RC cantilever retaining walls designed by Mn/DOT.

Criteria for choosing the panel to be instrumented were: (1) It needed to be at or close to the maximum height, thus giving the highest magnitude of earth pressures. (2) At least one adjacent panel on either side needed to be of equal height, in order to emulate plane strain conditions. (3) The wall foundation should be a spread footing. (4) Finally, a panel near the start of construction was preferred, since winter would likely interrupt construction for several months.

Two panels that met the selection criteria were Panel E near the west end of the retaining wall and Panel BJ towards the east end. Both were 26 ft high panels with at least one adjacent panel of equal height on either side. From soil borings near these panels, it was evident that the footings would rest on mostly granular soils, with some mixed soil (e.g. loamy sand) a few feet below the bottom of the footing. Mn/DOT estimated that vertical settlements would be less than 1 in. (25.4 mm) and differential settlements less than 0.5 in. (13 mm) over the length of the retaining wall. The water table was estimated to be 3 to 5 ft (1.0 to 1.5 m) below the bottom of the wall footings at the time of the boring. Due to construction issues, the contractor, Edward Kraemer and Sons, Inc., started at the east end of the retaining wall, with Panel CE. Therefore, Panel BJ was instrumented.

Instrumentation Plan

The instrumentation plan was developed with several principal themes in mind. Earth pressure on the wall needed to be determined, and the movement of the wall had to be measured to give context to the earth pressure measurements. Redundancy in measurements was essential since field conditions are often unpredictable and can be harsh on sensitive instruments.

Earth pressure was to be measured using two identical layouts of two quite different earth pressure cells (EPCs). One, manufactured by Kulite Semiconductor Products, Inc. (Leonia, New Jersey), was a diaphragm type [17], while the other, manufactured by Geokon Inc. (Lebanon, New Hampshire), was relatively larger and a hydraulic type [18].

A retaining wall, being a deformable body, may undergo three possible types of movements (Fig. 3.1):

a. rigid body translation,

b. rigid body rotation about a point, and

c. deformation or deflection.

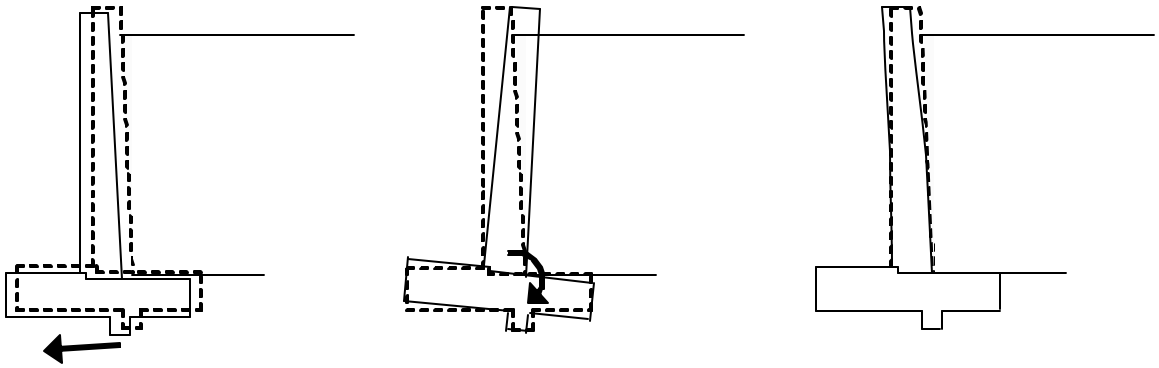

(a) (b) (c)

Figure 3.1. Modes of movement for a retaining wall.

The total movement of a retaining wall is a combination of all three modes. An instrumentation plan was devised to measure these components of movement. Translation was to be determined from a total station survey and extensometers. Rigid body rotation was to be estimated from tiltmeters and inclinometer measurements. An important point is that the rotation was assumed to be about the base of the stem; that is, the footing was assumed to be rigid. Deflection of the stem was to be determined from strain gages on the steel reinforcing bars, as well as tiltmeter and inclinometer readings referenced to the rigid body rotation of the footing.

Instrument Types

Over 60 sensors were installed on Panel BJ. These included 18 EPCs, 36 strain gages, 5 tiltmeters, 2 extensometers, and 2 inclinometer casings. All except the inclinometer casings were monitored automatically at regular intervals by a CR10X data acquisition system, manufactured by Campbell Scientific, Inc. (Logan, Utah). Five AM16/32 multiplexers were also used. A multiplexer expands the number of datalogger channels by up to 16 four-wire sensors (or 32 two-wire sensors). The datalogger was programmed to take readings every 15 minutes for the first week of backfilling; this interval was increased to every 30 minutes thereafter. The CR10X has 128 kilobytes of data storage, and a modem provided remote access for communication and data collection.

Earth Pressure Cells (EPCs)

Two types of EPCs were used in this study. The Kulite EPCs are diaphragm-type pressure cells (Fig. 3.2). They are 0.72 in. (18.3 mm) thick and 2.17 in. (55.1 mm) in diameter, but the active face is only 0.93 in. (23.7 mm) across. As a diaphragm cell, its output is related to deflection of a diaphragm, which is located below a small reservoir of fluid under the active face [17]. Semiconductor strain gages on this metal diaphragm serve as the sensing element.

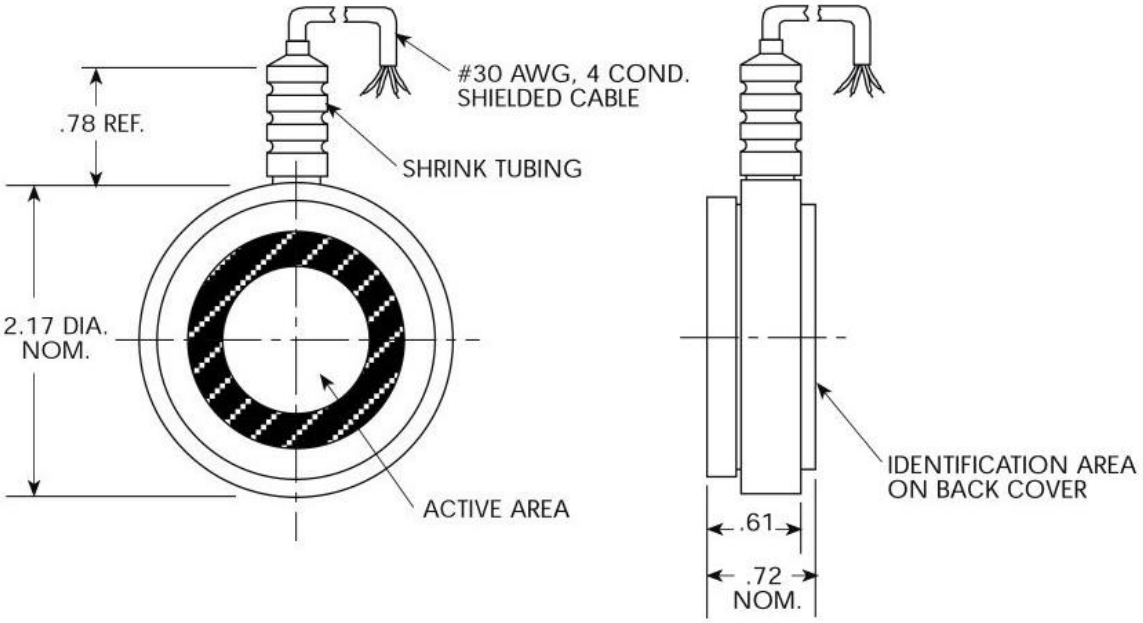

Figure 3.2. Diagram of Kulite model 0234 earth pressure cell (www.kulite.com).

The Geokon EPCs are hydraulic pressure cells 9 in. (230 mm) in diameter and 0.25 in. (6.4 mm) thick (Fig. 3.3). Those to be installed against concrete were twice as thick due to a sturdier backing plate. The principle of hydraulic cells is that the stress from soil on the face of the cell is balanced by the internal fluid pressure, which is measured by a pressure transducer. The pressure transducer is integrated with the cell and has a vibrating wire or strain gage based sensing element. The Geokon EPCs used in this study had semiconductor strain gage transducers. Each Geokon EPC also includes a thermistor (temperature probe) for temperature readings [18].

Figure 3.3. Geokon model 4800 earth pressure cell (www.geokon.com).

EPCs installed in contact with the retaining wall were attached with four concrete anchors per cell. Additionally, a 1/8 to 3/8 in. pad of quick-setting mortar was placed behind the EPC prior to tightening the anchors in order to ensure smooth contact with the structure. To facilitate the installation of those Kulite EPCs to be attached directly to the retaining wall, they were bonded to pre-drilled galvanized steel plates with silicon caulk (Fig. 3.4). Anchor bolts were used to fasten the EPC assembly to the wall. For those Geokon EPCs to be attached directly to the wall, screws with plastic concrete anchor sleeves were used (Fig. 3.5). Each Geokon EPC's external

pressure transducer was also secured to the retaining wall with a PVC U-clamp. All EPCs were installed within pockets of medium dense, uniform silica sand (Fig. 3.6).

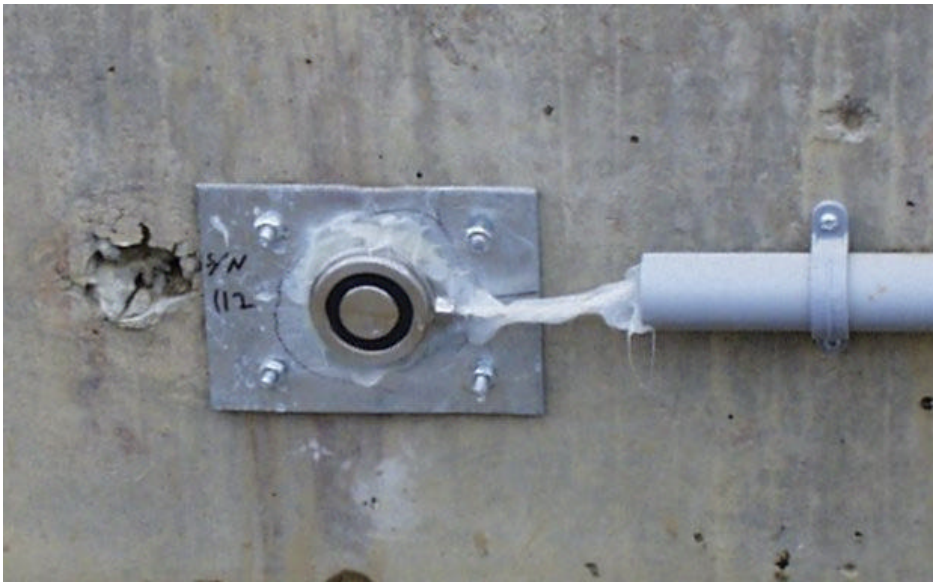

Figure 3.4. Kulite EPC attached to retaining wall.

Figure 3.5. Geokon EPC attached to retaining wall.

Figure 3.6. Kulite EPC within sand pocket.

Foil Strain Gages

Foil resistive strain gages manufactured by Tokyo Sokki Kenkyujo Company, Ltd. (Tokyo, Japan) were used to measure strain on steel reinforcing bars. A three lead-wire arrangement was used to compensate for temperature effects on lead wire resistance. The gages were 3.5 mm wide and 8.8 mm long. The gage length was 3 mm and the nominal resistance was 120 ohms.

Figure 3.7. Foil strain gage attached to epoxy-coated reinforcing bar.

At each strain gage location, an angle grinder was used to produce a uniform, flat surface where gages were placed on rebar (Fig. 3.7). This surface was cleaned further using a weak acid. After applying a neutralizing agent, gages were attached with cyanoacrylate adhesive. Protective butyl rubber tape was laid over each gage, and a final coating of either two-part epoxy or silicon caulk was applied. The epoxy required 24 hours to cure in temperatures above 50° F (10° C), while the silicon caulk could be used in temperatures as low as 32° F (0° C) and began to cure much more rapidly.

Tiltmeters

Tuff Tilt (Applied Geomechanics, Santa Cruz, California) electrolytic tiltmeters were used to measure rotations of the retaining wall. Each tiltmeter had an aluminum mounting bracket to allow for direct attachment to the wall with anchor bolts (Fig. 3.8). All tiltmeters were attached to the front face of the stem after the concrete was poured and stem forms were removed but before backfilling. This particular model had a range of ±0.5° (0.0087 radians), a resolution of 0.0001° (1.75 μradians), and a repeatability of 0.0002° (3.5 μradians). These electrolytic tiltmeters work in a manner analogous to a spirit level, whereby a conductive liquid flows within a glass tube containing electrodes as the sensor rotates. This changes the resistance between electrodes; the resistance is proportional to the rotation of the sensor [19].

Figure 3.8. Tiltmeter attached to base of retaining wall stem.

Borehole Extensometers

Borehole rod extensometers with a potentiometer reference head manufactured by Slope Indicator (Mukilteo, Washington) were used. The potentiometer had a resolution of 0.00024 in. (0.006 mm) and a repeatability of 0.012 in. (0.3 mm). A galvanized metal plate was used as the anchor for the fiberglass rod. During backfilling, once the fill was placed and compacted to one foot above the height of the bottom extensometer, a trench was dug down to the depth of the extensometer. The extensometer rod and metal anchor were then installed and the backfill replaced and hand-compacted.

Inclinometer

A Digitilt (Slope Indicator, Mukilteo, Washington) biaxial inclinometer was used to measure inclination of 2.75 in. (69.9 mm) diameter plastic casings embedded throughout the retaining wall stem and into the footing. Grooves oriented at 90° from each other allow for two perpendicular readings, with the probe tracking along the same orientation in the casing each time a measurement is taken. Measurements are taken at 2 ft (0.61 m) increments through the length of the casing (Fig. 3.9). Both the stated resolution and the repeatability are 0.0012 in. per 2 ft (0.05 mm per 1 m).

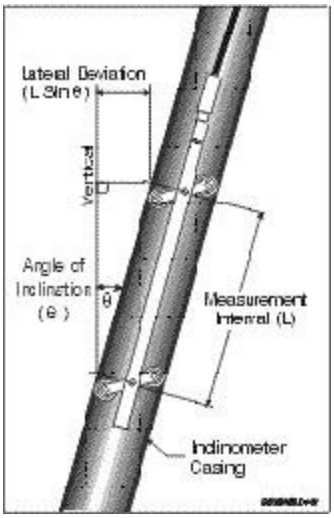

Figure 3.9. Diagram of inclinometer probe within casing (www.slopeindicator.com).

Total Station Survey

To capture the total movement of the retaining wall, a survey of wall position was performed with a total station that utilized a laser to measured distance. To reduce error associated with setting up the survey device each time a measurement was to be taken, a reinforced concrete monument 1 ft (0.305 m) in diameter was constructed opposite the wall on the north side of Interstate 494. It extended 4 ft (1.2 m) into the ground and 5 ft (1.5 m) above ground level (Fig. 3.10). A mounting bracket with a bull's-eye bubble level was embedded on the top of the monument, whereby the total station could be quickly placed in the same position each time. The level was checked each time a measurement was made to determine if the monument had moved. A backsight was established 165 ft (50 m) away to detect any movement by the monument.

Figure 3.10. Total station mounted on concrete monument.

Four prismatic reflectors were attached to the front face of the wall (Fig. 3.11). A coordinate system was set up with the monument was at the origin and the backsight along the *y*-axis. Hence, the wall was in the direction of the *x*-axis, although the line of sight to Panel BJ was rotated clockwise 7.6º from the *x*-axis (Fig. 3.12). Since the wall was nearly along the *x*-axis, distance measurements made using the total station's laser were predominantly responsible for determining the coordinates of the survey points. This also should have reduced error to less than 2 mm. For convenience, a second coordinate system, transformed by a rotation of 7.6º and a translation to the position of Panel BJ, was used throughout the project to describe the movement of the retaining wall and the locations of instruments. The *y'*-axis of this coordinate system was oriented along the length of the wall. The *z'*-axis was positive upwards, and the positive direction of the *x'*-axis was into the backfill. Consequently, wall displacements away from the backfill and wall rotations away from the backfill were both negative in sign.

Figure 3.11. Prismatic survey reflector fastened to front face of the wall.

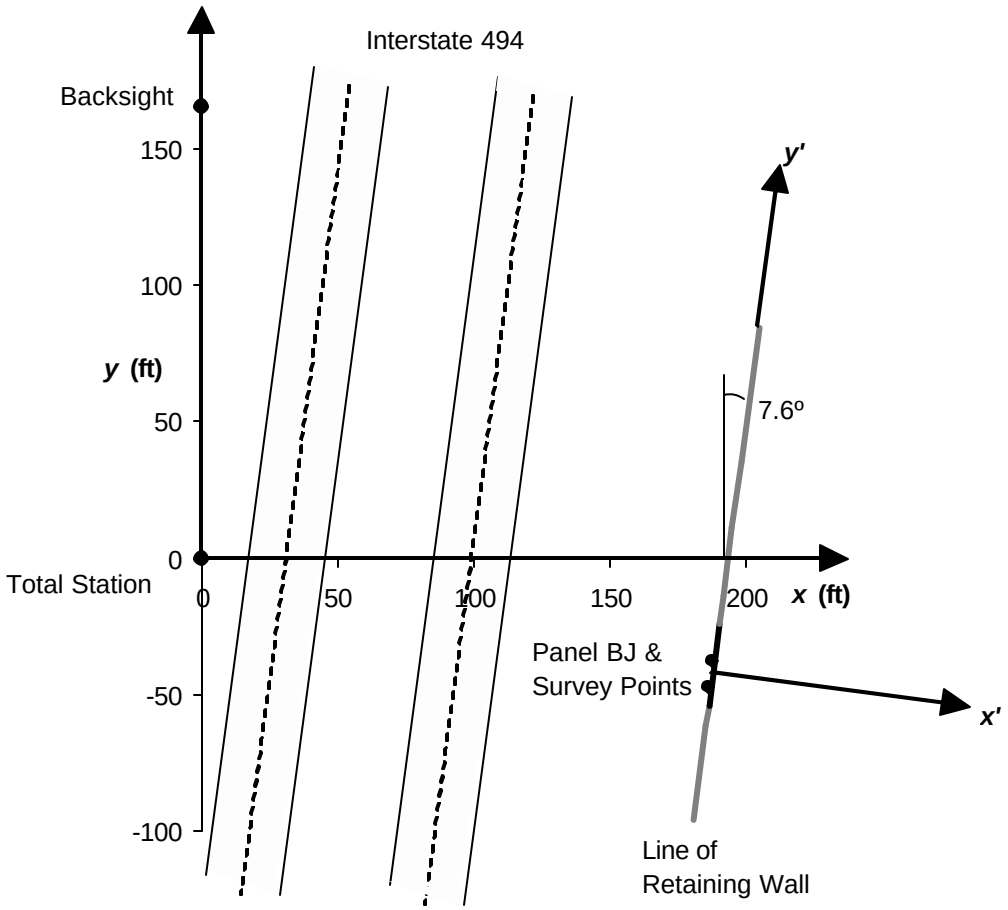

Figure 3.12. Layout of total station monument, backsight, and Panel BJ along Interstate 494 with coordinate system used for survey.

Error Estimates

The reported repeatability of the Kulite EPCs is 0.1% of the full scale operating range. The pressure transducers for the Geokon EPCs have an accuracy of 0.5% of the full scale operating range. The error for the EPC calibrations is covered in the following section. Inclinometer readings have a resolution in terms of displacements equal to 0.0012 in. per 2 ft (0.05 mm per 1 m), in terms of rotation equal to 0.0029° (50 μradians); the repeatability is the same as the resolution. Tiltmeter readings have a finer resolution of 0.0001° (1.75 μradians) and a repeatability of 0.0002° (3.5 μradians). Therefore, the tiltmeters were assumed to more accurately measure rigid body rotation and rotation due to elastic deflection of the wall. Total station measurements have an inherent resolution of about ±0.08 in. (2 mm). The resolution for the strain gages measured with the CR10X was expected to be $3*10^{-6}$. It was estimated that measurements of strain using strain indicator units were accurate to within $3*10^{-6}$, since this was the repeatability in the field. Table 3.1 summarizes the repeatability of the instruments, which in most cases was also the accuracy. The accuracy of the tiltmeters was determined from the EPC calibrations.

Table 3.1. Error estimates for retaining wall instrumentation.

Sensor	Repeatability (±)	Accuracy (±)
Kulite EPC	0.1% full scale	5%
Geokon EPC	0.5% full scale	5% (est.)
Inclinometer	0.0029° (1/20,000)	0.0029° (1/20,000)
Tiltmeter	0.0002° (1/286,000)	0.0002° (1/286,000)
Total station	0.08 in. (2 mm)	0.08 in. (2 mm)
Strain gages	$3*10^{-6}$	$3*10^{-6}$

EPC Calibration

Numerous papers have been published on the performance of various types of earth pressure cells. Theroux et al. [20] and Labuz and Theroux [21] have studied the performance of the Kulite, diaphragm-type EPC, where arching of the surrounding soil may be responsible for under-registration. These researchers developed a means of calibrating for the under-registration and proposed installing EPCs within a sand pocket to ensure consistent readings.

Due to this arching effect, the EPCs to be used in this study were calibrated in sand prior to field installation. Furthermore, the sand used for field installation was the same as that used for laboratory calibration. The techniques were based on those developed by Theroux et al. [20].

Kulite Calibration

The uniaxial calibration technique developed by Theroux et al. [20] was employed in calibrating the Kulite EPCs. Uniform, dry silica sand, which passed a #20 sieve and was retained on a #30 sieve, was used for the calibration. The uniaxial calibration device uses fluid pressure to induce stress in a column of soil above the active face of the EPC (Fig. 3.13). Comparing this soil calibration to the manufacturer's calibration factor, it is evident that these EPCs under-registered by up to 25%. A few of these calibration factors were checked by placing the EPC within a universal calibration chamber (Fig. 3.14). This chamber had about 7 in. (178 mm) of soil, a 1-in. (25-mm) water-filled rubber bladder, 7 in. of soil containing the EPC, another 1-in. rubber bladder, and 7 in. of soil at the bottom. The load applied to the steel platens was recorded, as was the pressure in the bladders. The uniaxial calibration factors predicted the stress in the soil to within 5% of the applied stress, as measured by the upper bladder. This was taken to be the error range for the Kulite EPCs. Plots from the uniaxial and universal calibration tests for the Kulite EPCs are included as Appendix A.

Geokon Calibration

These hydraulic cells were calibrated only in the universal calibration chamber (Fig. 3.14), due to their size. Geokon EPCs under-registered from 5 – 15%. It is thought that some arching of the soil across the EPC face was able to take place since the outer rim of the EPC face is stiffer than the inner part. This force was transferred through the structure of the sensor rather than through the hydraulic fluid inside the cell. The calibration supplied by the manufacturer is only for the pressure transducer, not the entire device; this explains the under-registration in soil. Calibration plots for the Geokon EPCs are also included in Appendix A.

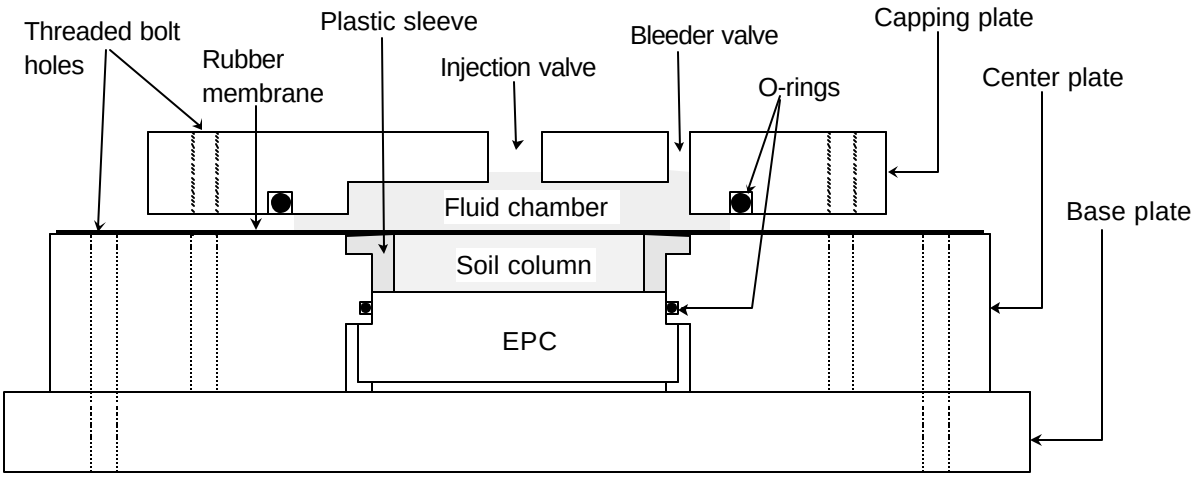

Figure 3.13. Uniaxial soil calibration device [20, 21].

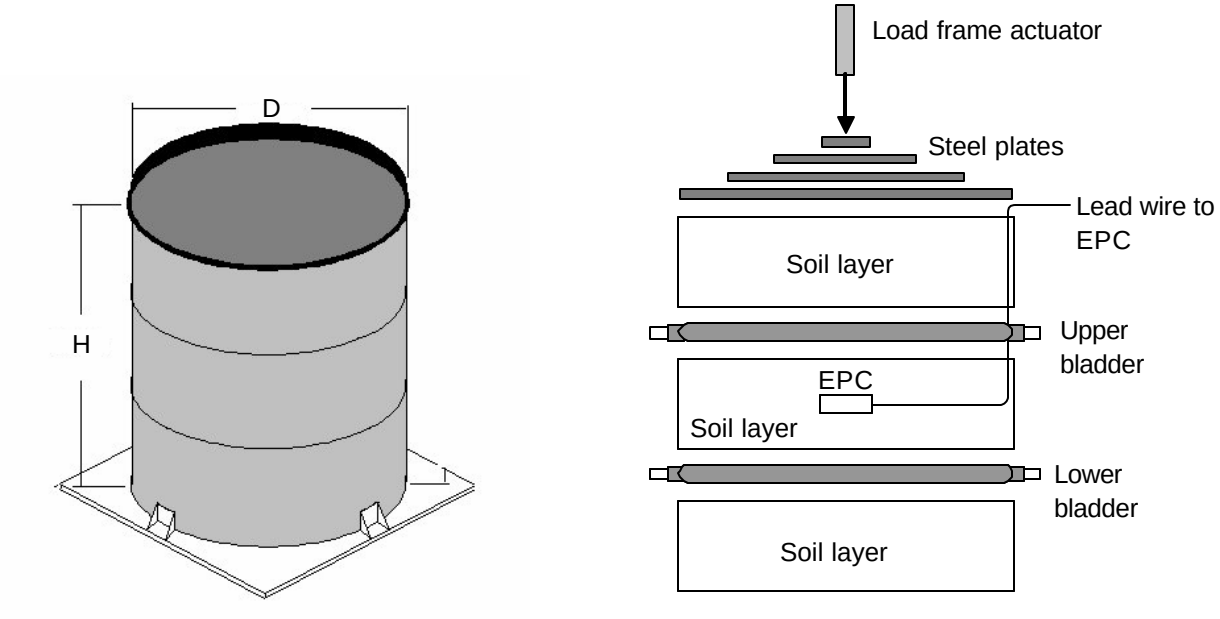

Figure 3.14. Universal EPC calibration device [20, 21].

Instrumentation Layout

Nine EPCs of each type (diaphragm and hydraulic), for a total of 18 EPCs, were installed, with similar placement locations for each set: 14 were oriented to measure lateral earth pressure, while four were oriented to measure vertical stress (Fig. 3.15).

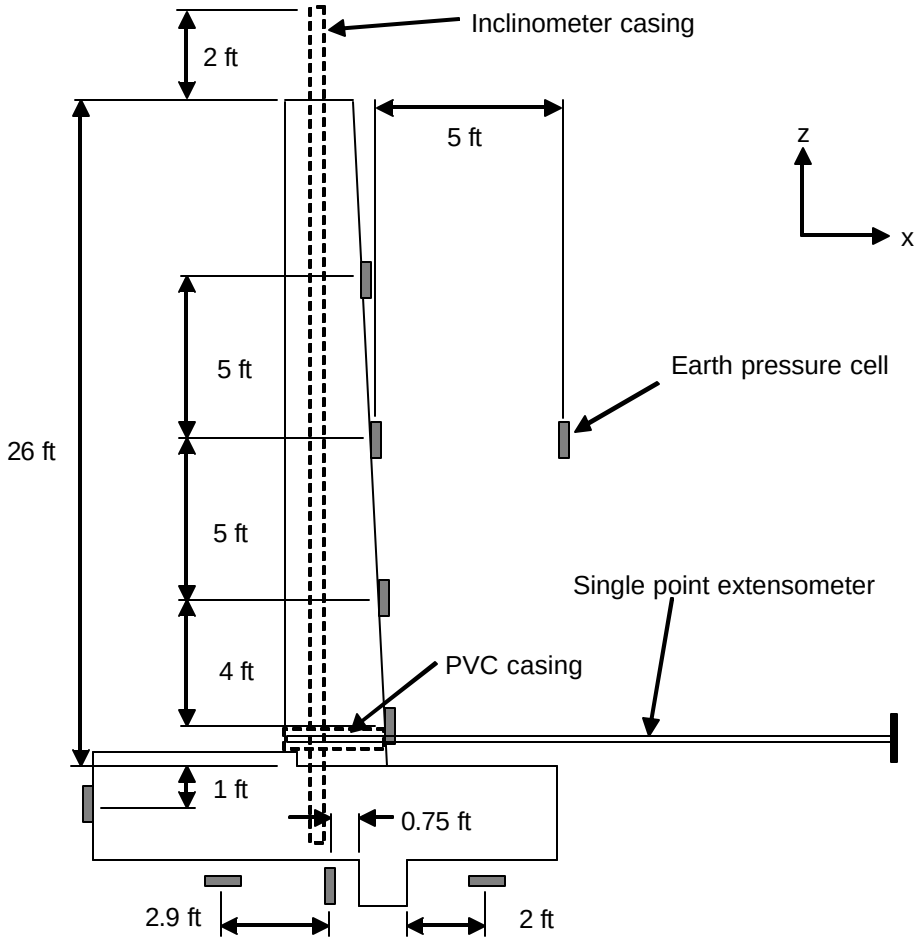

Figure 3.15. Locations of earth pressure cells and extensometers (1 ft = 0.305 m).

Of those EPCs measuring lateral pressure, two each were mounted at these positions:

a. on the face of the footing toe,

b. in front of the shear key,

c. at 1, 5, 10, and 15 ft (0.305, 1.52, 3.05, and 4.57 m) up from the footing on the back face of the stem, and

d. within the backfill, 10 ft (3.05 m) up from the footing and 5 ft (1.52 m) from the wall in the soil.

Two borehole rod extensometers were to be installed in the stem and anchored within the backfill. Two inclinometer casings were installed vertically within the stem, extending from

within the footing and up through the top of the stem. Four survey reflectors were mounted on the stem for total station measurements. Five tiltmeters were mounted on the stem, including one at the base of the stem to measure rigid body rotation (Fig. 3.16).

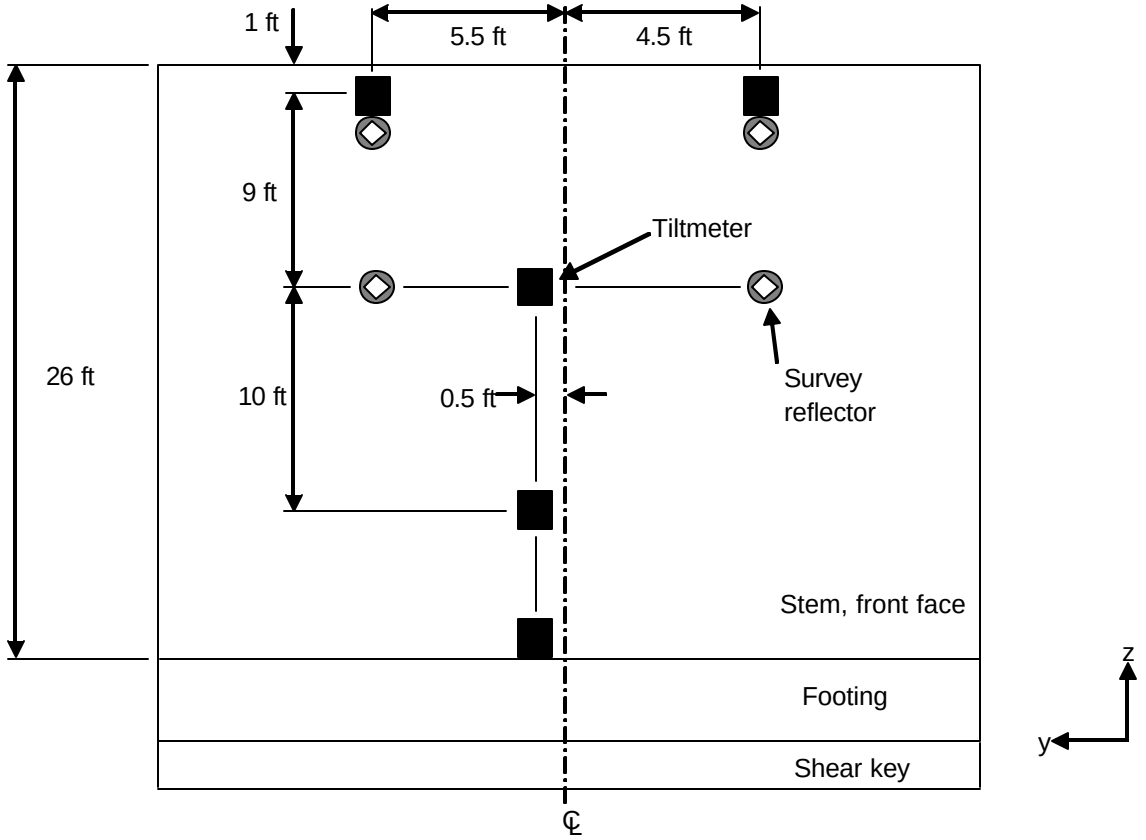

Figure 3.16. Locations of tiltmeters and survey reflectors on front face of stem (1 ft = 0.305 m).

A total of 36 strain gages were placed on the steel reinforcement. Eight strain gages were placed on the footing rebar, four were placed on the steel dowels, and 24 were placed on reinforcing bars within the stem (Figs. 3.17 and 3.18).

Half of the strain gages were installed at approximately the same cross-section (east section) through the wall as the Kulite EPCs, and half were installed at the same cross-section (west section) as the Geokon EPCs. Furthermore, an inclinometer casing was installed at each cross-section. Both the compression and tension reinforcement were instrumented (Fig. 3.18).

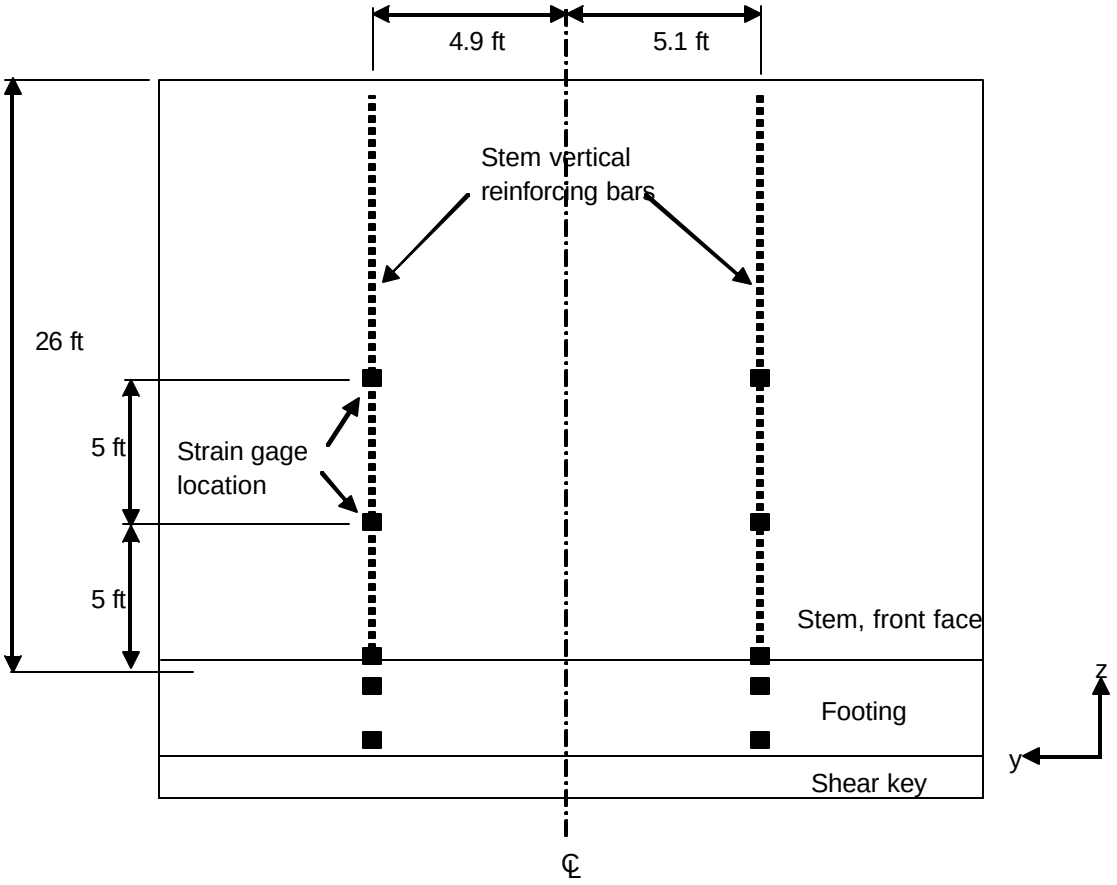

Figure 3.17. Strain gage locations along length of Panel BJ (1 ft = 0.305 m).

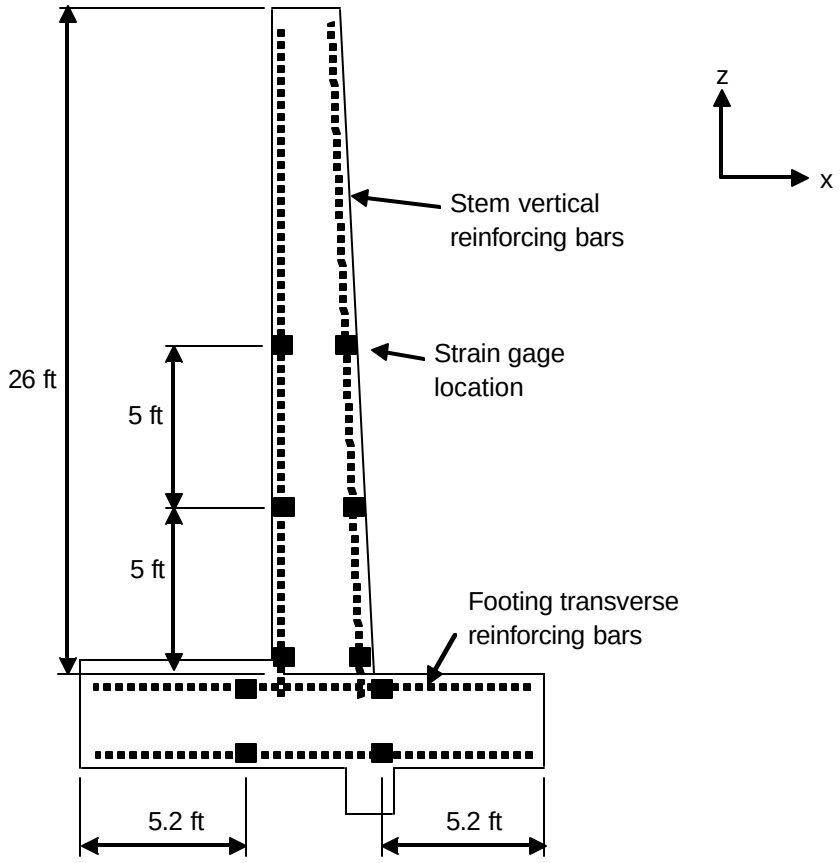

Figure 3.18. Strain gage locations on reinforcing bars through cross-section of Panel BJ (1 ft = 0.305 m).

Installation Procedures

It was important with all instrumentation, especially with the EPCs, that consistent and methodical procedures be used when installing instruments on the retaining wall. Weather conditions and other factors sometimes made this difficult.

Footing

A total of 16 sensors were used to instrument the footing of Panel BJ: eight EPCs and eight strain gages. In addition, the inclinometer casings extended into the footing. Foil strain gages were placed on the longitudinal rebar in the footing at two evenly spaced locations along the length of Panel BJ (Figs. 3.17 and 3.18). Due to the tight dimensions of the rebar cage and concrete forms, strain gages were attached to the appropriate pieces of rebar before they were wired in place. Gages were placed on both the top and bottom longitudinal reinforcing bars in two places approximately coinciding with the front face and back face of the stem. After the rebar cage was complete, lead wires were run through PVC pipe away from the footing before concrete was poured.

Following compaction of the soil and forming of the footing, four EPCs were placed to measure vertical stress below the footing (Fig. 3.15). In addition, two EPCs were placed on the passive side of the footing shear key. Finally, after the forms were removed, two EPCs were installed on the vertical face in front of the footing toe. All lead wires were protected within PVC conduit. To protect the footing instrumentation, concrete was not dumped or vibrated within a one-foot radius of the gages and earth pressure cells.

Stem

A total of 45 instruments were installed in and on the stem of Panel BJ: 10 EPCs, 28 strain gages, 2 extensometers, and 5 tiltmeters. The two inclinometer casings extended through the entire height of the stem. Four survey reflectors were also mounted on the front face of the stem for total station measurements.

Foil strain gages were placed in the stem at two evenly spaced locations corresponding to the strain gages in the footing. At each of these locations, gages were attached to both the compression and tension reinforcement at three different heights (0.5 ft, 5 ft, and 10 ft) above the top of the footing (Fig. 3.17). At each position, a gage was placed on both sides of the rebar (approximately corresponding to the individual bar's neutral axis).

The strain gages at 0.5 ft above the footing were attached to the rebar dowels projecting out of the footing and extending into the stem of the wall. These were installed shortly after the footing was poured. The strain gages at 5 ft and 10 ft above the footing were installed on reinforcing bars after the cage was tied, but before it was lifted into place. In order to compensate for drift and temperature changes, several identical gages were placed on 2 ft (0.61 m) pieces of debonded transverse rebar embedded in the stem.

Foil strain gages were also installed on two joint dowels in an attempt to measure the load transferred from Panel BJ to neighboring sections. The strain gages were applied to the proper pieces of epoxy-coated dowels before they were placed in the end forms of the stem. Two gages were placed on each side of the instrumented dowels, one on the soil side and one on the free side. One dowel was instrumented along each joint near the top of the wall (Fig 3.19). Two foil strain gages were placed 1 in. (25 mm) towards Panel BJ from the center of the 2 ft (0.61 m) long dowel.

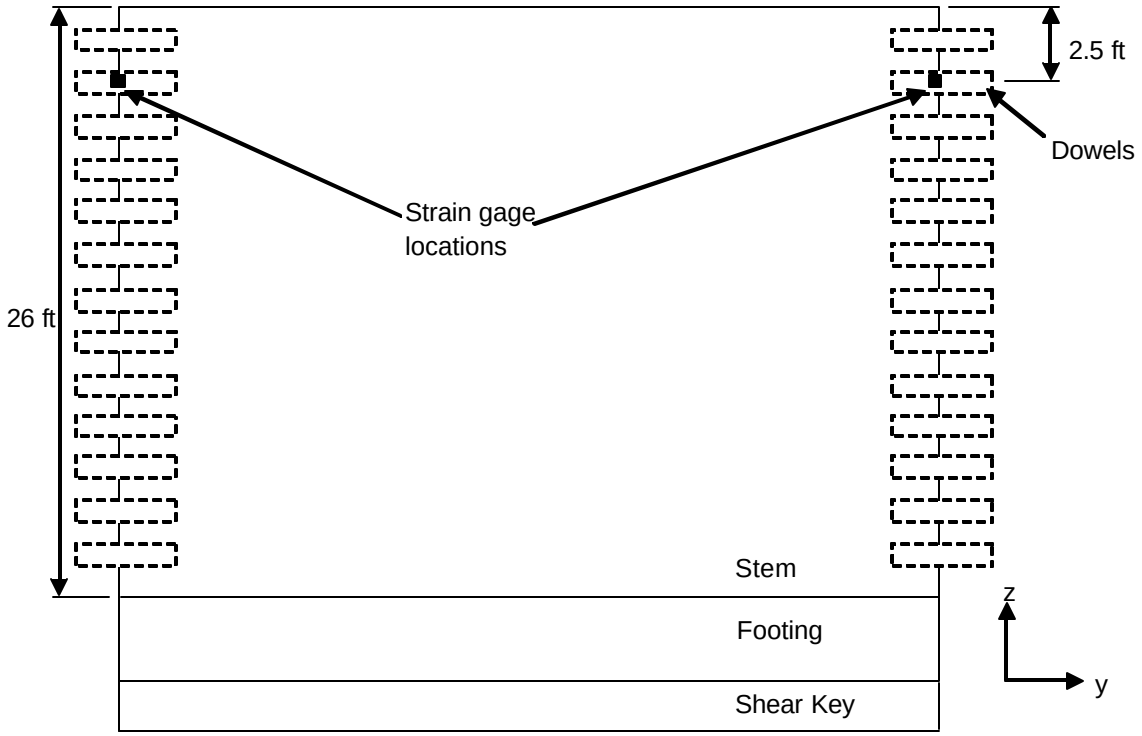

Figure 3.19. Location of instrumented dowels at joints of Panel BJ (1 ft = 0.305 m).

Two sections of 4 in. (102 mm) PVC pipe were placed vertically within the footing to serve as "block-outs" for inclinometer casings. After the rebar cage for the stem was placed, inclinometer casings were anchored into these PVC pipes with mortar and secured to the rebar cage as they extended up the height of the stem.

Four tiltmeters were placed on the exposed face of Panel BJ (Fig 3.16). These tiltmeters were to measure the longitudinal rotation of the wall. A fifth tiltmeter was placed at the base of the stem to measure the rigid body rotation of the footing.

The eight EPCs on the back face of the stem were fastened to the concrete after the concrete had hardened and forms were removed. During backfilling, pockets of sand were placed around the EPCs as the height of the backfill soil increased. Two EPCs were placed within the backfill. When backfill had been placed and compacted to about 2 ft (0.61 m) above the installation height for the EPCs, two trenches for the sensors and their signal cables were dug. The cells were placed within sand pockets, and the backfill soil was replaced and hand-compacted. The backfill process was observed to ensure that no instruments or signal cables were damaged.

Two borehole extensometers were to be placed in the stem and anchored into the fill behind Panel BJ. Both extensometer heads were to be anchored in the center of Panel BJ with respect to the length of the panel. One was installed at the bottom of the stem, while the other was to be installed near the top of the stem. The bottom extensometer head was installed, but the top extensometer head was destroyed upon placement of the back form for the stem. In addition, mud and silt from heavy rains prior to backfilling evidently caused the bottom extensometer to cease functioning. Repair efforts were unsuccessful.

Difficulties

Several difficulties were encountered:

1. The EPC at the shear key was difficult to place because the surrounding soil was not well compacted. This was due in part to the excavation and forming method for the shear key.
2. Two extensometers were destroyed, one accidentally by the contractor, and one by the elements (mud and rain), so the total station was the sole measure of total horizontal movement.
3. The readings from the Geokon EPCs, although still proportional to the actual earth pressure, were approximately an order of magnitude lower than those from the correspondingly located Kulite EPCs. This was due to a hardware problem with a multiplexer (Appendix B).
4. One inclinometer casing was damaged during placement of the concrete, although it was repaired. However, measurements from this casing were somewhat erratic.
5. Two gaps in the data (15:32 Nov 1 thru 12:32 Nov 3 and 12:47 Dec 1 thru 17:02 Dec 4) were due to difficulties with the CR10X datalogger.
6. All but one tiltmeter malfunctioned at some point. The tiltmeter at the base of the stem was buried under four feet of soil and could not be removed for repair, though others were repaired by the manufacturer and subsequently reattached. The tiltmeters were also sensitive to changes in ground potential; this showed up as a sudden, substantial increase in the baseline tiltmeter reading followed by an eventual drop to the original baseline reading.
7. Meaningful readings could not be obtained from the strain gages within Panel BJ. Interference in the signal produced noise levels in excess of the expected signal.

The following spring, ten additional strain gages were placed on the rebar within Panel E and monitored with a strain indicator and switch-and-balance unit. These sensors were installed to give supplementary data regarding the structural behavior of the wall. A Geokon EPC was also placed within the backfill (Fig. 3.20). The strain gages on Panel E gave satisfactory readings.

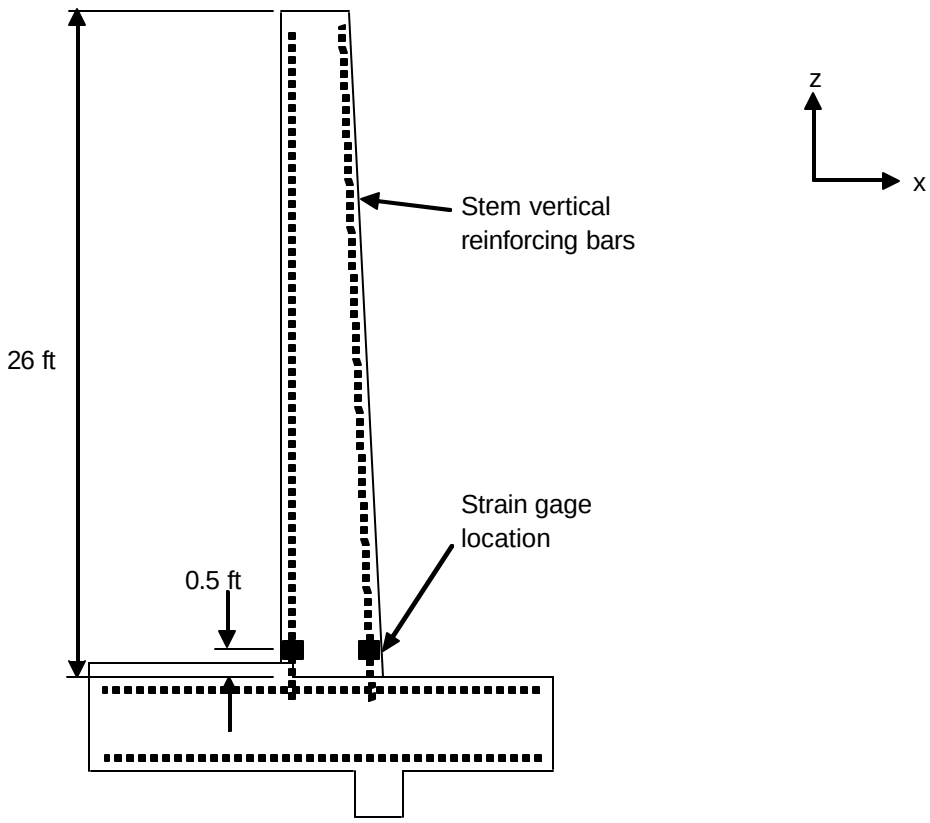

Figure 3.20. Strain gage locations for Panel E.

Chapter 4
Measurements and Analyses

Backfill Description

The backfill soil used behind Mn/DOT's retaining walls is designated modified select granular, with a limit of 10% by weight passing the No. 200 sieve [22]. Some larger pebbles and cobbles were observed during backfilling. From a standard sieve analysis, the effective size D_{10} = 0.005 in. (0.13 mm). The uniformity coefficient C_u = 3.23, and the coefficient of gradation C_z = 1.14 (Appendix C, Section 1). It was classified as SP (poorly graded sand) according to the Unified Soil Classification System. Its AASHTO classification was A-3(0).

Friction Angle

The angle of internal friction for the backfill material was found to be from 35° – 39° from consolidated-drained triaxial tests (Appendix C, Section 2). A friction angle of 37° was used when predicting loads on the wall. This is higher than the value of 35° used in Mn/DOT's design.

Unit Weight

A unit weight of 125 pcf (19.6 kN/m^3) is assumed in Mn/DOT's design specifications. Field measurements of unit weight by Mn/DOT inspectors using the sand cone method were consistently about 120 pcf (18.9 kN/m^3). This value was used for predictions of lateral loads and displacements.

Backfilling Procedure

Panel BJ's footing was poured on September 18, 2002, and the stem was poured September 30. Backfilling on Panel BJ began on October 28 and was up to 22 ft (7.62 m) by November 1. The soil was dumped by trucks and then spread by bulldozers into layers at most 8 in. (200 mm) thick. Compaction was achieved by smooth-wheel vibratory compactors. If necessary, water was added between lifts to achieve optimum moisture content. The backfill reached a height of 25 ft (7.6 m) on November 21; the final 1 ft (0.30 m) of soil was placed the following spring.

Sensor Notation

The following notation is used to describe instruments and locations in subsequent sections:

EPC IDs

EPC_back: Kulite EPC below heel of footing
EPC_front: Kulite EPC below toe of footing
EPC_key: Kulite EPC in front of footing's shear key
EPC_toe: Kulite EPC mounted on face of footing toe

EPC_1: Kulite EPC mounted to stem, 1 ft (0.3 m) up from footing
EPC_5: Kulite EPC mounted to stem, 5 ft (1.5 m) up from footing
EPC_10: Kulite EPC mounted to stem, 10 ft (3.0 m) up from footing
EPC_bf: Kulite EPC placed 5 ft (1.5 m) into backfill, 10 ft (3.0 m) up from footing
EPC_15: Kulite EPC mounted to stem, 15 ft (4.6 m) up from footing

Tiltmeter IDs

Tilt_0: Tiltmeter mounted at the base of the stem
Tilt_6: Tiltmeter mounted 6 ft (1.8 m) up the stem, at the center
Tilt_16: Tiltmeter mounted 16 ft (4.9 m) up the stem, at the center
Tilt_25E: Tiltmeter mounted 25 ft (7.6 m) up the stem, 5 ft (1.5 m) east of center
Tilt_25W: Tiltmeter mounted 25 ft (7.6 m) up the stem, 5 ft (1.5 m) west of center

Total Station Survey Point IDs

ts 25: Average of readings for two survey points 25 ft (7.6 m) up the stem
ts 16: Average of readings for two survey points 16 ft (4.9 m) up the stem

Vertical Soil Stress

The responses of the Kulite EPCs measuring vertical soil stress beneath the footing were directly proportional to the weight of the soil above. In fact, comparing the readings from EPC_back and EPC_front with field observations of the backfill height revealed a direct correlation (Fig. 4.1). Thus, these EPCs could be used to determine the height of the retaining wall backfill at a given time, so as to fill in gaps between observations of the backfill height. The observed soil depths, supplemented with those determined from EPC_back, are used throughout this report.

These measurements from EPCs below the footing were in contrast to the distribution of stress beneath a retaining wall footing presented in soil mechanics textbooks [23]. Standard design assumes the highest vertical stress below the footing toe (Fig. 4.2a), whereas a linear interpretation of stress measurements from EPC_back and EPC_front indicated the opposite (Fig. 4.2b). In fact, these measurements agree instead with numerical results such as those of Clough and Duncan [8] and Goh [12], which found greater vertical settlement at the footing heel than at the toe; this necessitates greater vertical stresses below the heel than below the toe.

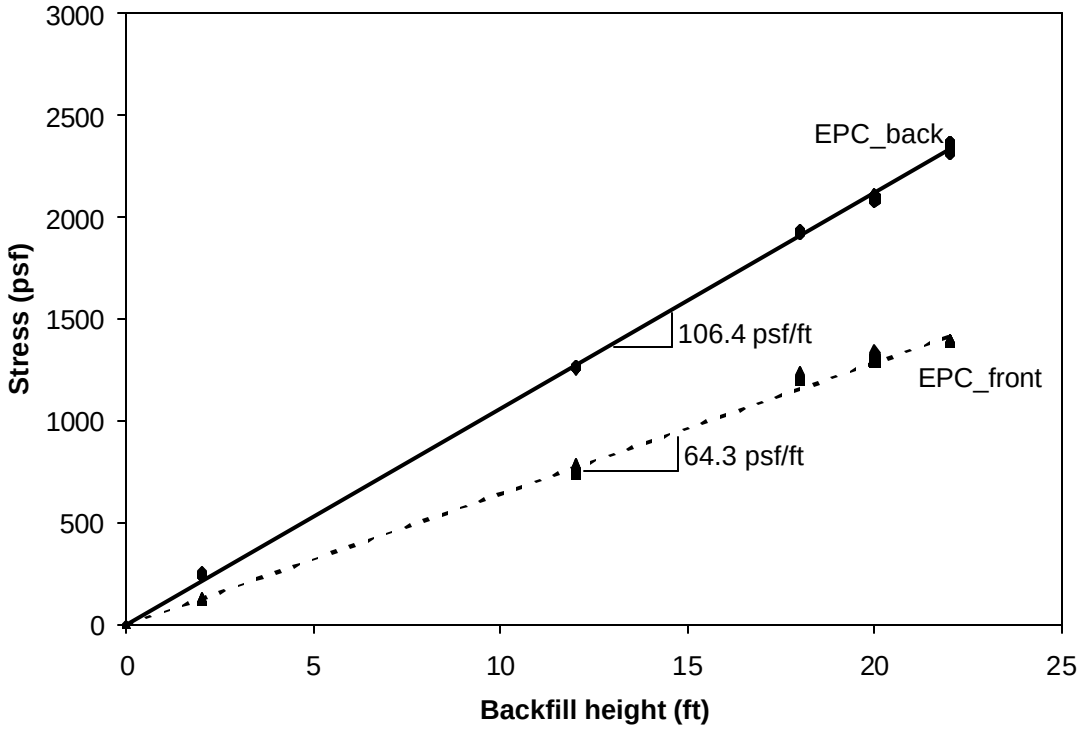

Figure 4.1. Measurements of vertical stress below footing versus backfill height.

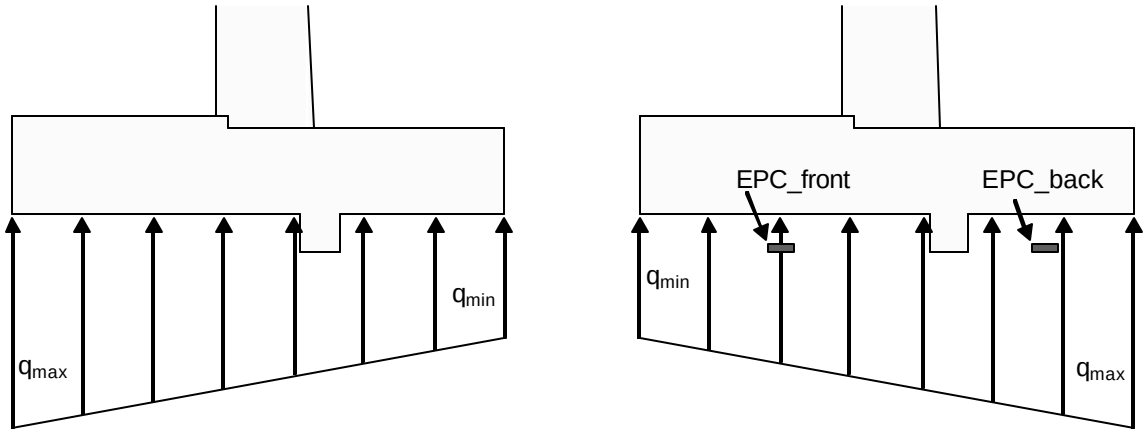

Figure 4.2. (a) Commonly assumed vertical stress distribution below retaining wall. (b) Estimated vertical stress distribution below Panel BJ, from EPC measurements.

A major difference between the problem as outlined in textbooks and the actual situation, which the numerical studies attempted to simulate, was the placement of the backfill beyond the footing heel. As backfill was placed behind the footing, its weight acted as a uniform load applied to the surface of the foundation subsoil (Fig. 4.3). Downward deflection of the subsoil occurred. Since the wall was founded on this subsoil, it displaced downward as well. Because much less soil was placed in front of the wall, differential settlements occurred between the footing heel and the toe (Fig. 4.4).

Given that measurements of vertical stress were taken approximately 5 in. (127 mm) below the bottom of the footing, it may be expected that the vertical stress below the edge of the heel at this depth should be nearly equal to the vertical stress at the same depth some distance away from the heel (Fig. 4.5). In fact, the values of q_{max} extrapolated from EPC_front and EPC_back compared very well with the vertical stress expected at the same elevation below backfill with a unit weight of 120 pcf (18.9 kN/m^3). Throughout the backfilling process, the expected vertical stress, γz, was within 5% of q_{max} (Fig. 4.6).

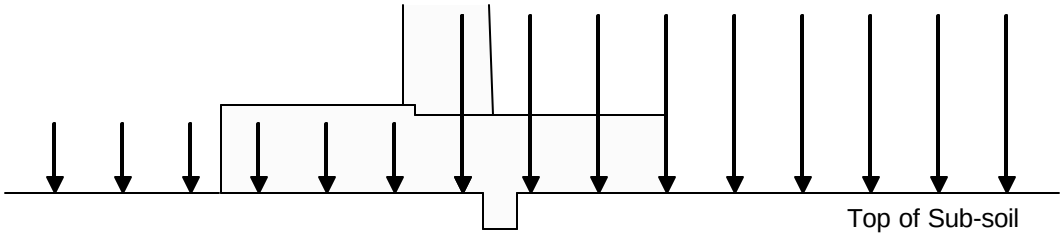

Figure 4.3. Idealized loading on surface of foundation subsoil due to weight of backfill.

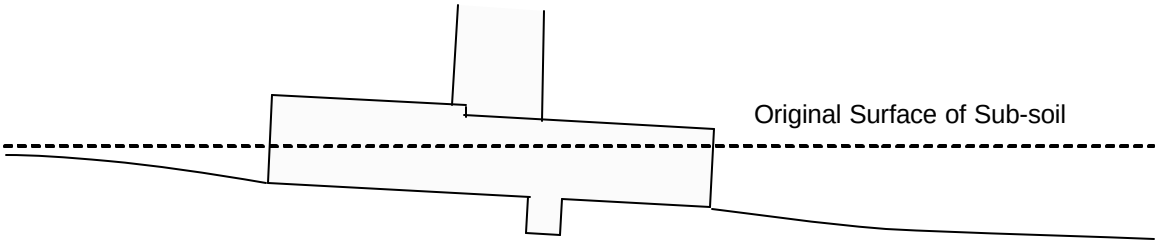

Figure 4.4. Qualitative settlement of foundation subsoil due to weight of backfill.

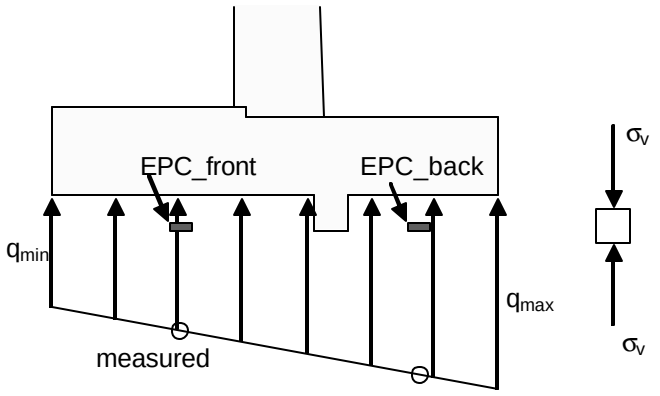

Figure 4.5. Soil element located near the edge of the footing heel; q_{max} was extrapolated from the measured data.

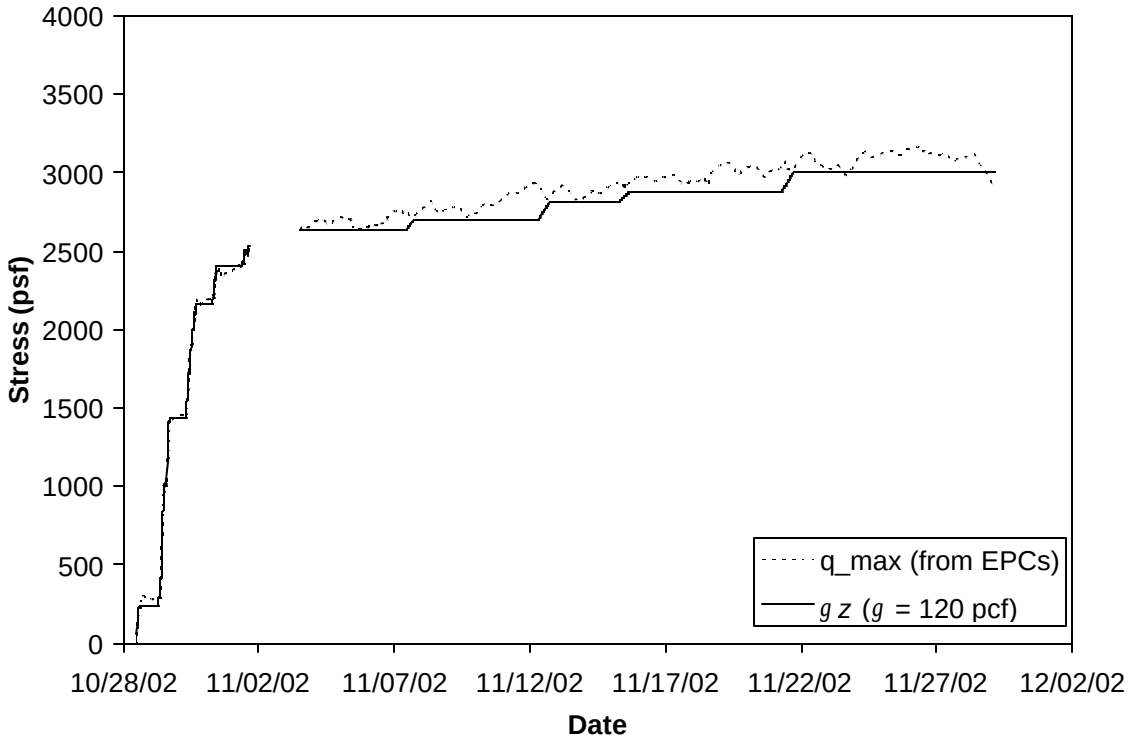

Figure 4.6. Estimated vertical stress at edge of footing heel.

Earth Pressure Distribution

The distribution of lateral earth pressure on the retaining wall stem at selected stages during backfilling is shown in Figs. 4.7, 4.8, and 4.9; note that t = 0 denotes the profile at 17:00 while t = 12 hr denotes the profile at 5:00 the following morning. It is evident that the lateral pressure was higher than the theoretical active pressure when the backfill height was at 12 ft (3.7 m), 18 ft

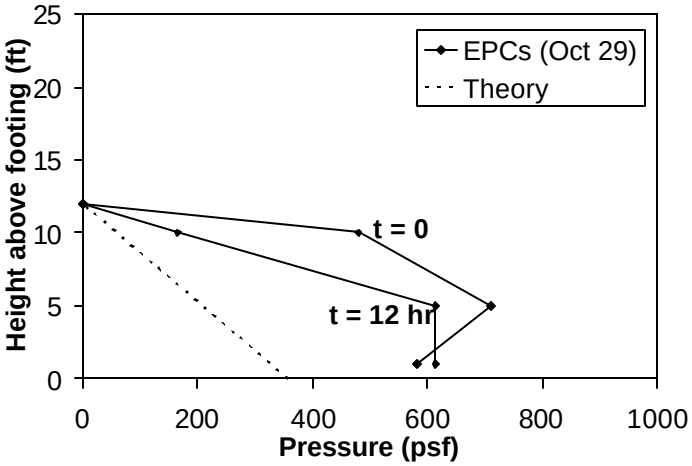

Figure 4.7. Earth pressure distribution for backfill height of 12 ft (3.7 m).

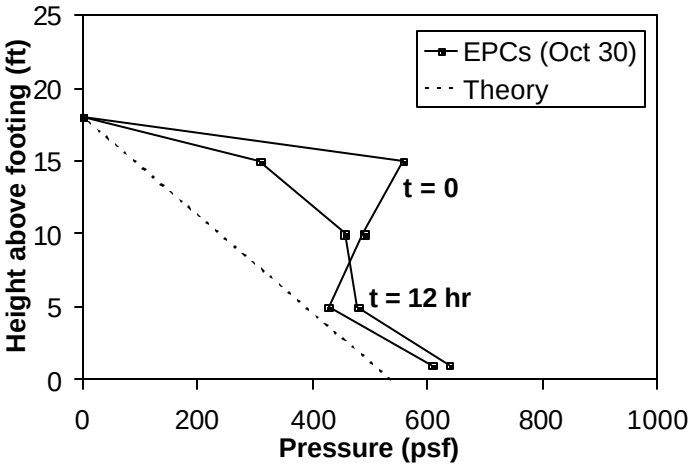

Figure 4.8. Earth pressure distribution for backfill height of 18 ft (5.5 m).

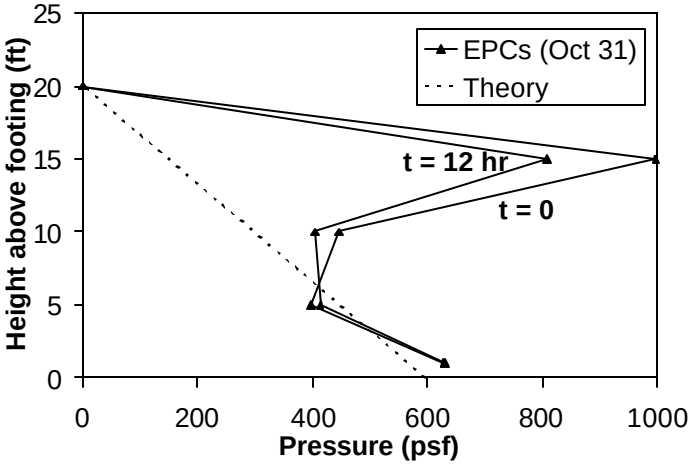

Figure 4.9. Earth pressure distribution for backfill height of 20 ft (6.1 m).

(5.5 m), and 20 ft (6.1 m). This was probably due to two factors. First, as is discussed in Section 4.3.6, very little rigid body translation had occurred by the time backfill reached 12 ft (3.7 m). Second, compaction of the backfill likely caused considerable residual lateral stresses.

Table 4.1 contains backfill heights and the EPC-determined lateral force on the stem for the first several days of backfilling, with values listed for every 12 hr. The lateral force was determined by assuming a linear distribution of pressure between the EPC measurements. Also included are theoretical values for the lateral force assuming the active condition. The EPC readings from 15:32 Nov 1 thru 12:32 Nov 3 were lost due to a problem with the data acquisition system. However, no backfilling occurred on Nov 2 and 3 since these dates were on the weekend. Two things are evident from the data. The first is that the lateral force on the stem was significantly more than the theoretical active force until about a week after backfilling began. Second, the lateral force measured by the EPCs at 5:00 was generally less than what it was 12 hr earlier (the backfilling usually ended just prior to 17:00). As is discussed in Section 4.3.6, this reduction of lateral force was due to translation of the wall overnight. This is also described in further detail in Section 5.1.2.

The resultant of the lateral earth pressure was calculated for the piecewise linear distribution of earth pressure from the EPCs (Fig. 4.10). Note that for the first day of backfilling, when only EPC_1 was covered with soil, the position of the resultant was one-third of the backfill height since the linear extrapolation of a single EPC reading was a triangle. After this initial day, however, the resultant was higher, with a peak of almost 50% of the soil height. This was due in large part to the higher earth pressure near the soil surface resulting from the compaction process. Again, translation of the wall was responsible for the decrease in pressure on the wall near the soil surface, with a corresponding lowering of the resultant's point of action after about five days of backfilling. Throughout the remainder of backfilling, the height of the resultant stayed between about 30 – 35% of the backfill height.

Table 4.1. Backfill height and lateral force on stem for selected times during backfilling.

Date	Time	Day	Backfill Height (ft)	Theoretical active lateral force (lb)	Lateral force on stem, from EPCs (lb)	Location of resultant (h/H)
28-Oct	5:00 AM	1	0	0	0	- -
28-Oct	5:00 PM	1	2	60	421	0.33
29-Oct	5:00 AM	2	2	60	222	0.33
29-Oct	5:00 PM	2	12	2148	6611	0.44
30-Oct	5:00 AM	3	12	2148	5189	0.37
30-Oct	5:00 PM	3	18	4832	8447	0.45
31-Oct	5:00 AM	4	18	4832	7598	0.43
31-Oct	5:00 PM	4	20	5966	10918	0.40
1-Nov	5:00 AM	5	20	5966	9846	0.39
1-Nov	5:00 PM	5	22	7219	- -	- -
3-Nov	5:00 PM	7	22	7219	6769	0.29
4-Nov	5:00 AM	8	22	7219	7723	0.31
4-Nov	5:00 PM	8	22	7219	7355	0.30

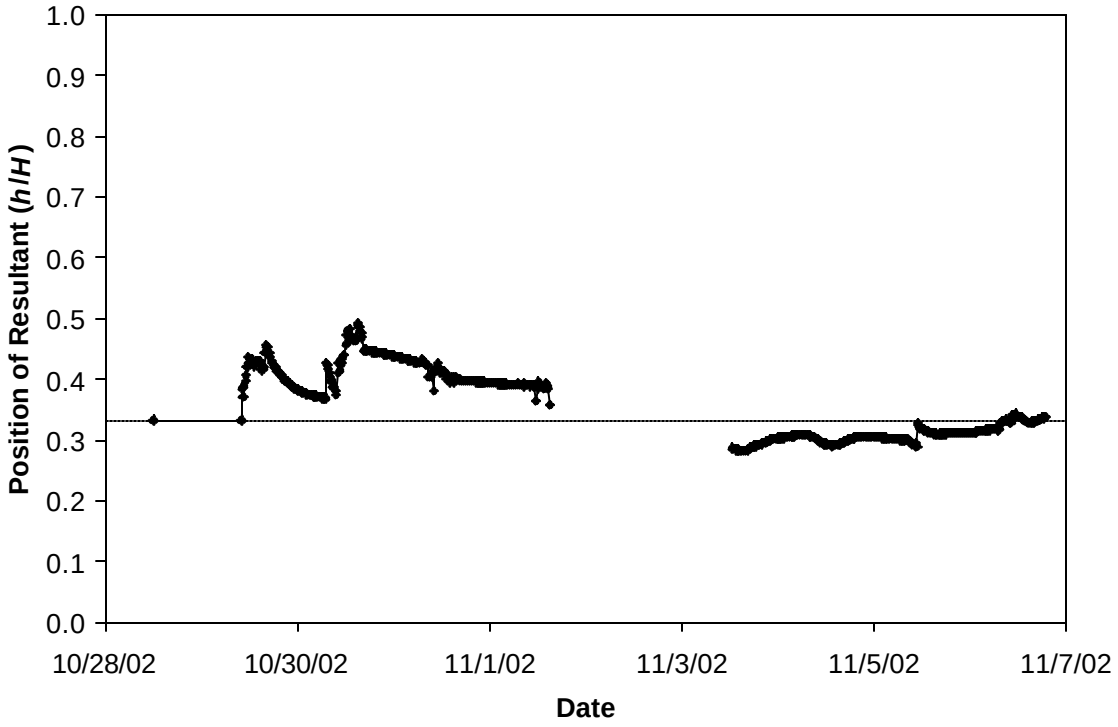

Figure 4.10. Ratio of the height of the resultant of lateral earth pressure to soil height during the early stages of backfilling.

When the backfill height reached 24 ft (7.3 m), the earth pressure distribution was much closer to the theoretical active distribution (Fig. 4.11). Although the EPC readings presented in Fig. 4.11 are for a moment in time at the end of the workday, the earth pressure distribution was essentially the same the following morning, unlike the earlier stages of backfilling. This was because relatively little soil had been placed and compacted the previous workday, so stresses within the soil had been mostly unaffected by those processes. The lateral force on the wall was 9480 lb, about 10% higher than the theoretical active force of 8591 lb.

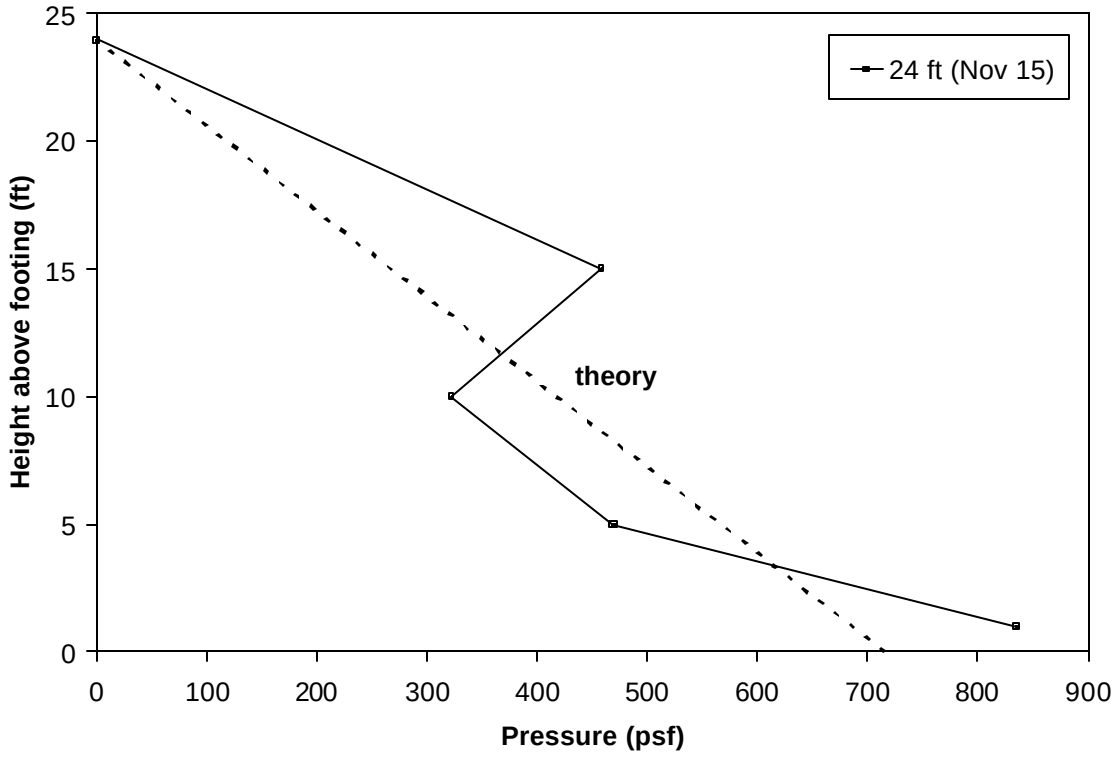

Figure 4.11. Comparison between theoretical active earth pressure and lateral earth pressure distribution for backfill height of 24 ft (7.3 m).

At the end of backfilling in late November 2002, the distribution of lateral earth pressure on the retaining wall stem was approximately bilinear in shape (Fig. 4.12). This general shape was similar to that found experimentally by Coyle et al. [5] and numerically by Goh [12]. Kulite EPC readings agreed fairly well with theoretical predictions of lateral stress based on active conditions. In fact, the values of earth pressure predicted using Rankine's theory were generally greater than the Kulite EPC measurements. This was likely because interface friction between the wall stem and the soil supported some of the soil's weight, thus reducing lateral earth pressure. However, Rankine's theory assumes a smooth wall, meaning there can be no force acting tangent to the soil-structure interface.

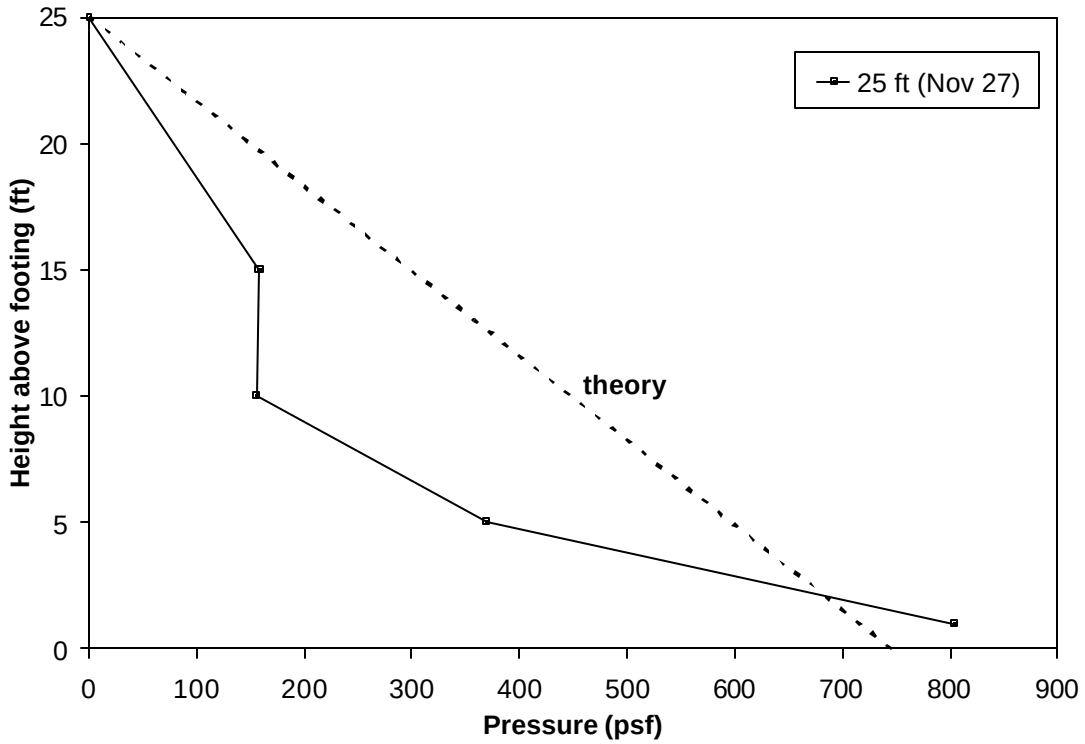

Figure 4.12. Comparison between theoretical active earth pressure and lateral earth pressure distribution at the end of backfilling (EPC readings represent average for day).

Rigid Body Rotation

The tiltmeter at the base of the stem showed that 0.03° of rigid body rotation into the backfill occurred as backfill was placed. Most of this had occurred by the time 23 ft (7.0 m) of backfill was placed. The footing rotation could also be used to find the differential settlement between the footing toe and heel, assuming the footing to be rigid. The differential settlement was thus found to be 0.08 in. (2 mm) between the toe and the heel (Fig. 4.13). Note that since more settlement occurred at the footing heel than at the toe, this corroborates the EPC readings from below the footing, which showed higher vertical stress below the heel than below the toe.

Inclinometer readings from within the footing also indicated rigid body rotation into the backfill, although 0.01° more rotation than Tilt_0. Recalling that the tiltmeters used in this study were more precise than the inclinometer probe, the reading from Tilt_0 was taken to be more accurate. Regardless, the important point is that the weight of the backfill on the footing heel caused rigid body rotation into the backfill.

Taken by itself, 0.03° of rigid body rotation would produce 0.16 in. (4 mm) of lateral movement at the top of the wall into the backfill. However, the displacement profile determined from tiltmeters showed that the effects of rigid body rotation and stem deflection essentially canceled each other in terms of net displacement (Fig. 4.14).

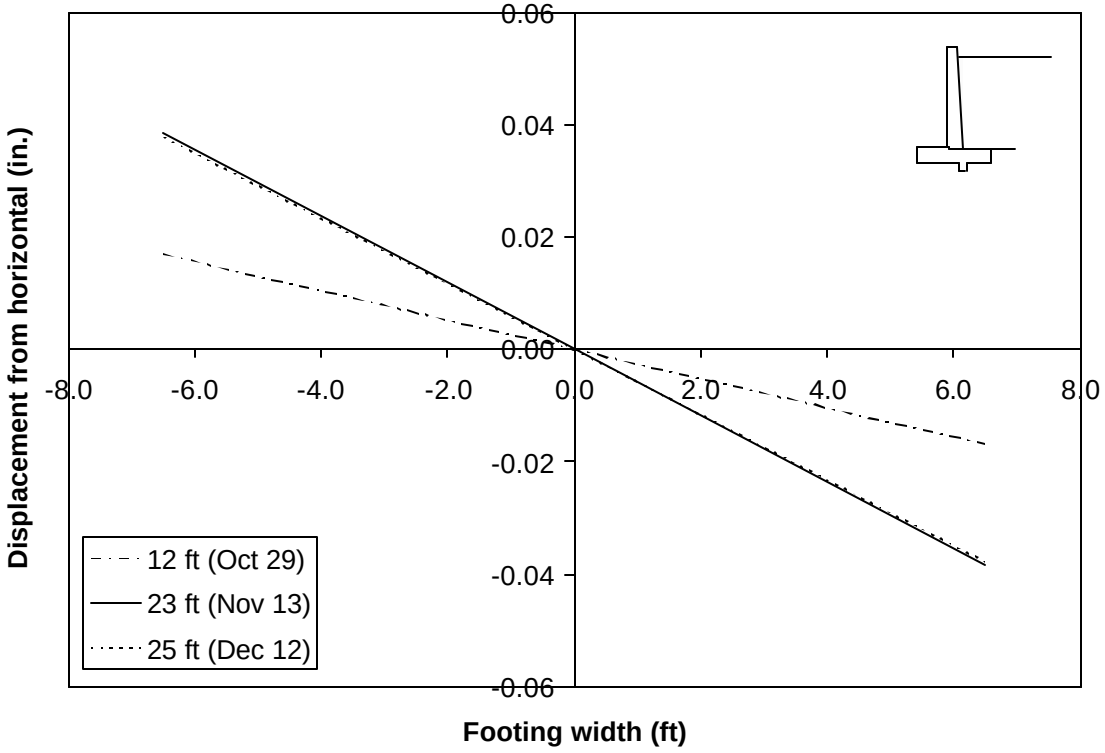

Figure 4.13. Rotation of footing, measured by tiltmeter at base of stem.

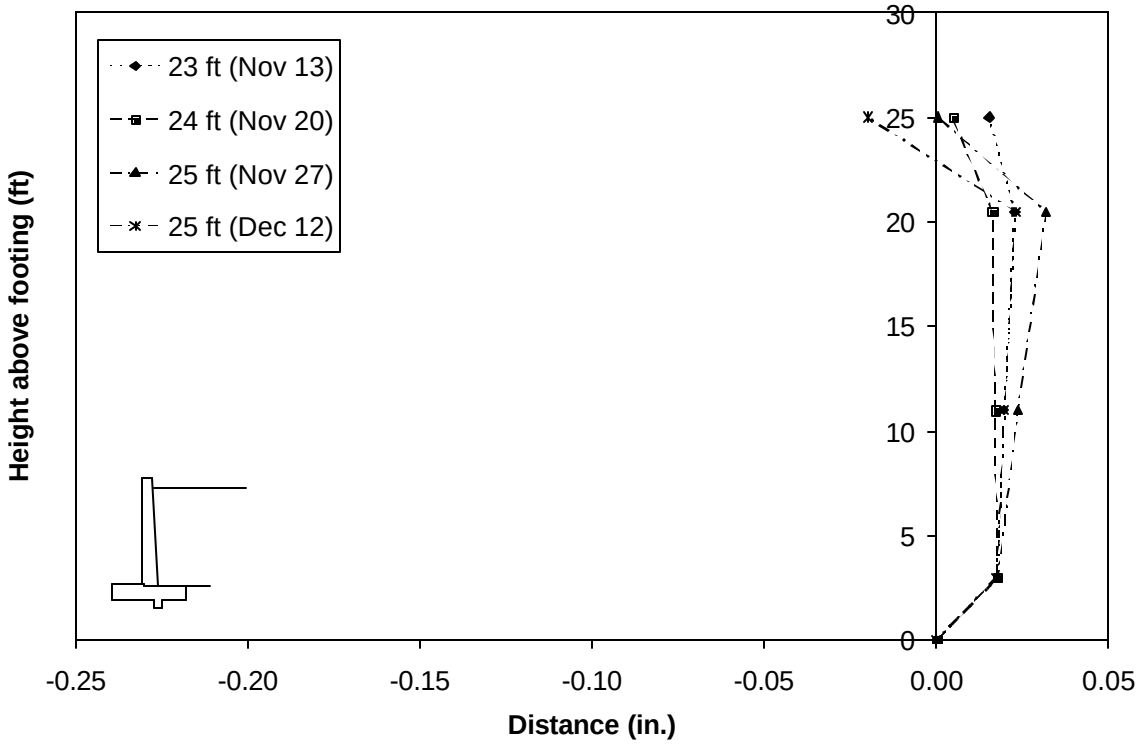

Figure 4.14. Stem displacement profile on selected dates, from tiltmeter measurements.

Elastic Deflection

Those tiltmeters on the stem, when referenced according to the rigid body rotation, showed the stem deflection, 0.16 in. (4.1 mm) at the top of the wall, to be near predicted values (Fig. 4.15). Note that the deflection was between that predicted using the theoretical active earth pressure loading (120 pcf and f = 37°) and that predicted using the EPC measurements. Also, recall that the effect of rigid body rotation at the top of the stem was a relative displacement of 0.16 in (4 mm) into the backfill. Hence the combined displacement due to rigid body rotation and stem deflection was essentially zero at the top of the wall.

Inclinometer readings were taken on the same days as total station measurements. One could readily observe a fair amount of scatter among the inclinometer readings. Recall that inclinometers were less accurate than tiltmeters. However, the magnitude of the displacements (and deflections) did corroborate the displacements from tiltmeter readings. Particularly, the deflection profiles were shaped the same (Fig. 4.16).

Stem deflections were predicted using engineering beam theory. A brief overview of the analysis and the computer code are included as Appendix D. The retaining wall was modeled as a cantilever beam with a clamped support. Euler-Bernoulli beam theory was assumed, using a Young's modulus of $3.6*10^6$ psi (25 GPa) for the concrete and a transformed section accounting for the steel reinforcement to calculate the moment of inertia [24]. For this purpose, the Young's modulus of steel was $29*10^6$ psi (200 GPa). The tapered stem was approximated as a piecewise constant beam (26 one-foot sections), with a piecewise constant distributed load (Fig. 4.17a, b).

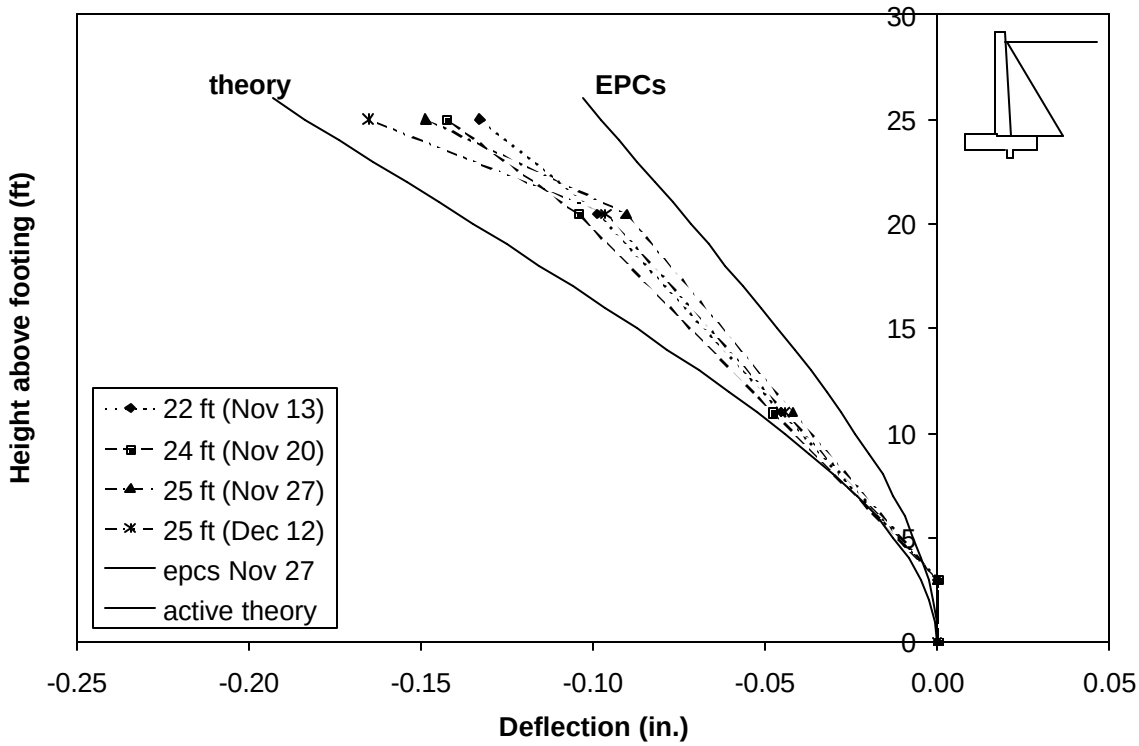

Figure 4.15. Stem deflection on selected dates, from tiltmeter measurements; the solid curves were calculated from the assumed loadings.

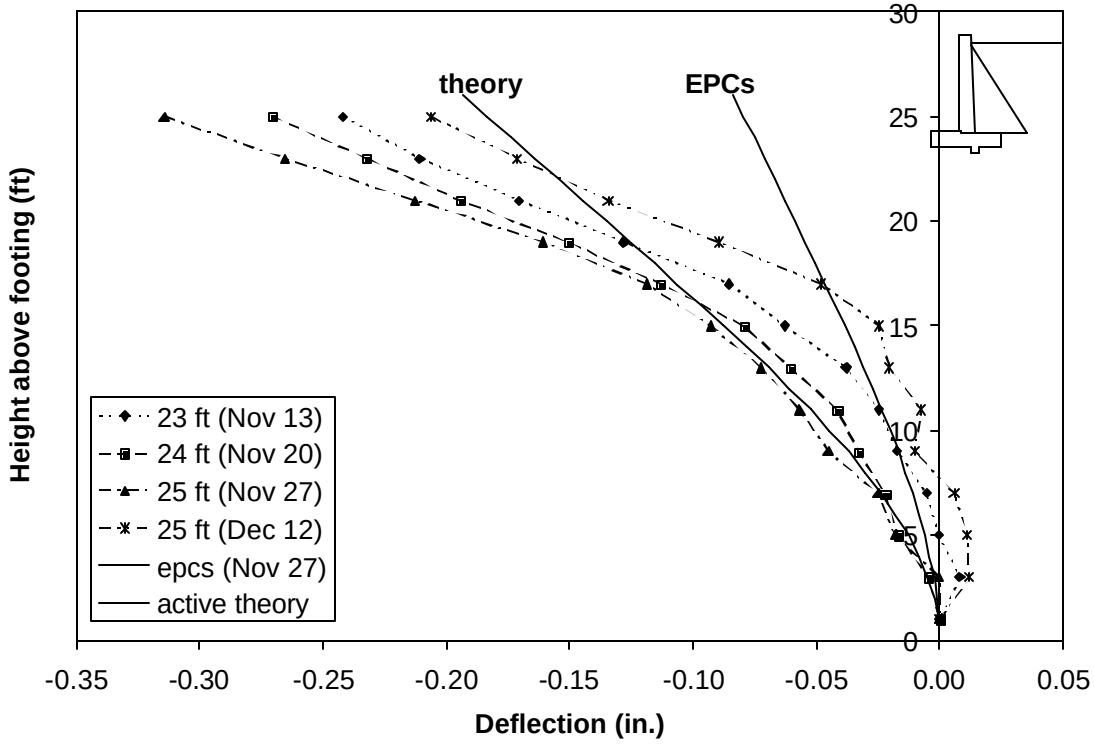

Figure 4.16. Stem deflection on selected dates, from inclinometer measurements; the solid curves were calculated from the assumed loadings.

A theoretical earth pressure distribution was obtained by assuming a friction angle of 37°, a unit weight of 120 pcf (18.9 kN/m^3), and active pressure. Deflections were calculated for both the theoretical lateral earth pressure distribution and for the EPC-measured earth pressure distribution. Linear interpolation was used to estimate the earth pressure distribution between EPCs. The observed deflections from the tiltmeters fell between these two predictions, as shown previously (Fig. 4.15).

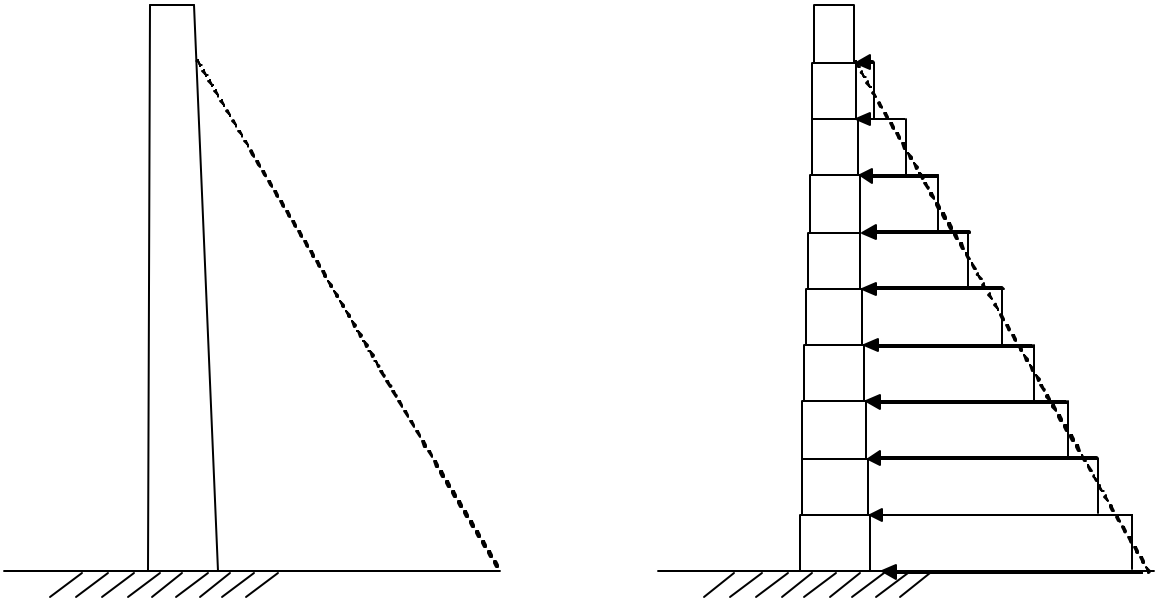

Figure 4.17. (a) Theoretical loading on retaining wall. (b) Approximated cross-section of retaining wall with piecewise constant distributed load.

Rigid Body Translation

Total station measurements indicated 0.46 in. (11.7 mm) of horizontal movement for the retaining wall at the end of backfilling (Fig. 4.18). Subtracting the effects of rigid body rotation and stem deflection, as measured by the tiltmeters, showed the horizontal rigid body translation to be 0.45 in. (11.4 mm), almost identical to the total horizontal movement. This was because the net effect of footing rotation and stem deflection was almost no absolute displacement. Thus, almost all wall displacement measured with the total station was due to translation.

Note that when 12 ft (3.7 m) of backfill had been placed, almost no translation had occurred (Fig. 4.19). Most translation took place when the final half of the backfill was placed. Translation of the wall also coincided with EPC readings showing increased lateral pressure on the face of the toe, in front of the wall (Fig 4.20). This indicated at least the partial development of passive earth pressure. Between the start and end of backfilling, the entire wall also moved downward 0.42 in. (10.7 mm).

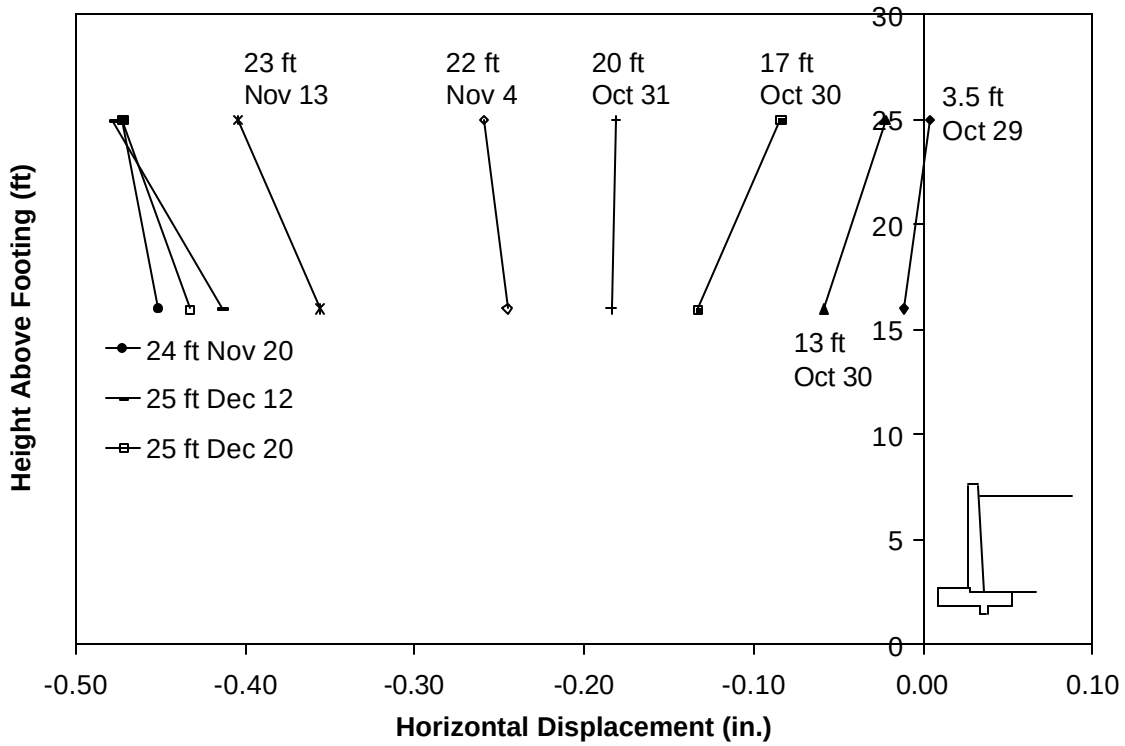

Figure 4.18. Total station measurements of horizontal movement at survey points.

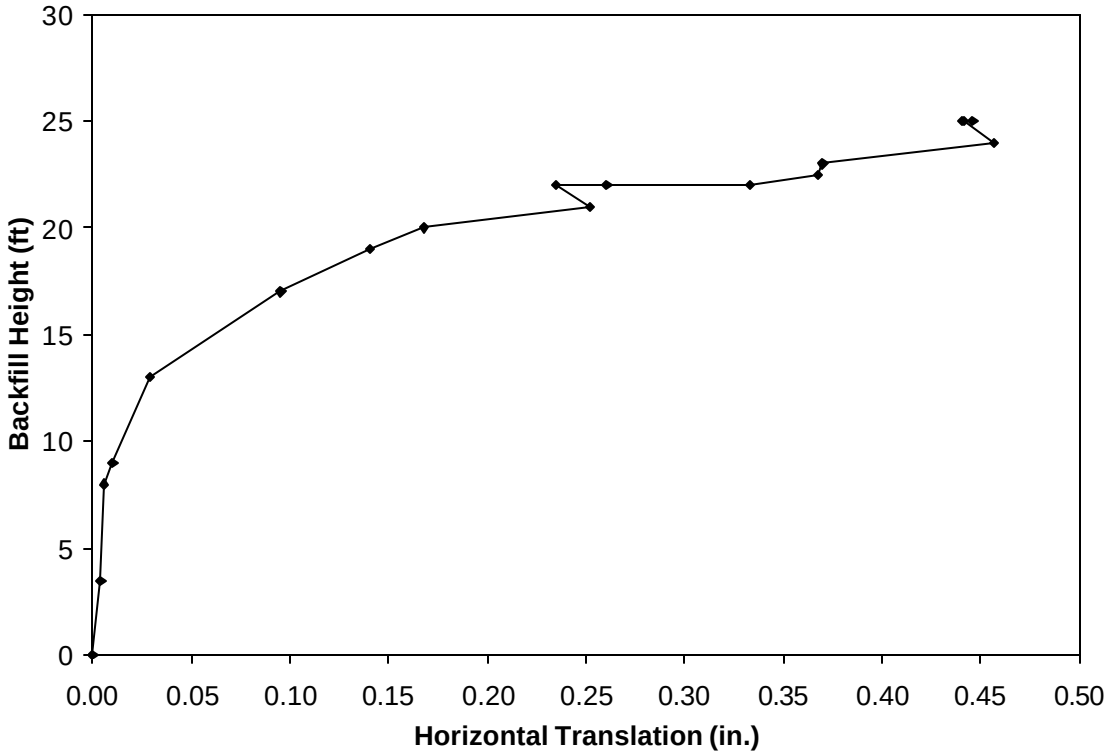

Figure 4.19. Height of backfill behind Panel BJ versus horizontal wall translation (average of all survey points).

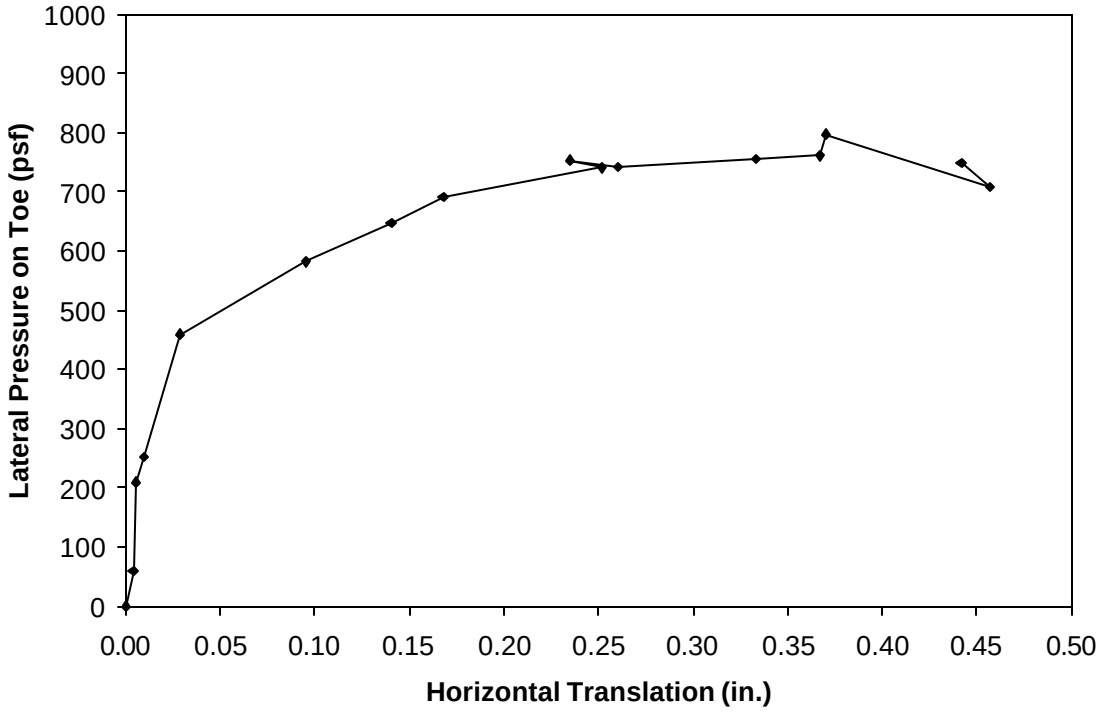

Figure 4.20. Increased lateral pressure at footing toe with horizontal translation (average of all survey points).

Table 4.2 lists the backfill heights and horizontal translation values plotted in Fig. 4.19, as well as the date, time, and the lateral force on the stem corresponding to when each reading was taken. The translation values were obtained by averaging the measurements for the four total station survey points and subtracting the tiltmeter readings. It is evident from Table 4.2 and Fig. 4.19 that translation of the wall was responsible for development of the active condition and reduction of the total lateral force on the stem. If the readings from November 4 are considered, it can be seen that the measured force and the theoretical active force agreed. The horizontal translation was 0.235 in. (6.0 mm), while the backfill height was 22 ft (6.7 m). This gives a displacement to soil height ratio of about 0.1%, which agrees with Terzaghi's finding for the movement necessary to bring about the active condition [4]. The lateral earth pressure coefficient, which is essentially the force on the stem, normalized by the integrated vertical stress, is plotted against the ratio of the wall translation to the backfill height in Fig. 4.21. Only readings from early in the morning were plotted, so as to reduce secondary effects from the backfilling process (i.e. compaction, vibration, movement of machinery, etc.). This plot also shows that a displacement to soil height ratio of about 0.1% was necessary for development of the active condition.

Table 4.2. Backfill height, horizontal wall translation, and lateral force on stem for selected times during backfilling.

Date	Time	Day	Backfill Height (ft)	Translation (in.)	Lateral force on stem, from EPCs (lb)	Theoretical active lateral force (lb)
28-Oct	11:00 AM	1	0	0.000	0	0
29-Oct	9:20 AM	2	3.5	0.004	572	183
29-Oct	11:55 AM	2	8	0.005	5006	955
29-Oct	2:40 PM	2	9	0.010	5118	1208
30-Oct	9:00 AM	3	13	0.029	7083	2521
30-Oct	2:25 PM	3	17	0.095	8035	4310
31-Oct	8:30 AM	4	19	0.140	8121	5384
31-Oct	12:10 PM	4	20	0.168	10485	5966
1-Nov	2:35 PM	5	21	0.252	10105	6578
4-Nov	10:55 AM	8	22	0.235	7157	7219
5-Nov	11:00 AM	9	22	0.260	7887	7219
7-Nov	10:55 AM	11	22	0.333	7838	7219
9-Nov	11:45 AM	13	22.5	0.367	8927	7551
13-Nov	11:20 AM	17	23	0.370	9743	7890
20-Nov	9:50 AM	24	24	0.457	7221	8591
27-Nov	11:20 AM	31	25	0.442	6411	9322
12-Dec	9:05 AM	46	25	0.441	5114	9322
20-Dec	11:10 AM	54	25	0.446	5344	9322

Note from the data in Table 4.2 that the maximum lateral force on the stem, as determined from the EPCs, did not occur when the backfill height was maximum. Rather, it occurred when 20 ft (6.1 m) of backfill had been placed. This was likely due to compaction-induced lateral stresses on the wall, which is discussed further in Section 5.1.3. The force on the stem was still less than the value of 11,500 lb (50.9 kN) calculated using Mn/DOT's design assumption of f = 35° and g = 125 pcf (19.6 kN/m^3) for a 26 ft (7.92 m) wall.

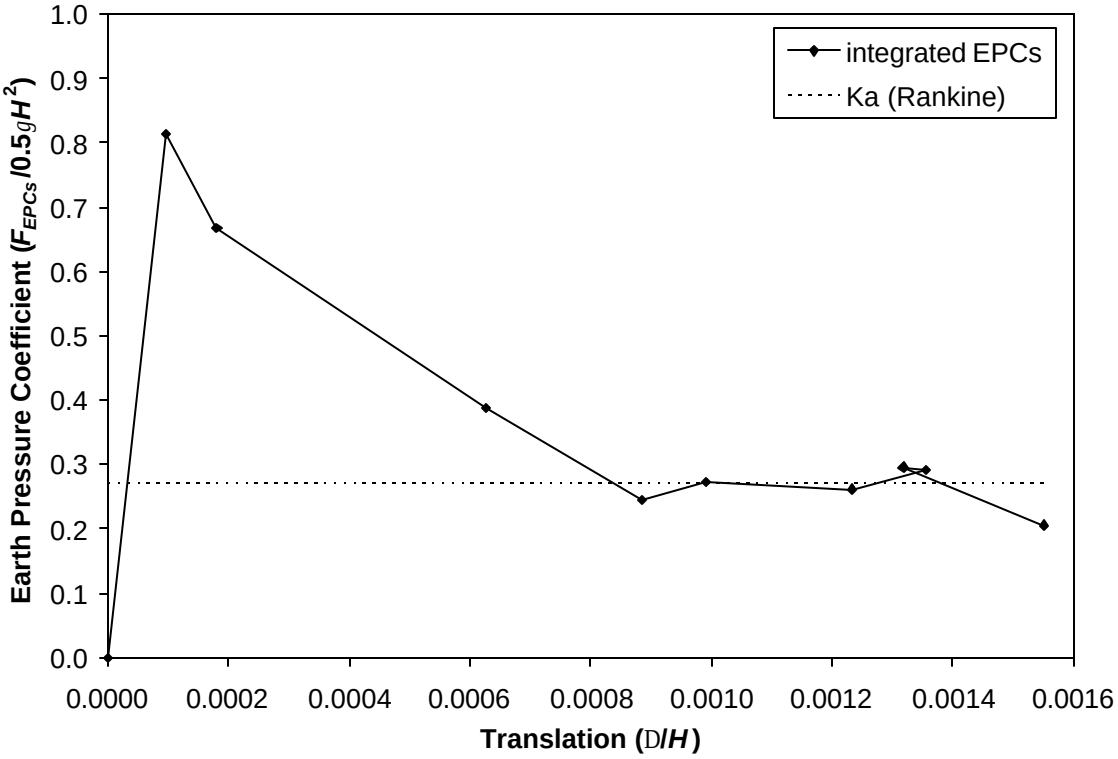

Figure 4.21. Change in normalized force on stem with wall translation.

Strain Gage Measurements

Meaningful readings could not be obtained from the strain gages on the reinforcing bars within Panel BJ. Interference in the signal produced noise levels in excess of the expected signal. Thus, strains in the steel reinforcement were unknown during the backfilling of Panel BJ.

As a result, ten foil strain gages were installed in June 2003 on the reinforcing bars anchoring the stem of Panel E to the footing. (Recall that Panel E also matched the selection criteria.) Two pairs of gages were attached to the compression reinforcement near the front face, and three pairs of gages were attached to the tensile reinforcement near the back face of the stem. The gages were approximately 6 in. (152 mm) up from the interface between the footing and the stem. These were installed in a similar manner as before but were read using a strain indicator with a ten-channel switch-and-balance unit; the unit was housed in a protective enclosure and left connected for ten days while strain readings were taken manually.

Panel E Strain Readings

Strain gage readings were taken six days after the stem was poured; these were used as the zero readings. Backfilling of this section of the retaining wall began the next day, and readings were taken at the end of the first day, with the backfill up to two feet. Readings were taken in the morning and late afternoon during the construction workday for backfilling. Though backfilling was completed after a week, strain readings were taken the next two mornings after backfilling had ended.

Qualitatively, the curves showing the compressive and tension strains increased with backfill height (Fig. 4.22). One of the gages on the tension rebar gave erroneous readings and was impossible to balance within the Wheatstone bridge. Nine of the gages, however, gave reasonable readings of strain. A heavy, dashed line shows the compressive strains predicted using the theoretical active earth pressure distribution. This curve is cubic, since the strain e at a distance y from the neutral axis is directly proportional to the moment M acting on the stem, and the moment is proportional to the cube of the backfill height h, assuming a uniform unit weight g and friction angle f:

$$e = \frac{s}{E} = \frac{1}{E}\frac{My}{I} \tag{4.1}$$

$$M = \frac{1}{6}h^3 g K_a = \frac{1}{6}h^3 g \frac{1-\sin f}{1+\sin f} \tag{4.2}$$

where E is the Young's modulus of the concrete and I is the moment of inertia of the section. Hence, the equation of the expected strains is given by

$$e = \frac{yh^3 g}{6EI}\left(\frac{1-\sin f}{1+\sin f}\right) \tag{4.3}$$

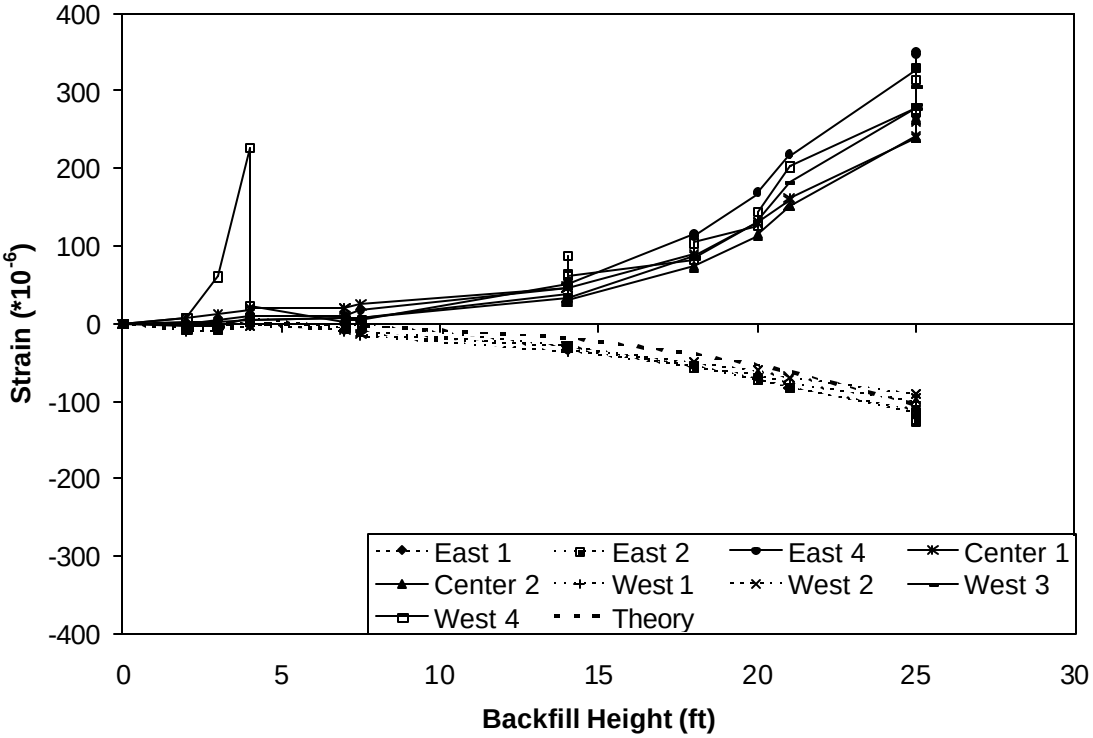

Figure 4.22. Strain gage readings from reinforcing bars within the stem of Panel E. (Solid lines indicate tensile strains; dashed lines indicate compressive strains.)

Back-calculation of Loading

For an assumed elastic response of the wall, the load could be back-calculated from strain measurements. As before, the retaining wall was modeled as a cantilever beam with a clamped support; the stem was approximated as a piecewise constant beam. The same material parameters were assumed, and the transformed section method was used to account for the steel reinforcement. Using the strains measured on the compression reinforcing bars of Panel E, the distributed load from lateral earth pressure was back-calculated to be 29 psf/ft (4.6 kPa/m). This loading corresponded approximately to active lateral earth pressure. Assuming a unit weight of 120 pcf (18.9 kN/m^3) and the active condition, the soil's angle of internal friction was back-calculated to be 37.5°. This compared well with the value of 37° used for estimating the loading and deflections of panel BJ.

"Jointed" Section

The strain gage readings from Panel E revealed a striking trend: the strain gages on the tension reinforcement gave readings that were two to three times the magnitude of the readings from gages on the compression reinforcement. Upon completion of backfilling, the median value of the tensile strains was $295*10^{-6}$ while the median value of the compressive strains was $108*10^{-6}$. Assuming a linear distribution of strains, this disparity in final readings suggested that the neutral axis of the stem was 9.22 in. (234 mm) from the front face. This is considerably closer to the

front face than the back face of the wall for the 31 in. (787 mm) thick cross-section at the base of the stem.

Performing a transformed-section analysis of the concrete and rebar put the neutral axis very near the centroid of the cross-section (Fig. 4.23a, b). However, assuming that a certain portion of the concrete in the tension zone has an effective Young's modulus of zero (i.e. a portion of the section acted as a joint), it was possible to adjust the location of the neutral axis to match that determined from strain readings (Fig. 4.23c) if the thickness of the concrete that was effectively acting in tension was 6.06 in. (154 mm). The forces in the reinforcing bars and the stress distribution in the concrete are shown for the jointed section (Fig. 4.24).

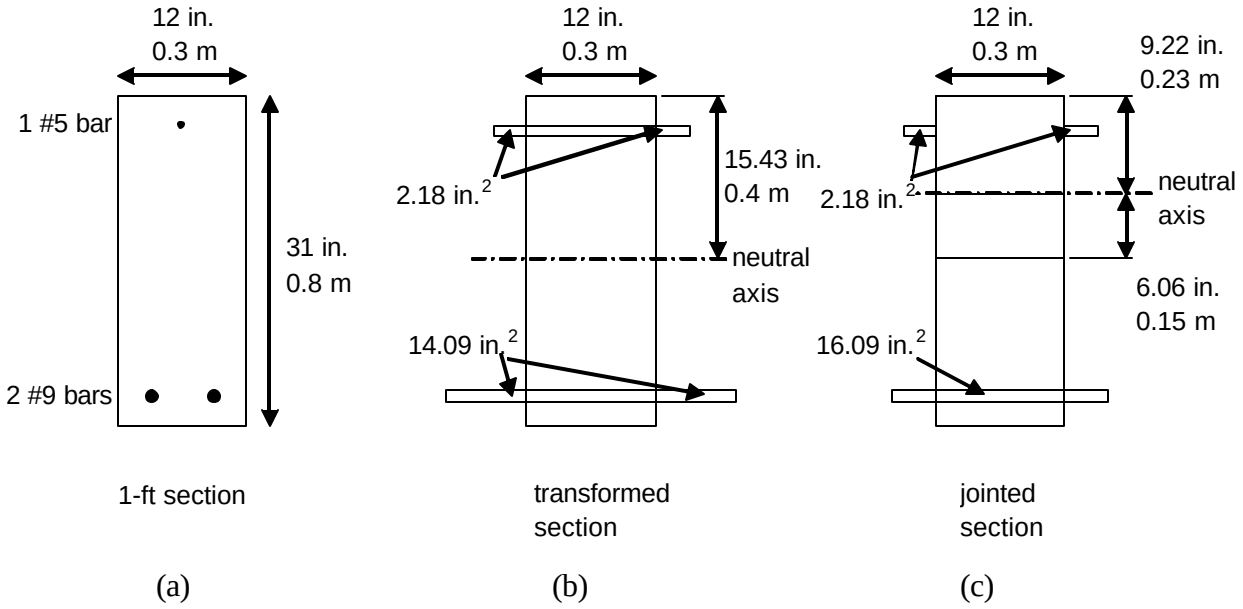

Figure 4.23. Cross-section of retaining wall at base of stem.

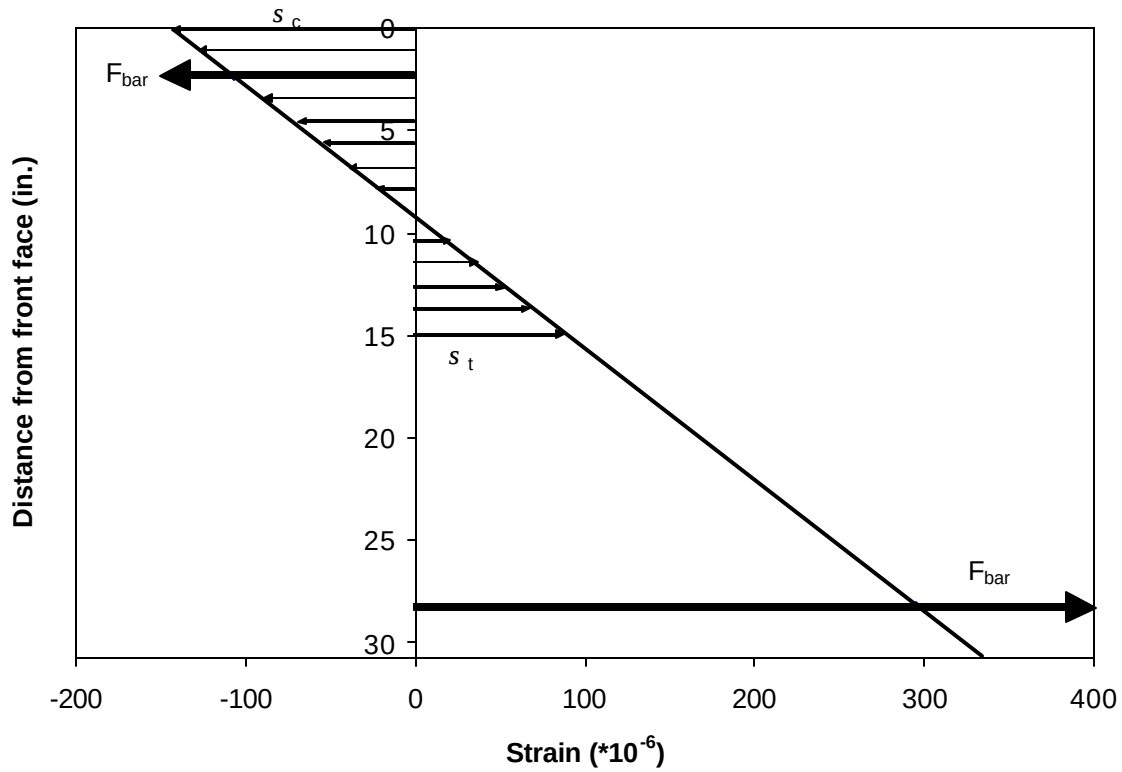

Figure 4.24. Forces in reinforcing bars and stress distribution in concrete for jointed section.

One way to think of this section is that a joint acts at the interface between the footing and the stem. This does not imply that any separation occurred between the footing and the stem, however, since the strains recorded did not include the compressive strains due to the self-weight of the vertical stem.

Load Test

Two trucks were parked end to end, centered on Panel BJ but extending partially onto the adjacent panels (Fig. 4.25). Their combined weight was about 90,000 lb (400 kN) over an area of about 400 ft^2 (37 m^2). Strain gages were read with strain indicators and switch-and-balance units. Inclinometer readings and total station measurements were taken before, during, and after the load was applied. EPC and tiltmeter readings were recorded almost continuously (every 5 min). The total movement of the wall was very small, below the 0.08-in. (2-mm) resolution of the total station, although the weight of the trucks was observed in the readings of EPCs under the footing.

Figure 4.25. View towards front face of retaining wall during load test.

In fact, the change in vertical stress registered by EPC_back could be predicted using the Boussinesq solution of stress distribution in a linearly elastic half-space [23]. For a point load at the surface of an elastic half-space (Fig. 4.26), the solution for the vertical stress increase at any point $Q(x, y, z)$ within the half-space is

$$\Delta s_z = \frac{P}{z^2}\left\{\frac{3}{2p}\left[\left(\frac{r}{z}\right)^2 + 1\right]^{-\frac{5}{2}}\right\} \tag{4.4}$$

where P is the applied force, z is the depth of the point Q, and r is the radius from the origin to a point on the surface directly above Q.

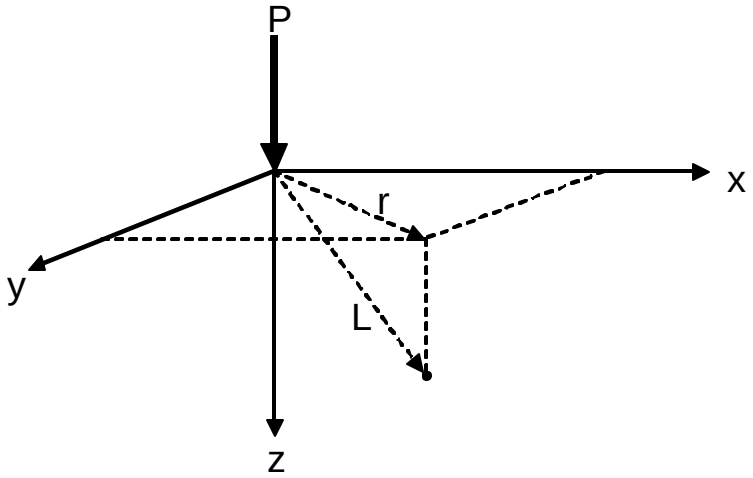

Figure 4.26. Point load at the surface of an elastic half-space.

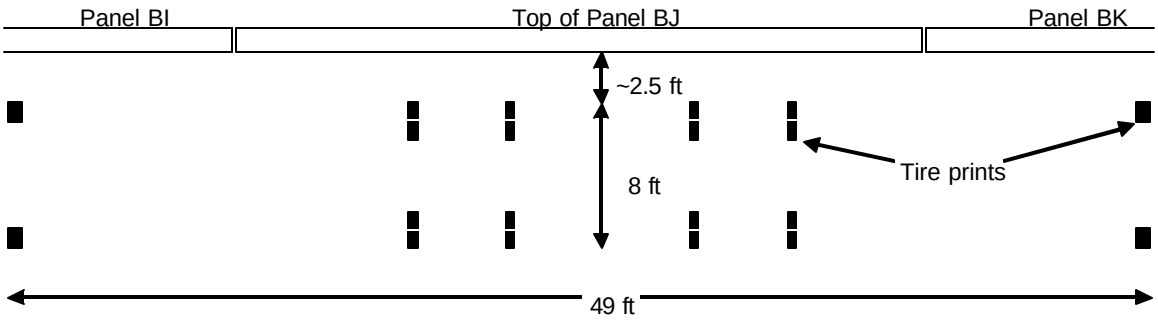

Figure 4.27. Wheel pattern of trucks parked on backfill during load test.

The loading pattern of the trucks' wheels is given in Fig. 4.27. One-sixth of a truck's weight was assumed to act as a point load at the center of each of its six tire prints (counting dual tires as one), and superposition was used to find the total increase in vertical stress at the depth of the footing due to the two trucks.

Indeed, the change in vertical stress registered by EPC_back (30 psf, or 1.4 kPa) matched the vertical stress increase due to point loads at the trucks' wheels predicted by the Boussinesq solution. Furthermore, it was obvious from the increase registered by the EPCs under the footing when the trucks were parked above the wall and likewise from the decrease in stress when they were removed (Fig. 4.28). However, lateral EPC readings for the stem actually decreased when the load was applied and increased when it was removed (Fig. 4.29). A similar phenomenon was observed by Duncan and Seed [16] during application of point loads at the soil surface behind a retaining wall. It should also be noted that only the immediate changes in EPC readings pertain to the load test. The gradual changes with time were due to temperature effects and are discussed in Section 5.2.

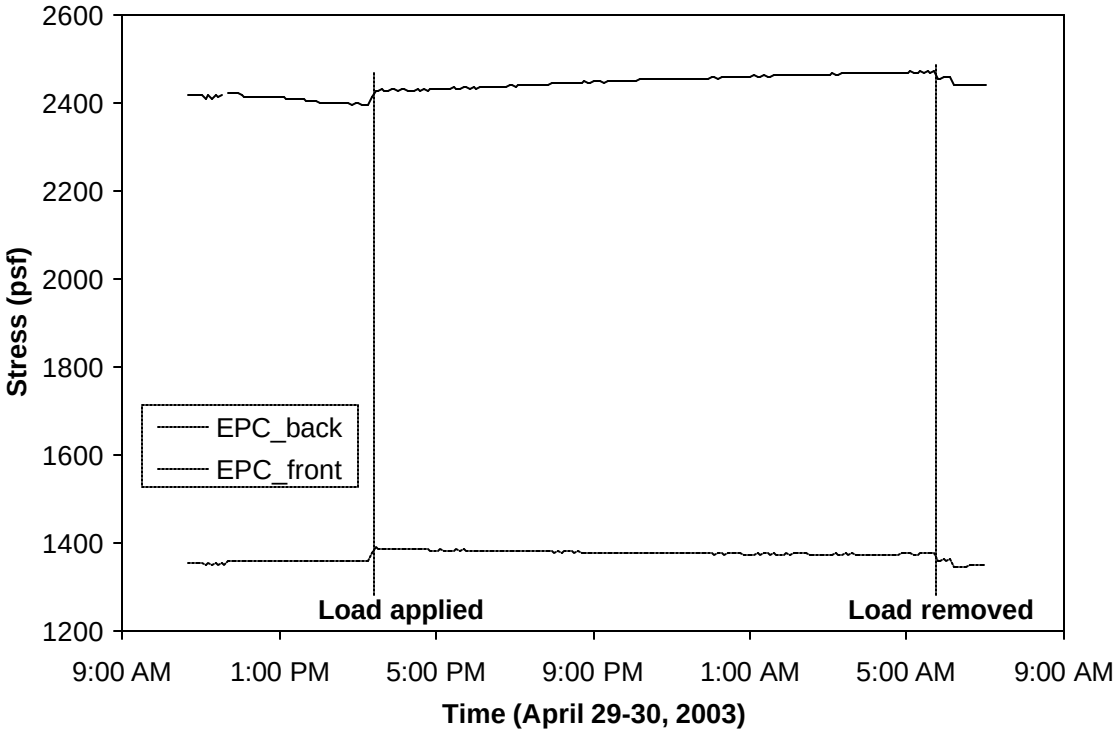

Figure 4.28. Change in vertical soil stress below footing during load test.

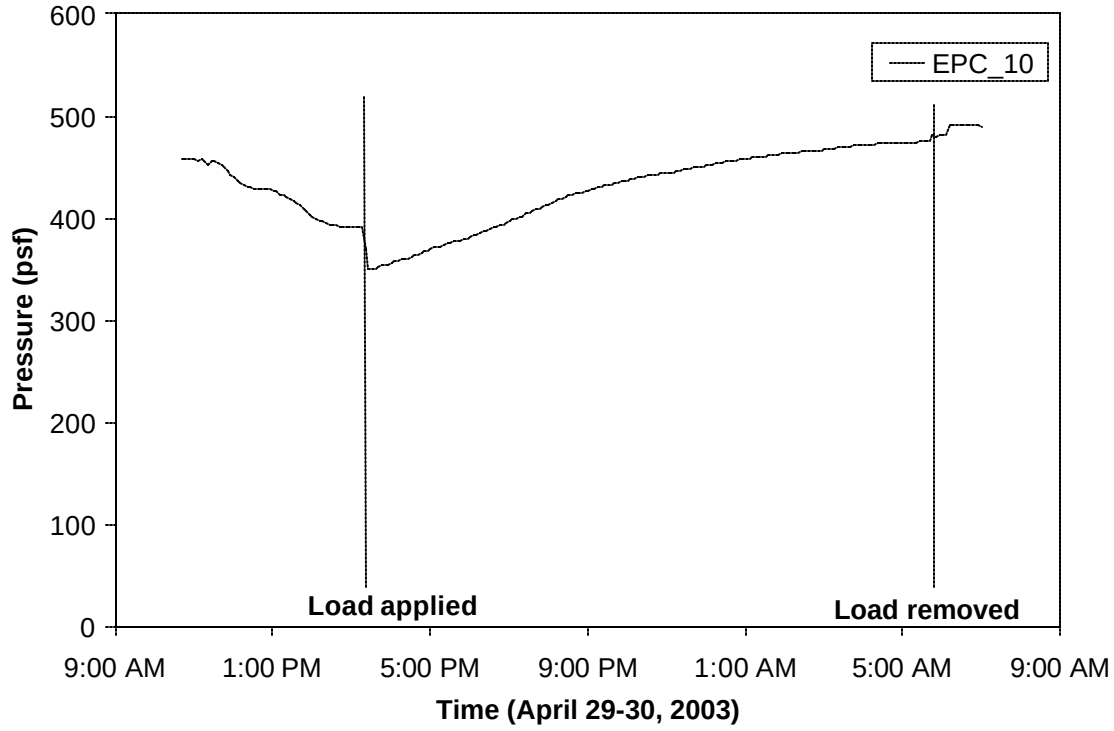

Figure 4.29. Example of change in stem EPC readings during load test.

An explanation for this decrease in stem EPC readings upon loading is that the lateral pressure increase on the wall was greatest near the applied load at the surface but quite small at the depths of the EPCs. Spangler [25] performed experiments showing that the lateral pressure increase on a retaining wall due to surface loads may be predicted by the Boussinesq solution, at least in a qualitative sense. For a point load at the surface of an elastic half-space, the solution for the lateral stress increase at any point $Q(x, y, z)$ within the half-space is

$$\Delta s_x = \frac{P}{2p}\left\{\frac{3x^2 z}{L^5} - (1-2n)\left[\frac{x^2 - y^2}{Lr^2(L+z)} + \frac{y^2 z}{L^3 r^2}\right]\right\} \tag{4.5}$$

where x, y, z are coordinates of the point Q relative to the origin set at the point load, L is the length from the origin to the point Q, P is the applied force, and n is the Poisson's ratio of the medium. A value of 0.33 was taken for Poisson's ratio n.

Again, the weight of the trucks was taken to be evenly distributed over the tires, and a point load was assumed to act at the location of each tire. While the assumed distribution of the truck's weight over its tires may affect the distribution of the stress increase on the wall, the emphasis for this analysis was placed upon the qualitative nature of the distribution.

Fig. 4.30 shows how the theoretical lateral stress increase was distributed on the wall. Notice how the majority of the effect was within 10 ft (3.0 m) of the surface. All EPCs were at least this depth below the surface. Therefore, it is thought that upon application of the load, the wall's deflection away from the soil had a greater effect on the EPCs than the surface load had. The movement of the wall away from the backfill must have decreased the lateral earth pressure on the EPCs. When the trucks were removed, the wall moved slightly into the backfill, and the stem EPCs increased by about the same magnitude as the earlier decrease.

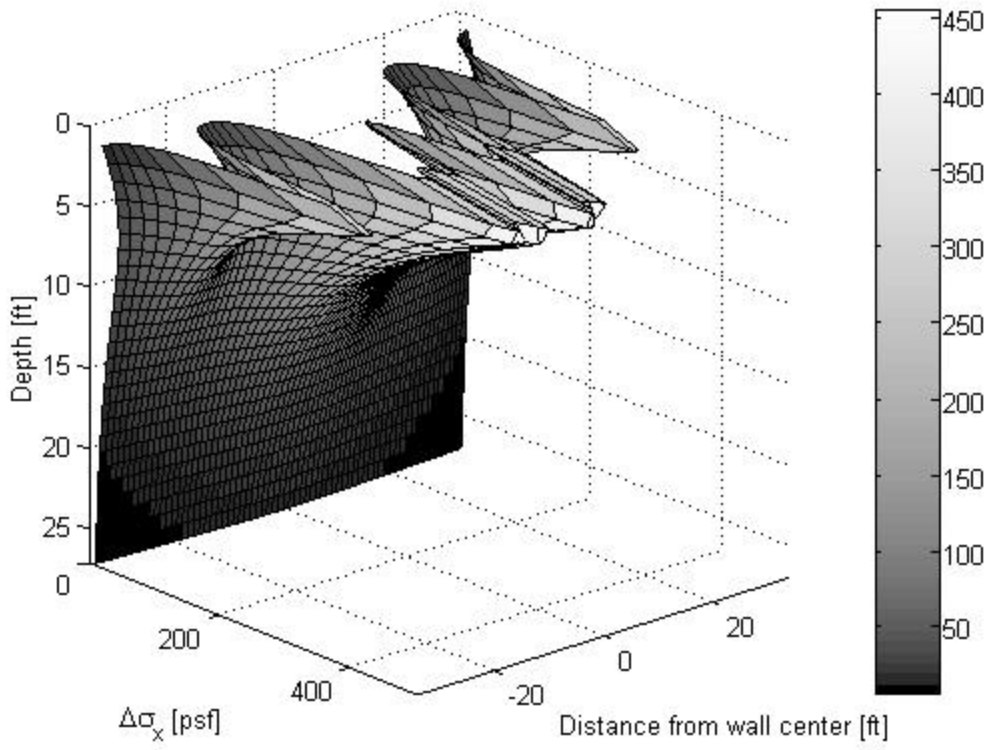

Figure 4.30. Theoretical distribution of lateral stress increase on wall due to load test.

Chapter 5
Interpretation

Continuous reading of sensors yielded vast amounts of data for examination and interpretation. (Readings from the Kulite stem EPCs and the tiltmeters through July 2003 are included as Appendix E). For example, the immediate response by EPCs and tiltmeters to placement of backfill, the evolution of the earth pressure distribution, and the changing stem deflection profile during backfilling were observed. Data from backfilling were interpreted as showing the effects of compaction. Long-term monitoring of sensors showed that earth pressure and stem deflection were affected by daily changes in air temperature and precipitation. Data from the EPCs could also be used to assess the effectiveness of the wall's design.

Backfilling Process

Numerous jumps and drops in the data from EPCs and tiltmeters were directly attributable to backfilling activities such as dumping of soil, movement of equipment, and vibratory compaction. Furthermore, the earth pressure distribution at the end of the construction workday was often quite different from the distribution the following morning. Evidence was also found for relatively large residual stresses due to compaction, which was achieved with smooth-wheel vibratory rollers.

Observations during the Workday

The readings from October 30, 2002, the third day of backfilling behind Panel BJ, exemplify the changes in readings from EPCs and tiltmeters during the construction workday. These display the evolution of the pressure distribution and displacements, as well as insight into how wall displacements and earth pressure affected each other.

Consider the earth pressure cell readings. EPC_10 increased suddenly just after 7:00 on this day, while EPC_1 dropped (Fig. 5.1). EPC_1 and EPC_5 increased until 10:00, while EPC_10 decreased slightly. These changes in the EPC readings were probably due to backfilling activities (e.g. dumping fill, vibratory compaction, and movement of heavy machinery), since EPC_back increased steadily during the day, and the backfill height could be directly determined from EPC_back (Fig. 5.1). Assuming that a load of sand was placed behind Panel BJ at 10:00, it would have caused wall movement away from the backfill, which could account for the decreased pressure in EPC_1 and EPC_5 at this time. This would also explain the jump in EPC_10 at 10:00. Since the backfill height was about 14 ft (4.3 m) at this time, EPC_10 would experience a significant stress increase due to the dumping of a load of fill above it.

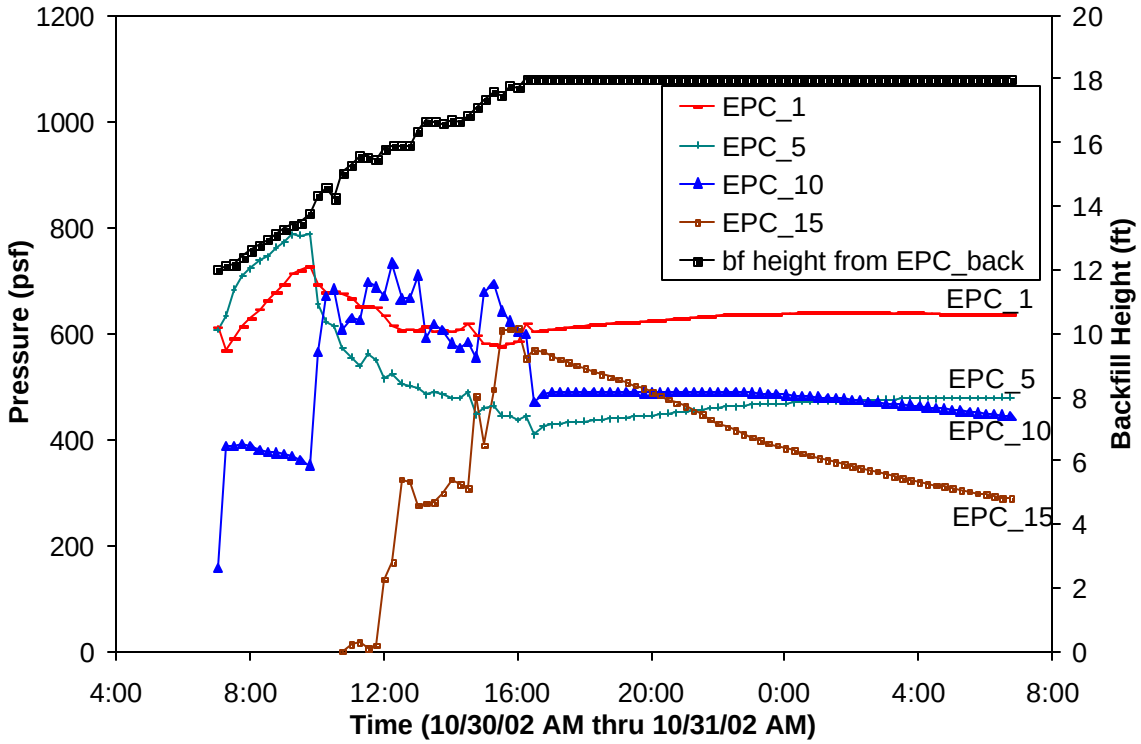

Figure 5.1. EPC and backfill heights during the third day of backfilling.

EPC_15 began registering pressure at noon, since the backfill level reached 15 ft (4.6 m) at that time (Fig. 5.1). It increased erratically thereafter during the workday, eventually registering higher pressure than any other stem EPC at 16:00. This may have been due to residual stresses from the compaction process.

Earth pressure distributions from selected times during the day show that the earth pressure was rather variable and not uniform in shape (Fig. 5.2). The reason for the variability was probably the ongoing backfilling process, which both increased the height of the backfill and compacted the soil.

(a)

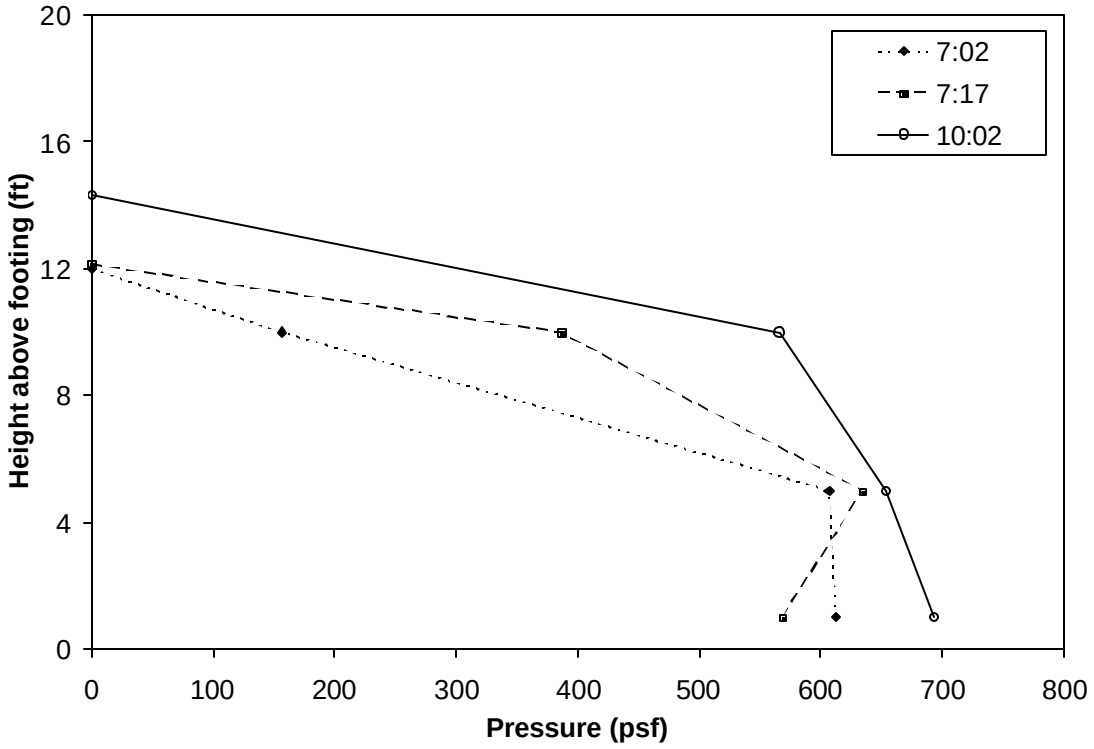

(b)

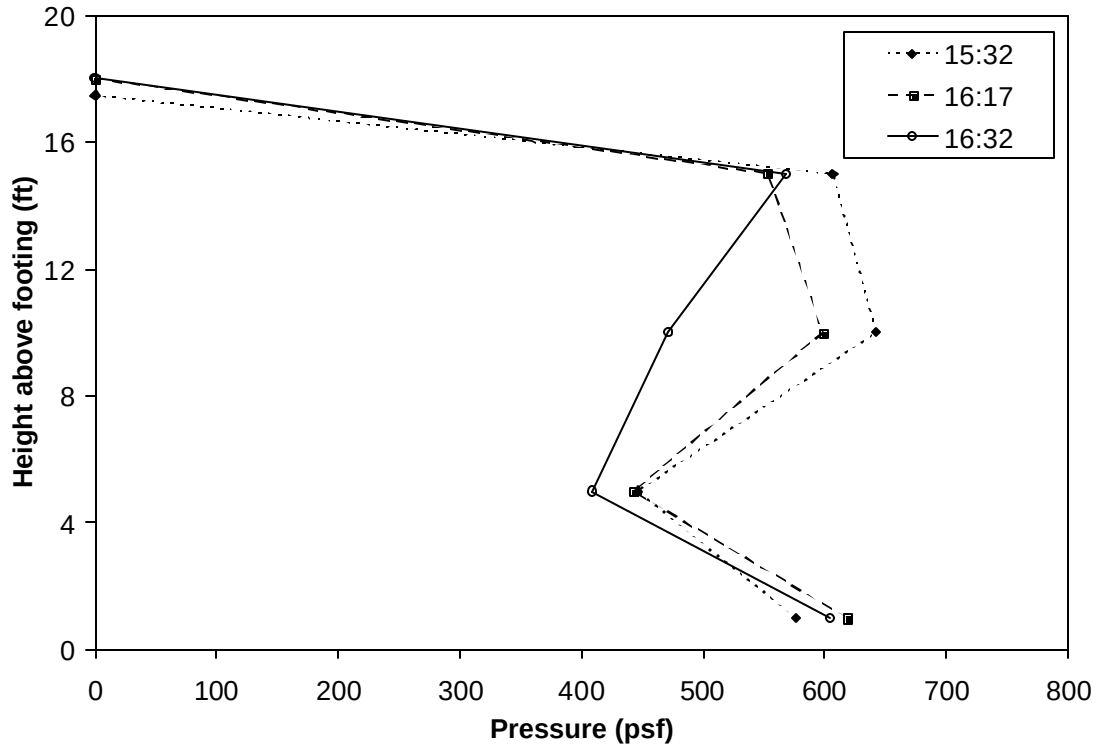

Figure 5.2. Earth pressure distribution at selected times during the third day of backfilling: (a) during the morning and (b) during the afternoon.

It is evident from Fig. 5.1 that EPC_1 and EPC_5 increased overnight, while EPC_10 and EPC_15 decreased overnight. Thus, the lateral soil pressure apparently redistributed somewhat between the end of this workday and the start of the next. This may have been due to wall movement away from the backfill. As illustrated in Fig 5.3, total station measurements showed that the wall displaced 0.06 in. (1.5 mm) away from the backfill from 9:00 to 14:25 and displaced again overnight, more so at 25 ft (7.6 m) than at 16 ft (4.9 m). This indicated horizontal translation of the wall, as well as somewhat increased deflection of the stem, during this time. Such motion allowed the active condition to begin developing within the backfill.

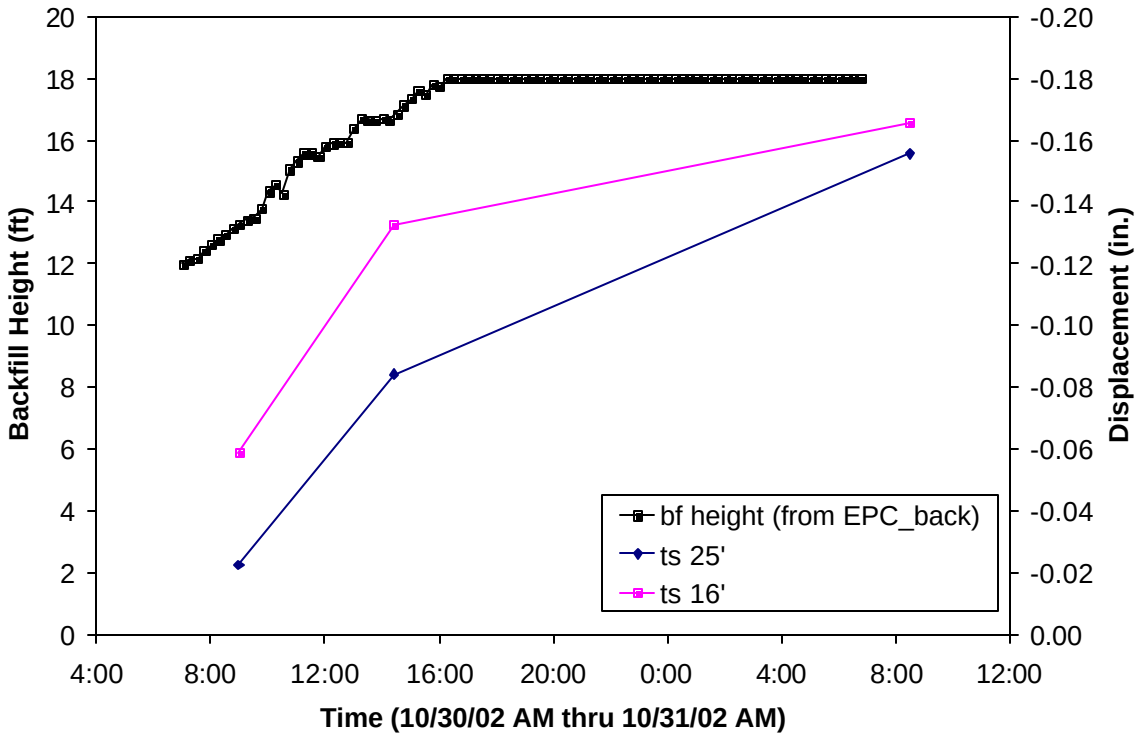

Figure 5.3. Total station measurements and backfill height during the third day of backfilling. (Note that negative displacement indicates displacement *away* from the backfill.)

Redistribution of Stresses

It was observed during backfilling that EPCs near the upper lifts of backfill tended to decrease overnight while EPCs at the bottom of the stem increased overnight (Figs. 5.4 and 5.5). Two mechanisms may have been involved. First, total station measurements showed that the wall moved away from the backfill overnight, thus allowing mobilization of the soil's strength and decreasing lateral earth pressure toward the active state in recently placed layers of soil (i.e. at the top of the wall). Second, since lateral pressure at EPC_1 and EPC_5 at the bottom of the stem increased overnight when the height of backfill was constant, it suggests that stresses within the soil redistributed somewhat. Movement of the wall could have facilitated this redistribution of stresses.

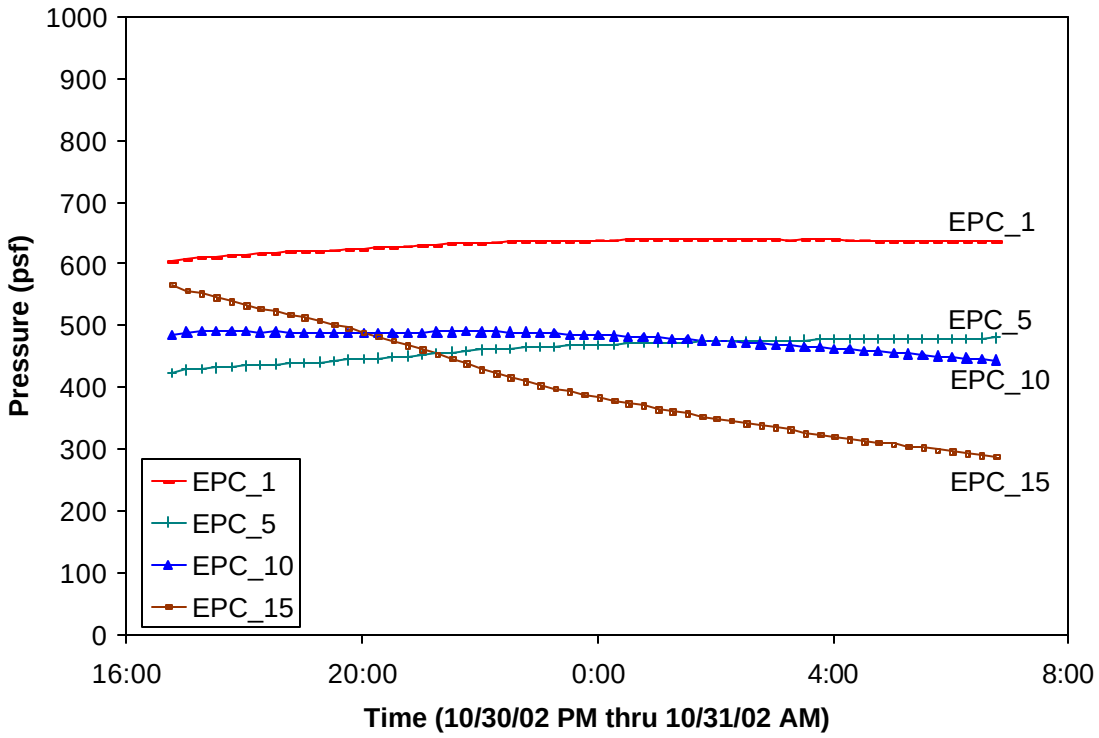

Figure 5.4. Stem EPC readings overnight following the third day of backfilling.

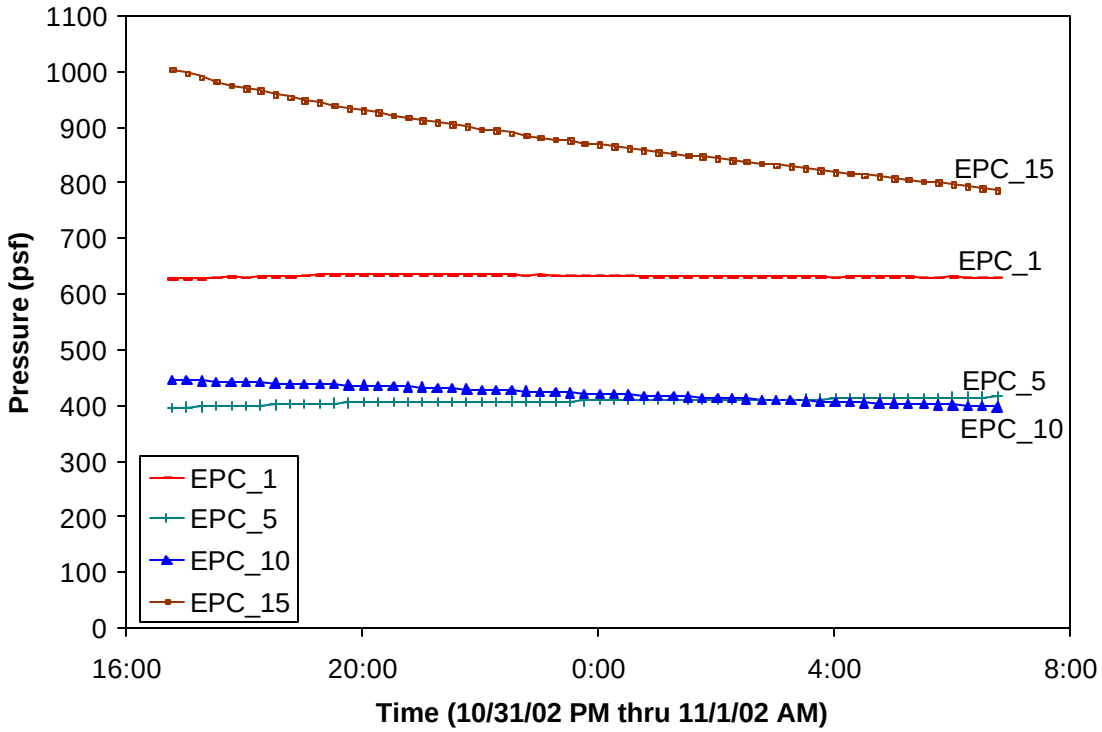

Figure 5.5. Stem EPC readings overnight following the fourth day of backfilling.

One way to envision this redistribution is if residual stresses from compaction existed such that the wall stem, through frictional stresses along the soil-structure interface, supported much of the weight of the uppermost layers of soil, which are shaded darker in Fig. 5.6a. When the wall translated overnight, however, it would decrease the lateral pressure in the top part of the backfill. It also would relieve some of the compaction-induced residual stresses. Moreover, wall translation could have disturbed the soil's frictional contact along the stem. This would increase the vertical and lateral stress at points deeper below the backfill surface (Fig. 5.6b). Vertical stresses in the soil below the footing would remain nearly constant.

There was evidence for this mechanism on the third day of backfilling (October 30, 2002), when an increase in backfill height, as recorded by EPC_back, was only partially recorded by EPC_1 and EPC_5 (Fig 5.7). The backfill height increased by 6 ft (1.8 m) to a height of 18 ft (5.5 m) on this day, but EPC_1 and EPC_5 increased only while the first 1.5 ft (0.46 m) of soil was placed. EPC_15, however, was covered when the final 3 ft (0.9 m) of soil was placed and registered a pressure reading approximately equal to that for EPC_1 at the end of the construction workday. Since the weight of the backfill was registered by EPC_back, it is known that the force was transmitted to the soil below the wall's footing. At the location of EPC_1 at the bottom of the stem, the weight of the additional lifts of backfill should have caused an increase in the vertical stress, as well as a corresponding increase in the lateral stress measured by EPC_1. Since EPC_1 showed no increase after about 10:00, it supports the hypothesis that interface friction allowed

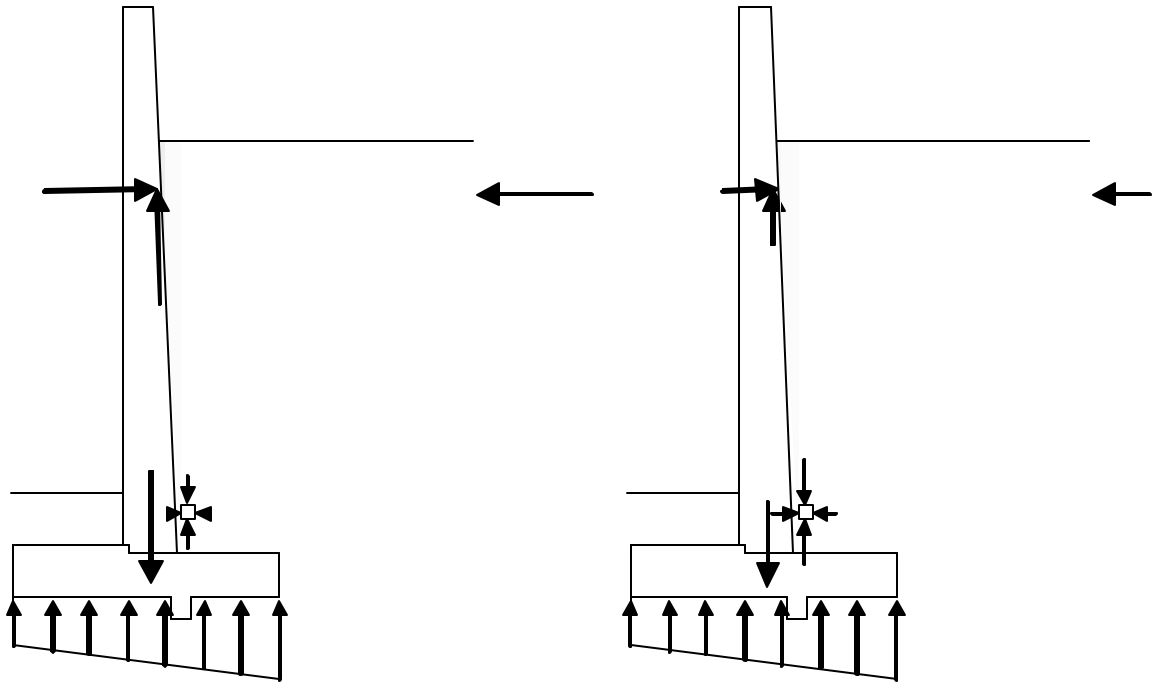

(a) (b)

Figure 5.6. Diagram showing possible soil stresses at the bottom of the stem (a) at the end of the workday and (b) the following morning, after wall translation.

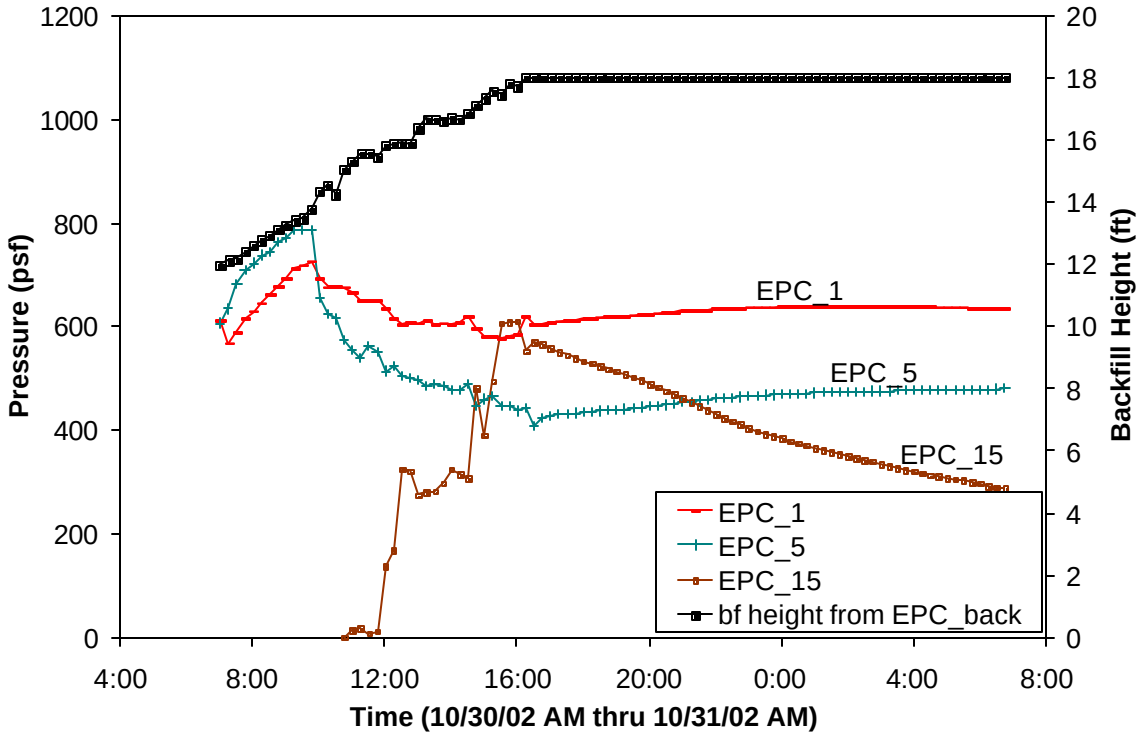

Figure 5.7. Output from EPC_1 and EPC_15 during the third day of backfilling.

the wall stem to temporarily support a significant portion of the weight of these newly placed upper lifts of sand until displacement occurred following the end of the workday. Residual stresses from compaction would have been the source of the large normal force required for a correspondingly large interface frictional force.

Movement of the wall, however, would cause disturbance of the sand grains, relieving the residual stresses, thus decreasing the normal force on the wall and in turn the interface friction. Moreover, the weight of the top layers of backfill would then increase stresses at the bottom of the stem. It is thought that this occurred overnight following the third day of backfilling, as EPC_15 and EPC_10 decreased while EPC_1 and EPC_5 slightly increased (Fig 5.4). Wall movement must have occurred for EPC_15 and EPC_10 to decrease. In fact, total station readings showed 0.05 in. (1.3 mm) of movement away from the backfill overnight. While this displacement is of the same magnitude as the inherent error of the instrument, it was determined from four survey points with two readings per point. Thus it does suggest the mechanism described above. Additionally, referenced tiltmeter readings from overnight show that the magnitude of the rotation due to deflection increased considerably at the top of the wall (Fig. 5.8). This increase in stem deflection further explains how EPC_15 and EPC_10 would have decreased.

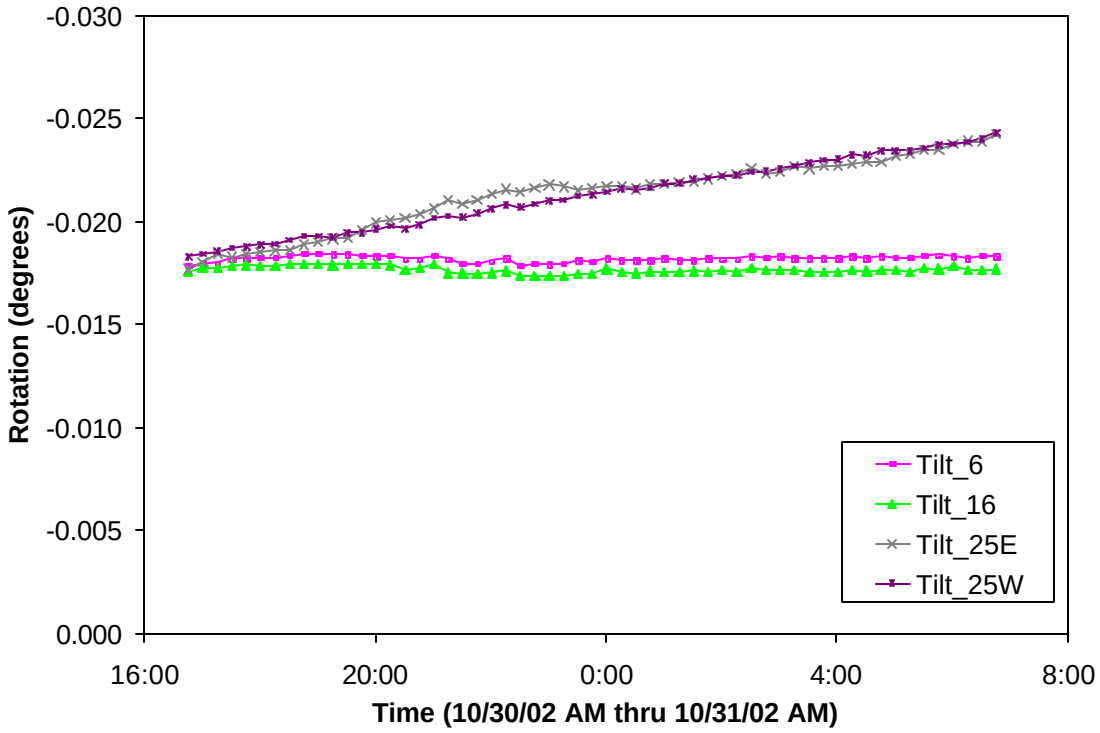

Figure 5.8. Referenced tiltmeter readings following the third day of backfilling. (Note that negative rotation is *away* from the backfill).

Also consider the readings following the fourth day of backfilling (October 31, 2002). EPC_15 and EPC_10 decreased while EPC_5 increased; EPC_1 increased almost negligibly (Fig. 5.5). Total station readings showed that the wall moved 0.08 in. (2.0 mm) away from the backfill overnight; this movement allowed EPC_15 and EPC_10 to decrease. Referenced stem tiltmeter readings decreased in magnitude overnight, only slightly at the heights of 6 ft (1.8 m) and 16 ft (4.9 m), but considerably more so at 25 ft (7.6 m) up the stem (Fig. 5.9). This drop in rotation due to elastic deflection of the stem high up the wall was directly attributable to the decrease in earth pressure behind the top part of the stem, which in turn was due to wall translation away from the soil. What this means is that outward translation of the wall overnight decreased the lateral earth pressure on the stem and in turn the stem deflection (Fig. 5.10).

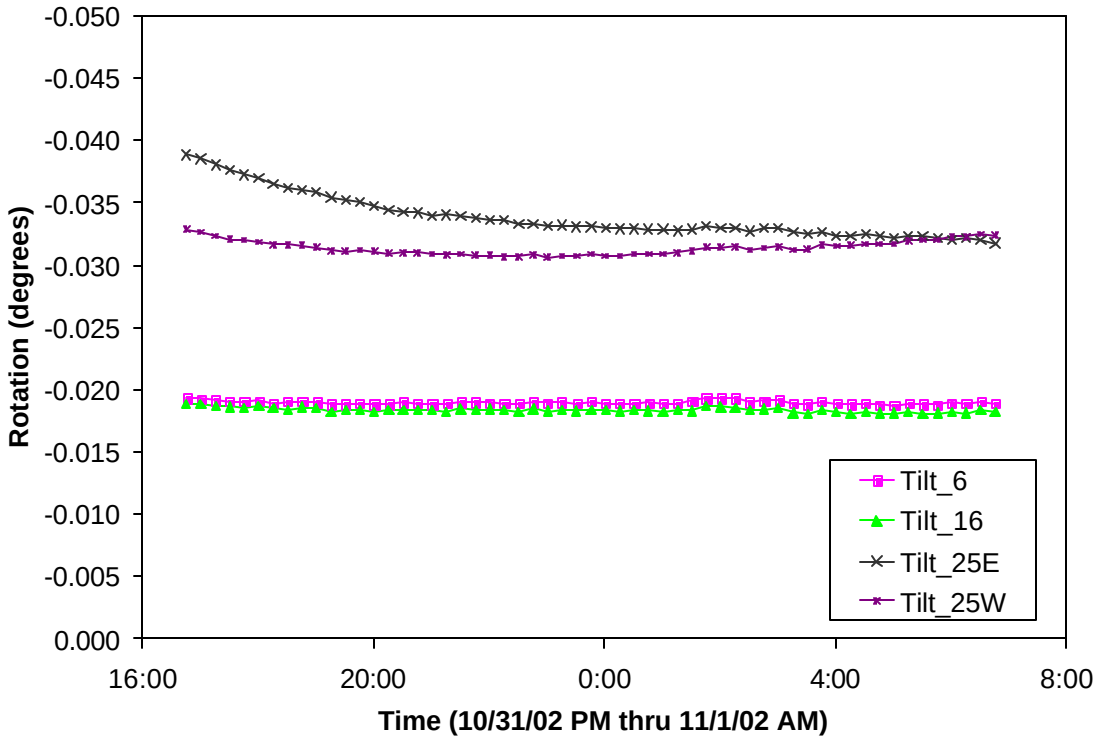

Figure 5.9. Referenced tiltmeter readings following the fourth day of backfilling. (Note that negative rotation is *away* from the backfill).

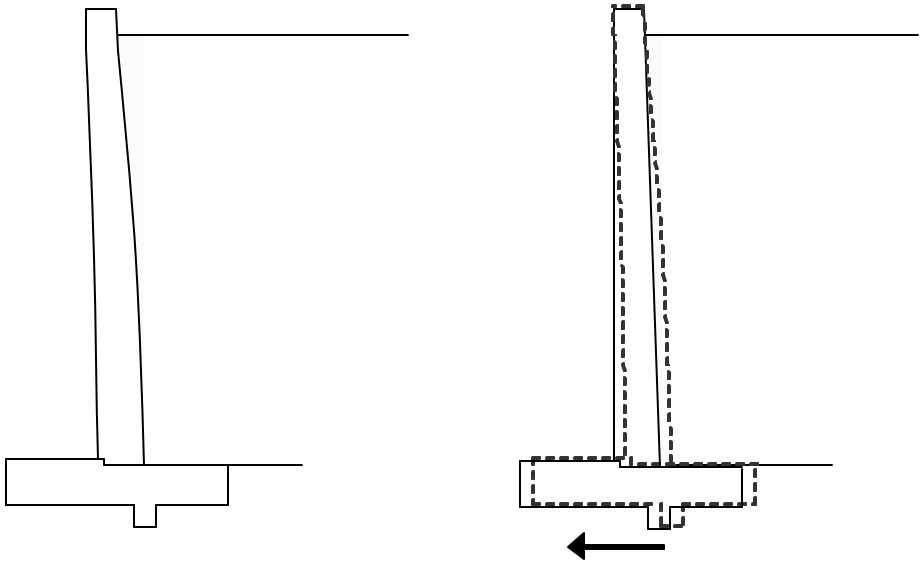

(a) (b)

Figure 5.10. Change in displacement of wall between (a) the end of the workday and (b) the following morning.

It is also notable that the tiltmeters' response following the fourth day of backfilling was different from the response following the third day. Whereas deflection increased following the third day, it decreased following the fourth day. While the change was a small percentage of the total deflection, the difference is evident in the deflection profiles (Fig. 5.11). One reason may be that more translation occurred following the fourth day. Translation would allow mobilization of the soil's strength, thus reducing lateral earth pressure on the stem. When the load on the stem decreased, the deflection decreased as well.

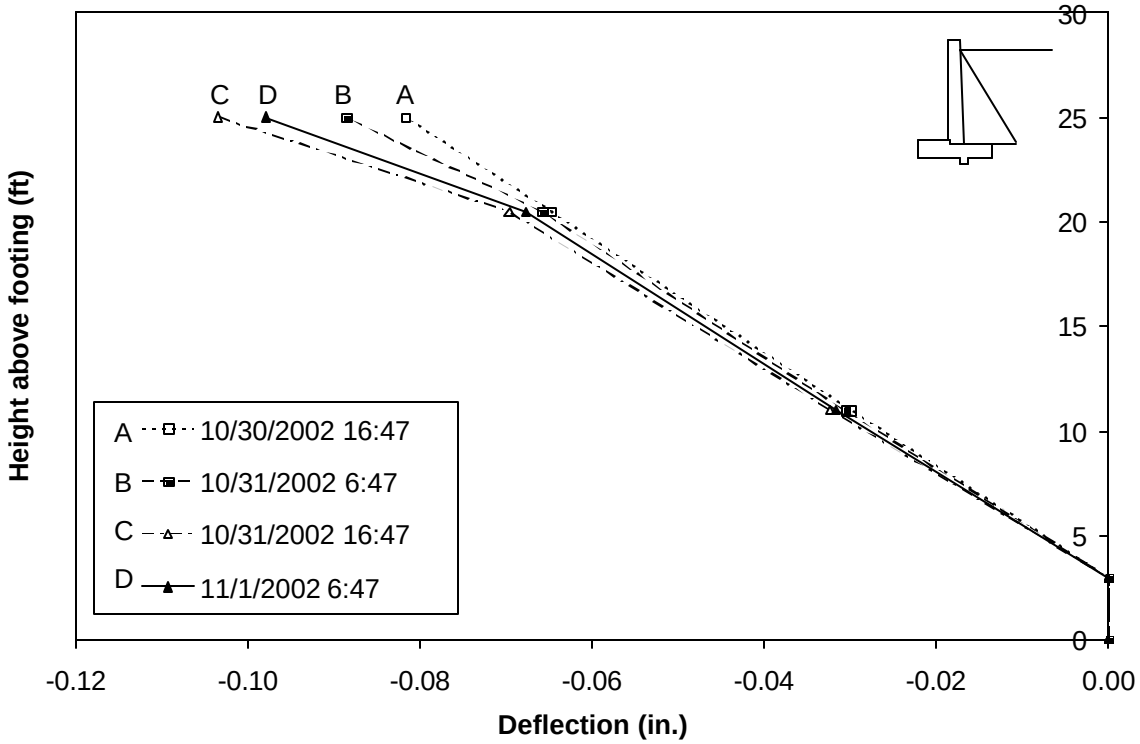

Figure 5.11. Change in stem deflection profile following the third and fourth days of backfilling.

Compaction

As previously alluded to, the readings from EPC_15 suggested the buildup of relatively high residual lateral stresses due to the compaction process. The readings from October 31, 2002, (the fourth day of backfilling behind panel BJ) are perhaps the best evidence for this. The backfill height increased from 18 ft (5.5 m) to about 20 ft (6.1 m) during the workday. Given that only about 2 ft (0.6 m) of soil was placed, a prominent feature of the EPC readings from this day was that the pressure at EPC_15 more than doubled by mid-afternoon. The resulting earth pressure distribution was not at all triangular (Fig. 5.12). In fact, it looks similar in shape to the final earth pressure distribution shown in Fig. 5.13 that was determined numerically by Aggour and Brown [14].

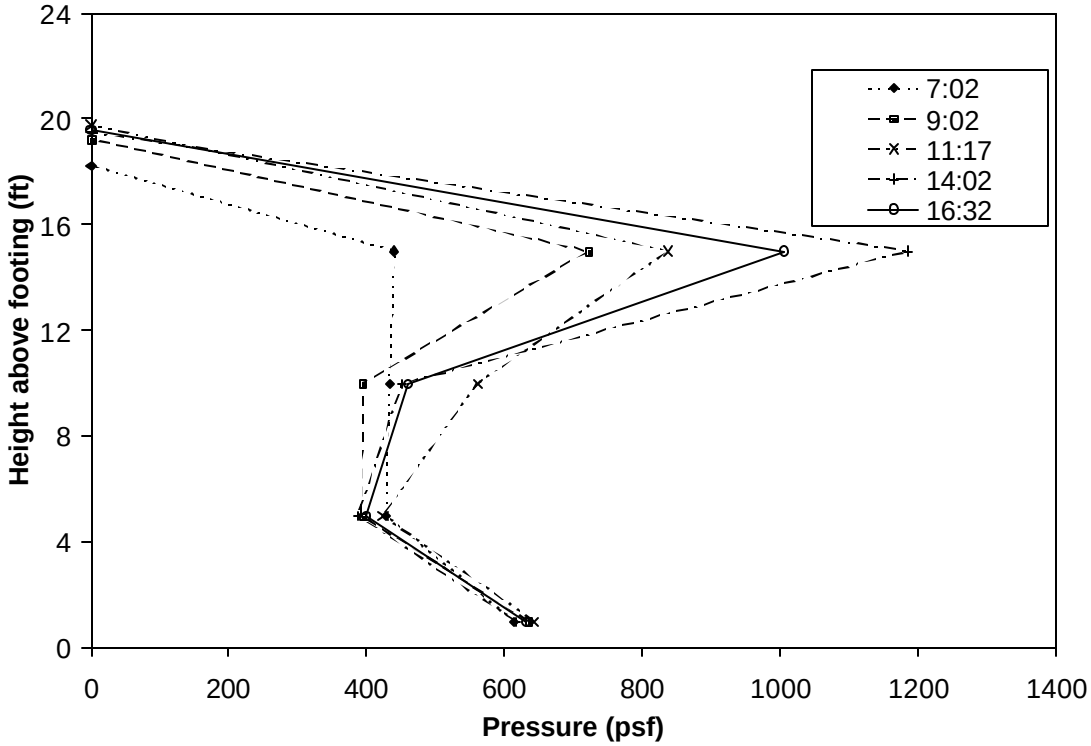

Figure 5.12. Earth pressure profiles at selected times during the fourth day of backfilling.

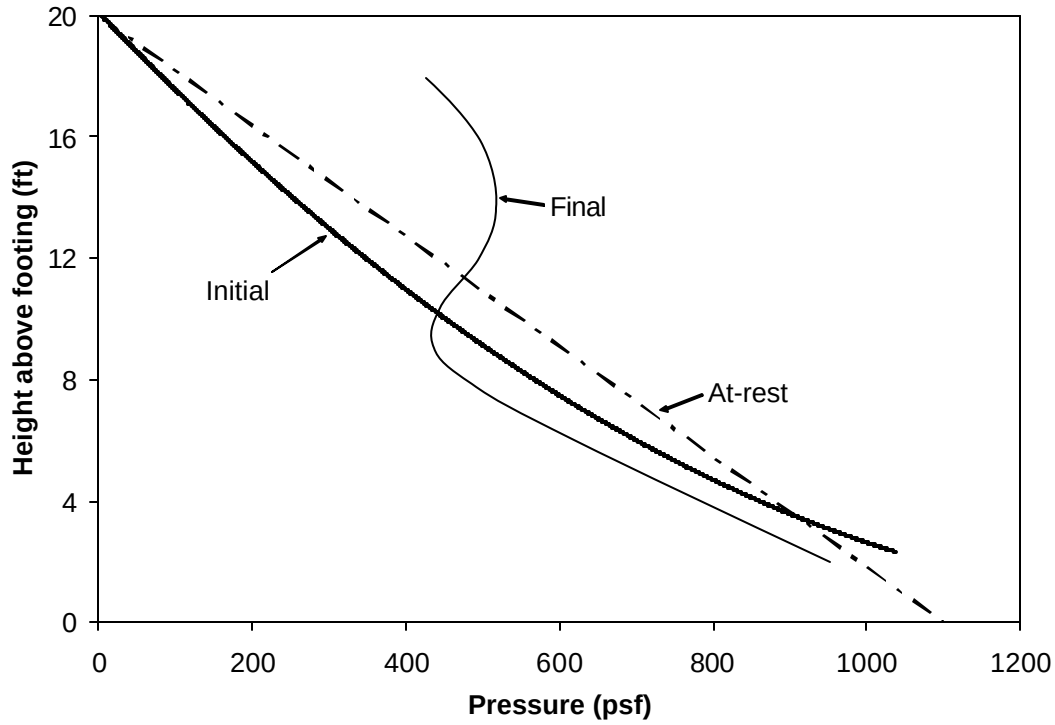

Figure 5.13. Earth pressure due to compaction, estimated from numerical analysis [14].

A plot of earth pressure readings versus time further shows the stark contrast between EPC_15 and the other stem EPCs (Fig. 5.14). EPC_15 increased to a peak of about 1200 psf (57 kPa) at 14:00 and then steadily decreased to about 800 psf (38 kPa) by the next morning. EPC_10 also decreased overnight, though not as significantly; all other stem EPCs held steady from about noon until the next morning.

Wall movement must have caused the lateral pressure registered by EPC_15 to reduce. As the tiltmeter readings suggested (Fig. 5.15), it was possible that deflection of the stem allowed the pressure at EPC_15 to decrease. Also, total station readings indicated increased displacement away from the backfill between 8:30 and 12:00 (Fig. 5.14), which would have allowed the active condition to develop.

An interesting feature was that the rotation readings of Tilt_25E and Tilt_25W changed sharply at 7:00 and again at 9:00, just as EPC_15 did (Fig. 5.15). They also peaked at the same time (14:00) and decreased thereafter. In fact, the response of the tiltmeters at 25 ft (7.6 m) almost exactly matched the signal from EPC_15. Tilt_6 and Tilt_16 also matched this trend, although the variation was much less significant and the magnitude of the changes was very small. Not shown in Fig. 5.15 is that Tilt_0 showed almost no change, indicating that no measurable rigid body rotation occurred.

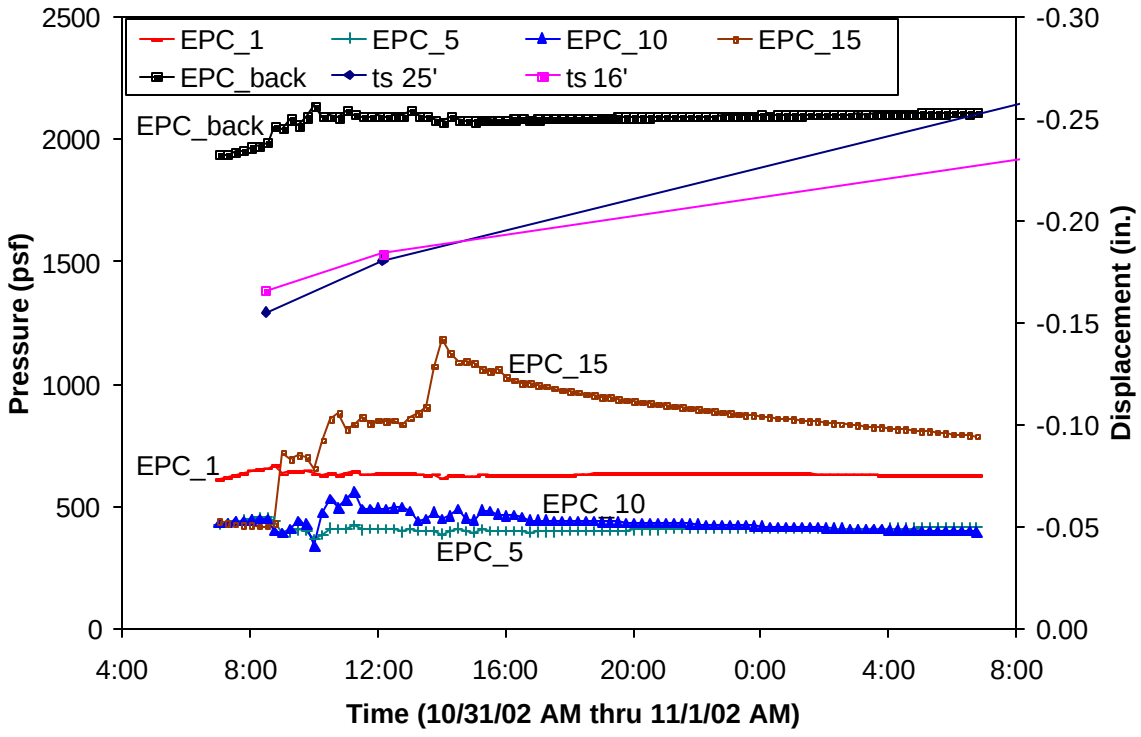

Figure 5.14. EPC and total station readings for the fourth day of backfilling.

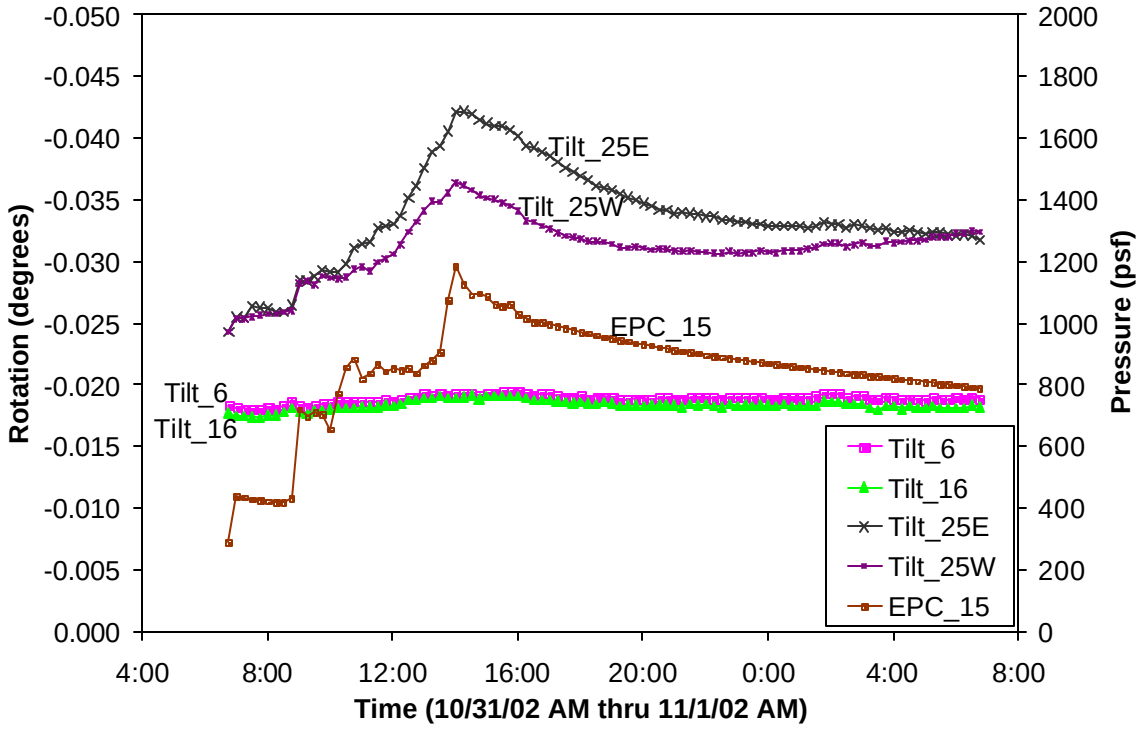

Figure 5.15. EPC_15 and referenced tiltmeter readings for the fourth day of backfilling.

As a whole, the tiltmeter readings indicated that the deflection at the top of the wall increased significantly more than in the middle (Fig. 5.15). More deflection occurred in the top half of the wall than the bottom half. This was due in part to the change in stem thickness with height, as well as the distance from the fixed base of the stem. It was also due to the greater lateral pressure that acted higher up the wall (Fig. 5.12). Since only 2 ft (0.6 m) of soil was placed this day, this increase in deflection was largely induced by compaction. The high lateral stresses from compaction caused the stem to deflect. However, it was not permanent. As described in Section 5.1.2, translation of the wall relieved the compaction-induced lateral stresses, thus also reducing the deflection of the stem.

While the readings of EPC_15, Tilt_25E, and Tilt 25W from the fourth day of backfilling demonstrated the effects of compaction, all stem EPCs showed evidence for large temporary increases in lateral stress due to compaction. These occurred shortly after the backfill covered each EPC and lasted until the backfill was about 5 ft (1.5 m) above the EPC. The stress tended to decrease overnight. The effect of compaction can be illustrated by the normalized lateral earth pressure, which can be defined as an earth pressure coefficient K:

$$K = \frac{s_l}{gz} \tag{5.1}$$

where s_l is the measured lateral earth pressure, g is the unit weight of the backfill, and z is the height of soil above the EPC. The peak value of K for each EPC was at least 1.9 or higher (Fig. 5.16). The backfill (bf) height is included on these plots, since placement of backfill was

generally immediately followed by compaction. As stated before, the EPCs eventually decreased to values that were approximately active (recall K_a = 0.249 for f = 37°). It can be seen that EPC_1, EPC_5, and EPC_10 all registered active earth pressure at the end of the workday on Friday, November 1, 2002. EPC_15 decreased to active earth pressure later in November (Fig. 5.17). Movement of the wall, primarily horizontal translation, relieved the residual compaction stresses within the soil.

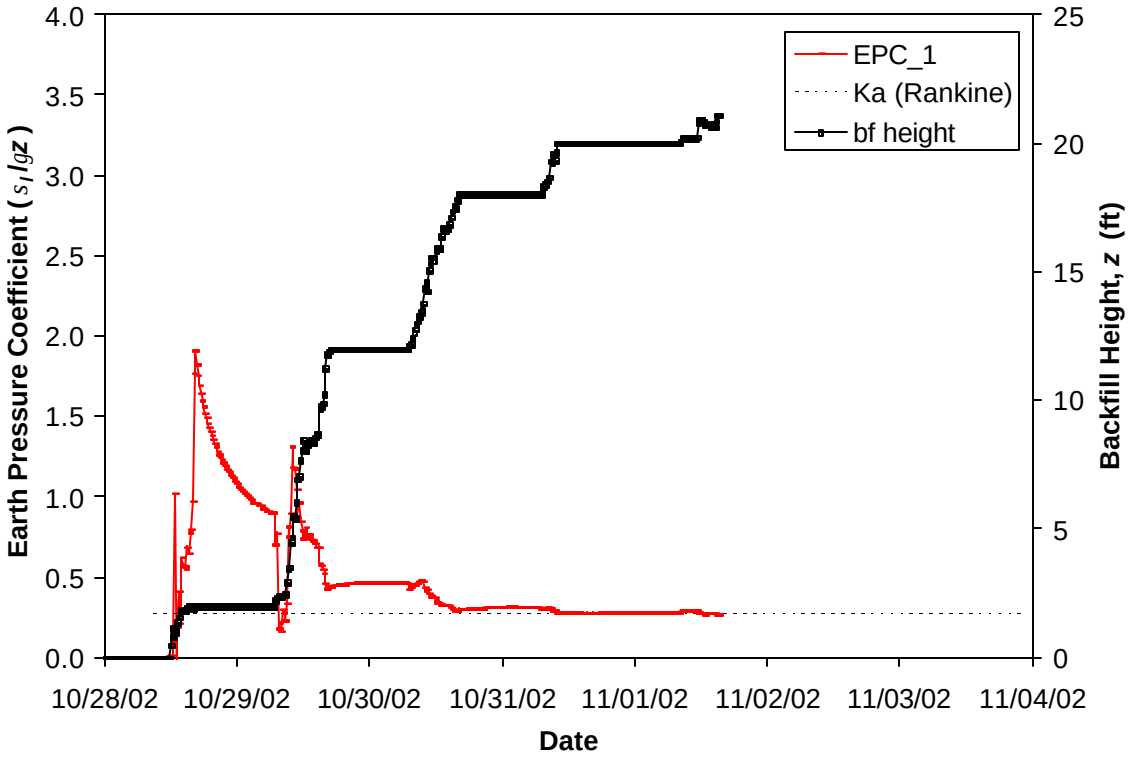

Figure 5.16a. Normalized lateral earth pressure 1 ft (0.3 m) up from the base of the stem (bf = backfill).

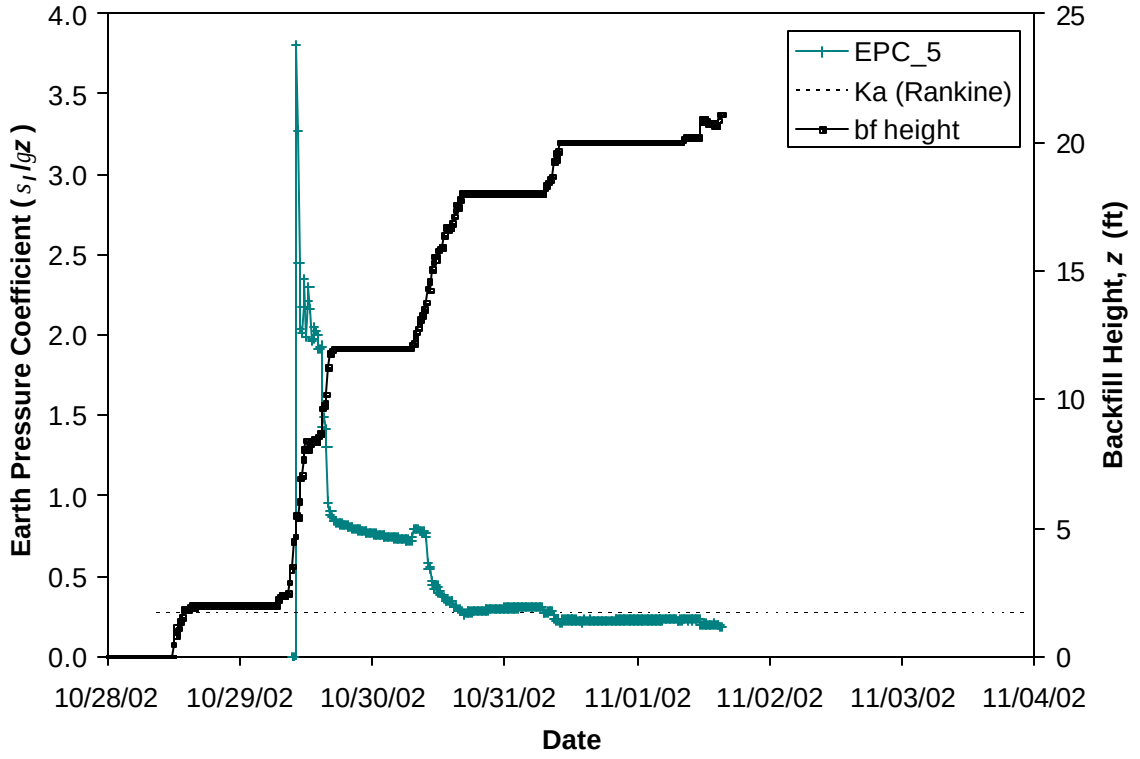

Figure 5.16b. Normalized lateral earth pressure 5 ft (1.5 m) up from the base of the stem.

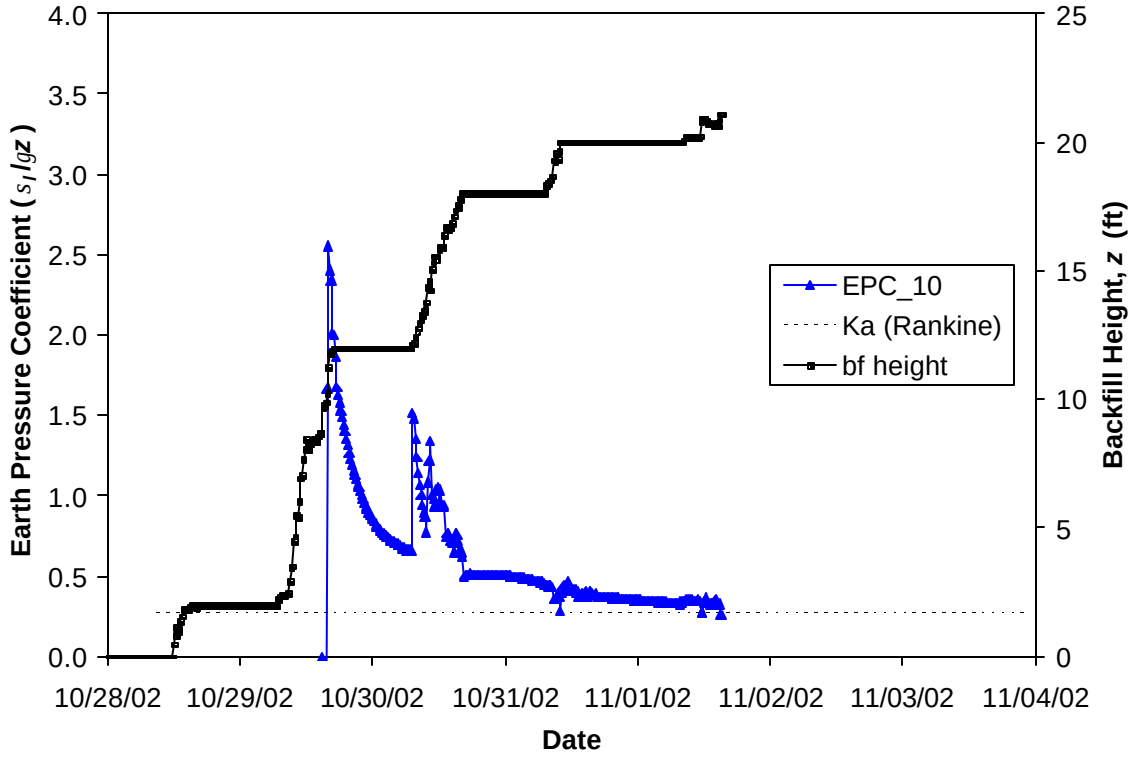

Figure 5.16c. Normalized lateral earth pressure 10 ft (3.0 m) up the stem.

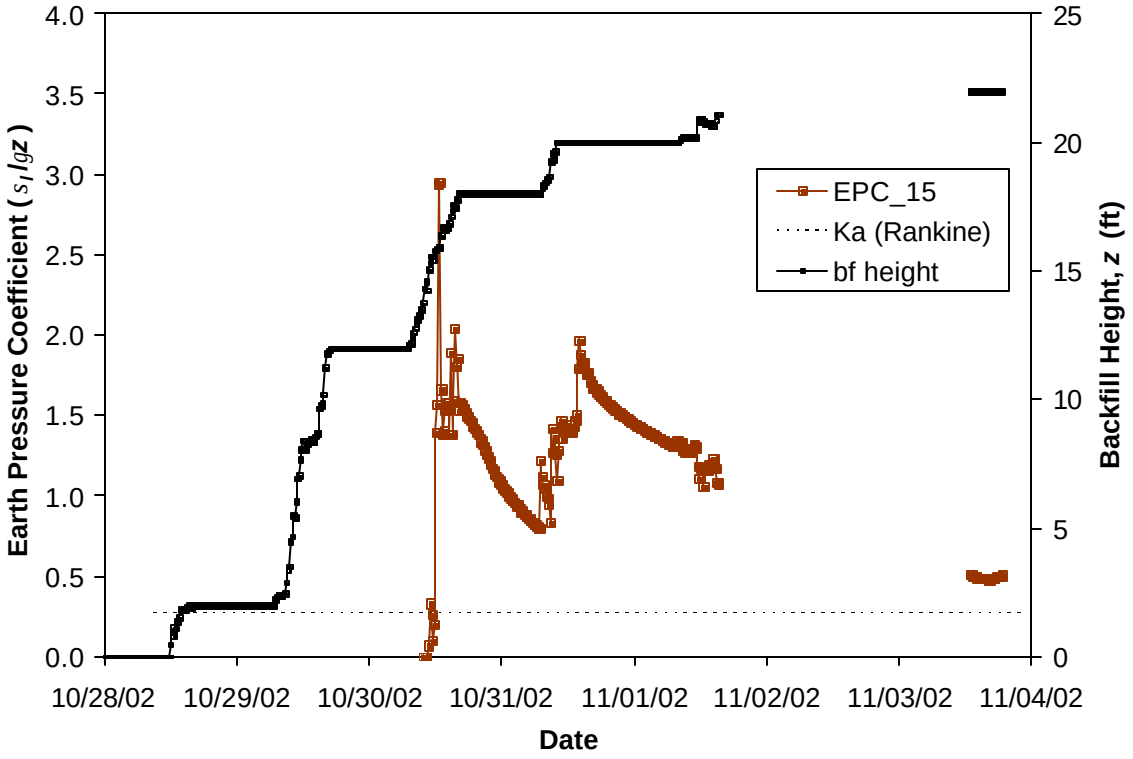

Figure 5.16d. Normalized lateral earth pressure 15 ft (4.6 m) up the stem.

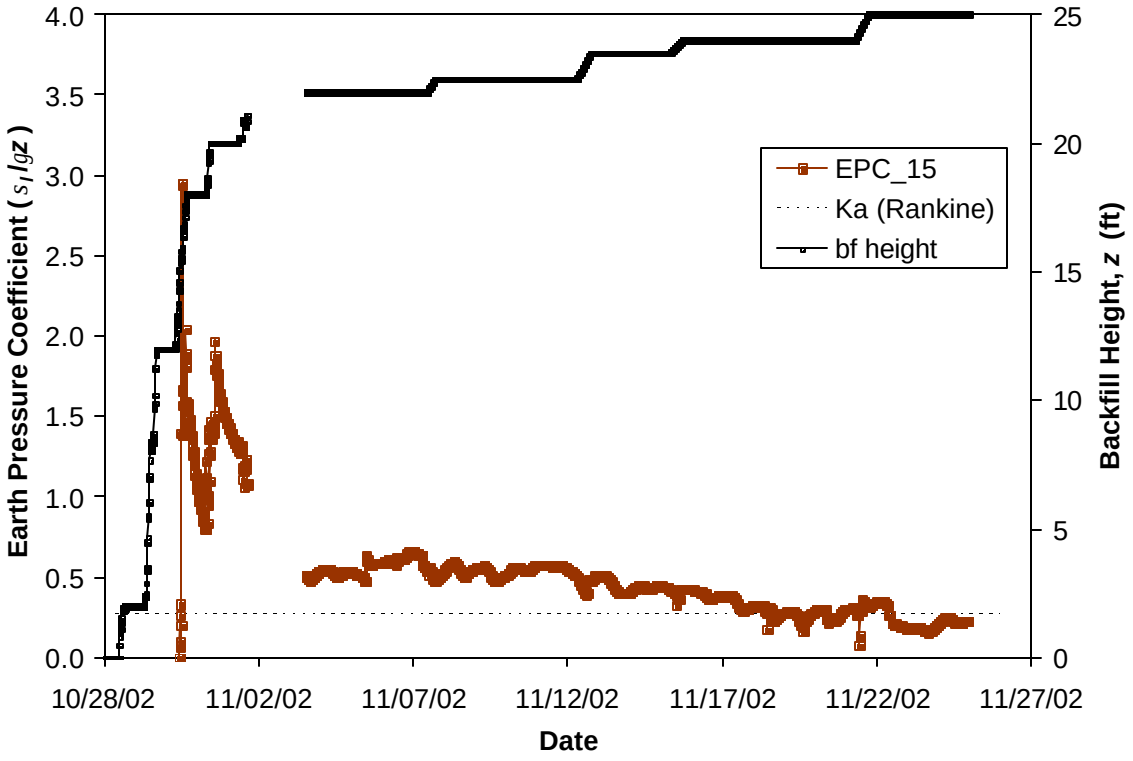

Figure 5.17. Normalized lateral earth pressure 15 ft (4.6 m) up from the base of the stem over the entire course of backfilling behind Panel BJ.

Temperature Behavior

Once a retaining wall is constructed and backfilled, and after movements of the wall and the surrounding soil associated with backfilling have stopped, classical earth pressure theory suggests that the lateral earth pressure on the retaining wall remains constant. However, Coyle and Bartoskewitz [7] observed a seasonal variation in earth pressure readings (decrease in winter, increase in summer). Readings from the EPCs and tiltmeters on Panel BJ also indicated that changes in temperature affect lateral earth pressure on a retaining wall.

Daily Cycle

Throughout the monitoring of the wall, EPCs and tiltmeters showed a daily rise and fall in readings that was associated with the daily change in the temperature (Figs. 5.18 & 5.19). The output from the Geokon EPCs showed the same qualitative behavior as the Kulite EPCs (Appendix B). The temperature recorded was that of the datalogger; this was assumed to be about the same as air temperature, and the daily high and low readings compared well with those reported by the National Weather Service (obtained at http://climate.umn.edu). Temperature corrections were applied to the tiltmeters mounted on the stem above ground, but not Tilt_0, which was covered with soil. However, since the temperature of each Kulite EPC was unknown, and since the thermal sensitivity has been measured to be rather small for these sensors [20, 21], no temperature corrections were applied to the EPC readings.

If the daily cyclic variations were due to the thermal properties of the sensors or the data acquisition system, the EPCs should have all responded in a similar manner to changes in temperature. However, when the air temperature increased, for example, stem EPCs decreased while EPC_toe increased. The main difference between these EPCs was location. Again, for the tiltmeters, if the observed change in readings with temperature were due to the data acquisition system, all the tiltmeters would have shown nearly the same response. However, the change with temperature was more pronounced for Tilt_25E and Tilt_25W than for Tilt_16; in fact, Tilt_6 decreased when the other tiltmeters increased. Tilt_0 showed almost no change with temperature when compared to the other tiltmeters. Hence, the daily change in the measurements (Figs. 5.18 and 5.19) was due to physical changes in the interaction between the structure and the soil.

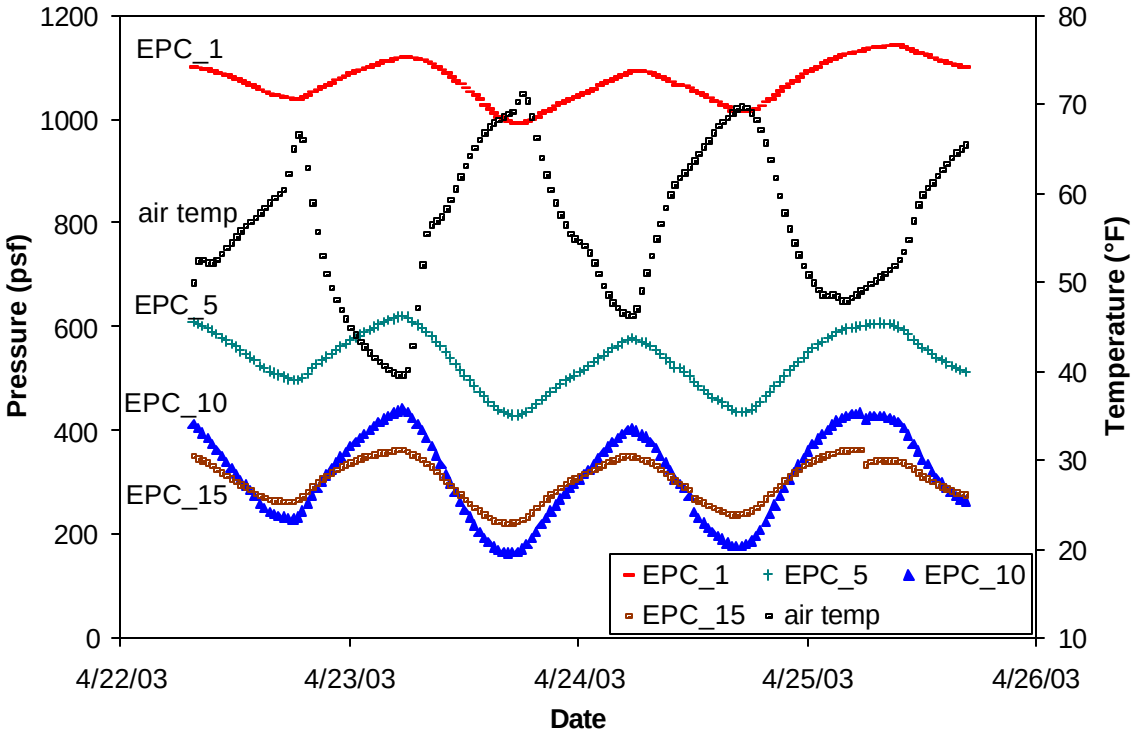

Figure 5.18. Example of daily cyclic variation of Kulite EPCs and temperature.

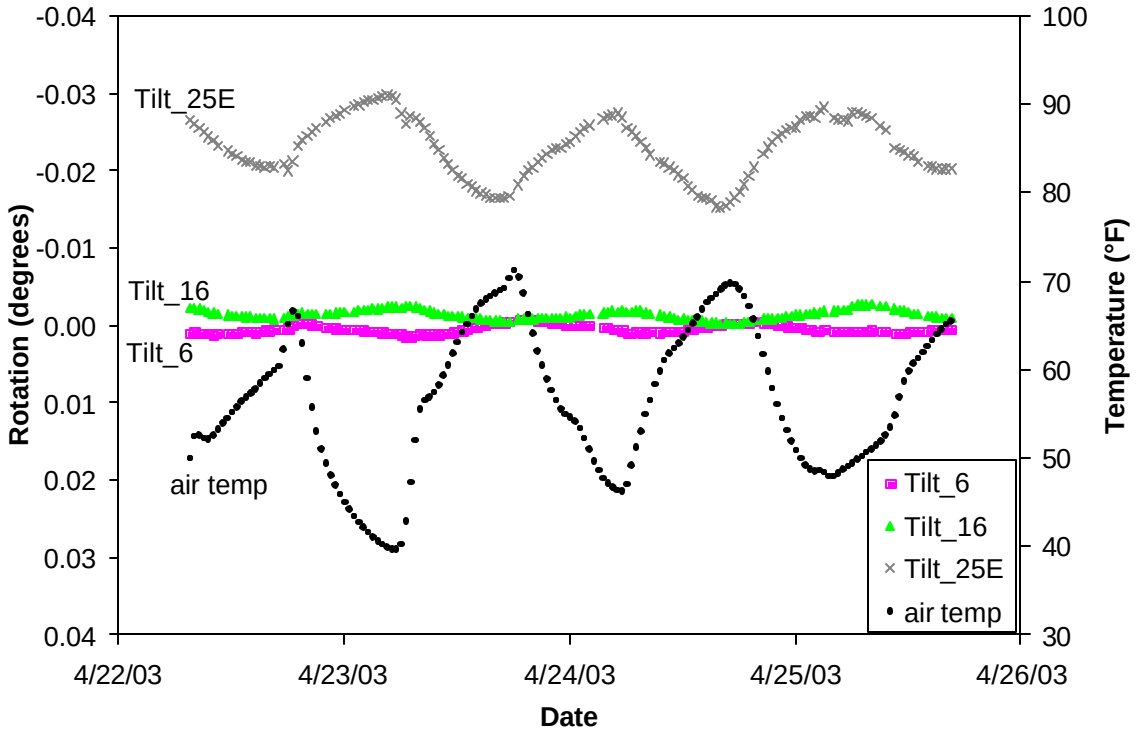

Figure 5.19. Example of daily cyclic variation of tiltmeters and temperature.

The EPC data revealed that the earth pressure on the stem decreased when the air temperature increased (Fig. 5.20), which usually occurred between morning and evening. Overnight, when the air temperature decreased, earth pressure on the stem increased. Assuming that no rigid body rotation of the footing occurred, the tiltmeter readings indicated that the top of the stem moved into the backfill when the air temperature increased (Fig. 5.21). Conversely, when the air temperature decreased, the top of the stem moved back away from the soil. However, EPC_toe increased when the temperature increased (Fig. 5.22). Although the data shown are not for the same period of time as previous figures since EPC_toe malfunctioned on April 18, 2003, Fig. 5.22 shows the typical response at EPC_toe to changes in air temperature.

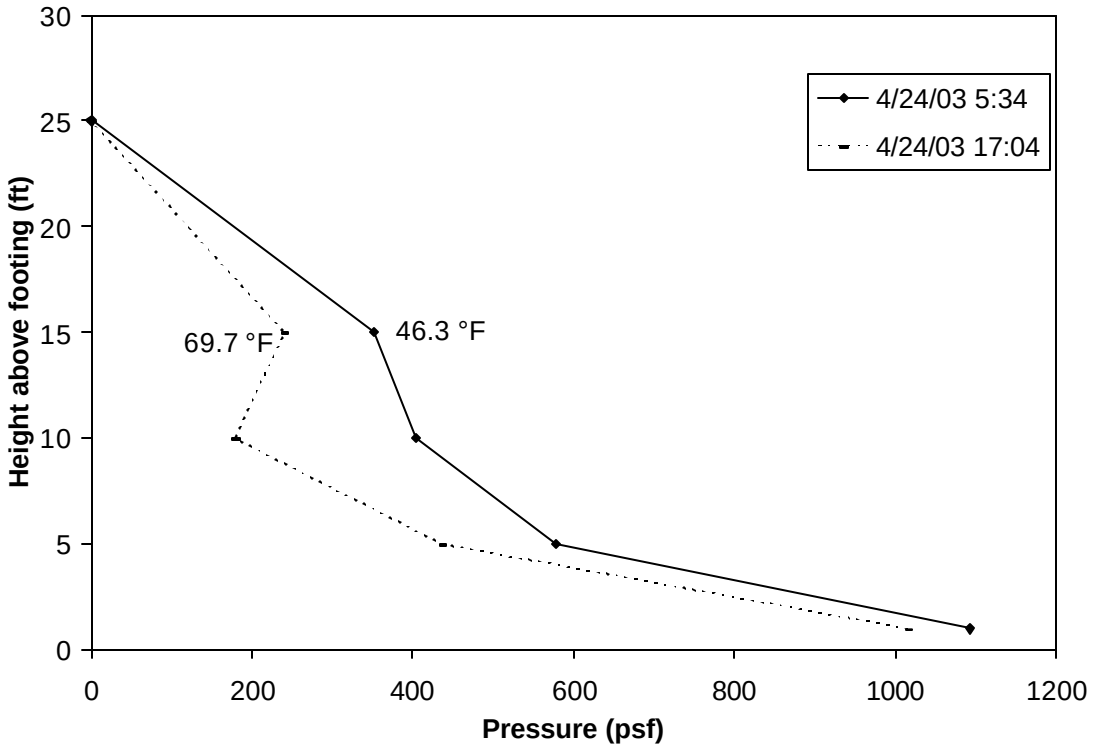

Figure 5.20. Example of change in earth pressure profile due to change in air temperature.

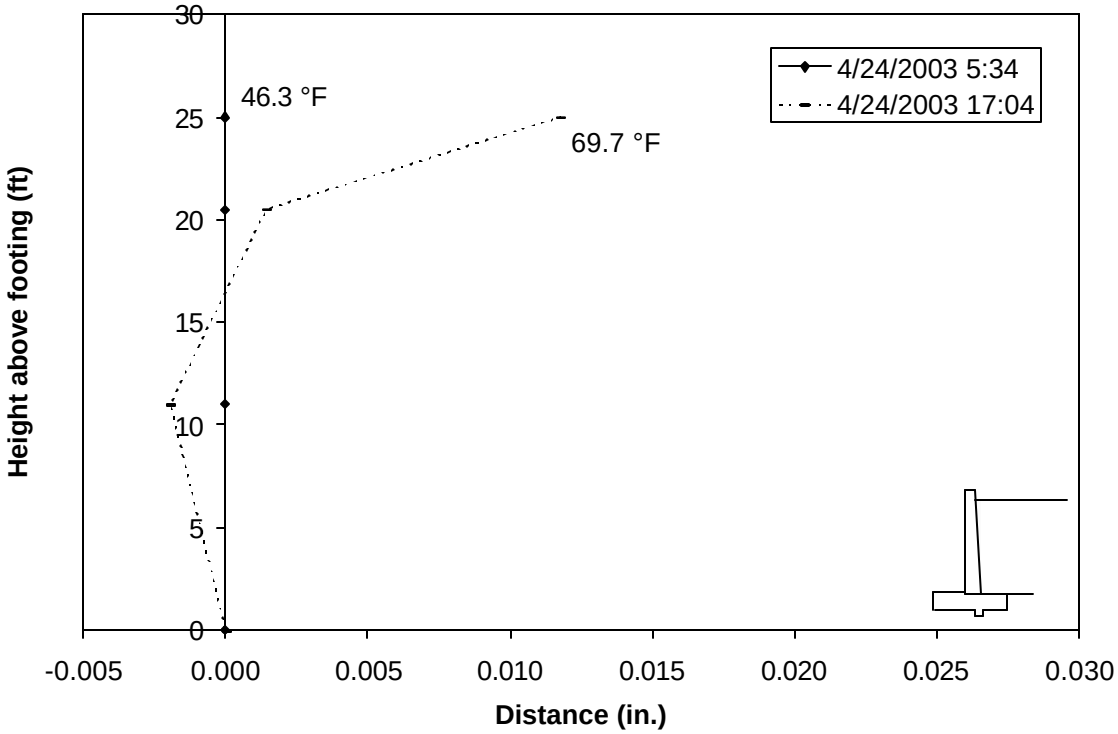

Figure 5.21. Example of incremental change in deflection profile due to change in air temperature.

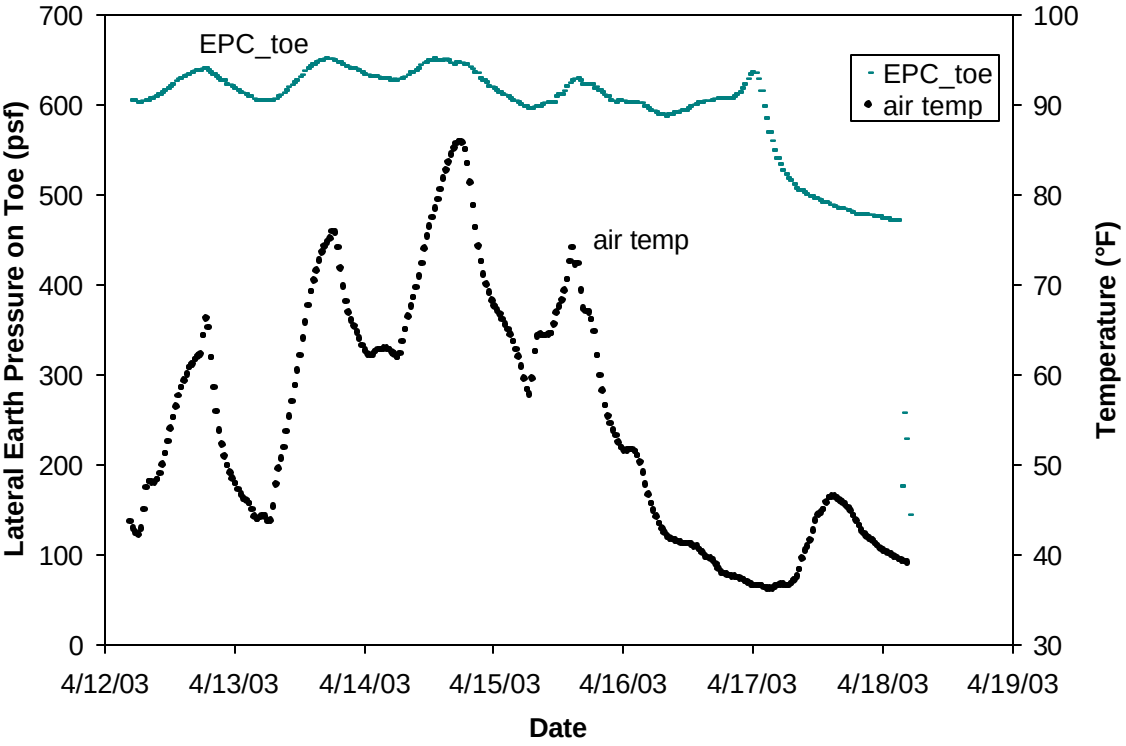

Figure 5.22. Example of response at EPC_toe with daily change in air temperature.

To reiterate, an increase in air temperature was associated with both a decrease in earth pressure on the stem and movement of the top of the stem into the backfill. Conversely, a decrease in air temperature was associated with an increase in earth pressure on the stem and movement of the top of the stem away from the backfill. It should be noted that the movement described includes stem deflection and rigid body rotation. Unfortunately, total station readings are not available for this period of time, so the wall translation is unknown.

The change in tiltmeter readings and the change in the stem EPC readings are most likely connected. Two possibilities exist: (1) the earth pressure was affected by temperature, and the stem moved due to the change in earth pressure or (2) the stem moved due to the temperature, and the earth pressure was affected by the stem movement. The first possibility is not considered reasonable since changes in temperature (other than changes around the freezing point) should have little effect on stresses within dry soil. The second possibility is reasonable since there is likely a temperature gradient through the thickness of the retaining wall stem. The air temperature is much more variable than the soil temperature, which at a given time in the spring is probably at or below the air temperature averaged over a week's time. For a concrete pavement, a gradient in temperature between the air and the subgrade is known to cause curling of the slab in the manner shown in Fig. 5.23 [27, 28]. The tiltmeter readings (Fig. 5.21) suggested that a similar change in shape of the retaining wall occurred.

This change in shape for the retaining wall could have caused the bottom of the stem to push out away from the soil (Fig. 5.24a). The change in the stem's shape could have caused wall translation away from the soil. This movement would account for the decreased pressure on the stem EPCs. Furthermore, the effect of the change in air temperature was more pronounced for EPC_5 and EPC_10 than for EPC_1 and EPC_15 (Fig. 5.20). In fact, the change in stem profile determined from the tiltmeters and shown in Fig. 5.24a suggests the highest magnitude of movement occurred in the lower middle of the stem. Translation away from the soil would also be expected to have caused an increase in the pressure measured by EPC_toe in front of the wall footing. Indeed, EPC_toe showed an increase in pressure when, according to this mechanism, the wall should have been moving away from the soil. Moreover, EPC_toe decreased when the temperature decreased. This would imply that the wall moved back into the soil when the temperature decreased (Fig. 5.24b). Hence, over a 24-hr period, the net movement of the wall would have been essentially zero.

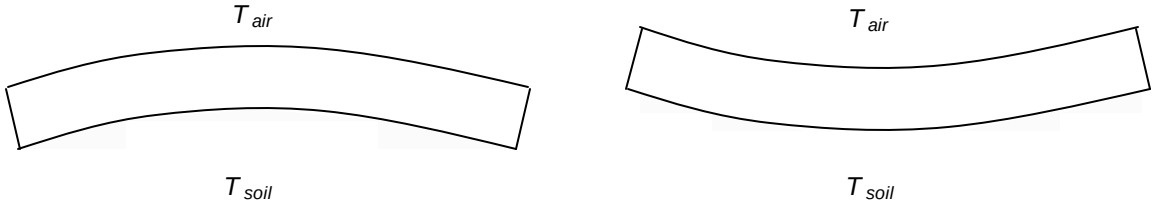

(a) (b)

Figure 5.23. Curling of a concrete slab on soil for (a) $T_{air} > T_{soil}$ and (b) $T_{air} < T_{soil}$.

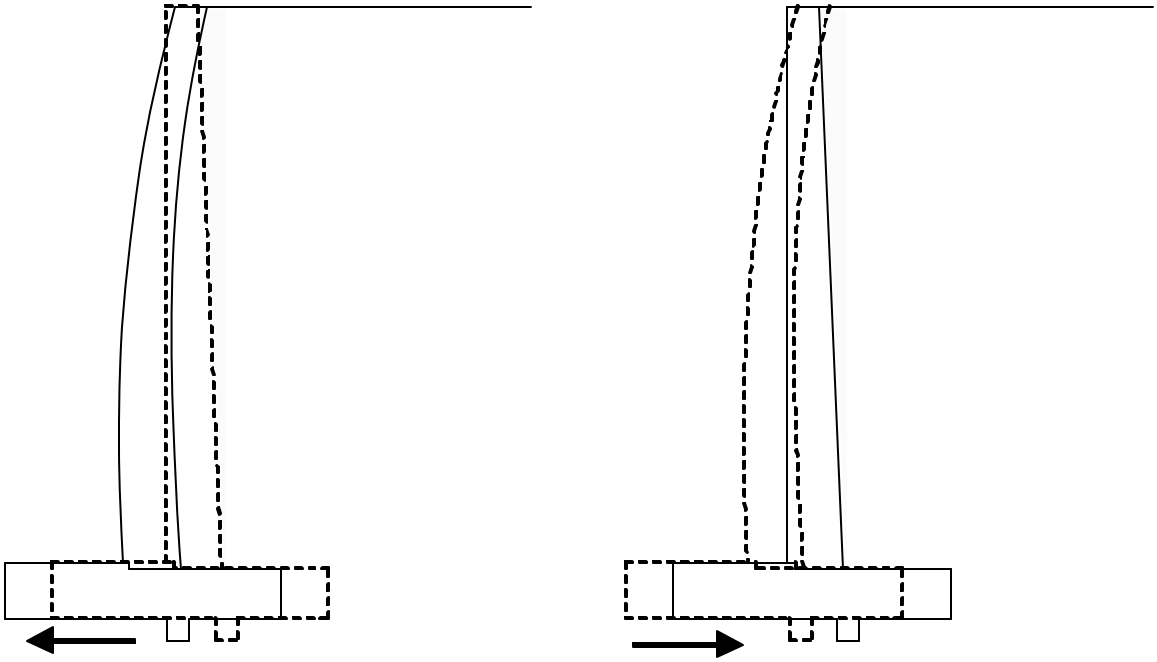

(a) (b)

Figure 5.24. Change in shape and corresponding movement of retaining wall during one day when (a) air temperature is highest and (b) air temperature is lowest.

Effect of Sub-freezing Temperatures

For climates with sub-freezing winter temperatures, freezing of moist soil may effectively create a temporary cohesion in the upper layers of the backfill. Evidence for this was recorded in January and February 2003 (Fig. 5.25). EPC_15 recorded no pressure for a period in mid-January and again in mid-February. This was interpreted to mean that the upper 10 ft (3.05 m) of backfill temporarily ceased to exert pressure on the wall. Meanwhile, lateral earth pressure increased at EPC_10 and EPC_5. Air temperatures were mainly in the range of -10° to 20° F (-23.3° to -6.7° C). By mid-March, however, the earth pressure distribution was similar to what it had been in late December (Fig. 5.26).

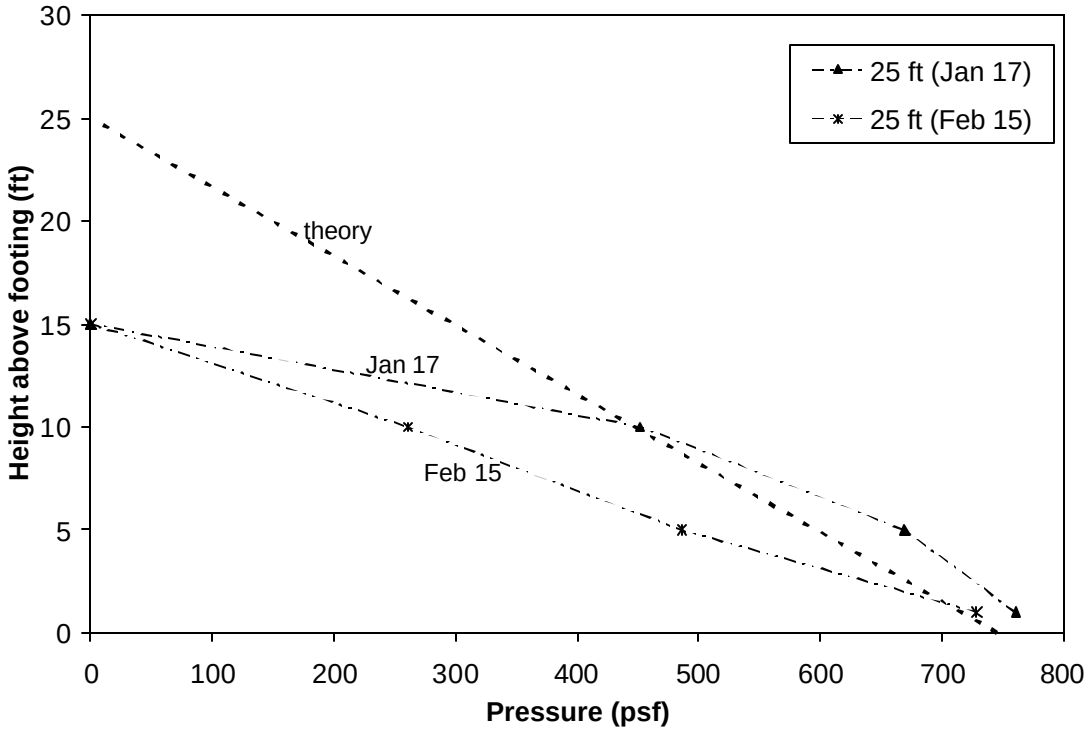

Figure 5.25. Distribution of earth pressure on stem during January and February 2003.

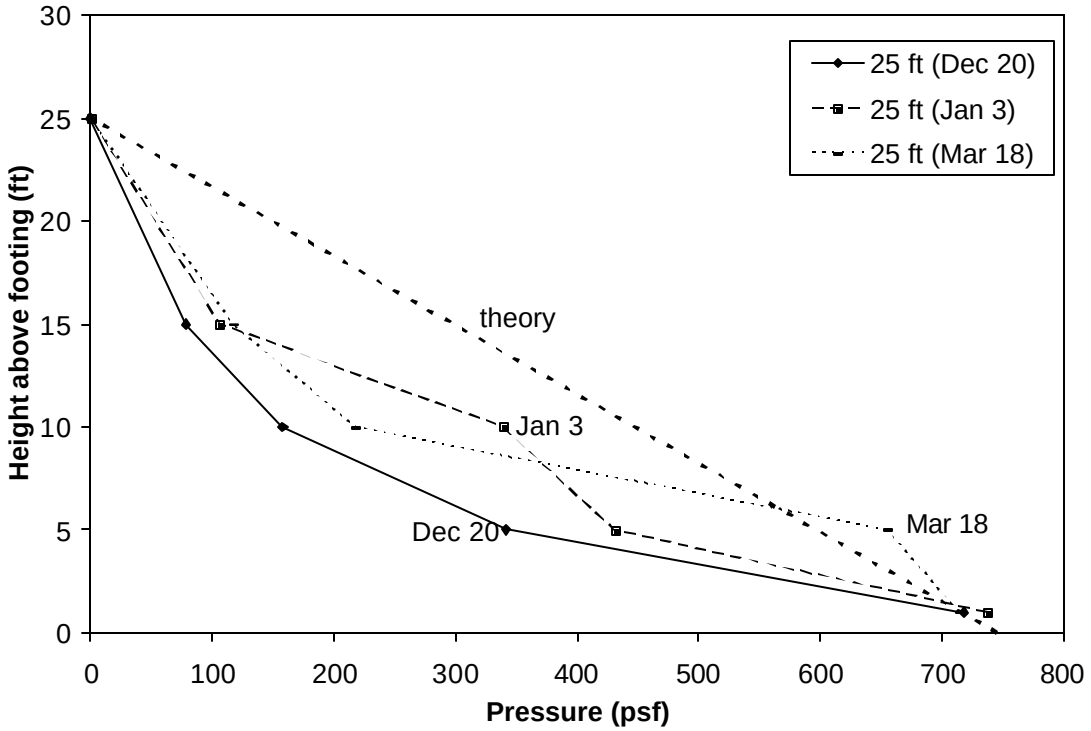

Figure 5.26. Distribution of earth pressure on stem during winter 2002 – 2003.

Response to Precipitation

National Weather Service records of daily precipitation were obtained through the state climatology office Web site (http://climate.umn.edu). Using this data, it was apparent that the earth pressure on the wall, as well as the soil stress below the footing, was affected by precipitation. For example, readings from selected EPCs on the stem and footing for the middle of April 2003 show that a rather large rainfall over a few days increased both the soil stress below the footing and the earth pressure on the stem (Fig. 5.27). The EPCs readings in Fig. 5.27 have been adjusted to account for temperature effects to isolate the influence of precipitation. The correction factors were determined by plotting the EPC readings against the air temperature (Fig. 5.28) for a typical April day (April 13, 2003) when no rain fell.

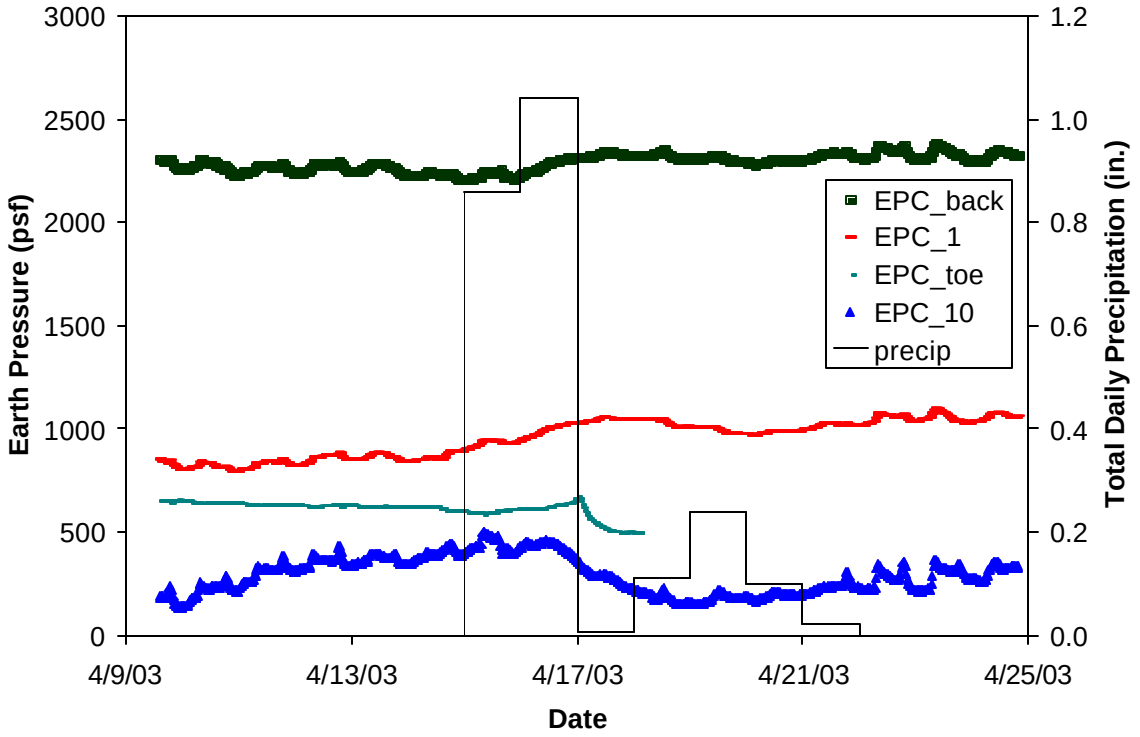

Figure 5.27. Change in temperature-corrected EPC readings due to heavy rainfall in April 2003.

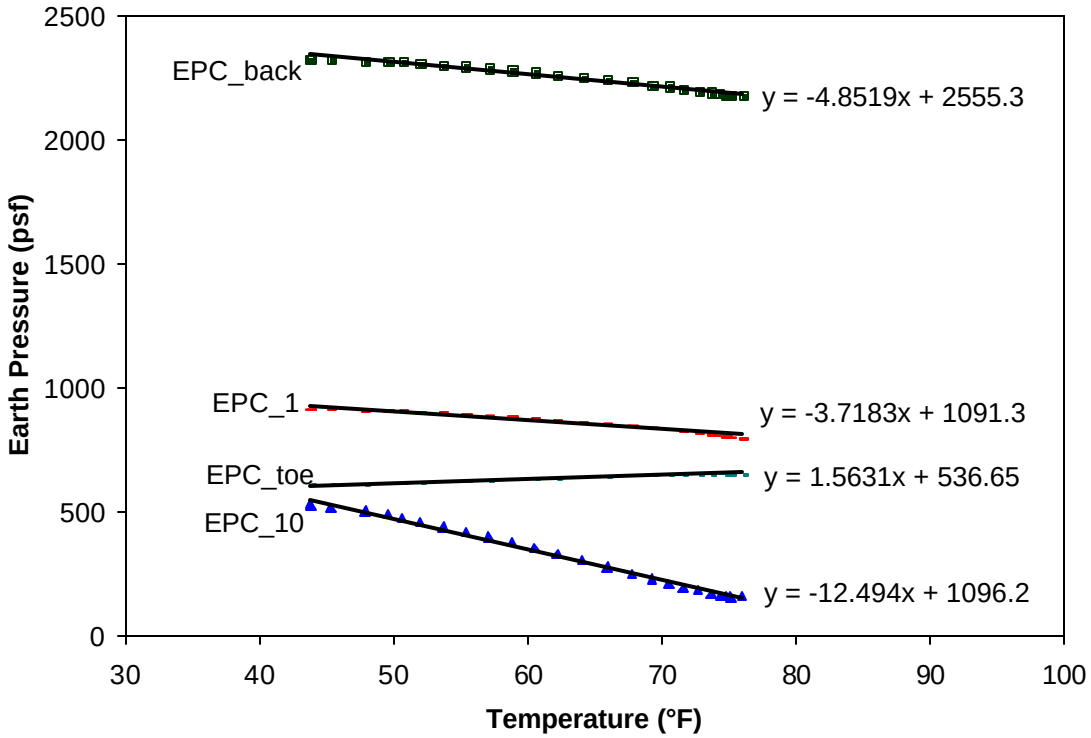

Figure 5.28. Temperature corrections for EPCs in mid-April 2003.

Fig. 5.27 shows that the stress below the footing (EPC_back) decreased slowly in the days following the rainfall, presumably due to drainage of the backfill. EPC_1 at the bottom of the stem did not seem to decrease significantly, although EPC_10 did, even prior to the end of this period of rain. It is possible that the increase in lateral earth pressure due to the rain caused outward translation of the wall, which decreased the pressure on the upper part of the stem, such as at EPC_10.

The rainfall also evidently caused EPC_toe to malfunction for several weeks, perhaps because moisture penetrated the seal around a splice in the lead wire. In another case, heavy rainfall on June 24-25, 2003, coincided with the permanent ending of readings from EPC_1 and EPC_toe.

Sliding Resistance

Since Panel BJ translated horizontally about 0.45 in. (11 mm) as a rigid body, it was worthwhile to consider the resistance to sliding for the retaining wall. Two scenarios were examined: (1) the maximum possible resistive force and (2) the mobilized (or developed) resistive force. While the factor of safety calculations in Section 5.5 consider the maximum possible forces resisting sliding, the readings from Panel BJ could be used to determine the mobilized resistive force for the actual wall. The lateral translation that was measured should then be interpreted as the displacement required for the resisting forces to develop, both along the bottom of the footing and in the soil in front of the retaining wall.

Interface Friction

Using the EPC readings, it was possible to determine the mobilized coefficient of friction at the interface between the wall footing and the soil below it. The lateral force P_h on the stem can be determined by integrating the stem EPC readings. However, several forces that could not be directly determined from the EPC readings had to be assumed (Fig. 5.29). First, the lateral force P_{heel} on the heel of the footing was assumed to be that due to the theoretical active earth pressure distribution acting on the back face of the footing heel. Second, since initial readings for the EPCs installed around the footing were not taken until after soil had been placed in front of the

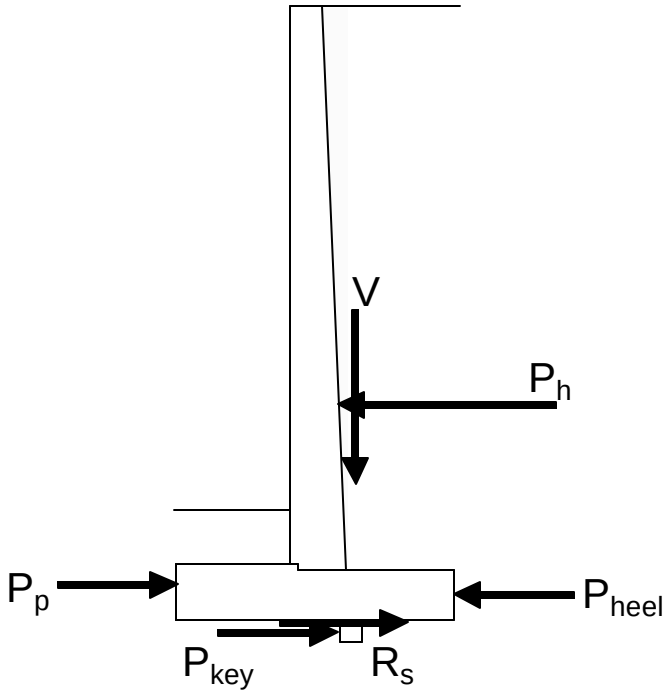

Figure 5.29. Forces on cantilever retaining wall, including the frictional resistance to sliding R_s.

footing, an existing lateral pressure was assumed for EPC_toe and EPC_key. Jaky's [1] expression for K_0 was used to estimate the at-rest earth pressure. Also, the distribution of lateral earth pressure in front of the toe was taken to be linear; thus, EPC_toe was used to determine the total resistance P_p of the soil in front of the footing. Finally, the total normal force V at the

interface was estimated using the dimensions of the retaining wall and the backfill height, as well as a unit weight of 150 pcf (23.6 kN/m^3) for the concrete and 120 pcf (18.9 kN/m^3) for the backfill.

After these other forces were determined, the net tangential force R_s, which is the frictional resistance to sliding, was found using equilibrium of horizontal forces:

$$R_s = P_h + P_{heel} - P_p - P_{key} \tag{5.2}$$

The coefficient of interface friction is then found by dividing the frictional force by the normal force, which is the vertical force V:

$$m = \frac{R_s}{V} \tag{5.3}$$

Finally, the angle of interface friction d can be found from the coefficient of friction:

$$d = \arctan m \tag{5.4}$$

The mobilized interface friction angle during the backfilling of Panel BJ is plotted along with the pressure at EPC_toe in Fig. 5.30. The highest value measured for the mobilized friction angle was 21º, which occurred in the afternoon of the fourth day of backfilling (October 31, 2002). The mobilized interface friction decreased after this, partly due to the further development of the passive resistance of the soil in front of the footing and partly due to the decrease in earth pressure on the stem toward the active case. Such changes decreased the amount of frictional resistance required for equilibrium.

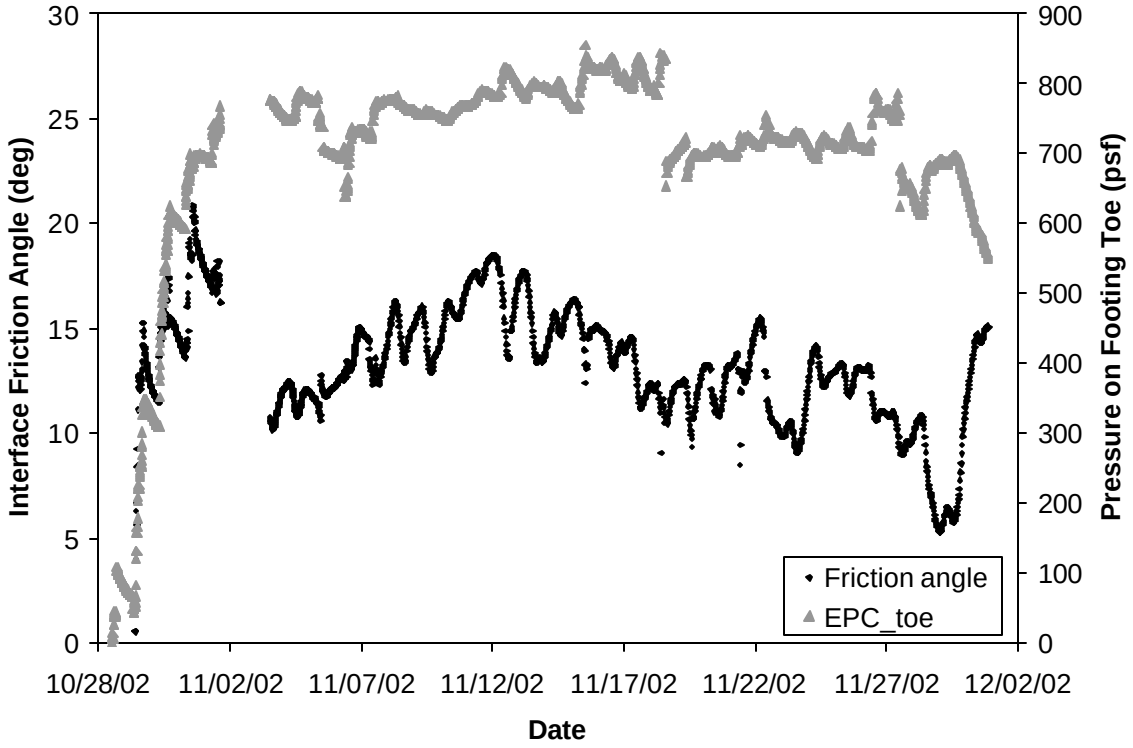

Figure 5.30. Mobilized friction angle at soil-footing interface and earth pressure on footing toe during backfilling.

"Passive" Earth Pressure

Since the footing toe was covered with soil before initial measurements of EPCs were taken, the pressure recorded at EPC_toe was the increase in pressure from at-rest. Therefore, in comparing the readings from EPC_toe to the theoretical passive pressure, it was necessary to account for the lateral stress that was not measured. EPC_toe was covered by approximately 3.5 ft (1.1 m) of soil. This soil, though suitable for backfilling, was not of the same quality as that placed behind the wall. Assuming a more conservative friction angle of 35º and a unit weight of 110 pcf (17.3 kN/m^3), this gives 164 psf (7.9 kPa) for the at-rest pressure. For 3.5 ft (1.1 m) of soil, the fully passive pressure would be 1421 psf (68.0 kPa), so the maximum expected increase in pressure would be 1257 psf (60.2 kPa). In comparison, the maximum pressure recorded for EPC_toe was about 840 psf (40.2 kPa).

In contrast, 25 ft (7.6 m) of soil had been placed above EPC_key at the end of backfilling in November 2002. Hence, the fully passive pressure at the shear key would be 12,068 psf (578 kPa), assuming a friction angle of 35º and a unit weight of 120 pcf (18.9 kN/m^3). Subtracting the at-rest pressure of 1195 psf (57 kPa) gives the maximum expected increase in pressure at EPC_key of 10,873 psf (521 kPa). However, the maximum earth pressure recorded by EPC_key in fall 2002 was only about 550 psf (26 kPa). The pressure reached a maximum of 800 psf in late June 2003; EPC_key ceased functioning shortly thereafter.

Readings from EPC_toe and EPC_key showed that the toe provided more resistance to sliding than the shear key (Fig. 5.31). In fact, the pressure at EPC_key was less than half of what would be expected simply for the placement of 25 ft (7.6 m) of soil above it (Fig. 5.32). This is consistent with the observation that the soil around the shear key was relatively loose.

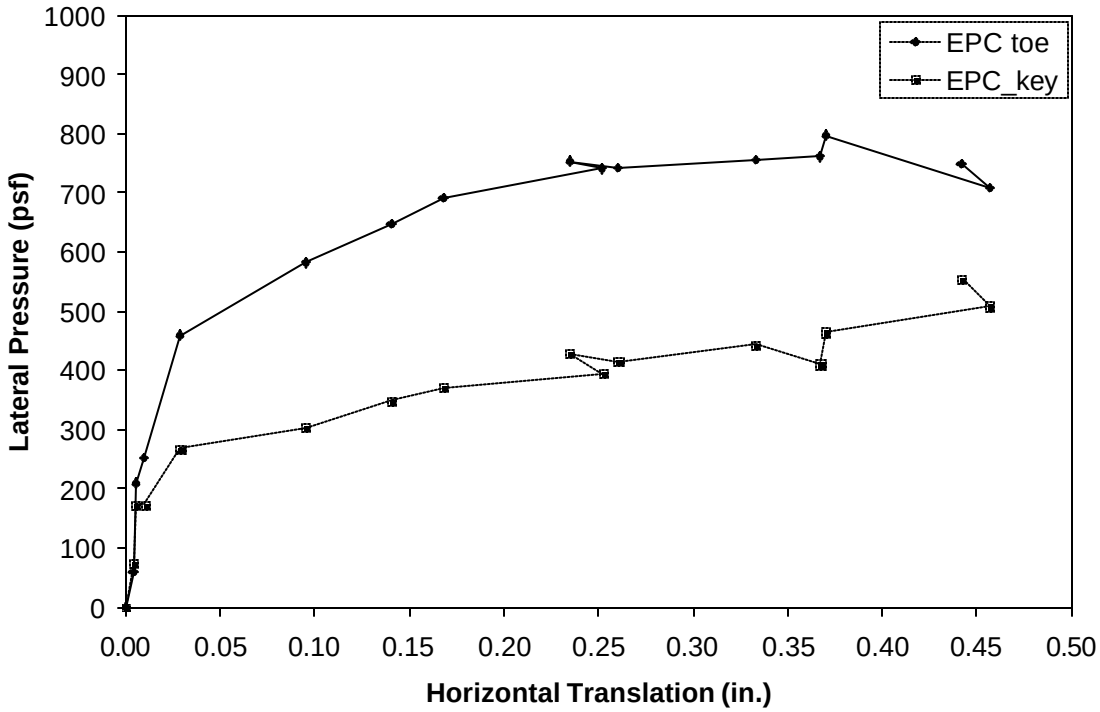

Figure 5.31. Change in lateral pressure at toe and in front of shear key with horizontal translation.

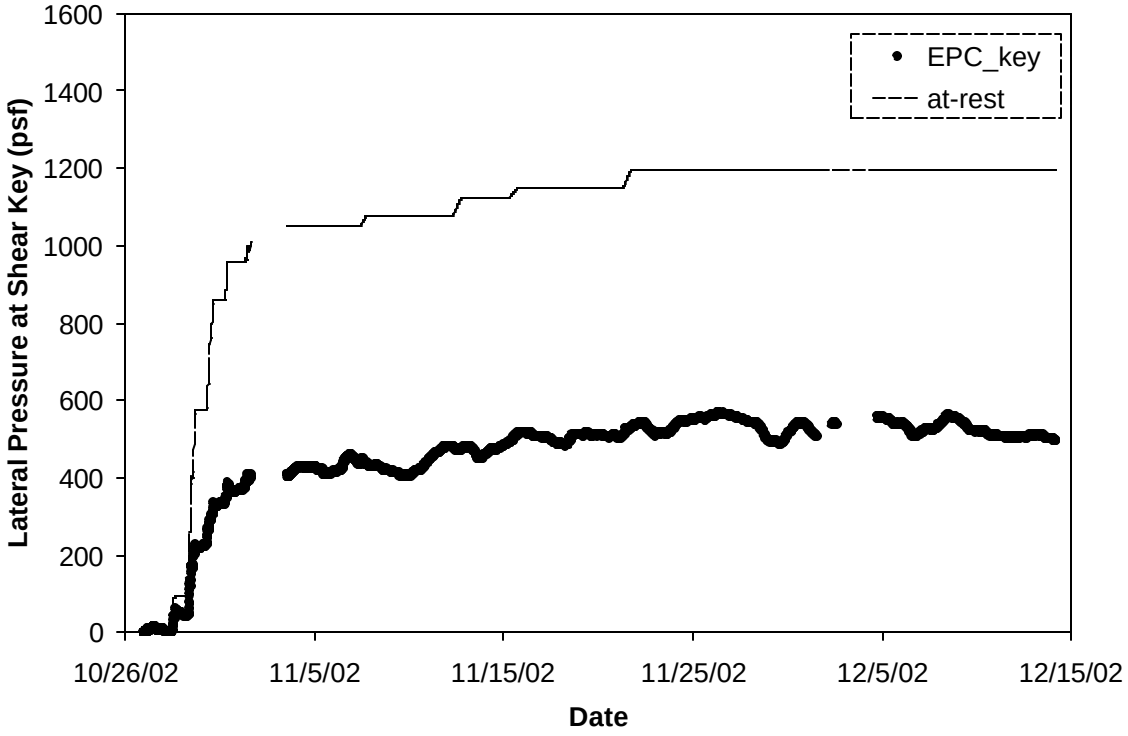

Figure 5.32. Comparison between lateral pressure in front of shear key and at-rest pressure.

Shear Key Performance

The readings from EPC_key demonstrated that the earth pressure on the shear key was much less than the fully passive earth pressure commonly assumed in design. One reason is that the amount of displacement required to completely mobilize passive earth pressure is about an order of magnitude higher than that required to achieve the active condition [4, 8]. Another factor is that the method in which the shear key is commonly constructed inhibits its performance. For example, the soil beneath the footing was compacted with a vibratory roller after it had been excavated to the proper elevation. Then a small backhoe was used to dig the 1 ft (300 mm) wide by 1 ft (300 mm) deep trench for the shear key. Plywood sheets with wooden spacers were used to keep the sides of the trench from collapsing. Once the shear key form was in place, little or no mechanical compaction was performed on the soil that had been disturbed by the excavation process. This was because compaction using a vibratory roller would have likely caused collapse of the formwork.

It seems that a shear key is effective only as a safeguard to prevent ultimate failure by sliding. If the wall were to translate several inches, passive pressure developed at the shear key would likely stop further movement of the wall. However, this situation is probably rare [29].

Comparison to Footing Toe

The footing toe developed lateral earth pressure that was over two-thirds of the theoretical fully passive pressure. In contrast, the shear key did not develop increased pressure beyond what would be expected due to the placement of backfill (Fig. 5.32). There was no evidence for passive pressure at the shear key. In addition, it is debatable that even the expected at-rest pressure conditions would exist were no wall movement to occur, since the soil surrounding the shear key was relatively loose and uncompacted due to the construction method. This suggests a difference between design assumptions and actual load conditions.

Furthermore, the passive resistance on the front face of the wall and the face of the footing toe is commonly ignored in design. Since the depth of soil is much less in front of the retaining wall than behind the wall, the amount of movement required to mobilize the full passive resistance on the face of the footing toe is considerably less than that required for a shear key located anywhere between directly below the stem and the footing heel. Consider Panel BJ. For the soil behind the wall, the depth was 25 ft (7.62 m) when construction was halted due to winter. The soil surface was 27.75 ft (8.46 m) above the shear key. For the soil in front of the wall covering the footing toe, the soil height was 4.75 ft (1.45 m). This difference in the effective wall height at the two positions may not be considered in designs where the passive resistance due to the shear key is included but the passive resistance due to the soil in front of the footing is ignored. Estimates of the amount of movement required to achieve the fully passive state range from $0.005H$ in dense sand [23] to $0.02H$ for medium dense sand [8]. If a value of $0.01H$ is assumed [4], the lateral movement necessary to bring about the fully passive condition at the shear key of Panel BJ was 3.3 in. (84 mm) but only 0.57 in. (14 mm) at the footing toe. Recall that the horizontal translation of Panel BJ was about 0.45 in. (11 mm) at the end of backfilling and that EPC_toe registered lateral earth pressure that was about 67% of the theoretical fully passive pressure.

Calculation of $FS_{sliding}$

The evidence, therefore, points to the conclusion that a shear key adds little benefit to the performance of a cantilever retaining wall at working loads. While it is evident that a shear key would add significant resistance in preventing a retaining wall from undergoing a catastrophic sliding failure, such a scenario is unlikely assuming sound construction practices [29]. However, let us consider the retaining wall in this study and calculate the factor of safety against sliding, for which the required value is 1.5. The interface friction angle δ is often taken to be one-half to two-thirds of ϕ. However, Mn/DOT assumes the coefficient of friction μ along the base to be 0.55, equivalent to $\delta = 28.8^{\circ}$, or 82.3% of $\phi = 35^{\circ}$. While this may seem somewhat unconservative, the footing for these walls is poured on site. The concrete adheres to the particles of the base soil, and upon curing its bottom surface is essentially rough. Potyondy [30] found that for rough concrete on sand, the ratio of the interface friction angle δ to the soil's friction angle ϕ exceeded 0.9. Thus, using $\delta = 0.832\phi$ may be justified for poured footings. Following Mn/DOT's design procedure, the coefficient of friction μ is 0.55, while the effect of the soil in front of the wall is ignored. The backfill has a unit weight $\gamma = 125$ pcf (19.6 kN/m^3) and a friction angle $\phi = 35^{\circ}$. Thus, the factor of safety for a wall with a 26-ft (7.92-m) stem is calculated from

$$FS_{sliding} = \frac{\sum F_R}{\sum F_D} = \frac{mV + \frac{h + \left(h + d_{key}\right)}{2} K_p d_{key} g}{\frac{1}{2} K_a \left(h + d_{key}\right)^2 g} \tag{5.5}$$

where the total vertical force V is

$$V = g h_{bf} \frac{\left(L_1 + L_2\right)}{2} + g_c A_c \tag{5.6}$$

For a wall with a 26-ft stem (i.e. h_{bf} = 26 ft), the area of the concrete A_c is 84.5 ft^2 (7.85 m^2). The lengths L_1, L_2, and L_3 are dimensions of the wall defined as shown in Fig. 5.33. Hence the total vertical force is

$$V = 125 * 26 * \frac{\left(5 + 6.08\right)}{2} + 150 * 84.5 = 30{,}680 \text{ lb} \tag{5.7}$$

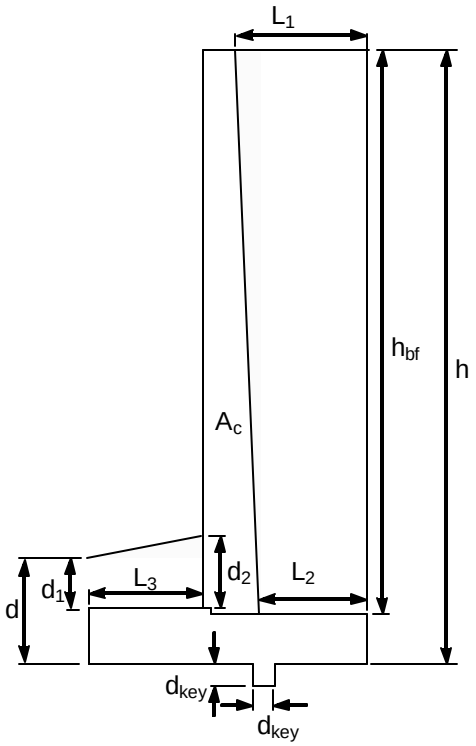

Figure 5.33. Dimensions of cantilever retaining wall.

and the factor of safety is

$$FS_{sliding} = \frac{0.55*30680 + \frac{28.25+(28.25+1)}{2}*3.69*1*125}{\frac{1}{2}*0.271*(28.25+1)^2*125} = 2.08 \quad (5.8)$$

where d_{key} is the height of the shear key (1 ft in this case) and h is 28.25 ft (8.61 m).

Values for the factor of safety against sliding were calculated using Mn/DOT's design procedure, both without a shear key and with a shear key, for stem heights from 20 – 30 ft (6.1 – 9.1 m). These values are given in columns 2 and 3, respectively, of Table 5.1. Note that the wall with a 20-ft stem has no shear key and has $FS_{sliding}$ = 1.52. When using Mn/DOT's design assumptions, the taller walls do not meet the required factor of safety of 1.5 if they do not have a shear key. Conversely, when the factor of safety is calculated with the shear key, the values are in excess of the required value of 1.5.

Table 5.1. Factor of safety against sliding for Mn/DOT cantilever retaining walls.

Stem height (ft)	FS w/o shear key	FS with shear key	FS w/o key, using P_p
20 (no key)	1.52	n/a	2.27
21	1.41	2.45	2.12
22	1.32	2.33	1.98
23	1.31	2.26	1.90
24	1.27	2.20	1.83
25	1.25	2.14	1.76
26	1.24	2.09	1.71
27	1.22	2.04	1.66
28	1.20	1.99	1.60
29	1.18	1.94	1.55
30	1.19	1.92	1.53

However, considering the experimental finding that the soil in front of the wall provided considerable resistance to sliding while the shear key provided little resistance, it is reasonable to use a modified factor of safety calculation, one which includes the effect of the soil in front of the wall but ignores the shear key. Hence, consider the same 26-ft (7.92-m) high wall, but with no shear key. The concrete area is then 83.5 ft^2 (7.76 m^2). The resistance of the soil in front of the wall is included in the following equation:

$$FS_{sliding} = \frac{\sum F_R}{\sum F_D} = \frac{mV + \frac{1}{2}K_p d^2 g}{\frac{1}{2}K_a h^2 g} \quad (5.9)$$

where d = 4.74 ft (1.44 m) is the depth from the soil surface to the bottom of the footing toe. The total vertical force V includes the weight of the soil on the toe, which is assumed to have the same properties as the backfill:

$$V = gh_{bf}\frac{(L_1 + L_2)}{2} + g\frac{(d_1 + d_2)}{2} * L_3 + g_c A_c \tag{5.10}$$

where d_1, d_2, and L_3 are defined as shown in Fig. 5.33. Also note that for this case, A_c = 83.5 ft^2 (7.76 m^2) since the shear key has been removed. Then the total vertical force is

$$V = 125 * 26 * \frac{(5 + 6.08)}{2} + 125 * \frac{(2.20 + 3.95)}{2} * 5.25 + 150 * 83.5 = 32{,}548 \text{ lb} \tag{5.10}$$

Therefore, the factor of safety against sliding for no shear key is

$$FS_{sliding} = \frac{0.55 * 32548 + \frac{1}{2} * 3.69 * 4.74^2 * 125}{\frac{1}{2} * 0.271 * 28.25^2 * 125} = 1.71 \tag{5.12}$$

Values for the factor of safety against sliding for this modified design procedure, which takes into account the passive resistance in front of the toe, are given for stem heights from 20 – 30 ft (6.1 – 9.1 m) in the fourth column of Table 5.1.

Horvath [31] performed a finite element analysis following the general approach of Clough and Duncan [8] to explore the behavior of cantilever retaining walls with five different footing shapes: flat bottom, sloped bottom, shear key at the toe, key below the stem, and key at the heel. It was found that at working stresses, the walls all performed essentially the same with regard to rigid body rotation and translation. At peak stresses (~4 times the active pressure), the sloped bottom performed the best, followed by the key at the heel, the key below the stem, the flat bottom, and finally the key at the toe. Horvath's numerical finding supports the observation from this research that the shear key did not noticeably affect the performance of Panel BJ.

Chapter 6
Conclusions

The purpose of this research was to determine the earth pressure behind a reinforced concrete cantilever retaining wall designed by the Minnesota Department of Transportation (Mn/DOT). Mn/DOT's specified backfill material was classified as a poorly graded sand from a sieve analysis. Triaxial compression tests on several samples of the soil put the angle of internal friction in the range of 35° – 39°. A value of 37° was used for the prediction of earth pressures and stem deflections.

Instrumentation consisting of about 60 individual sensors was installed on a 26 ft (7.9 m) high panel of a cantilever wall along Interstate 494 in Bloomington, Minnesota. Earth pressure cells (EPCs) and tiltmeters were monitored for 12 months with nearly continuous data acquisition and remote modem access. Monitoring of strain gages on the reinforcing bars was also attempted, although the noise level exceeded the expected signal. In addition to this automated data acquisition, manual readings of wall movements were taken. A total station was used to monitor the position of four survey points on the wall during backfilling in fall 2002. An inclinometer probe was used to monitor two inclinometer casings within the wall during this time. Readings from strain gages installed within a second 26 ft (7.9 m) high panel were taken manually while it was backfilled in spring 2003.

The lateral earth pressure on the stem was observed to be active near the end of backfilling, with a resultant located at approximately one-third of the backfill height. The wall translated horizontally 0.45 in. (11 mm) away from the backfill and also moved downward about 0.42 in. (11 mm) as a rigid body. Throughout the backfilling process, wall translation of about 0.1% of the backfill height was necessary to develop the active condition. A tiltmeter mounted at the base of the stem showed that the wall rotated 0.03° into the backfill as a rigid body. Measurements of vertical stress below the footing confirmed that the wall rotated into the backfill, since the vertical stress was greater under the footing heel than under the footing toe. The stem deformed elastically such that the top of the wall deflected 0.16 in. (4 mm) away from the backfill.

In order to predict deflections, the wall was modeled as a cantilever beam with a clamped support, and the stem was approximated as a piecewise constant beam, taking into account the presence of the steel reinforcement using the transformed section method. The measured deflections were between deflections predicted using the loading due to the theoretical earth pressure and those predicted using the integrated EPC measurements. Strains measured on the reinforcing bars within a second panel were used to back-calculate the load on the wall stem. This was found to compare very well with the theoretical active force, and, assuming a unit weight of 120 pcf (18.9 kN/m^3), a friction angle of 37.5° was determined from this back-calculated force.

A load test performed by parking two 45,000 lb (200 kN) trucks on the backfill above the wall produced little wall movement and had the observed effect of decreasing the earth pressure at the EPCs, which were all at least 10 ft (3 m) below the soil surface. However, noting that elasticity theory predicts the lateral stress increase due to a point load to be greatest relatively close to the surface, it was thought that the wall's small deflection away from the soil had a greater effect on

the EPCs than the surface load had. The movement of the wall away from the backfill decreased the lateral earth pressure on the EPCs.

Sensor readings during the backfilling process showed the complexity of the evolution of the earth pressure distribution on the wall. Evidence for residual lateral stresses from the compaction process was found in the readings of the stem EPCs, and the tiltmeter readings also suggested residual effects from compaction. Translation of the wall overnight following the construction workday reduced both the compaction-induced lateral stresses and stem deflections. Furthermore, it allowed stresses within the soil to redistribute, a phenomenon recorded by the stem EPCs.

Changes in lateral earth pressure weeks after backfilling were attributed to changes in temperature and rainfall events. Daily variations in air temperature apparently created a gradient in temperature through the thickness of the wall stem, resulting in small changes in shape and subsequent movements of the wall that affected earth pressure. However, there appeared to be no permanent effect from the daily changes in temperature. Air temperatures well below the freezing point coincided with readings showing zero lateral earth pressure on the top part of the stem. This was attributed to water freezing within the soil and consequently creating a temporary cohesion. In warmer weather, rainfall caused a transient increase in lateral earth pressure because the water increased the unit weight of the soil until the backfill dried.

The behavior of the wall in sliding was examined. The mobilized friction angle along the interface between the footing and the soil below was determined to be 21° at its highest value. Horizontal translation of the wall caused the development of earth pressure in front of the footing toe that was about two-thirds of the fully passive pressure. The wall movement was 0.8% of the soil height at this location, which is comparable to Terzaghi's prediction of 1% for the fully passive condition. In contrast, it was found that the earth pressure in front of the shear key on the bottom of the footing was less than would have been expected simply due to the placement of backfill above. This was likely due to the difficulty in constructing the shear key, which caused the surrounding soil to be poorly compacted. Furthermore, the wall movement was only about 0.1% of the soil height above the shear key. With this in mind, the factor of safety against sliding was calculated using Mn/DOT's design assumptions and using a modified method that accounted for the resistance of the soil in front of the wall but disregarded the shear key. Using this modified approach, the factor of safety against sliding was calculated for walls with no shear key. For walls with stem heights up to 30 ft (9.1 m), $FS_{sliding}$ still exceeded 1.5.

Recommendations

The data from this study show that Mn/DOT's design for cantilever retaining walls is reasonable, as active pressure developed. It is proposed that Mn/DOT's cantilever retaining wall design could be made more efficient by removing the shear key in certain situations. These situations would be limited to retaining walls 30 ft (9.1 m) or less in height, founded on granular soils, and for which the toe of the footing is covered with soil before the wall is completely backfilled. This "front-fill" should be granular and have properties similar to the design backfill material (γ = 125 pcf and f = 35°).

Future Work

Collection of data over a 12-month period suggested that some seasonal changes in earth pressure can occur. To make well-informed conclusions about this possible phenomenon, additional EPC and tiltmeter data spanning two complete seasonal cycles (essentially two years) is thought necessary. To this end, data collection is ongoing.

A finite element analysis of this retaining wall could help to better understand the earth pressure on the wall, as well as to possibly provide information that could further improve retaining wall design. It would also help in correlating the results of this study to numerical studies of other retaining walls. As previous numerical analyses and the results from this study show, an incremental analysis would be necessary to model the wall, since wall construction and especially backfilling are incremental processes.

References

1. J. Jaky (1944). The coefficient of earth pressure at rest. *Journal of the Society of Hungarian Architects and Engineers*, vol. 7: 355-358.
2. A.W. Bishop (1958). Test requirements for measuring the coefficient of earth pressure at rest. *Proceedings of the Brussels Conference on Earth Pressure Problems*, vol. I: 2-14.
3. N.R. Morgenstern and Z. Eisenstein (1970). Methods of estimating lateral loads and deformations. *Proceedings of ASCE Specialty Conference on Lateral Stresses in the Ground and Design of Earth Retaining Structures*. New York, NY: ASCE. 51-102.
4. K. Terzaghi (1934). Large retaining-wall tests—I. *Engineering News Record*, vol. 112: 136-140.
5. H.M. Coyle, R.E. Bartoskewitz, L.J. Milberger, and H.D. Butler (1974). Field measurements of lateral earth pressures on a cantilever retaining wall. *Transportation Research Record*, no. 517: 16-29.
6. R.B. Peck and H.O. Ireland (1961). Full-scale lateral load test of a retaining wall foundation. *Proceedings of the 5th International Conference on Soil Mechanics and Foundation Engineering*, vol. II: 453-458.
7. H.M. Coyle and R.E. Bartoskewitz (1976). Earth pressure on precast panel retaining wall. *Journal of the Geotechnical Engineering Division*, vol. 102, no. 5: 441-456.
8. G.W. Clough and J.M. Duncan (1971). Finite element analysis of retaining wall behavior. *Journal of the Soil Mechanics and Foundations Division*, vol. 97, no. 12: 1657-1673.
9. F.H. Kulhawy (1974). Analysis of a high gravity retaining wall. *Proceedings of the ASCE Conference on Analysis and Design in Geotechnical Engineering*. New York, NY: ASCE. 159-172.
10. L.E. Goodman and C.B. Brown (1963). Dead load stresses and the instability of slopes. *Journal of the Soil Mechanics and Foundations Division*, vol. 89, no. 3: 103-134.
11. R.W. Clough and R.J. Woodward (1967). Analysis of embankment stresses and deformations. *Journal of the Soil Mechanics and Foundations Division*, vol. 93, no. 4: 529-549.
12. A.T.C. Goh (1993). Behavior of cantilever retaining walls. *Journal of Geotechnical Engineering*, vol. 119, no. 11: 1751-1770.
13. G.F. Sowers, A.D. Robb, C.H. Mullis, and A.J. Glenn (1957). The residual lateral pressures produced by compacting soils. *Proceedings of the 4th International Conference on Soil Mechanics and Foundation Engineering*, vol. II: 243-247.
14. M.S. Aggour and C.B. Brown (1974). The prediction of earth pressure on retaining walls due to compaction. *Geotechnique*, vol. 24, no. 4: 489-502.
15. T.S. Ingold (1979). The effects of compaction on retaining walls. *Geotechnique*, vol. 29, no. 3: 265-283.

16. J.M Duncan and R.M. Seed (1986). Compaction-induced lateral pressure under K_0 conditions. *Journal of Geotechnical Engineering*, vol. 112, no. 1: 1-22.

17. Kulite Semiconductor Products, Inc. (2003). Leonia, NJ. Internet. www.kulite.com.

18. Geokon, Inc. (2003). Lebanon, NH. Internet. www.geokon.com.

19. Applied Geomechanics, Inc. (2003). *Tiltmeter temperature coefficients: source, definition, and use to improve accuracy*. Report no. B-95-1005, Rev. C.

20. B.A. Theroux, J.F. Labuz, and A. Drescher (2000). *Calibration of an earth pressure cell*. Report no. MN/RC-2000-34. St. Paul: Minnesota Department of Transportation.

21. J.F. Labuz and B.A. Theroux (2004). Laboratory calibration of earth pressure cells. *Geotechnical Testing Journal*. In press.

22. Minnesota Department of Transportation (2000). *Standard Specifications for Construction*. 717-720.

23. B.M. Das (2000). *Fundamentals of Geotechnical Engineering*. Pacific Grove, CA: Brooks/Cole.

24. J.G. MacGregor (1997). *Reinforced Concrete: Mechanics and Design*. 3rd ed. Upper Saddle River, NJ: Prentice Hall. 337-340.

25. M.G. Spangler (1938). Horizontal pressures on retaining walls due to concentrated surface loads. *Bulletin of the Iowa Engineering Experiment Station*. No. 140.

26. Minnesota Climatology Working Group, Historical Climate Data Retrieval (cited April 2004). Internet. http://climate.umn.edu/doc/historical.htm.

27. H.M. Westergaard (1926). Analysis of stresses in concrete pavements due to variations of temperature. *Proceedings of the Highway Research Board*. U.S. Bureau of Public Roads, vol. 6, 201-215.

28. M.E. Haar and G.A. Leonards (1959). Warping stresses and deflections in concrete pavements. *Proceedings of the Highway Research Board*. U.S. Bureau of Public Roads, vol. 33, 167-184.

29. R.B. Peck, H.O. Ireland, and C.Y. Teng (1948). A study of retaining wall failures. *Proceedings of the 2nd International Conference on Soil Mechanics and Foundation Engineering*. Rotterdam, vol. III, 296-299.

30. J.G. Potyondy (1961). Skin friction between various soils and construction materials. *Geotechnique*, vol. 11, no. 4: 339-353.

31. J.S. Horvath (1991). Effect of footing shape on behavior of cantilever retaining wall. *Journal of Geotechnical Engineering*, vol. 117, no. 6: 953-978.

Additional References

[1] J. Dunnicliff (1993). *Geotechnical Instrumentation for Monitoring Field Performance*. New York, NY: John Wiley & Sons.

[2] R.E. Sennett (1994). *Matrix Analysis of Structures*. Prospect Heights, IL: Waveland Press.

Appendix A

Earth Pressure Cell Calibrations

Kulite Uniaxial Calibrations

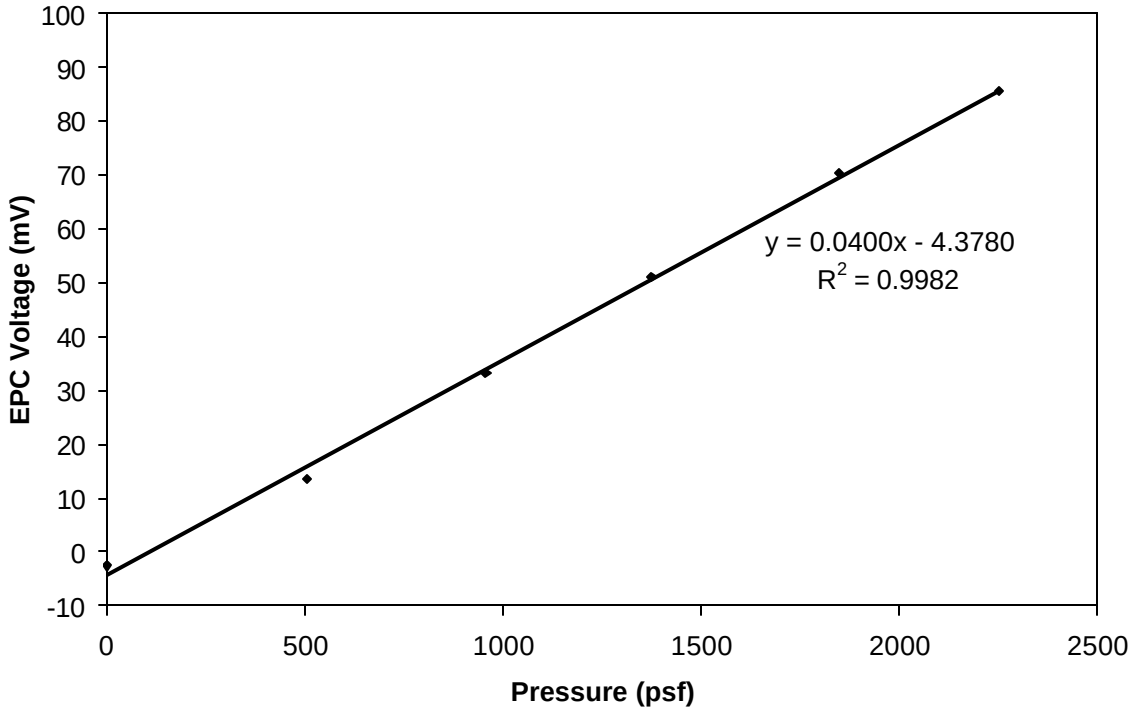

Figure A.1. Uniaxial calibration plot for Kulite EPC_1.

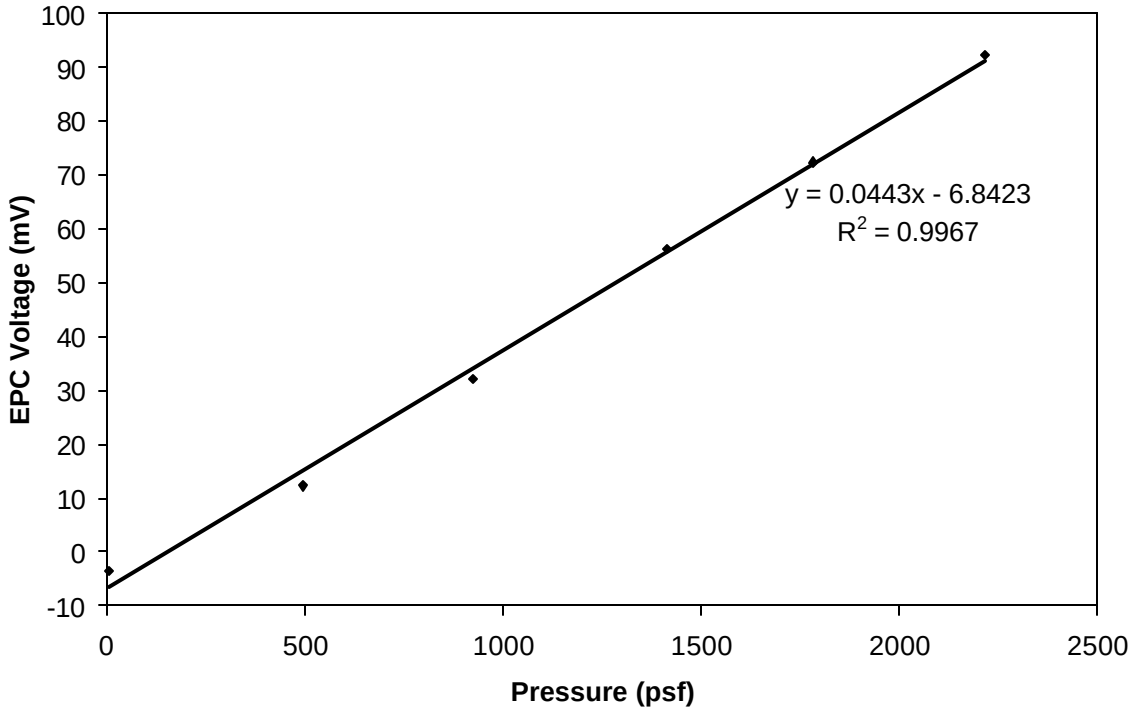

Figure A.2. Uniaxial calibration plot for Kulite EPC_5.

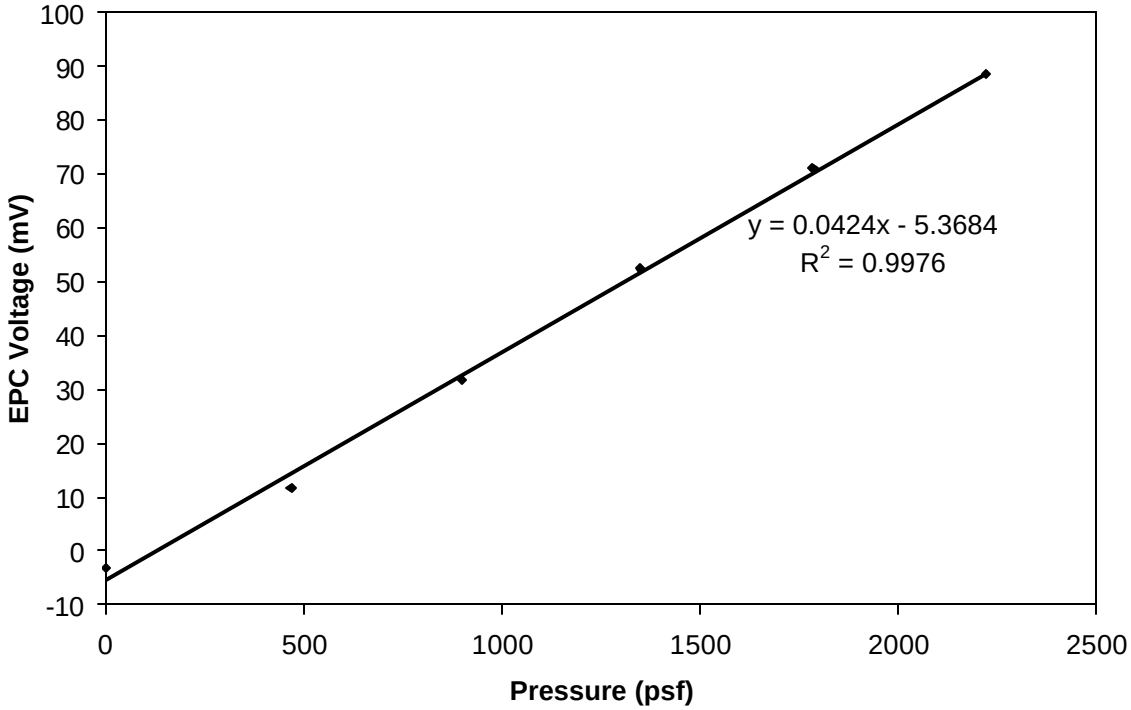

Figure A.3. Uniaxial calibration plot for Kulite EPC_10.

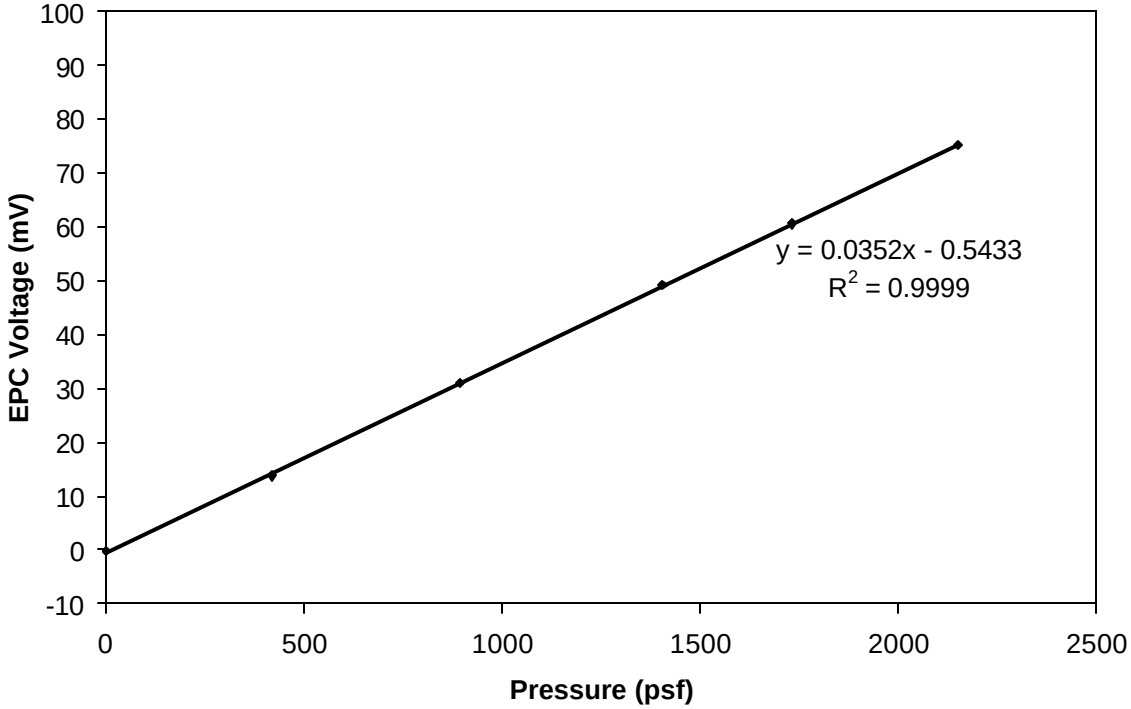

Figure A.4. Uniaxial calibration plot for Kulite EPC_15.

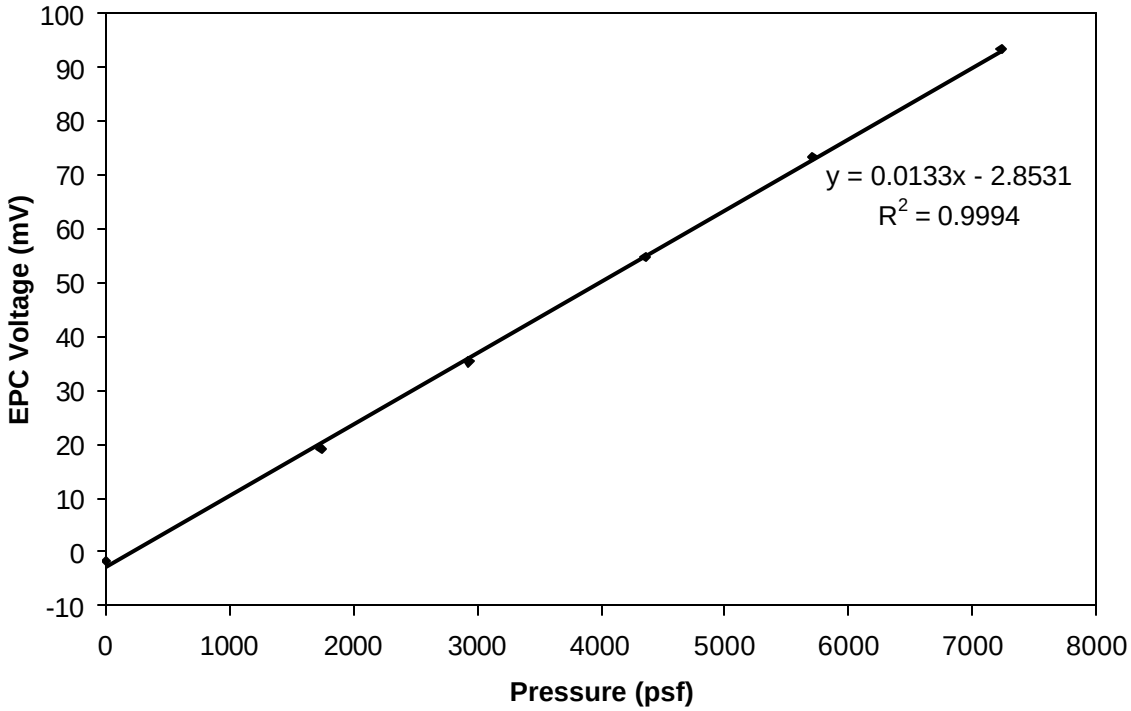

Figure A.5. Uniaxial calibration plot for Kulite EPC_front.

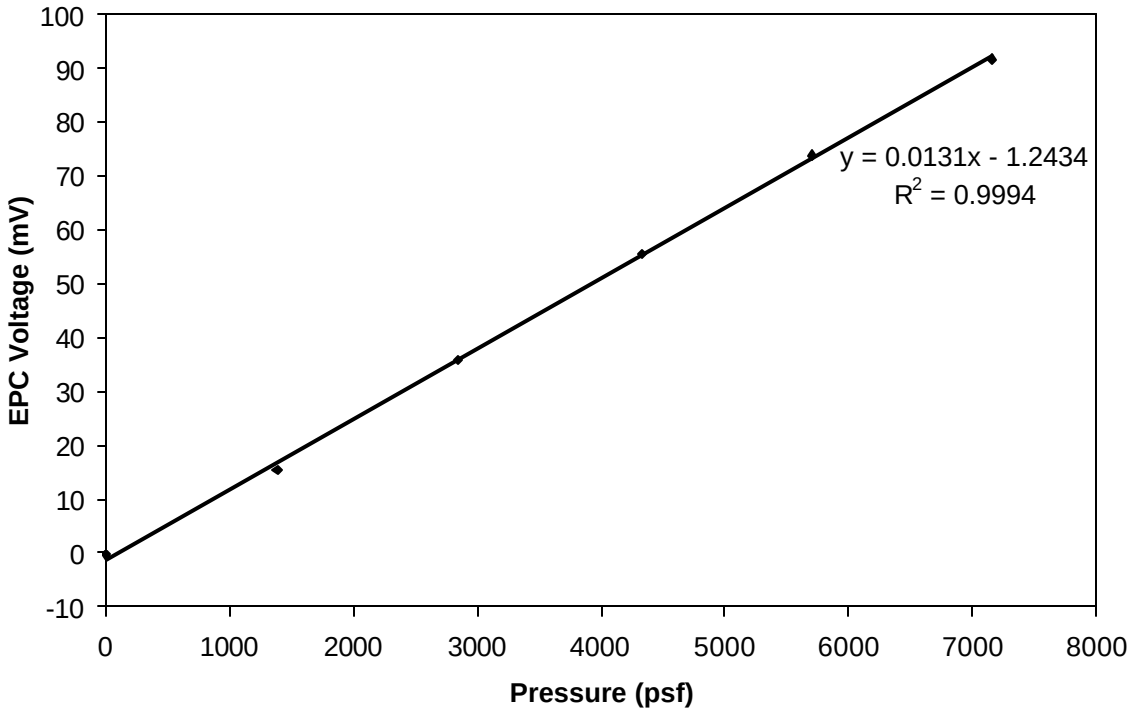

Figure A.6. Uniaxial calibration plot for Kulite EPC_back.

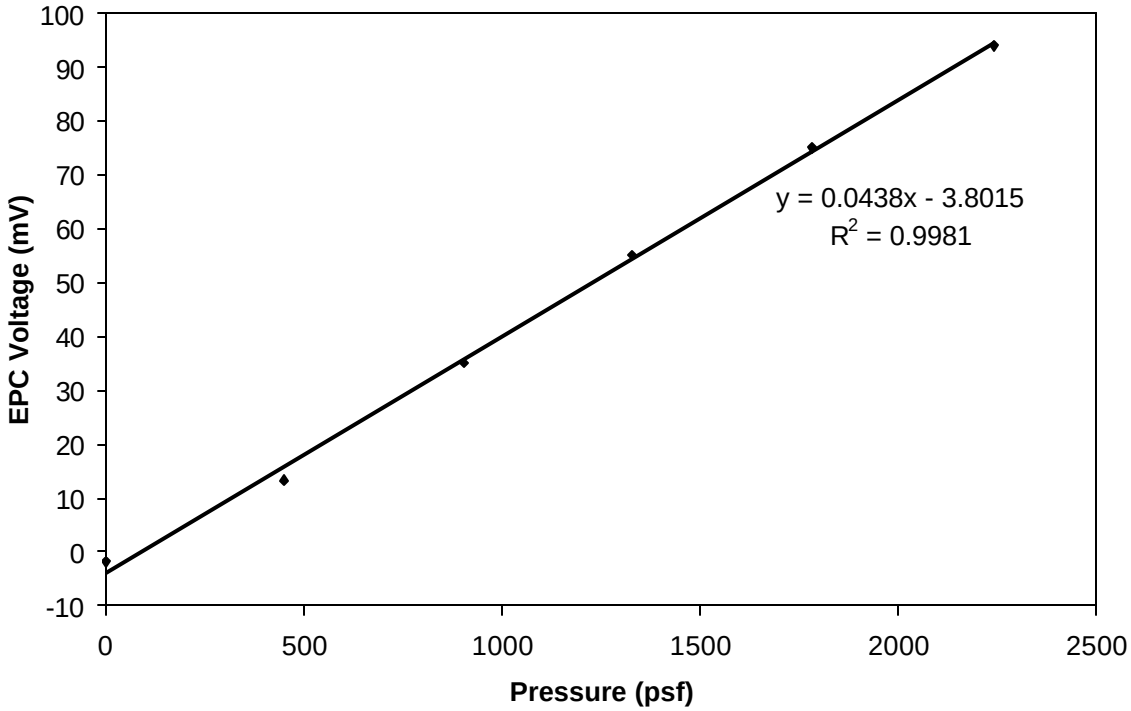

Figure A.7. Uniaxial calibration plot for Kulite EPC_toe.

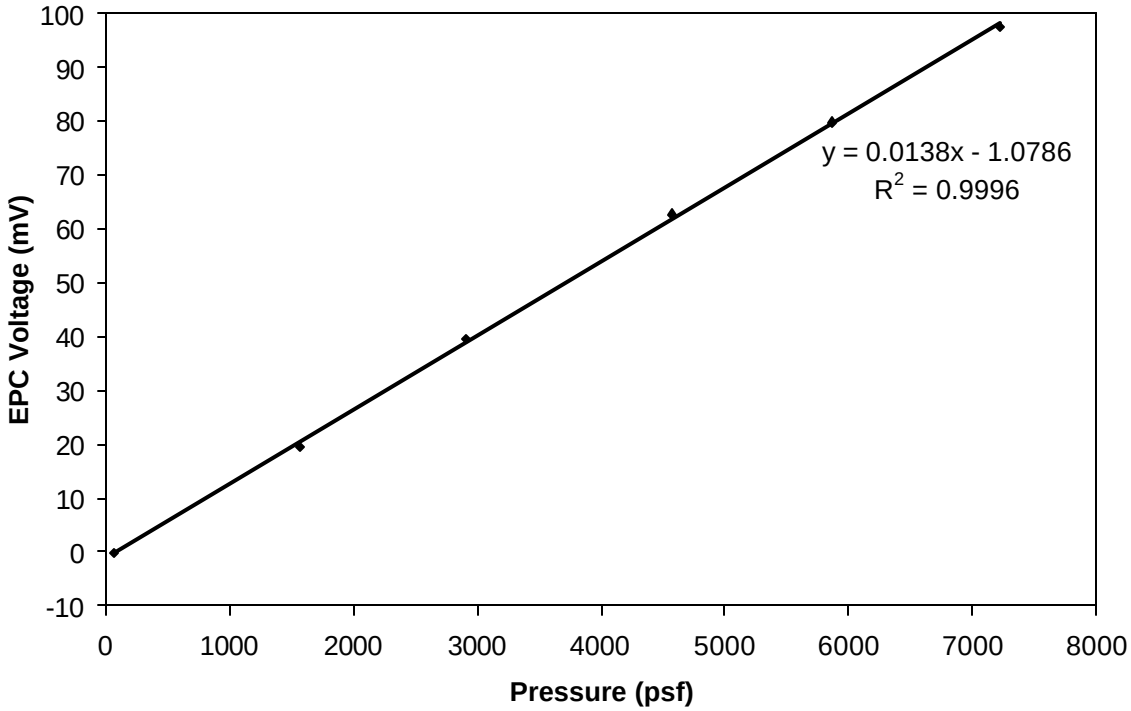

Figure A.8. Uniaxial calibration plot for Kulite EPC_key.

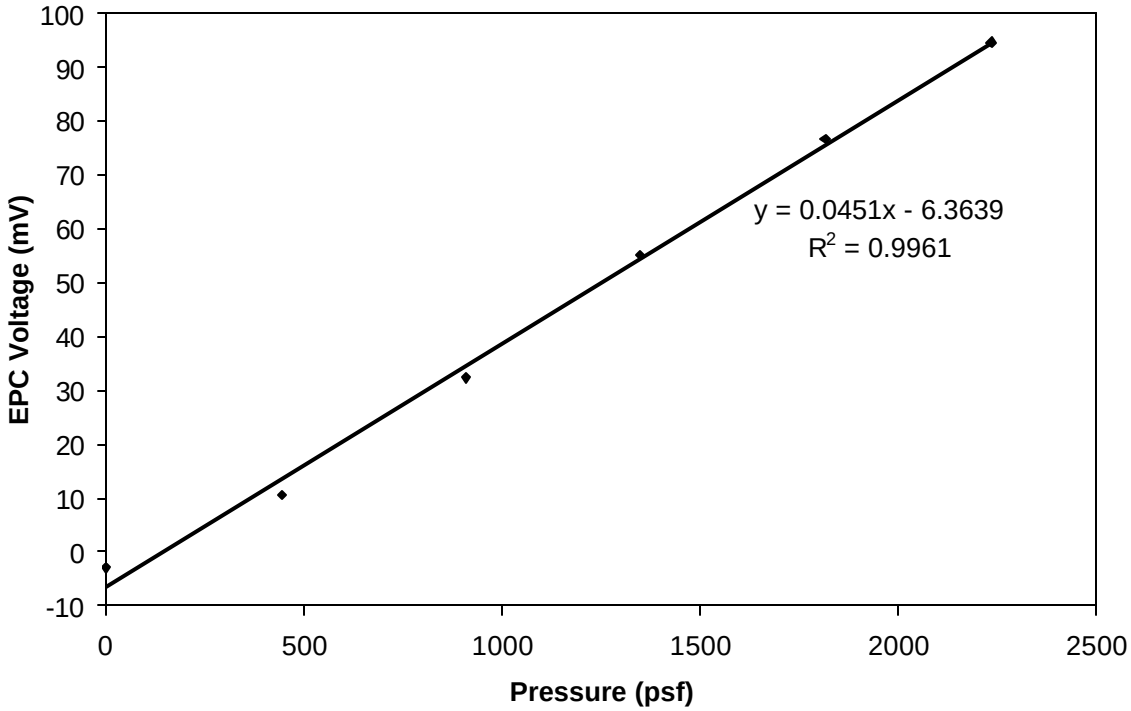

Figure A.9. Uniaxial calibration plot for Kulite EPC_bf.

Kulite Universal Calibrations

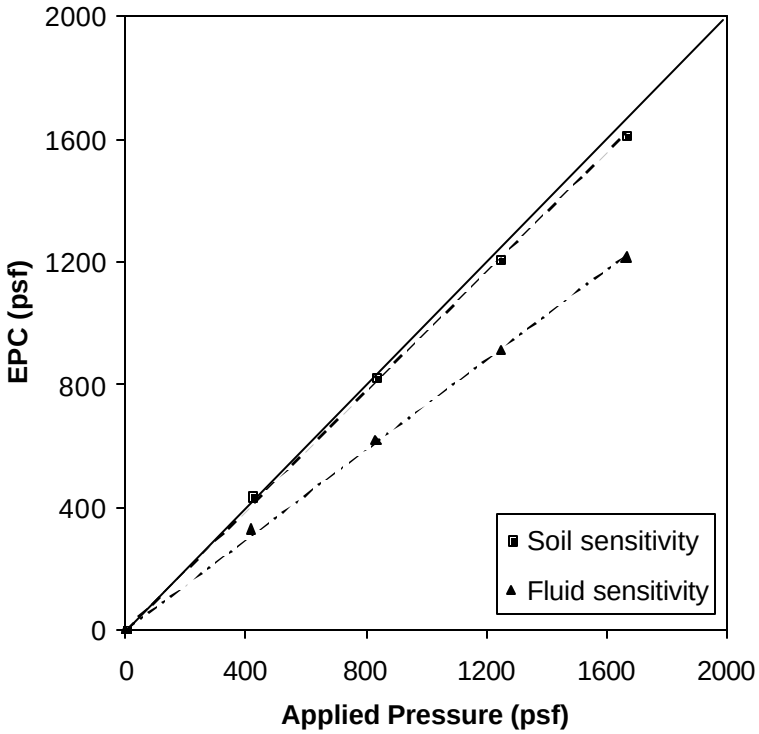

Figure A.10. Response of Kulite EPC_bf within universal calibration chamber.

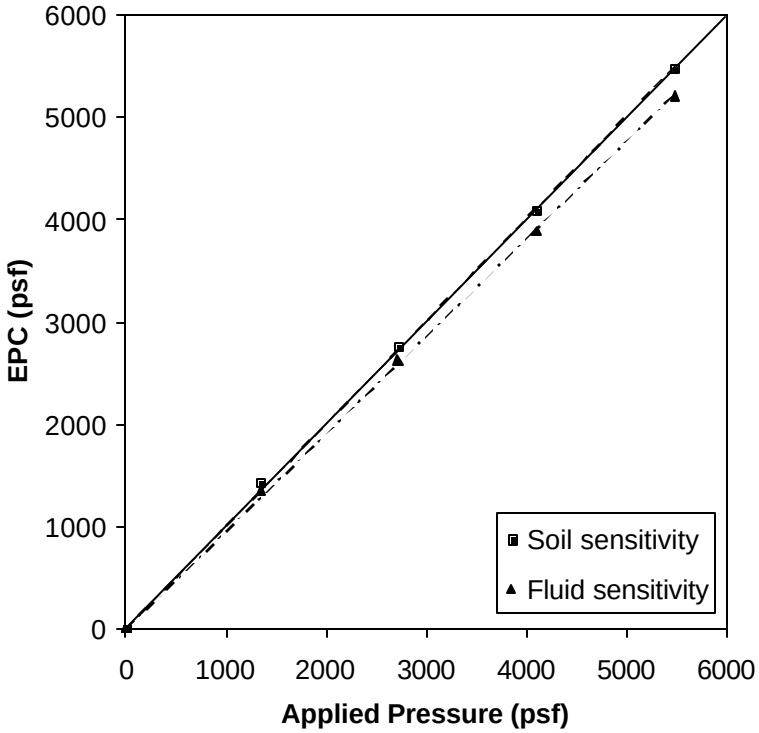

Figure A.11. Response of Kulite EPC_front within universal calibration chamber.

Geokon Universal Calibrations

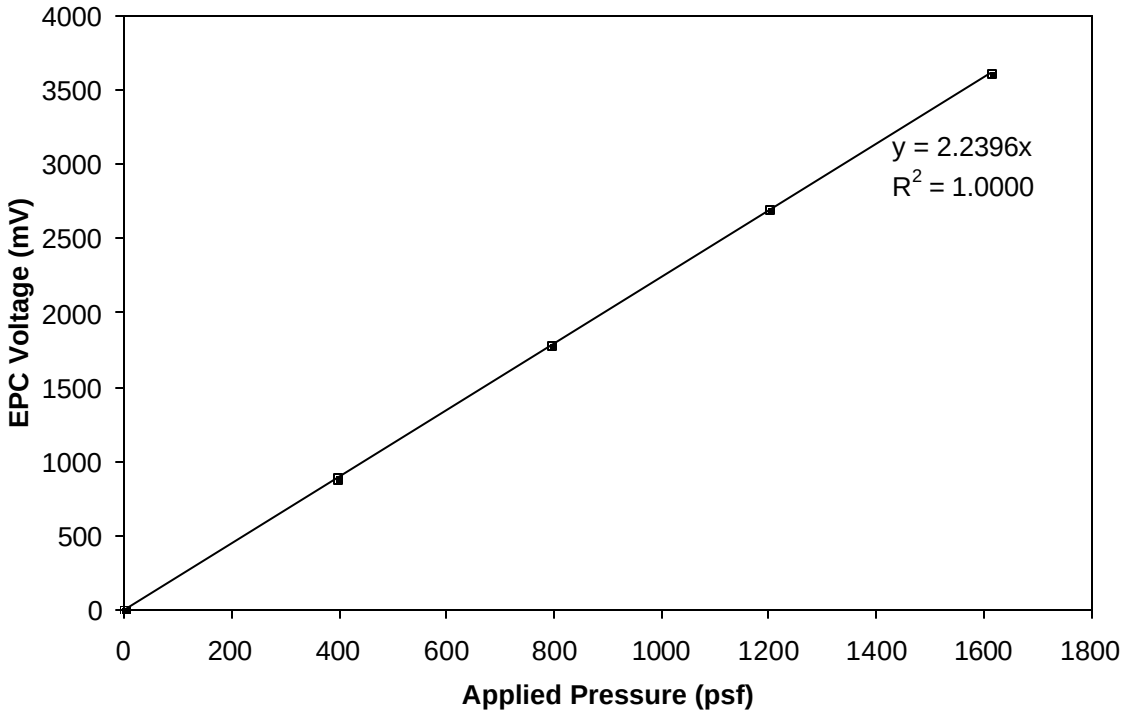

Figure A.12. Universal calibration plot for Geokon EPC_1.

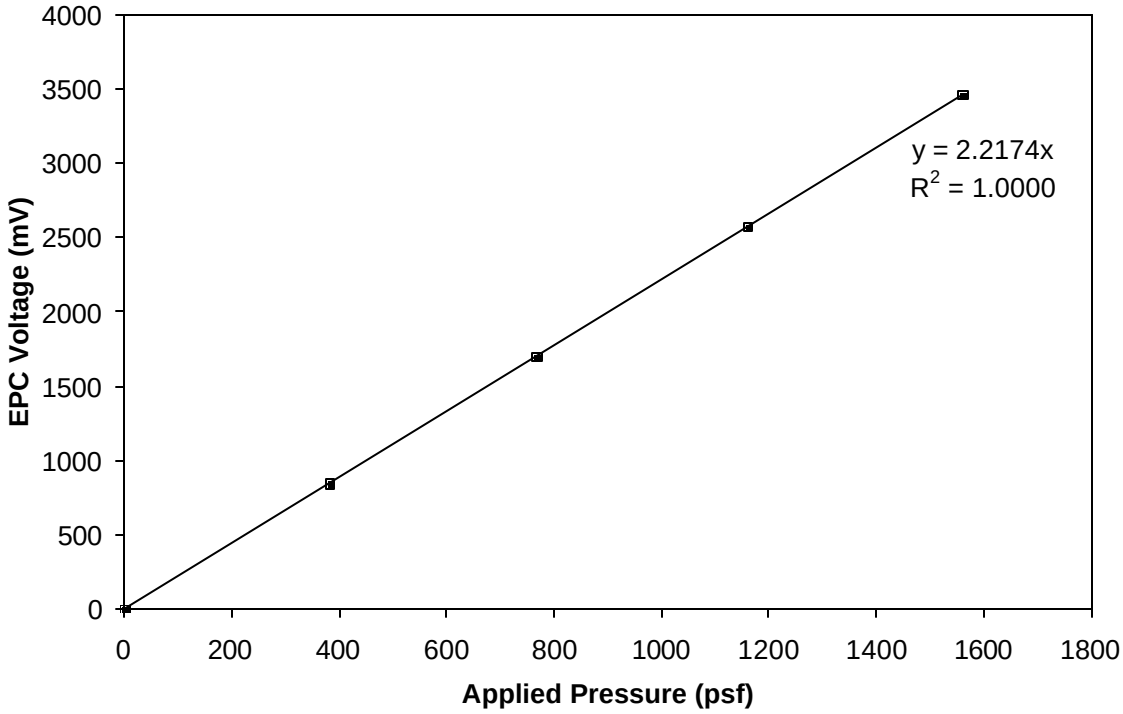

Figure A.13. Universal calibration plot for Geokon EPC_5.

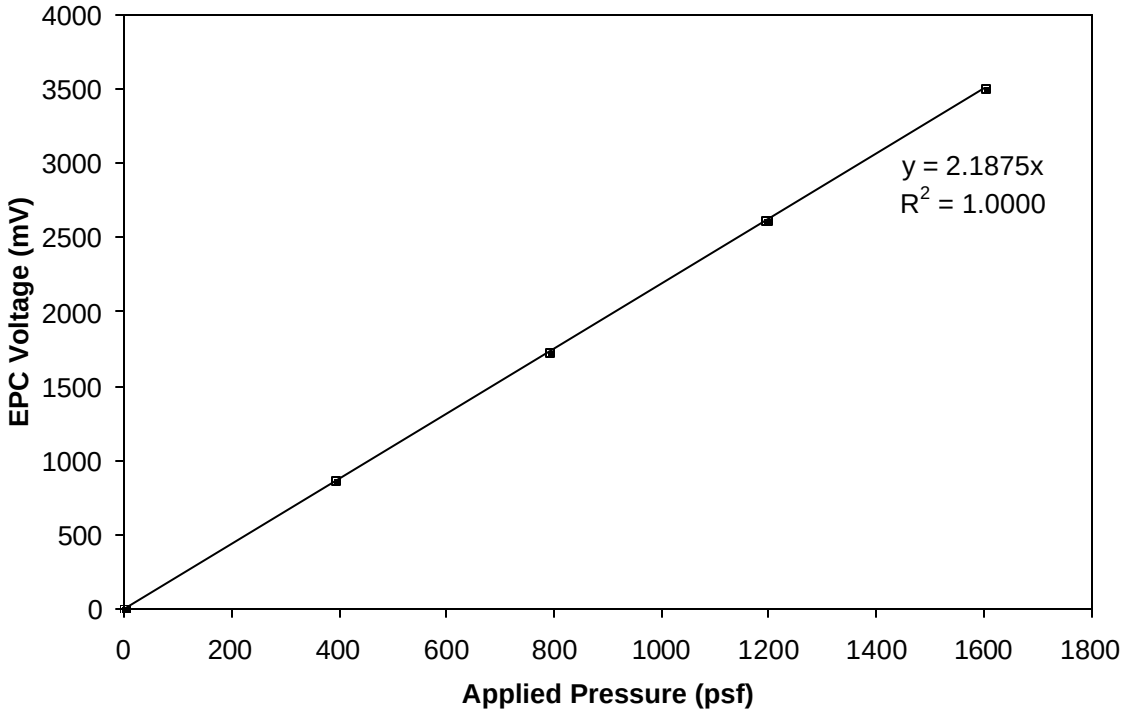

Figure A.14. Universal calibration plot for Geokon EPC_10.

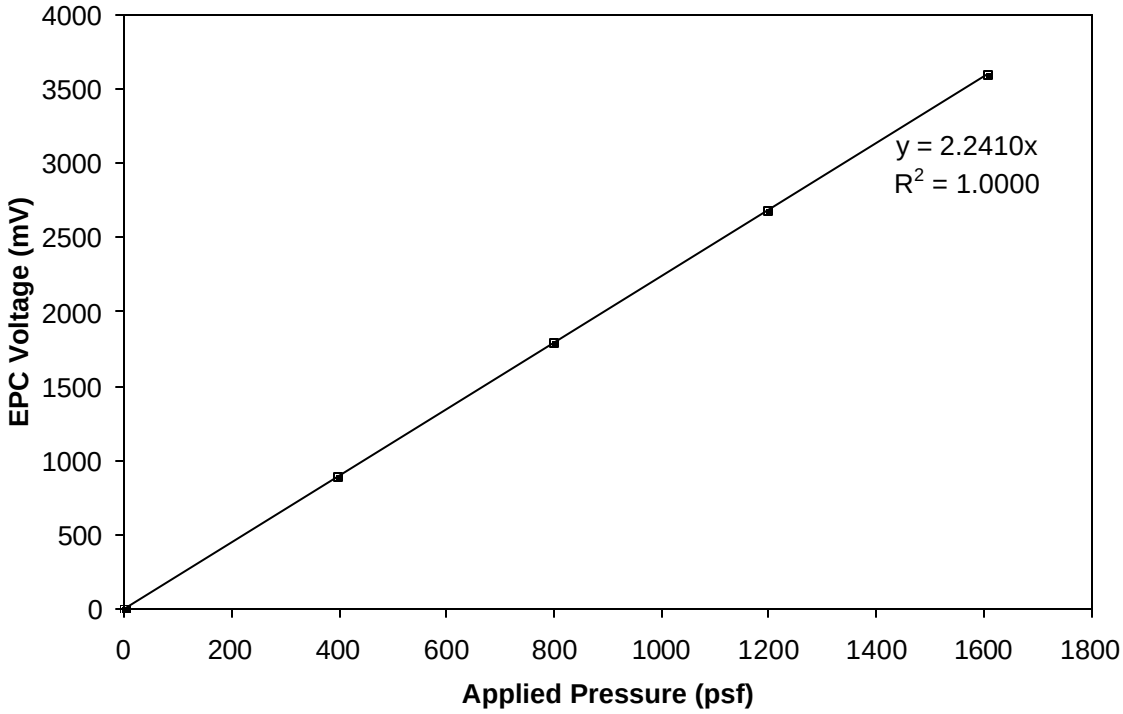

Figure A.15. Universal calibration plot for Geokon EPC_15.

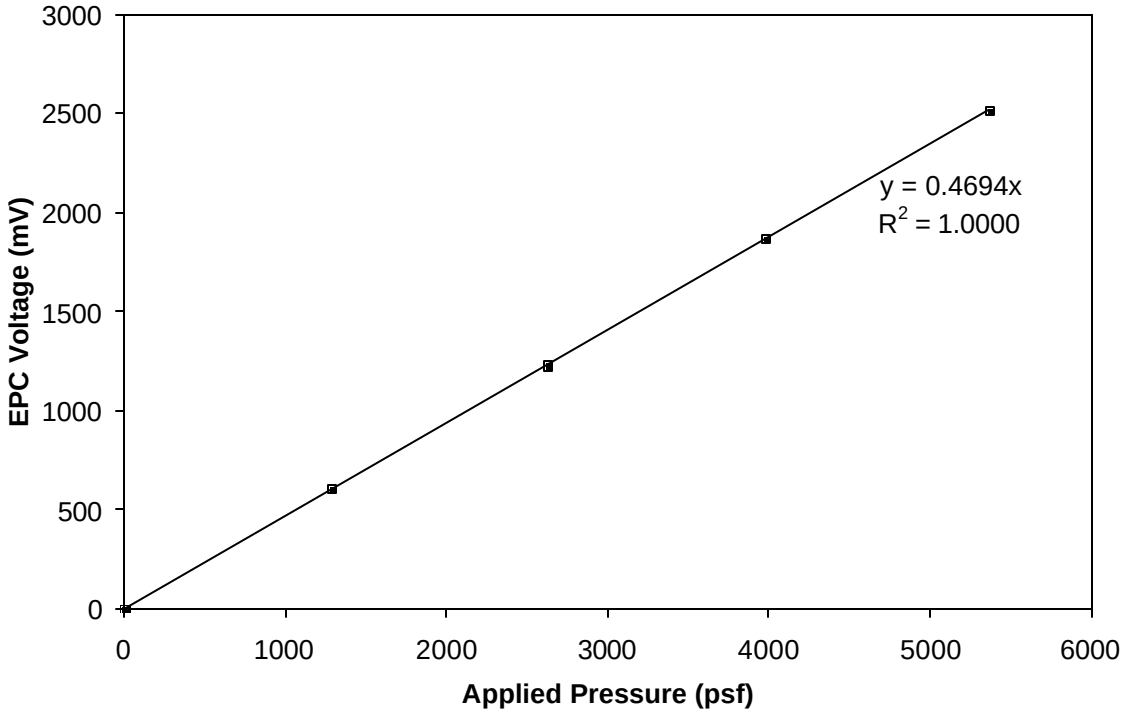

Figure A.16. Universal calibration plot for Geokon EPC_front.

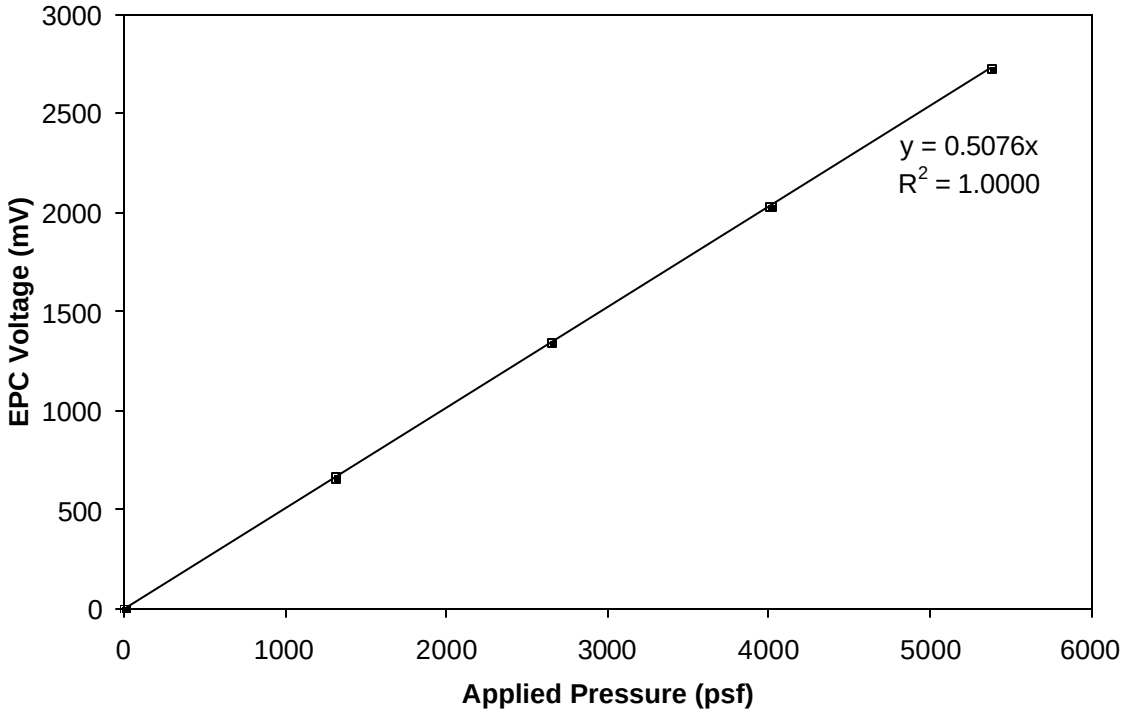

Figure A.17. Universal calibration plot for Geokon EPC_back.

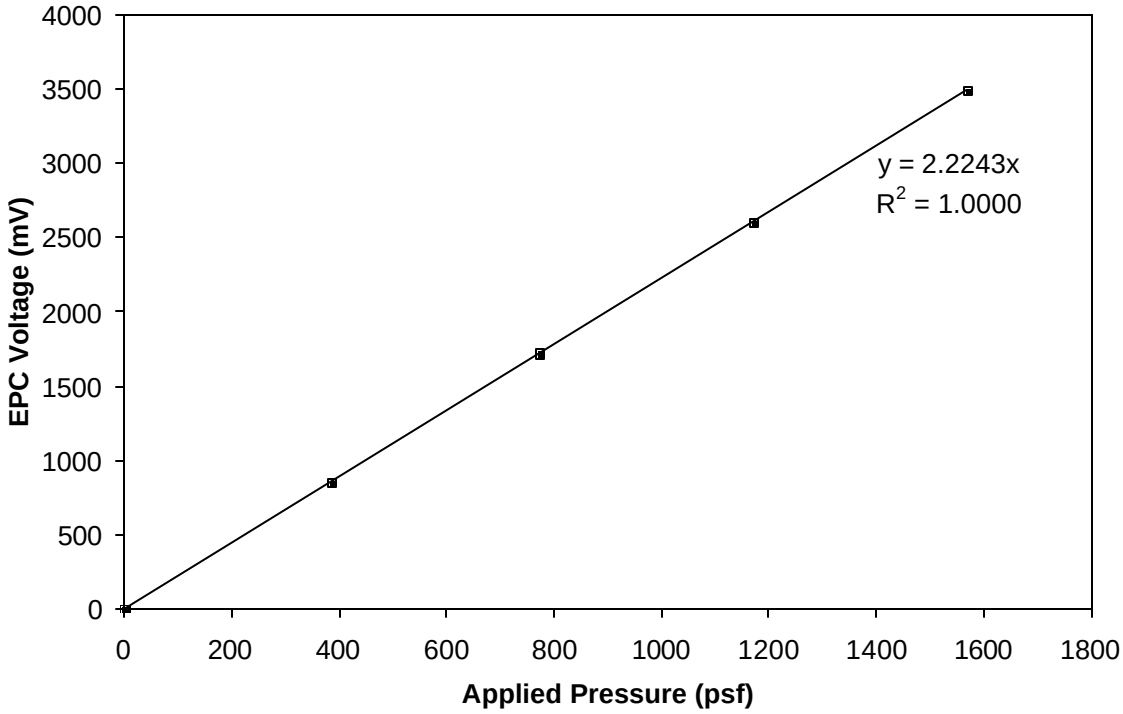

Figure A.18. Universal calibration plot for Geokon EPC_toe.

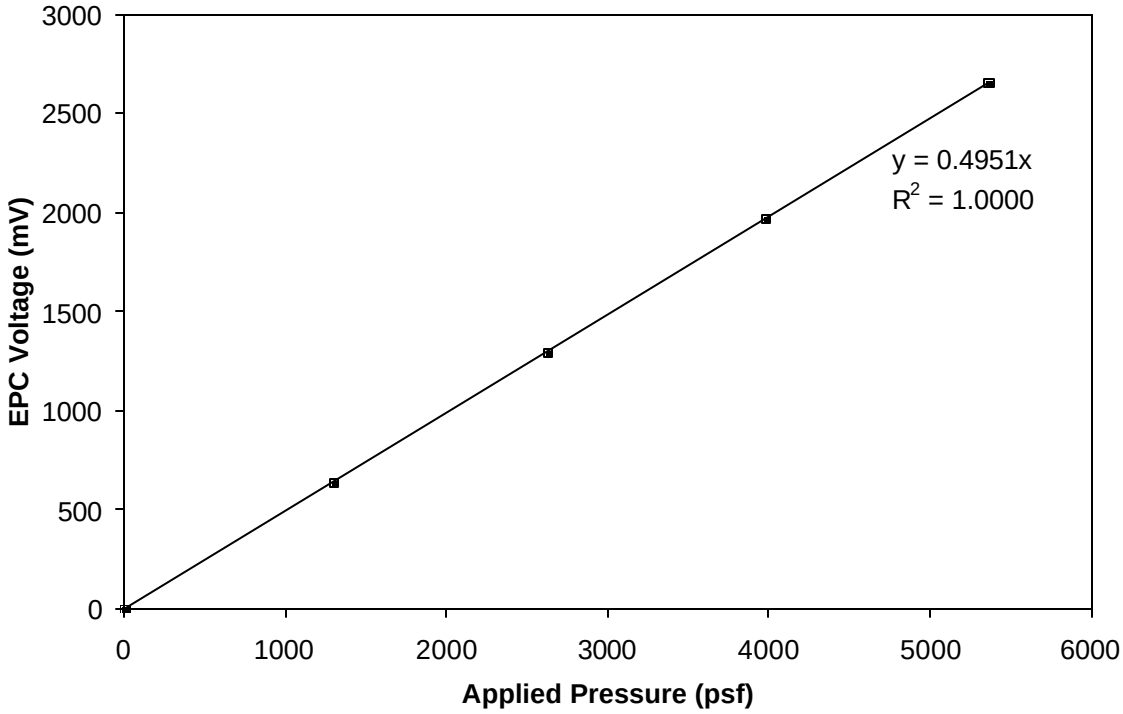

Figure A.19. Universal calibration plot for Geokon EPC_key.

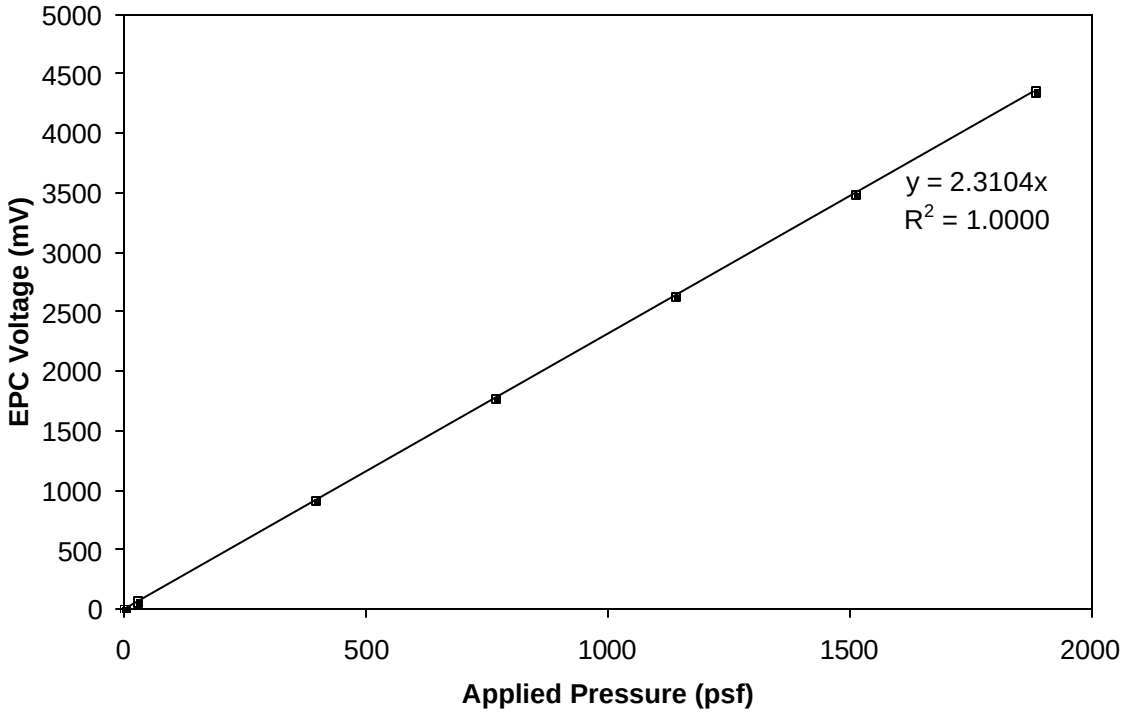

Figure A.20. Universal calibration plot for Geokon EPC_bf.

Appendix B

Geokon Earth Pressure Cells

A problem encountered with the Geokon EPCs was that the earth pressures were approximately an order of magnitude lower than those from the correspondingly located Kulite EPCs. After considerable effort was spent to determine the reason for this discrepancy, it was found that a hardware malfunction in a multiplexer caused the voltage output from the Geokon EPCs to be different from the voltage measured manually with a voltmeter when the EPCs were hooked up directly to the power supply. However, the output from the Geokon EPCs was still proportional to the earth pressure acting on them. Thus, when multiplied by an appropriate (unknown) value, the Geokon readings were useful in corroborating the daily changes during backfilling and the seasonal fluctuations in earth pressure observed with the Kulite EPCs (Figs. B.1 and B.2).

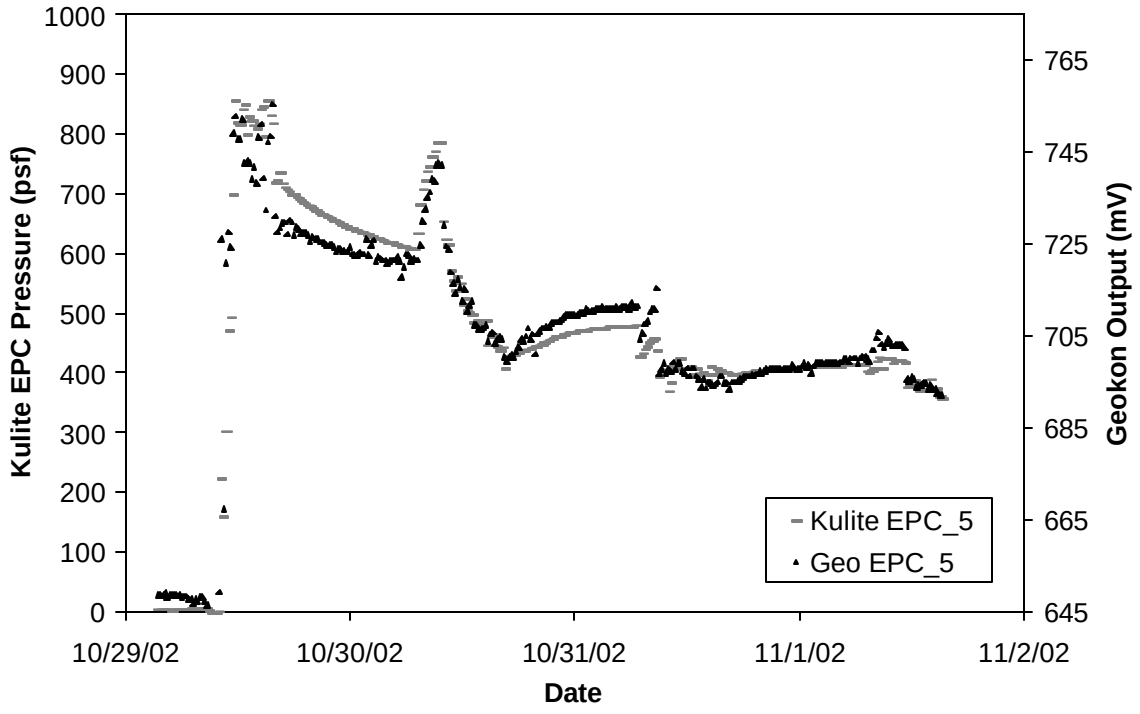

Figure B.1. Example response of Kulite and Geokon EPCs during backfilling.

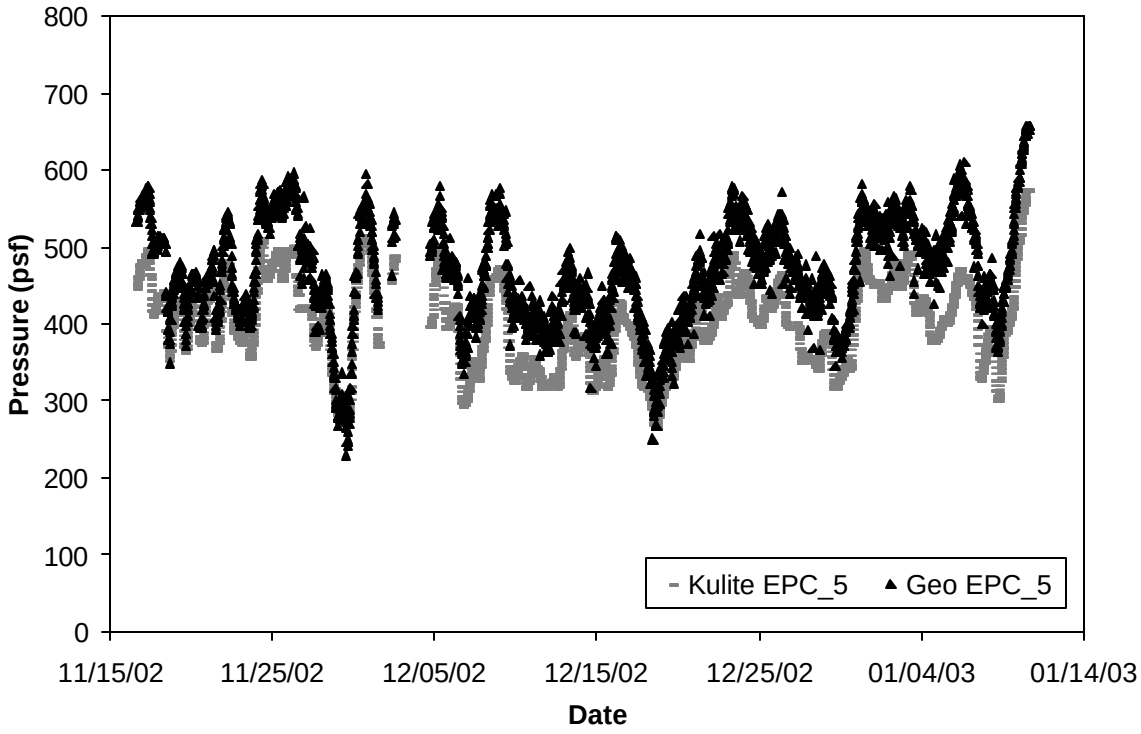

Figure B.2. Example variation of Kulite and Geokon EPCs with time corresponding to the daily temperature cycle.

Appendix C

Soil Tests

Grain-Size Analysis

A standard sieve analysis was performed on a sample of typical Mn/DOT backfill soil in fall 2001 (Fig. C.1). It was classified as poorly graded sand (SP) according to the Unified Soil Classification System (USCS). The results from the sieve analysis are summarized in Table C.1.

Table C.1. Results from sieve analysis.

Quantity	Value
D_{60}	0.42 mm
D_{30}	0.25 mm
Effective size, D_{10}	0.13 mm
Uniformity coefficient, C_u	3.23
Coefficient of gradation, C_z	1.14
USCS classification:	SP
AASHTO classification:	A-3(0)

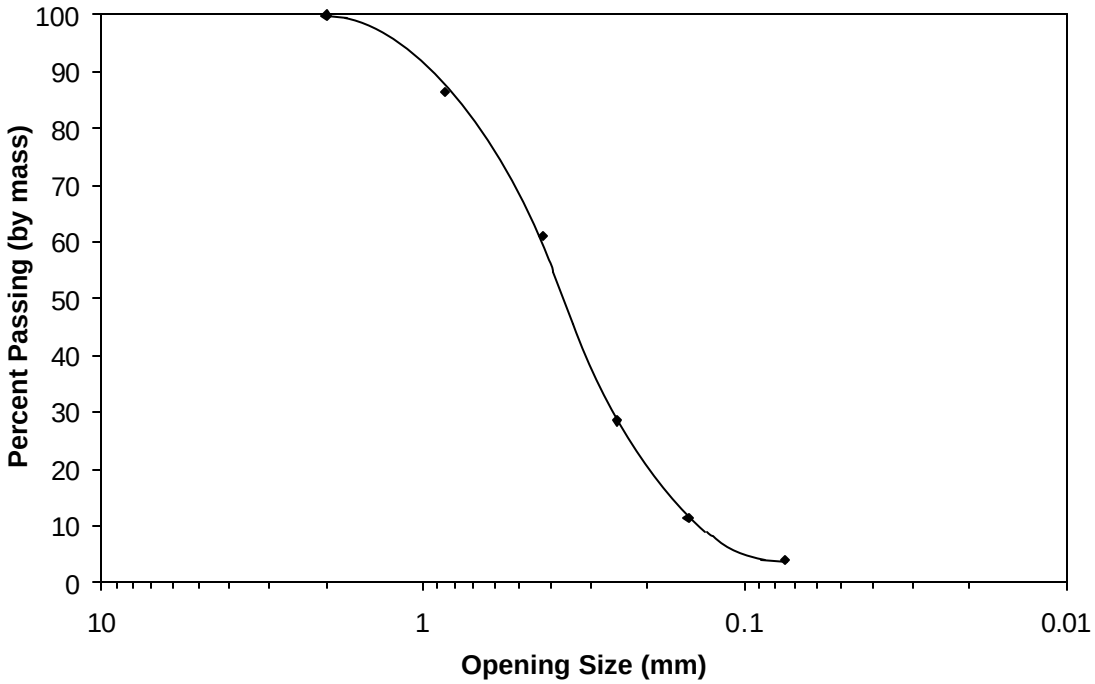

Figure C.1. Grain-size distribution curve.

Triaxial Tests

Laboratory strength tests were performed on several samples of typical Mn/DOT retaining wall backfill to determine the angle of internal friction for the soil. These were consolidated-drained triaxial tests.

Six tests were performed on a soil sample taken from the backfill material behind Panel BJ. These tests were performed at approximately 42-kPa, 50-kPa, 80-kPa, 100-kPa, 200-kPa, and 265-kPa confinement (Table C.2). The failure envelope from these tests gave a friction angle of 37° (Fig. C.2).

Table C.2. Triaxial test results for backfill behind Panel BJ.

Confining Pressure		Unit Weight		Void Ratio
(kPa)	(psf)	(kN/m^3)	(pcf)	
41.9	876	15.3	97.7	0.71
50	1044	15.1	96.1	0.73
80	1670	14.9	94.9	0.76
100	2088	15.3	97.3	0.71
200	4176	14.5	92.2	0.81
265.5	5544	14.5	92.5	0.80

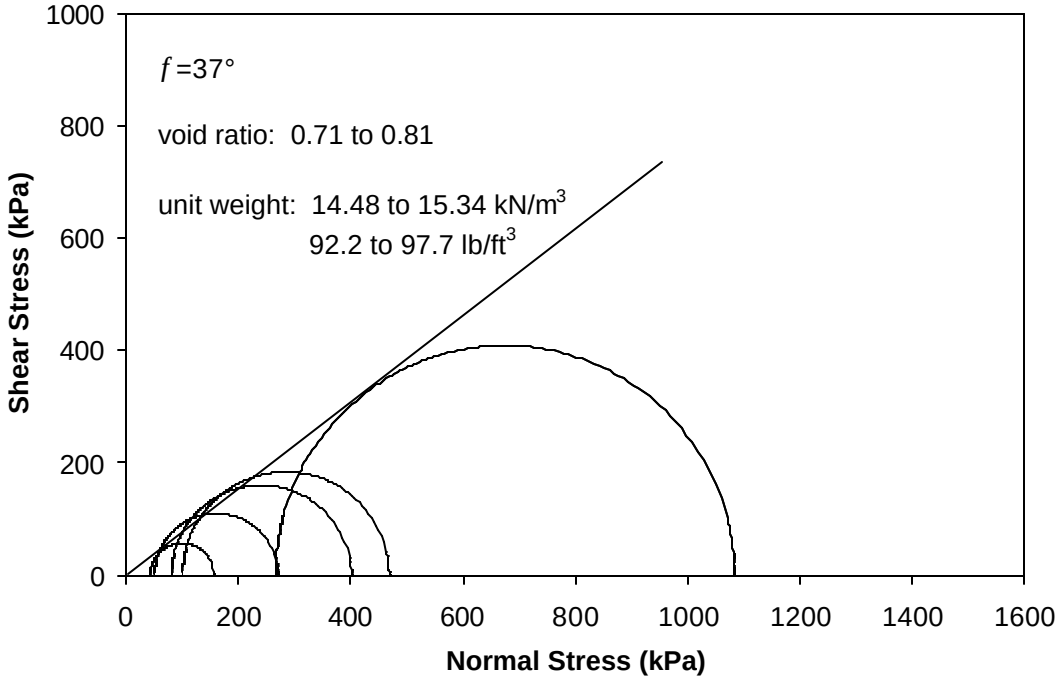

Figure C.2. Consolidated-drained triaxial test results for backfill behind Panel BJ.

Three consolidated-drained tests were performed on a soil sample taken from a stockpile of modified select granular soil at the retaining wall site. These tests were performed at approximately 100-kPa, 200-kPa, and 300-kPa confinement (Table C.3). The failure envelope from these tests gave a friction angle of 39° (Fig. C.3).

Table C.3. Triaxial test results for stockpiled construction site backfill material.

Confining Pressure		Unit Weight		Void
(kPa)	(psf)	(kN/m^3)	(pcf)	Ratio
101.4	2117	16.5	105	0.59
200	4176	15.6	99.3	0.67
301.3	6293	16.3	104	0.61

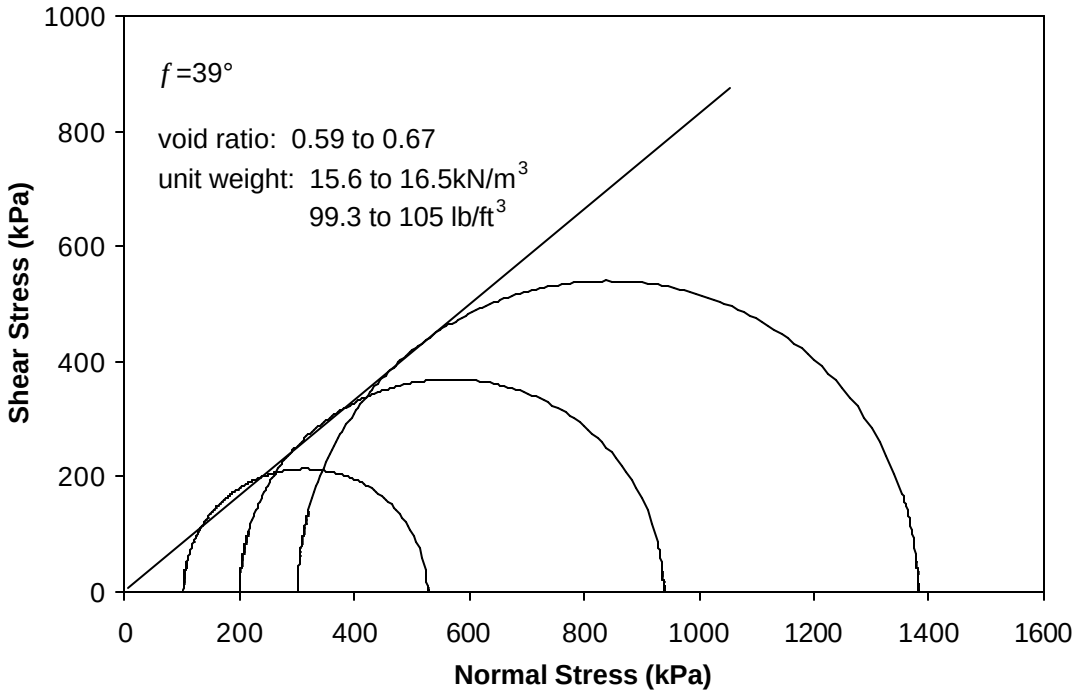

Figure C.3. Consolidated-drained triaxial test results for construction site backfill material.

In fall 2001, three triaxial tests were performed on a sample of typical Mn/DOT backfill (Table C.4). Figure C.4 shows the failure envelope obtained from these triaxial tests. The friction angle was found to be 35°.

Table C.4. Triaxial test results for typical retaining wall backfill.

Confining Pressure		Unit Weight		Void Ratio
(kPa)	(psf)	(kN/m^3)	(pcf)	
57	1195	14.6	92.9	0.80
200	4176	14.5	92.1	0.81
343	7200	14.2	90.4	0.84

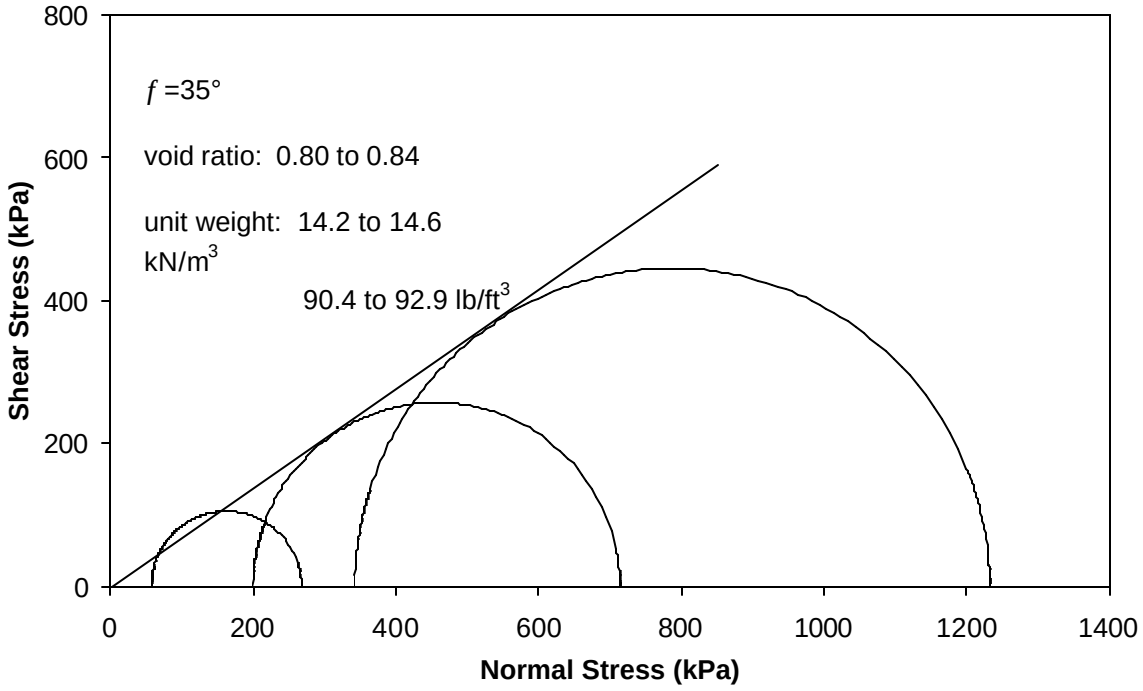

Figure C.4. Consolidated-drained triaxial test results for typical retaining wall backfill.

Appendix D

Structural Analysis

Stem deflections were predicted using engineering beam theory. The retaining wall was modeled as a cantilever beam with a clamped support (Fig. D.1a). Euler-Bernoulli beam theory was assumed, using a Young's modulus of $3.6*10^6$ psi (25 GPa) for the concrete and a transformed section accounting for the steel reinforcement to calculate the moment of inertia (MacGregor 1997). Steel has a Young's modulus of $29*10^6$ psi (200 GPa). The tapered stem was approximated as a piecewise constant beam (26 one-foot sections), with a piecewise constant distributed load (Fig. D.1b). This series of beams was treated as a frame and solved using a stiffness approach. An outline of the method follows.

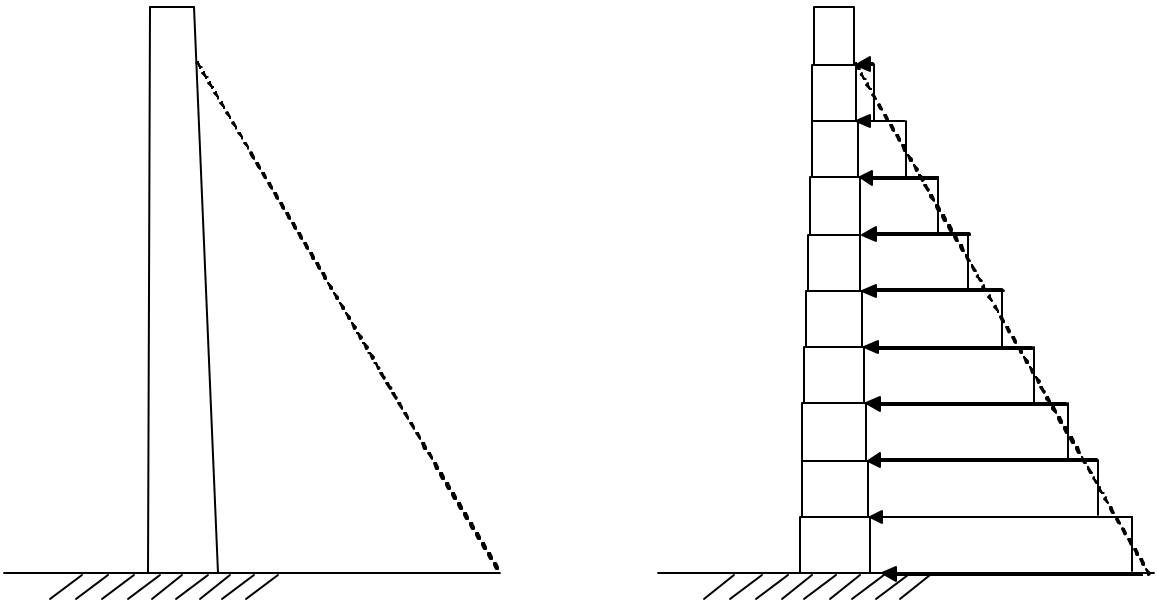

(a) (b)

Figure D.1. (a) Theoretical loading on retaining wall. (b) Approximated cross-section of retaining wall with piecewise constant distributed load.

The element stiffness matrix for a member in a frame is given by

$$\underline{K}_e = \frac{EI_e}{L_e^3}\begin{pmatrix} \frac{AL_e^2}{I} & 0 & 0 & -\frac{AL_e^2}{I} & 0 & 0 \\ 0 & 12 & 6L_e & 0 & -12 & 6L_e \\ 0 & 6L_e & 4L_e^2 & 0 & -6L_e & 2L_e^2 \\ -\frac{AL_e^2}{I} & 0 & 0 & \frac{AL_e^2}{I} & 0 & 0 \\ 0 & -12 & -6L_e & 0 & 12 & -6L_e \\ 0 & 6L_e & 2L_e^2 & 0 & -6L_e & 4L_e^2 \end{pmatrix} \quad \text{(D.1)}$$

where L_e is the length of the element, A is the cross-sectional area of the element, E is the Young's modulus, and I_e is the average moment of inertia for the length of the wall stem

represented by the beam element. Since the thickness of the wall stem changes linearly with height, this is given by

$$I_e = \frac{I_i + I_j}{2} \tag{D.2}$$

where I_i and I_j are the moments of inertia at the respective ends of the beam element.

The element stiffness matrix is based on a local coordinate system with the x-axis along the length of the beam. To change to the global coordinate system chosen for the structure, the element stiffness matrix must be transformed. The transformation matrix is given by

$$\underline{T} = \begin{pmatrix} \cos a & -\sin a & 0 & 0 & 0 & 0 \\ \sin a & \cos a & 0 & 0 & 0 & 0 \\ 0 & 0 & 1 & 0 & 0 & 0 \\ 0 & 0 & 0 & \cos a & -\sin a & 0 \\ 0 & 0 & 0 & \sin a & \cos a & 0 \\ 0 & 0 & 0 & 0 & 0 & 1 \end{pmatrix} \tag{D.3}$$

where a is the angle by which the local coordinate system for the member is rotated from the global coordinate system. The transformation operation is as follows:

$$\underline{K}_e^{global} = \underline{T}\,\underline{K}_e\,\underline{T}^{-1} \tag{D.4}$$

Each member stiffness matrix must then be assembled into the global stiffness matrix for the structure. The vector of nodal forces $\underline{F}$ is then related to the vector of nodal displacements $\underline{d}$ using the global stiffness matrix $\underline{K}$:

$$\underline{F} = \underline{K}\,\underline{d} + \underline{f} \tag{D.5}$$

where $\underline{f}$ is the fixed end forces arising from the distributed load over each member. This vector is determined in a manner analogous to the stiffness matrix, with elemental fixed end force vectors in local coordinate systems and the global vector $\underline{f}$.

After eliminating rows and columns corresponding to nodal displacements that are fixed, the above equation may be solved for the unknown nodal displacements:

$$\underline{d} = \underline{K}^{-1}\left(\underline{F} - \underline{f}\right) \tag{D.6}$$

In turn, Eq. D.5 may be used to find the unknown nodal forces. The computer code used to implement the analysis follows. It is written in Microsoft Visual Basic and is designed to interface with Microsoft Excel.

```
'Microsoft Visual Basic for Excel program
'Written Dec 2001 by Joseph Bentler
'Solves a 2D frame with rigid connections and distributed load that is constant over a member
'   using matrix stiffness methods
Option Base 1 'make lowest index of a matrix equal to 1 rather than 0
Sub matrix()
Dim NJ, NDJ, ndimensions, NM, NCD As Integer

NDJ = 3     '2D frame has 3 DOF
'Read NJ, ndimensions, NM, NCD from "input" worksheet
NJ = Sheets("input").Cells(1, 2)        'number of joints
NM = Sheets("input").Cells(2, 2)        'number of members
ndimensions = Sheets("input").Cells(3, 2) 'number of dimensions (2 or 3)
NCD = Sheets("input").Cells(4, 2)       'number of different materials

Dim BIGK(300, 300), MIJ(4, 150), XYZ(3, 100), AJ(6, 100), PMAT(4, 26), IFIX(3, 100)
Dim EK(6, 6), DIS(300), RHS(300), EFzero(6), Fzero(150), Mforces(150, 6)
Dim Count1, Count2, Count3 As Integer
Dim maxD, minD, aveD As Double
Dim NRC, MC As Integer

'Zero BIGK, DIS, RHS, MIJ, Mforces, XYZ, AJ, IFIX, PMAT, Fzero
   For Count1 = 1 To 300
      DIS(Count1) = 0
      RHS(Count1) = 0
      For Count2 = 1 To 300
         BIGK(Count1, Count2) = 0
      Next Count2
   Next Count1

   For Count1 = 1 To 6
      For Count2 = 1 To 150
      Mforces(Count2, Count1) = 0
      Next Count2
      For Count2 = 1 To 100
      AJ(Count1, Count2) = 0
      Next Count2
   Next Count1

   For Count1 = 1 To 3
      For Count2 = 1 To 150
         MIJ(Count1, Count2) = 0
         MIJ(4, Count2) = 0
         Fzero(Count2) = 0
      Next Count2
      For Count2 = 1 To 100
```

```
            XYZ(Count1, Count2) = 0
            IFIX(Count1, Count2) = 0
        Next Count2
        For Count2 = 1 To 26
            PMAT(Count1, Count2) = 0
            PMAT(4, Count2) = 0
        Next Count2
    Next Count1

'Read in coordinates of nodes, support conditions, nodal external loads
    For Count1 = 1 To NJ
        For Count2 = 1 To NDJ
            XYZ(Count2, Count1) = Sheets("input").Cells((1 + Count1), (4 + Count2))
            IFIX(Count2, Count1) = Sheets("input").Cells((1 + Count1), (10 + Count2))
            AJ(Count2, Count1) = Sheets("input").Cells((1 + Count1), (15 + Count2))
        Next Count2
    Next Count1

 'Read in material properties
    For Count1 = 1 To NCD
        For Count2 = 1 To 3
            PMAT(Count2, Count1) = Sheets("input").Cells((1 + Count1), (21 + Count2))
        Next Count2
        PMAT(4, Count1) = Count1    'assign ID numbers to each material
    Next Count1

'Read in node numbers, cross-sectional materal property number
    For Count1 = 1 To NM
        For Count2 = 1 To 4
            MIJ(Count2, Count1) = Sheets("input").Cells((1 + Count1), (26 + Count2))
        Next Count2
    Next Count1

'Form BIGK and Fzero
    For MC = 1 To NM
        Call FormEK(MC, MIJ, XYZ, PMAT, EK, EFzero, Fzero)
        Call AddEK(MC, MIJ, EK, BIGK, NDJ, EFzero, Fzero)
    Next MC

'Form RHS
    For Count1 = 1 To NDJ
        For Count2 = 1 To NJ
            RHS((Count2 - 1) * NDJ + Count1) = AJ(Count1, Count2)
        Next Count2
    Next Count1
```

```
'subtract Fzero from RHS
   For Count1 = 1 To NJ * NDJ
      RHS(Count1) = RHS(Count1) - Fzero(Count1)
   Next Count1

'Find average entry on main diagonal
minD = BIGK(1, 1)
maxD = BIGK(1, 1)
   For Count1 = 2 To NJ * NDJ
      CF = BIGK(Count1, Count1)
      If CF > maxD Then maxD = CF
      If CF < minD Then minD = CF
   Next Count1
aveD = (1 / 2) * (maxD + minD)

'Introduce support conditions and modify BIGK
   For Count1 = 1 To NDJ
      For Count2 = 1 To NJ
         If IFIX(Count1, Count2) = 1 Then
            NRC = (Count2 - 1) * NDJ + Count1
            For Count3 = 1 To NJ * NDJ
               BIGK(Count3, NRC) = 0
               BIGK(NRC, Count3) = 0
            Next Count3
            RHS(NRC) = 0
            BIGK(NRC, NRC) = aveD
         Else: End If
      Next Count2
   Next Count1

'Solve resulting equations to get displacements (DIS)
    Call GaussElim(BIGK, RHS, DIS, NJ, NDJ)

'Print Displacements to sheet titled "output"
   For Count1 = 1 To NJ
      Sheets("output").Cells(1 + Count1, 1) = "node " & Count1
      For Count2 = 1 To NDJ
         Sheets("output").Cells(1 + Count1, 1 + Count2) = DIS((Count1 - 1) * NDJ + Count2)
      Next Count2
   Next Count1

'Find member forces
   For MC = 1 To NM
      Call FindForces(MC, MIJ, NDJ, XYZ, PMAT, DIS, Mforces)
   'Print Member Forces to worksheet titled "output"
      Sheets("output").Cells(1 + MC, 6) = "Member " & MC
```

```
      For Count2 = 1 To 6
         Sheets("output").Cells(1 + MC, 6 + Count2) = Mforces(MC, Count2)
      Next Count2
   Next MC

'Change screen to "output" worksheet
   Sheets("output").Select
End Sub

'Subroutine to generate element stiffness matrix and element fixed-end forces
Sub FormEK(MC, MIJ, XYZ, PMAT, EK, EFzero, Fzero)
Dim Count1, Count2, Count3 As Integer
Dim T(6, 6), T_inv(6, 6), T_EK(6, 6), EFzero_hat(6)
Dim i, j, MatNo As Integer
Dim XI, XJ, YI, YJ, ZI, ZJ As Double
Dim E, A, Inertia, q As Double      'Young's modulus, area, moment of inertia, dist. load
Dim DX, DY, DZ, EX, EY, EZ As Double
Dim EL, CF, total As Double

'zero EK, T, and T_inv
   For Count1 = 1 To 6
      For Count2 = 1 To 6
         EK(Count1, Count2) = 0
         T(Count1, Count2) = 0
         T_inv(Count1, Count2) = 0
       Next Count2
   Next Count1

'Find node I and node J
i = MIJ(1, MC)
j = MIJ(2, MC)
MatNo = MIJ(3, MC)
q = MIJ(4, MC)          'distributed load on member
'Find XI, XJ, YI, YJ
XI = XYZ(1, i)
XJ = XYZ(1, j)
YI = XYZ(2, i)
YJ = XYZ(2, j)
ZI = XYZ(3, i)
ZJ = XYZ(3, j)
'Find material properties
A = PMAT(1, MatNo)
E = PMAT(2, MatNo)
Inertia = PMAT(3, MatNo)

'Formulate EK for frame member
```

```
    DX = XJ - XI
    DY = YJ - YI
    EL = Sqr((DX ^ 2) + (DY ^ 2))
    CF = E * Inertia / (EL ^ 3)
    EX = DX / EL          'same as cosine alpha
    EY = DY / EL          'same as sine alpha
'Fill in non-zero terms in stiffness matrix
    EK(1, 1) = CF * A * (EL ^ 2) / Inertia
    EK(1, 4) = -EK(1, 1)
    EK(2, 2) = CF * 12
    EK(2, 3) = CF * 6 * EL
    EK(2, 5) = -EK(2, 2)
    EK(2, 6) = EK(2, 3)
    EK(3, 2) = EK(2, 3)
    EK(3, 3) = CF * 4 * (EL ^ 2)
    EK(3, 5) = -EK(2, 3)
    EK(3, 6) = CF * 2 * (EL ^ 2)
    EK(4, 1) = -EK(1, 1)
    EK(4, 4) = EK(1, 1)
    EK(5, 2) = -EK(2, 2)
    EK(5, 3) = -EK(2, 3)
    EK(5, 5) = EK(2, 2)
    EK(5, 6) = -EK(2, 3)
    EK(6, 2) = EK(2, 3)
    EK(6, 3) = EK(3, 6)
    EK(6, 5) = -EK(2, 3)
    EK(6, 6) = EK(3, 3)

'Form T and T_inv
    T(1, 1) = EX
    T(1, 2) = -EY
    T(2, 1) = EY
    T(2, 2) = EX
    T(3, 3) = 1
    T(4, 4) = EX
    T(4, 5) = -EY
    T(5, 4) = EY
    T(5, 5) = EX
    T(6, 6) = 1

    T_inv(1, 1) = EX
    T_inv(1, 2) = EY
    T_inv(2, 1) = -EY
    T_inv(2, 2) = EX
    T_inv(3, 3) = 1
    T_inv(4, 4) = EX
```

```
    T_inv(4, 5) = EY
    T_inv(5, 4) = -EY
    T_inv(5, 5) = EX
    T_inv(6, 6) = 1

'Transform elemental stiffness matrix to global coordinates
'multiply T*EK
    For Count1 = 1 To 6
        For Count2 = 1 To 6
            total = 0
            For Count3 = 1 To 6
            total = total + T(Count1, Count3) * EK(Count3, Count2)
            Next Count3
        T_EK(Count1, Count2) = total
        Next Count2
    Next Count1
'multiply (T*EK)*T_inv to get EK in terms of global coordinates
    For Count1 = 1 To 6
        For Count2 = 1 To 6
            total = 0
            For Count3 = 1 To 6
            total = total + T_EK(Count1, Count3) * T_inv(Count3, Count2)
            Next Count3
        EK(Count1, Count2) = total
        Next Count2
    Next Count1

'determine fixed-end forces due to distributed load q (positive q is "upwards" in local
coordinates)
    EFzero_hat(1) = 0
    EFzero_hat(2) = -q * EL / 2
    EFzero_hat(3) = -q * (EL ^ 2) / 12
    EFzero_hat(4) = 0
    EFzero_hat(5) = -q * EL / 2
    EFzero_hat(6) = q * (EL ^ 2) / 12
    For Count1 = 1 To 6
    Next Count1
'multiply T times EFzero to transform to global coordinate systems
    For Count1 = 1 To 6
            total = 0
            For Count3 = 1 To 6
            total = total + T(Count1, Count3) * EFzero_hat(Count3)
            Next Count3
        EFzero(Count1) = total
    Next Count1
```

```
End Sub

'Subroutine to assemble global stiffness matrix
Sub AddEK(MC, MIJ, EK, BIGK, NDJ, EFzero, Fzero)
Dim i, j, p, q As Integer   'p and q counters
Dim NRCI, NRCJ As Integer

'Find node I and node J
i = MIJ(1, MC)
j = MIJ(2, MC)
NRCI = (i - 1) * NDJ
NRCJ = (j - 1) * NDJ

'Assemble EK into BIGK and Assemble EFzero into Fzero
For p = 1 To NDJ
   Fzero(NRCI + p) = Fzero(NRCI + p) + EFzero(p)
   Fzero(NRCJ + p) = Fzero(NRCJ + p) + EFzero(p + NDJ)
   For q = 1 To NDJ
      BIGK(NRCI + p, NRCI + q) = BIGK(NRCI + p, NRCI + q) + EK(p, q)
      BIGK(NRCI + p, NRCJ + q) = BIGK(NRCI + p, NRCJ + q) + EK(p, q + NDJ)
      BIGK(NRCJ + p, NRCI + q) = BIGK(NRCJ + p, NRCI + q) + EK(p + NDJ, q)
      BIGK(NRCJ + p, NRCJ + q) = BIGK(NRCJ + p, NRCJ + q) + EK(p + NDJ, q + NDJ)
   Next q
Next p

End Sub

'Subroutine to find member forces
Sub FindForces(MC, MIJ, NDJ, XYZ, PMAT, DIS, Mforces)
Dim i, j, MatNo, NRI, NRJ As Integer
Dim EK(6, 6), T(6, 6), T_inv(6, 6), T_EK(6, 6), EDIS(6), EDIS_hat(6), EFzero_hat(6)
Dim XI, XJ, YI, YJ, ZI, ZJ As Double
Dim E, A, Inertia, q As Double      'Young's modulus, area, moment of inertia, dist. load
Dim DX, DY, DZ, EX, EY, EZ As Double
Dim EL, CF, total As Double

'Find node I and node J
i = MIJ(1, MC)
j = MIJ(2, MC)
NRI = (i - 1) * NDJ
NRJ = (j - 1) * NDJ
MatNo = MIJ(3, MC)
q = MIJ(4, MC)
'Find XI, XJ, YI, YJ
XI = XYZ(1, i)
XJ = XYZ(1, j)
```

```
YI = XYZ(2, i)
YJ = XYZ(2, j)
ZI = XYZ(3, i)
ZJ = XYZ(3, j)
'Find material properties
A = PMAT(1, MatNo)
E = PMAT(2, MatNo)
Inertia = PMAT(3, MatNo)
'Find direction cosines and the length of the current member
DX = XJ - XI
DY = YJ - YI
DZ = ZJ - ZI
EL = Sqr((DX ^ 2) + (DY ^ 2) + (DZ ^ 2))
EX = DX / EL
EY = DY / EL
EZ = DZ / EL

   CF = E * Inertia / (EL ^ 3)
'zero EK, T, and T_inv
   For Count1 = 1 To 6
      For Count2 = 1 To 6
         EK(Count1, Count2) = 0
         T(Count1, Count2) = 0
         T_inv(Count1, Count2) = 0
       Next Count2
   Next Count1

'Fill in non-zero terms in stiffness matrix
   EK(1, 1) = CF * A * (EL ^ 2) / Inertia
   EK(1, 4) = -EK(1, 1)
   EK(2, 2) = CF * 12
   EK(2, 3) = CF * 6 * EL
   EK(2, 5) = -EK(2, 2)
   EK(2, 6) = EK(2, 3)
   EK(3, 2) = EK(2, 3)
   EK(3, 3) = CF * 4 * (EL ^ 2)
   EK(3, 5) = -EK(2, 3)
   EK(3, 6) = CF * 2 * (EL ^ 2)
   EK(4, 1) = -EK(1, 1)
   EK(4, 4) = EK(1, 1)
   EK(5, 2) = -EK(2, 2)
   EK(5, 3) = -EK(2, 3)
   EK(5, 5) = EK(2, 2)
   EK(5, 6) = -EK(2, 3)
   EK(6, 2) = EK(2, 3)
   EK(6, 3) = EK(3, 6)
```

```
    EK(6, 5) = -EK(2, 3)
    EK(6, 6) = EK(3, 3)

'Form T and T_inv
    T(1, 1) = EX
    T(1, 2) = -EY
    T(2, 1) = EY
    T(2, 2) = EX
    T(3, 3) = 1
    T(4, 4) = EX
    T(4, 5) = -EY
    T(5, 4) = EY
    T(5, 5) = EX
    T(6, 6) = 1

    T_inv(1, 1) = EX
    T_inv(1, 2) = EY
    T_inv(2, 1) = -EY
    T_inv(2, 2) = EX
    T_inv(3, 3) = 1
    T_inv(4, 4) = EX
    T_inv(4, 5) = EY
    T_inv(5, 4) = -EY
    T_inv(5, 5) = EX
    T_inv(6, 6) = 1

'create elemental displacement vector for nodes I and J
    For Count1 = 1 To 3
       EDIS(Count1) = DIS(NRI + Count1)
       EDIS(Count1 + 3) = DIS(NRJ + Count1)
    Next Count1
'multiply T_inv by EDIS to get EDIS_hat in terms of local coordinates
    For Count1 = 1 To 6
          total = 0
          For Count3 = 1 To 6
          total = total + T_inv(Count1, Count3) * EDIS(Count3)
          Next Count3
       EDIS_hat(Count1) = total
    Next Count1
'multiply EK by EDIS_hat to get Mforces
    For Count1 = 1 To 6
          total = 0
          For Count3 = 1 To 6
          total = total + EK(Count1, Count3) * EDIS_hat(Count3)
          Next Count3
       Mforces(MC, Count1) = total
```

```
    Next Count1

'determine fixed-end forces due to distributed load q (positive q is "upwards" in local
coordinates)
    EFzero_hat(1) = 0
    EFzero_hat(2) = -q * EL / 2
    EFzero_hat(3) = -q * (EL ^ 2) / 12
    EFzero_hat(4) = 0
    EFzero_hat(5) = -q * EL / 2
    EFzero_hat(6) = q * (EL ^ 2) / 12
'add fixed-end forces to member forces
    For Count1 = 1 To 6
        Mforces(MC, Count1) = Mforces(MC, Count1) + EFzero_hat(Count1)
    Next Count1

End Sub

'Gaussian Elimination subroutine
Sub GaussElim(BIGK, RHS, DIS, NJ, NDJ)
Dim i, j, k As Integer      'counters
Dim dimensions As Integer
Dim A, B, C, D As Double    'intermediate variables for calculations

dimensions = NJ * NDJ
'forward eliminate to make BIGK upper triangular
    For i = 1 To (dimensions - 1)
        B = BIGK(i, i)
        For j = (i + 1) To dimensions
            A = BIGK(j, i)
            For k = i To dimensions
                BIGK(j, k) = BIGK(j, k) - ((BIGK(i, k)) * (A) / (B))
            Next k
            RHS(j) = RHS(j) - ((RHS(i)) * (A) / (B))
        Next j
    Next i
'Backward substitute to find DIS
    For i = dimensions To 1 Step -1
        D = 0
        For k = (dimensions - 1) To i Step -1
            D = D + BIGK(i, k + 1) * DIS(k + 1)
        Next k
        C = RHS(i) - D
        DIS(i) = C / (BIGK(i, i))
    Next i

End Sub
```

Appendix E

Sensor Readings

The following pages include figures showing the readings from the stem Kulite earth pressure cells and tiltmeters for an eight-month period, from backfilling in fall 2002 thru summer 2003. During the first week of backfilling in fall 2002, readings are presented for each day from before the workday to the start of the next workday. Thereafter, plots show readings for periods of increasing length, ranging from a week a time to a month at a time.

Readings during Backfilling

Below is a brief summary of daily activities during construction and backfilling as they pertain to Panel BJ. This information is intended to give context to the sensor readings presented in Figs. E.1 thru E.18 on the following pages.

Date	Activity
Sep 18	Footings poured for Panels BJ thru BF.
Sep 30	Stem poured for Panel BJ.
Oct 28	First day of backfilling behind Panel BJ. Mud removed from footings of Panels BK thru BF. Panel BJ backfilled 2 ft with sand.
Oct 29	Panel BJ backfilled up to total of 12 ft. EPC_10 installed on the stem (10 ft up from the footing), and EPC_bf installed within the backfill (10 ft up from the footing and 5 ft into backfill).
Oct 30	Panel BJ backfilled up to total of 18 ft.
Oct 31	Panel BJ backfilled up to total of 20 ft.
Nov 1	Continued backfilling panels to the west. Panel BJ backfilled up to total of 22 ft.
Nov 2 & 3	Weekend, no construction occurred; data lost from CR10X during this time.
Nov 4	Continued backfilling panels to the west of Panel BJ.
Nov 7	Granular borrow added above and behind backfill area to approximately 6 ft above the top of panel BJ.
Nov 12	Panel BJ backfilled up to total of 23.5 ft
Nov 15	Panel BJ backfilled up to total of 24 ft.
Nov 21	Panel BJ backfilled up to total of 25 ft.

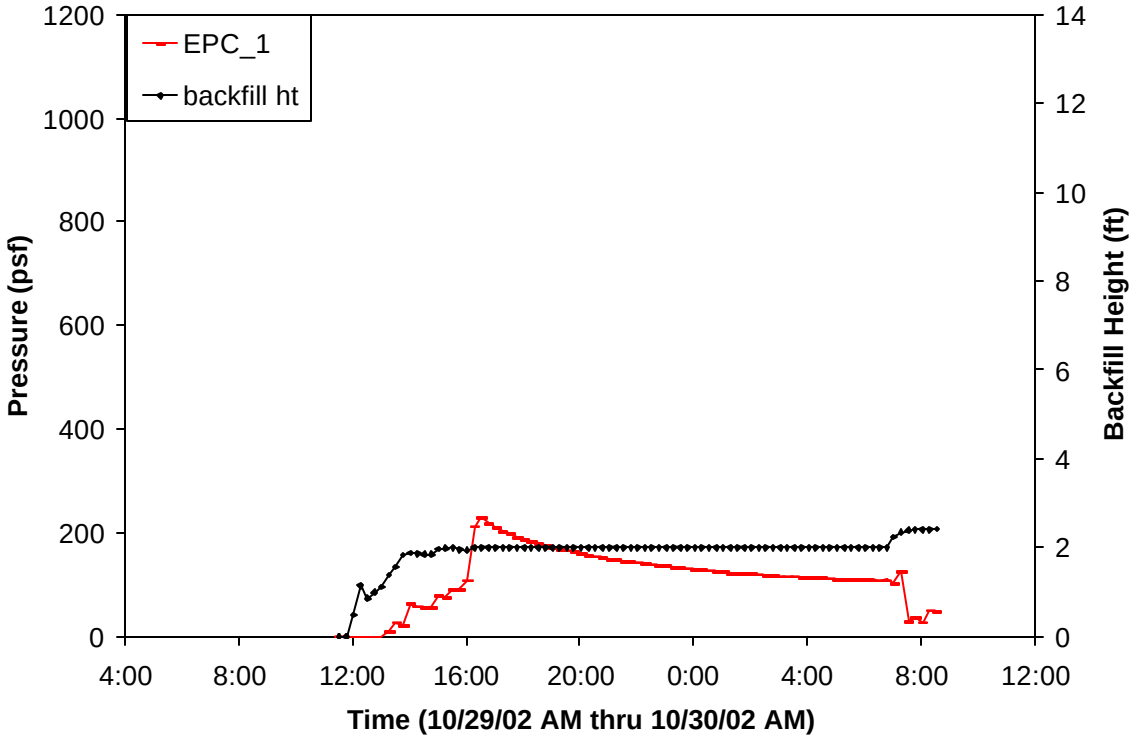

Figure E.1. Stem EPC readings and backfill heights for the first day of backfilling.

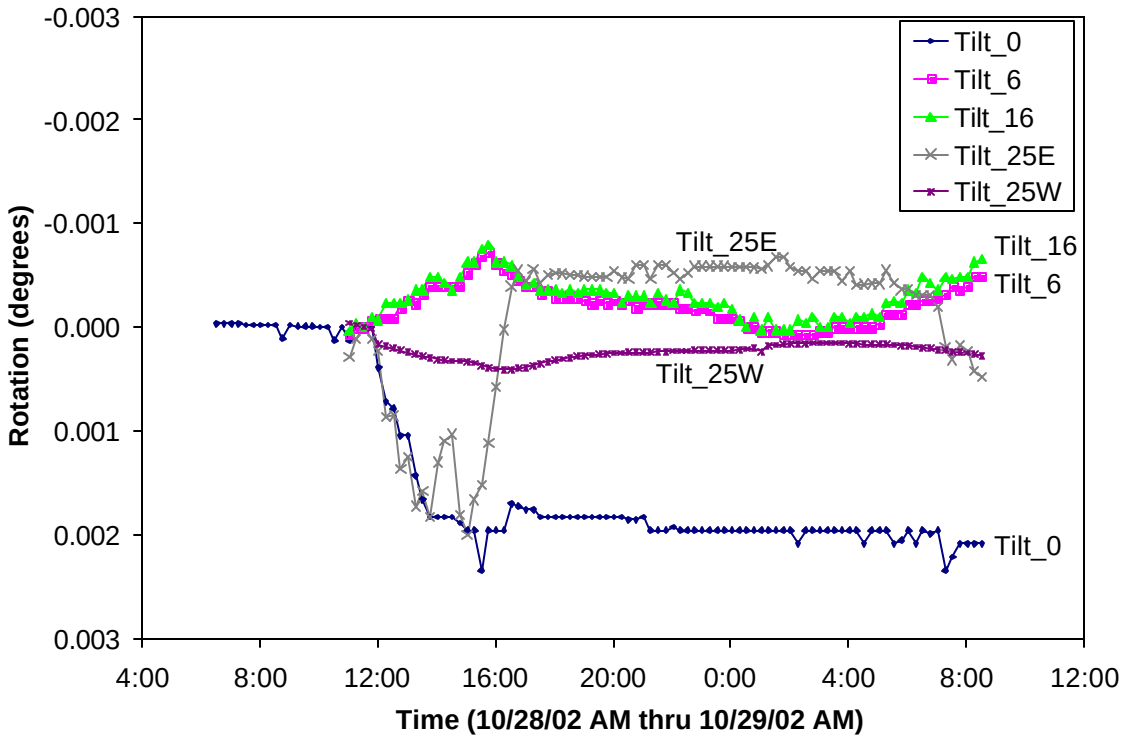

Figure E.2. Tiltmeter readings for the first day of backfilling.

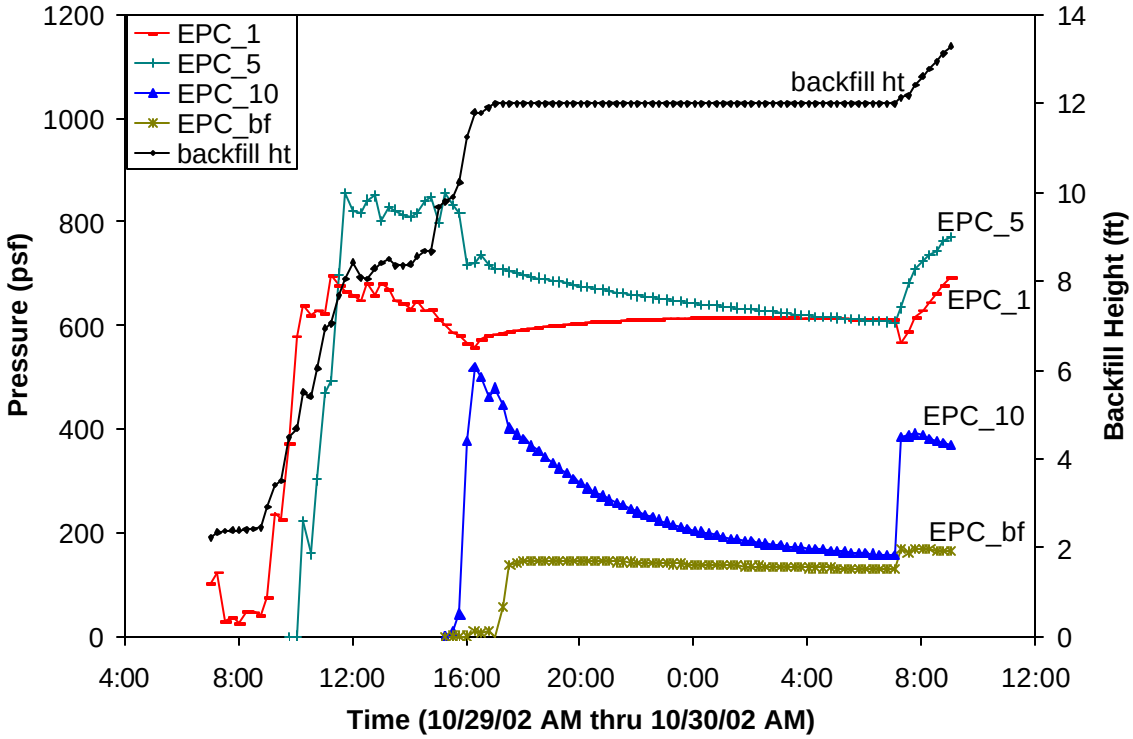

Figure E.3. Stem EPC readings and backfill heights for the second day of backfilling.

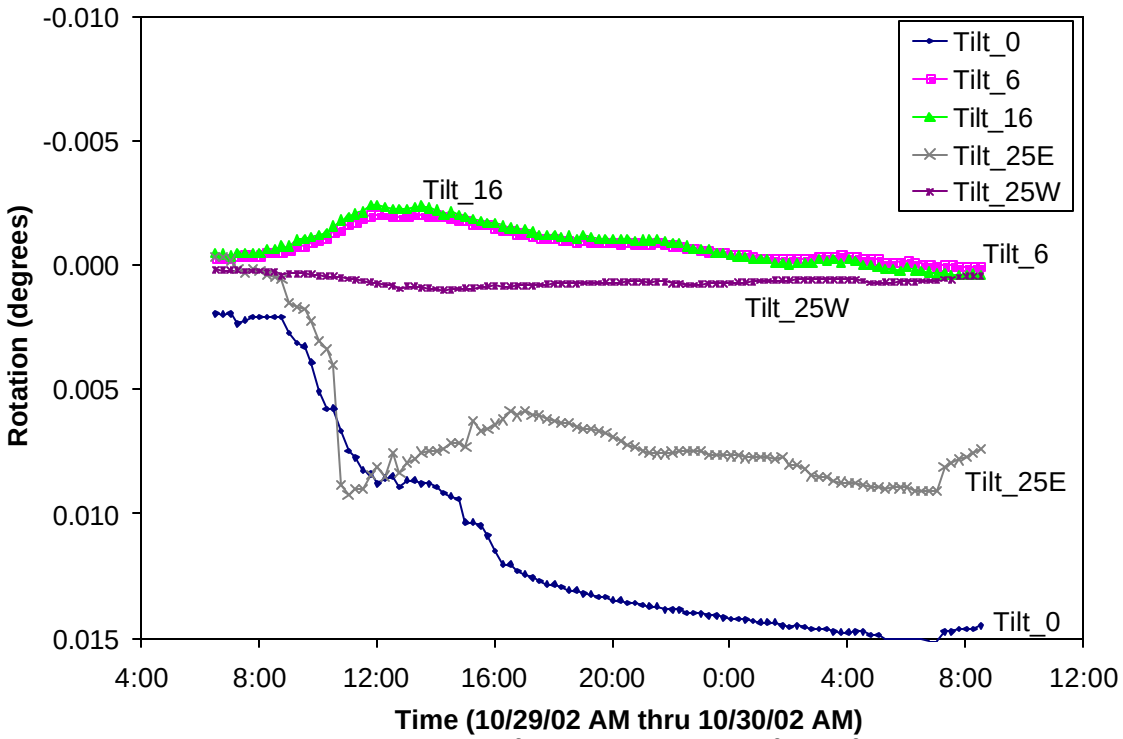

Figure E.4. Tiltmeter readings for the second day of backfilling.

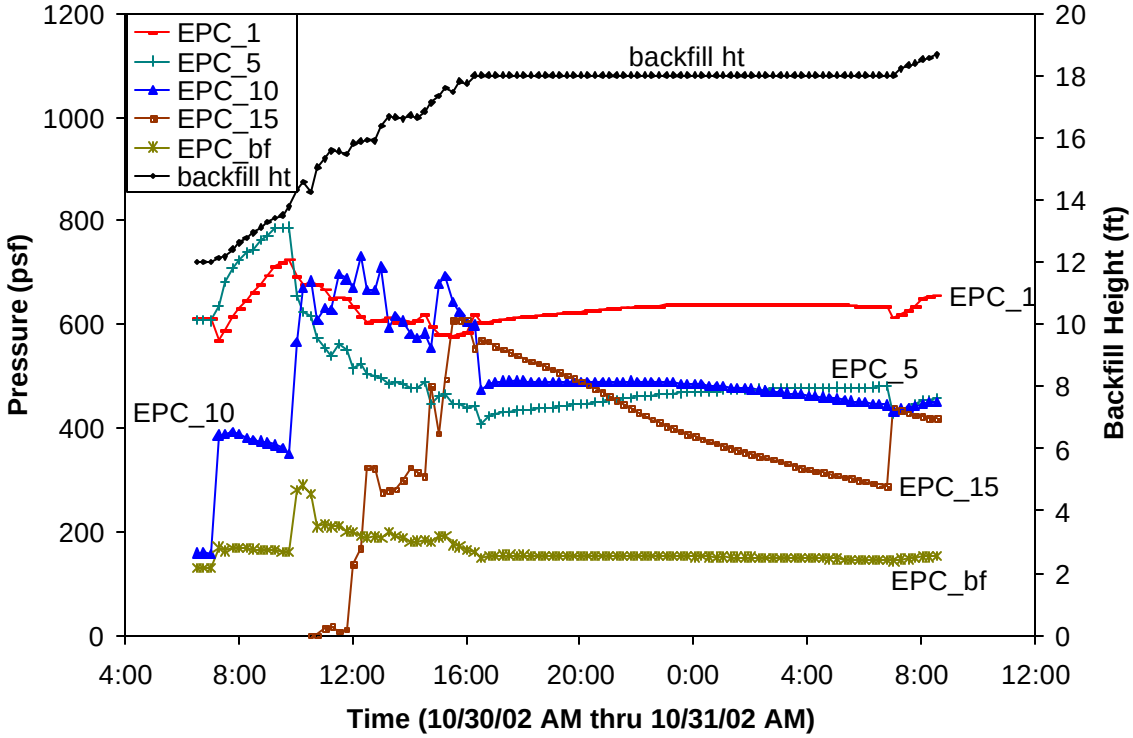

Figure E.5. Stem EPC readings and backfill heights for the third day of backfilling.

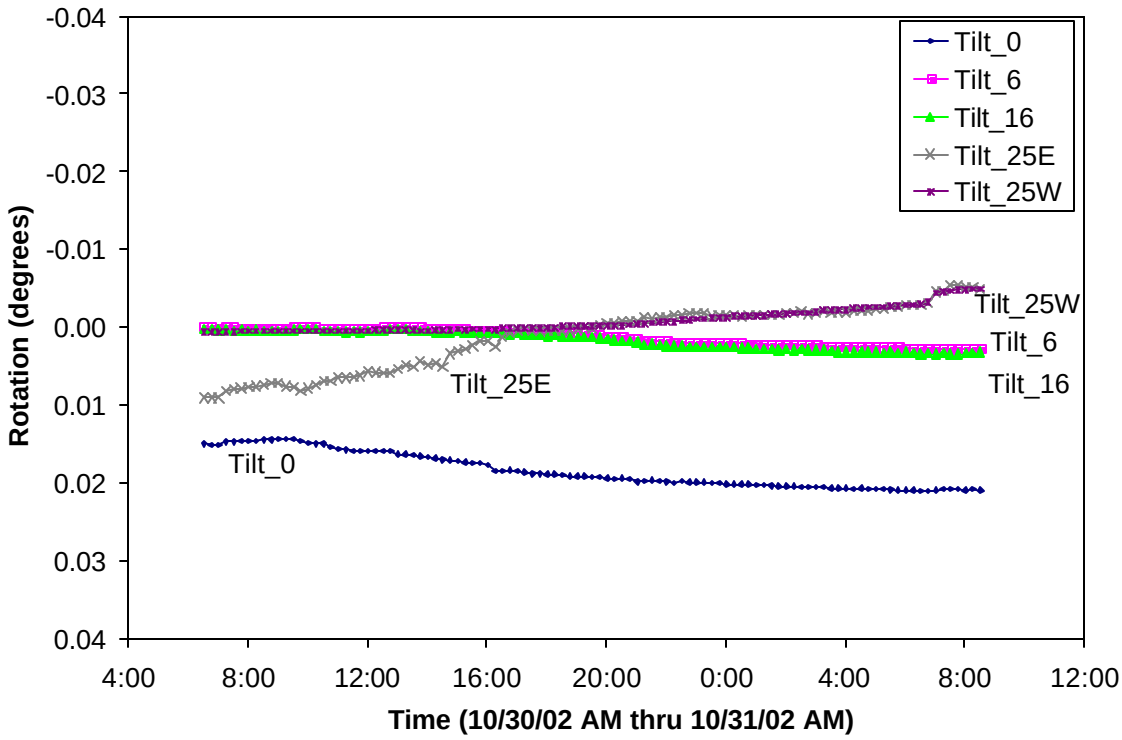

Figure E.6. Tiltmeter readings for the third day of backfilling.

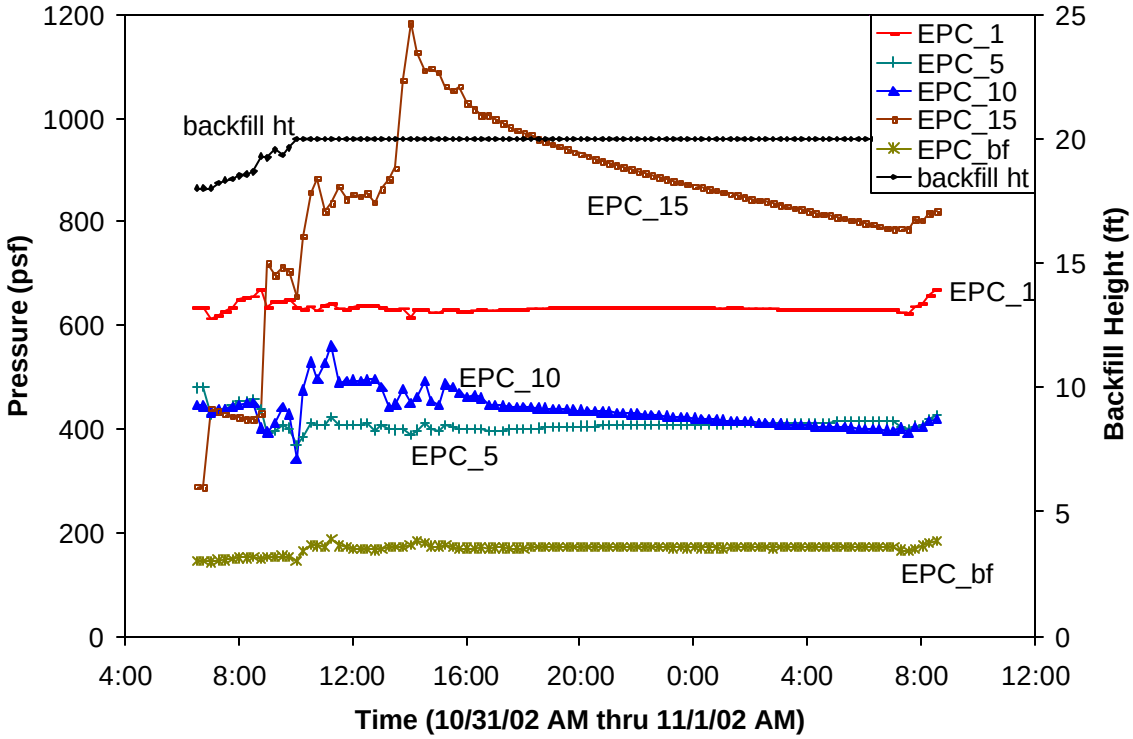

Figure E.7. Stem EPC readings and backfill heights for the fourth day of backfilling.

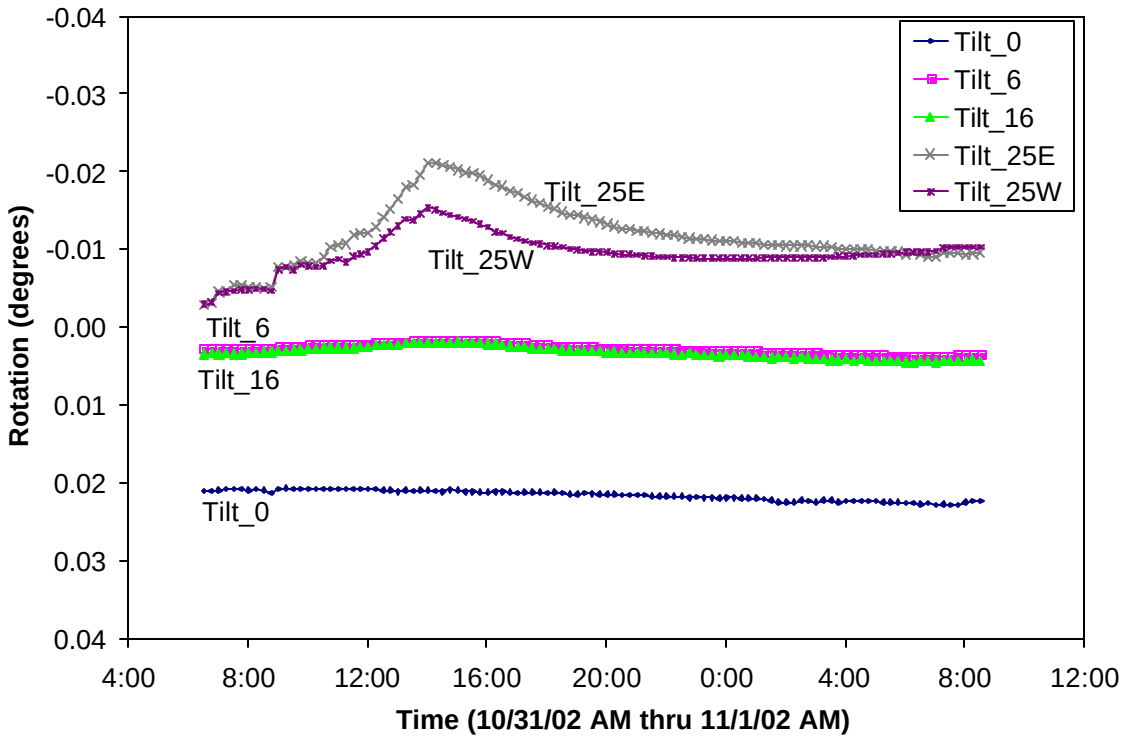

Figure E.8. Tiltmeter readings for the fourth day of backfilling.

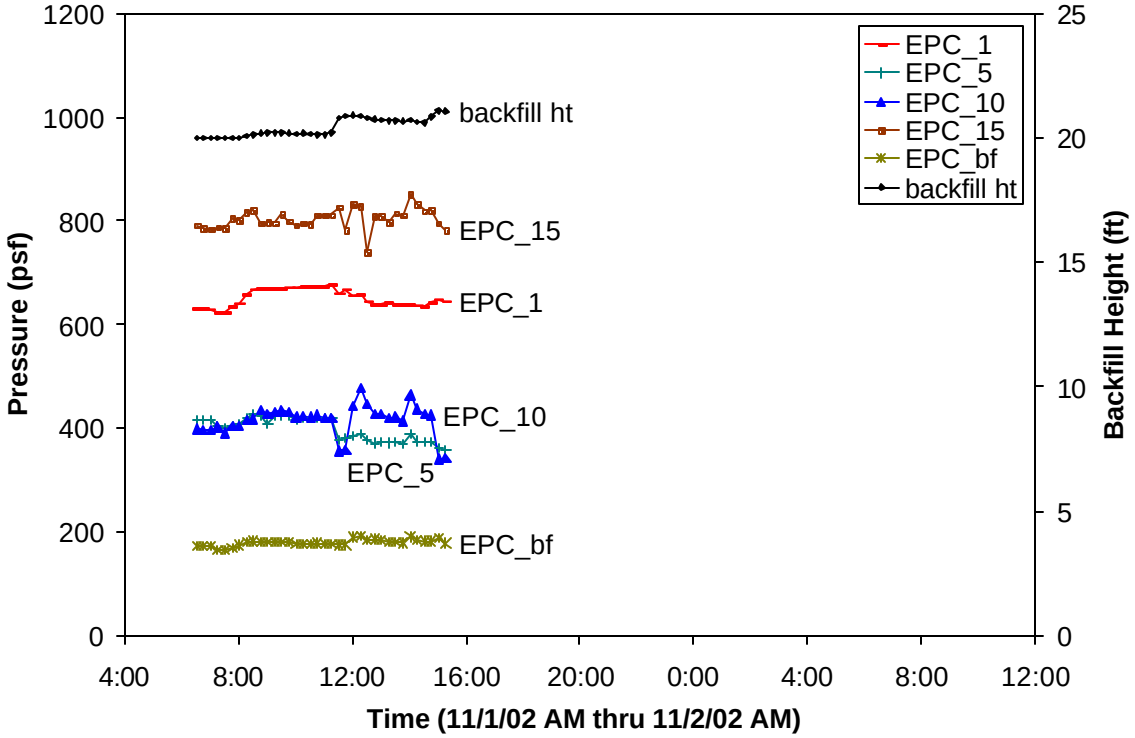

Figure E.9. Stem EPC readings and backfill heights for the fifth day of backfilling.

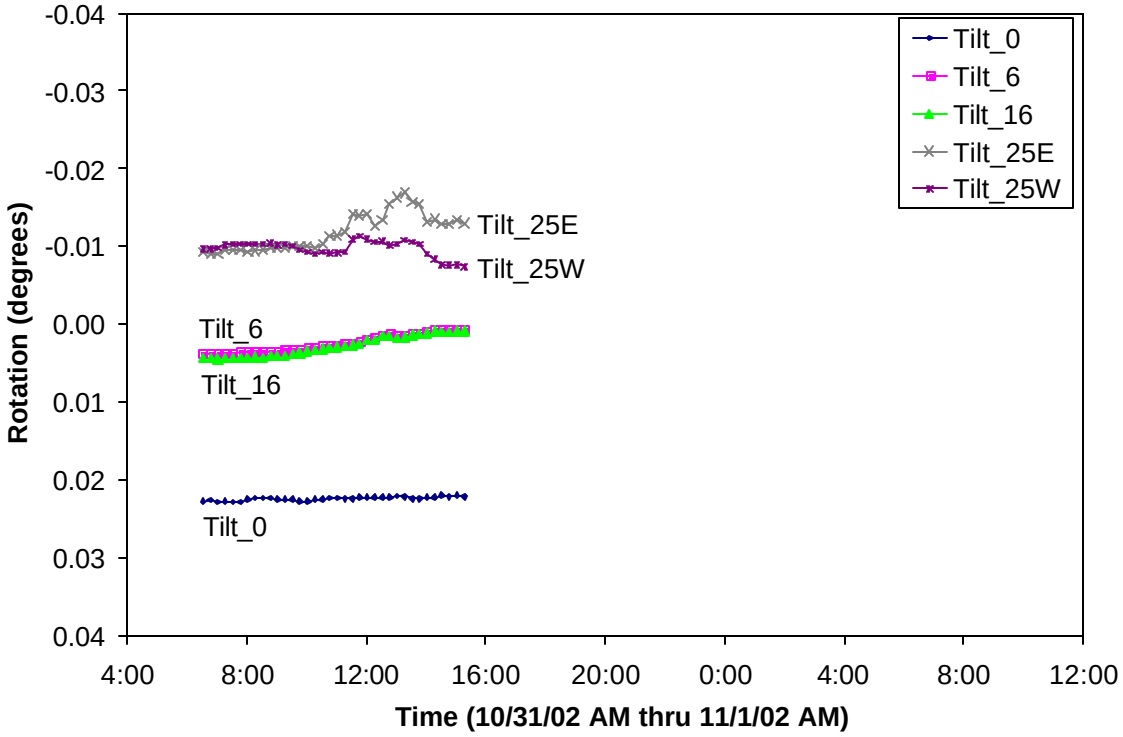

Figure E.10. Tiltmeter readings for the fifth day of backfilling.

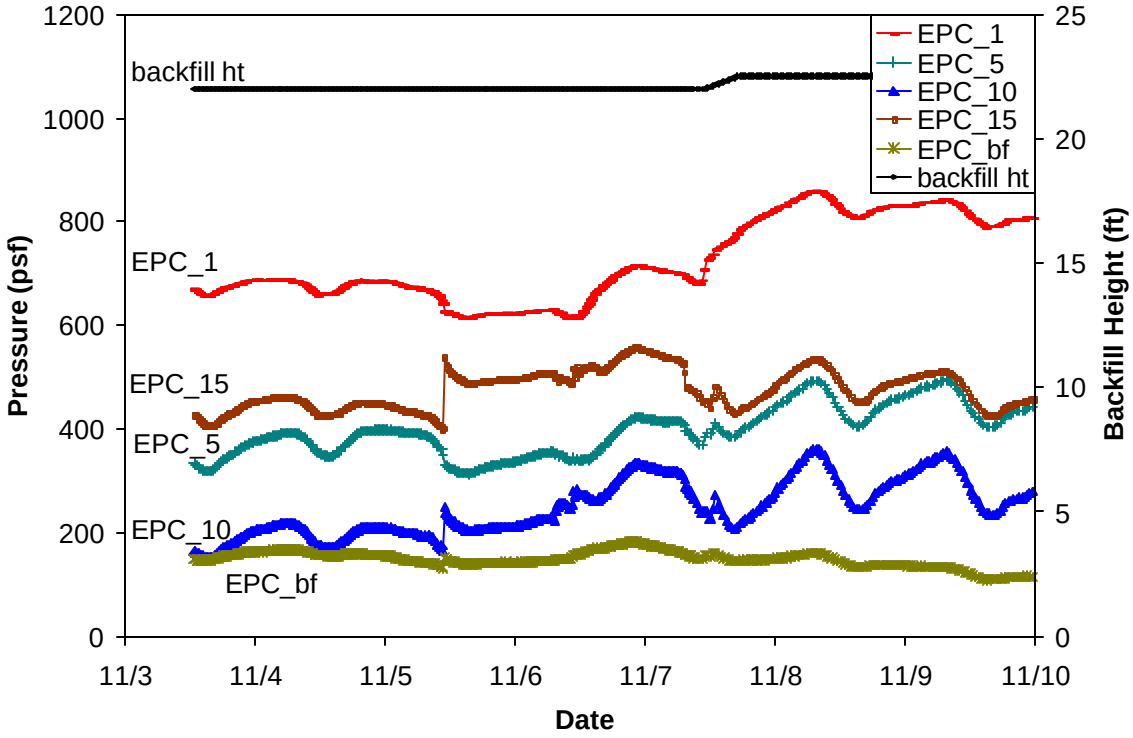

Figure E.11. Stem EPC readings and backfill heights for November 3-9, 2002.

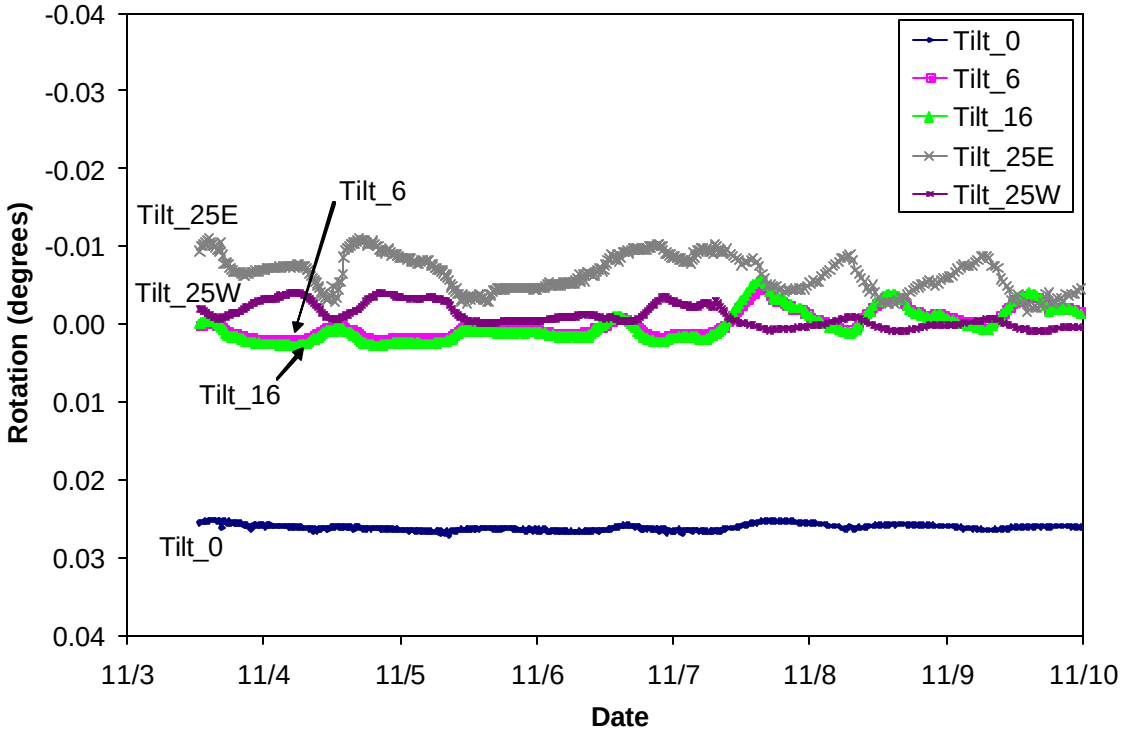

Figure E.12. Tiltmeter readings for November 3-9, 2002.

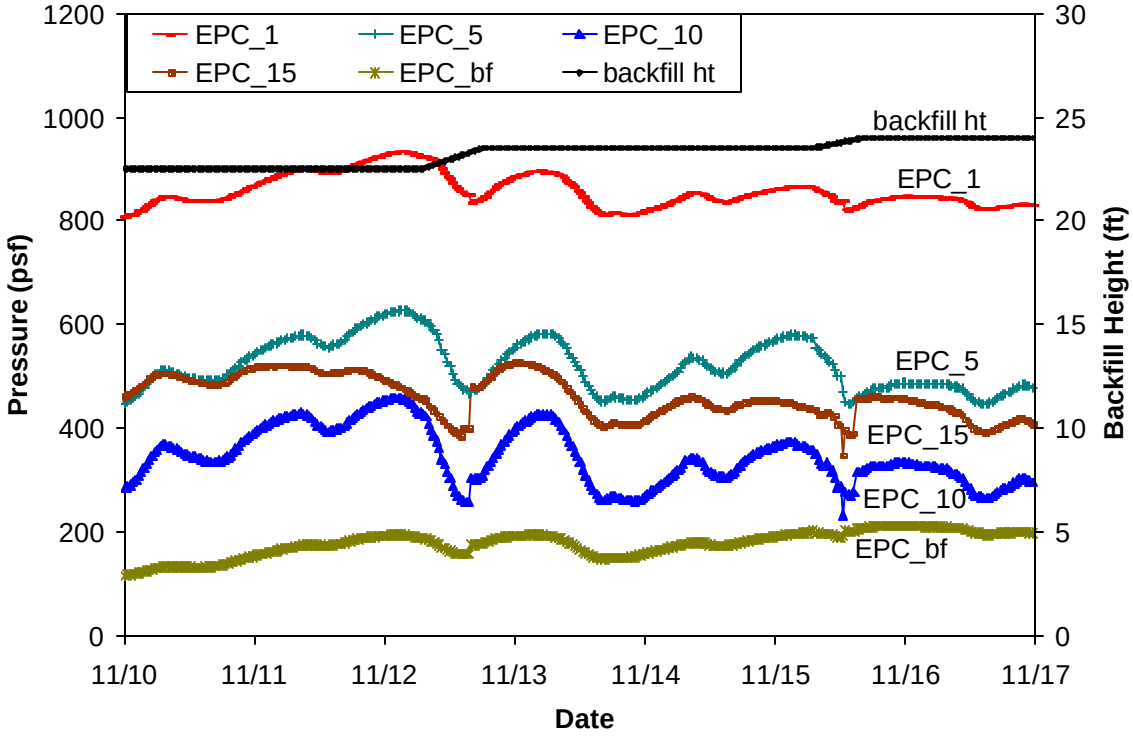

Figure E.13. Stem EPC readings and backfill heights for November 10-16, 2002.

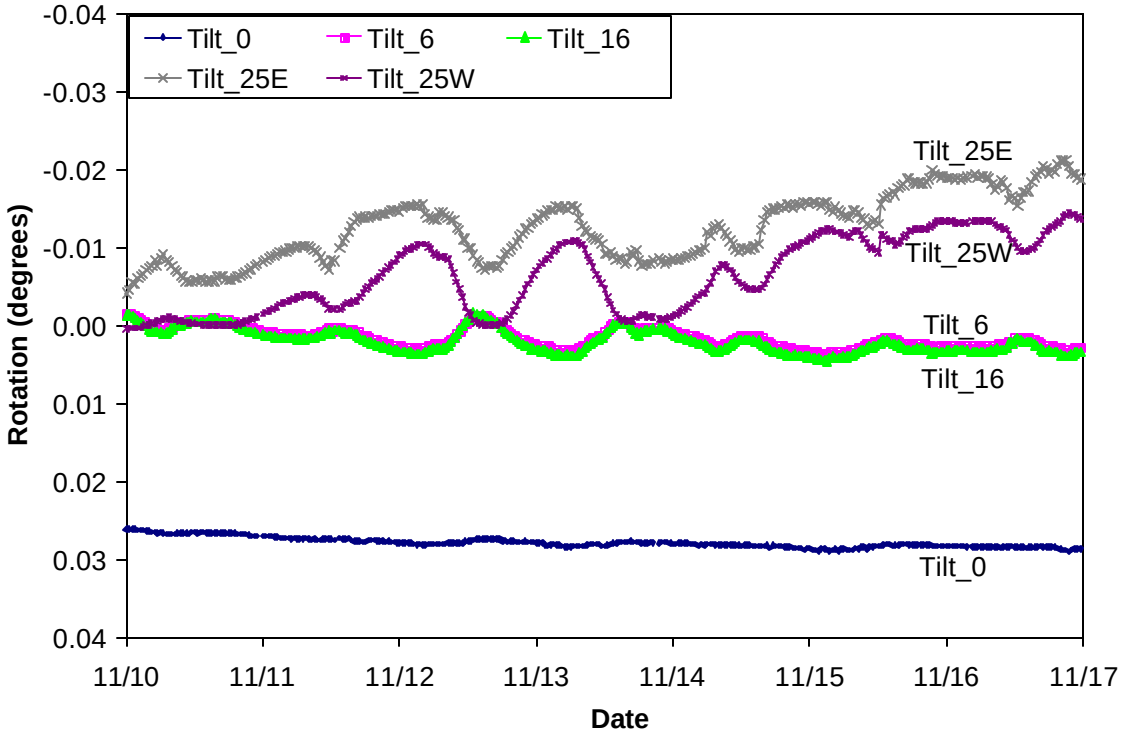

Figure E.14. Tiltmeter readings for November 10-16, 2002.

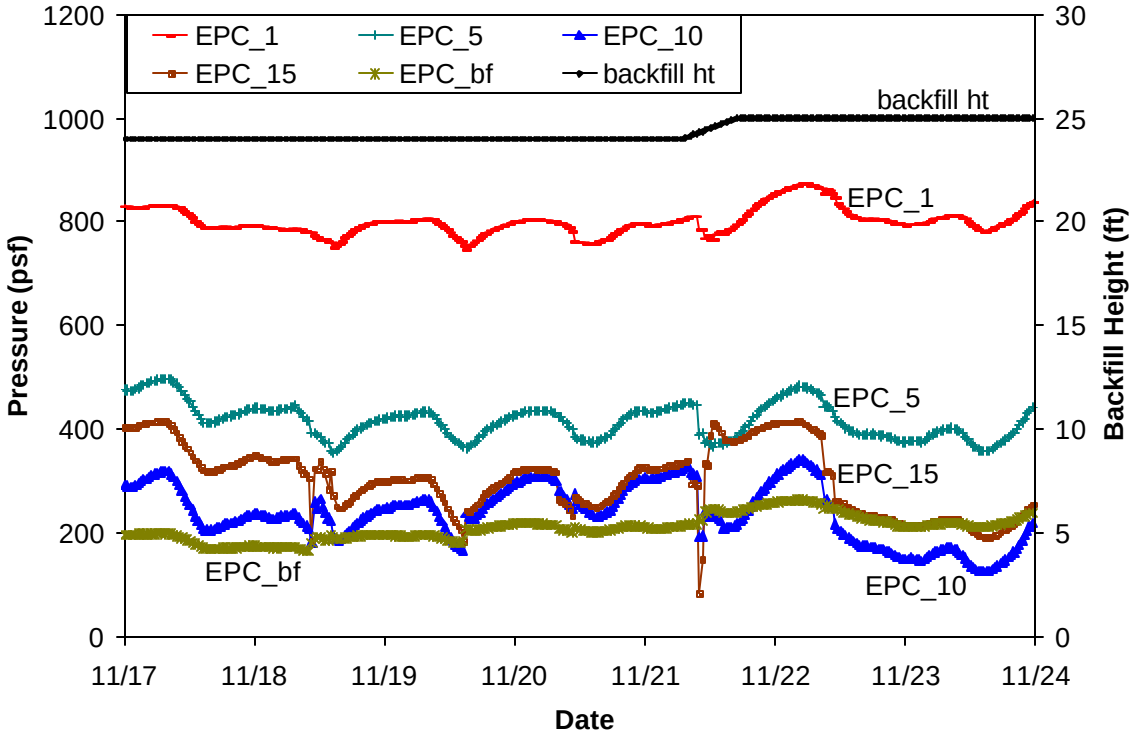

Figure E.15. Stem EPC readings and backfill heights for November 17-23, 2002.

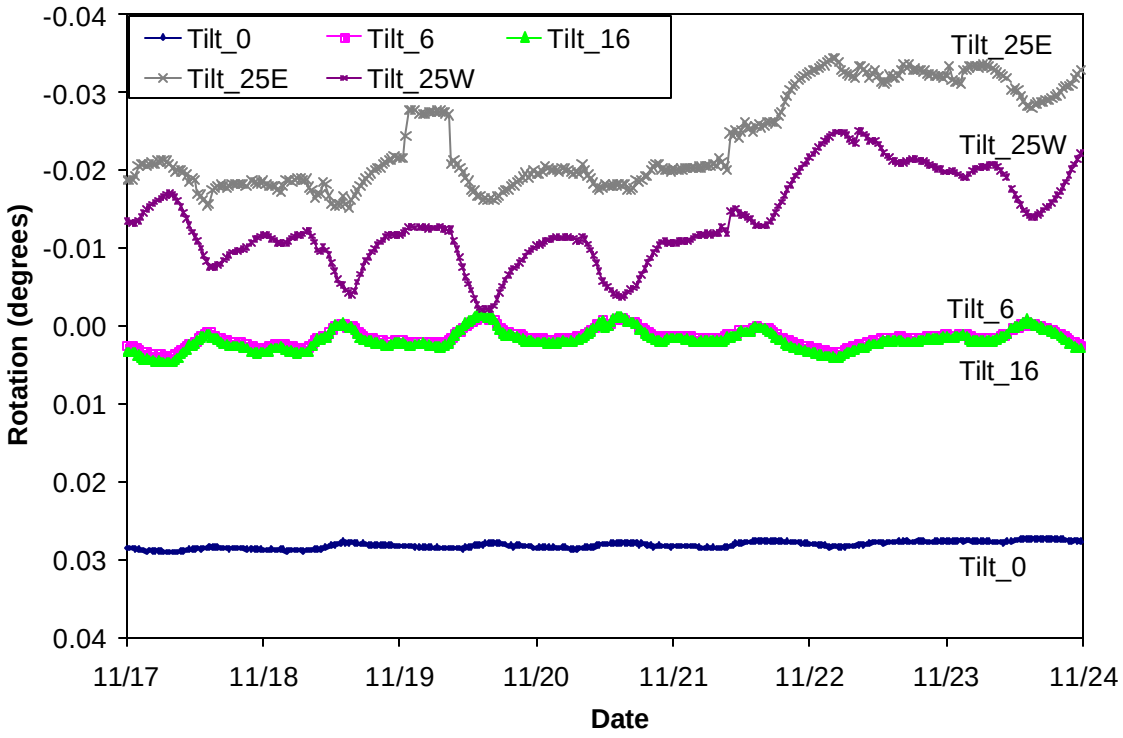

Figure E.16. Tiltmeter readings for November 17-23, 2002.

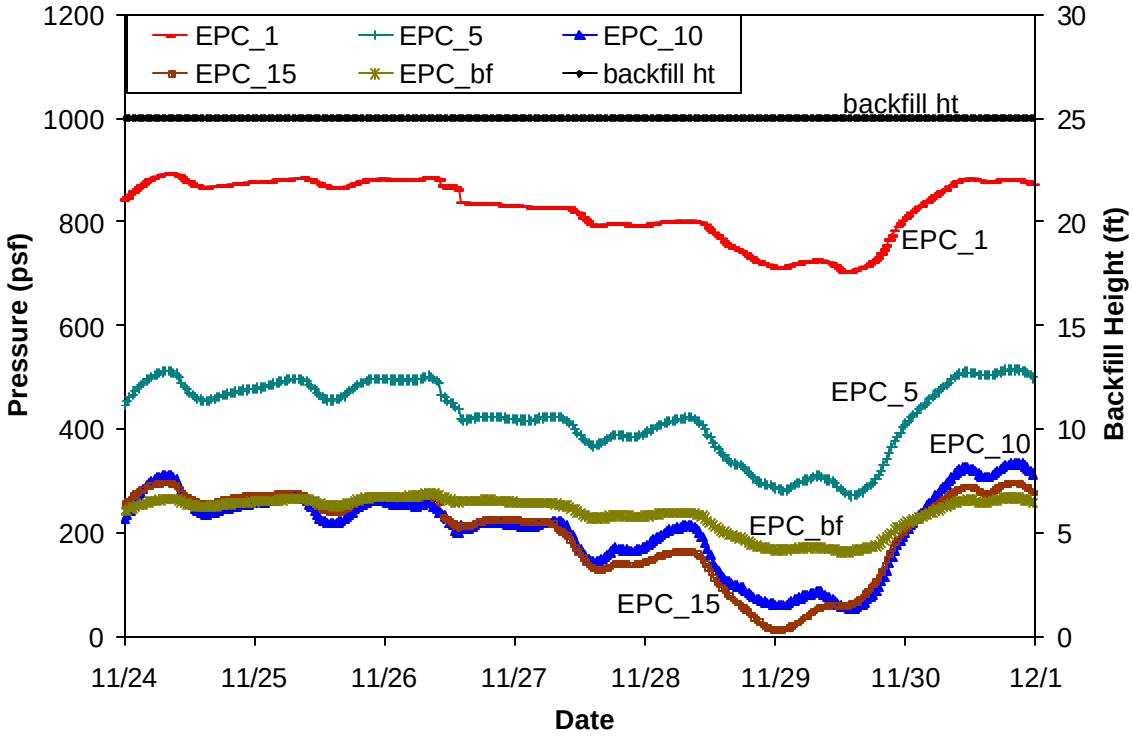

Figure E.17. Stem EPC readings and backfill heights for November 24-30, 2002.

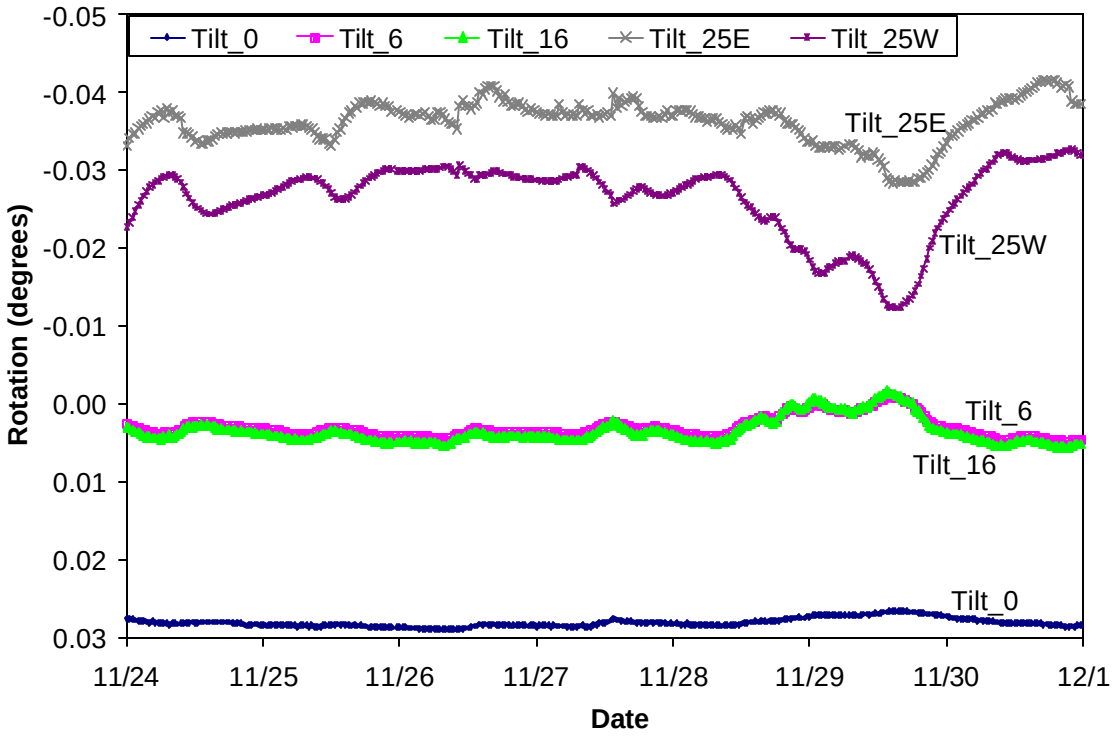

Figure E.18. Tiltmeter readings for November 24-30, 2002.

Readings after Backfilling

The following pages show sensor readings from December 2002 thru July 2003, eight months after the completion of backfilling. The sensors are plotted weekly for the first half of December, then monthly after that. Recall that a malfunction of the CR10X data acquisition unit occurred during the first week of December. This is reflected as two gaps in the readings shown in Figs. E.19 and E.20. The influence of temperature is evident throughout the figures, both through the daily cycle and sub-freezing temperatures.

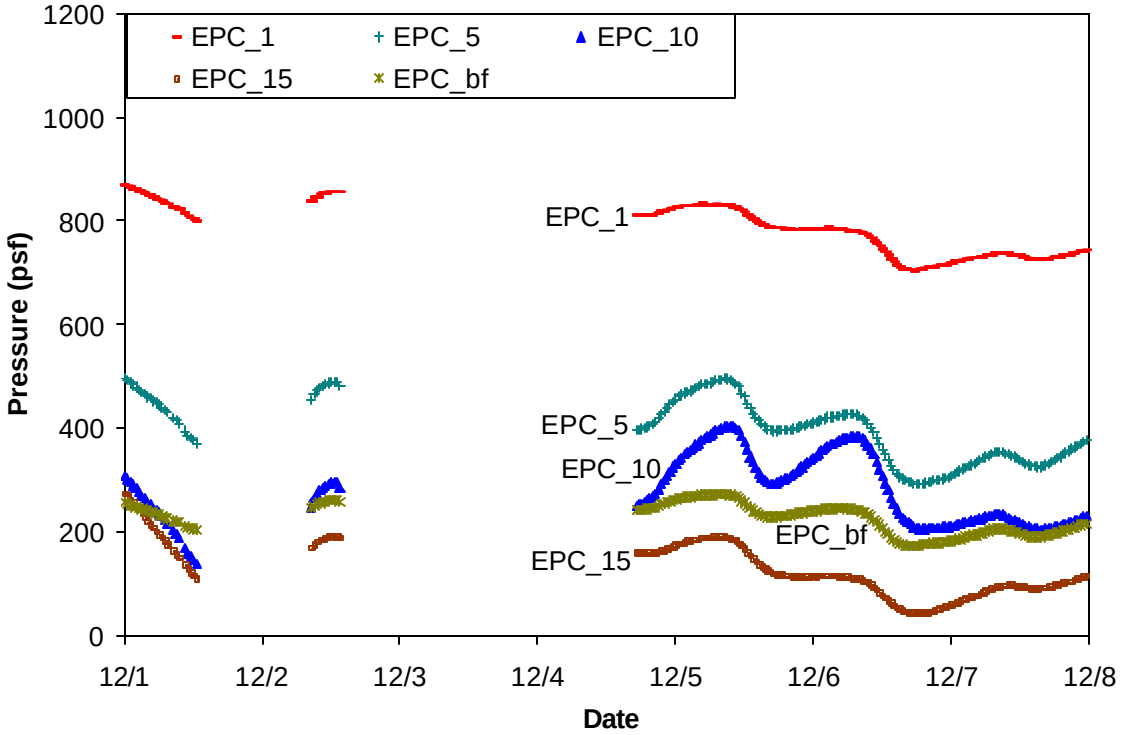

Figure E.19. Stem EPC readings for December 1-7, 2002; the gaps are due to malfunctioning of the data acquisition system.

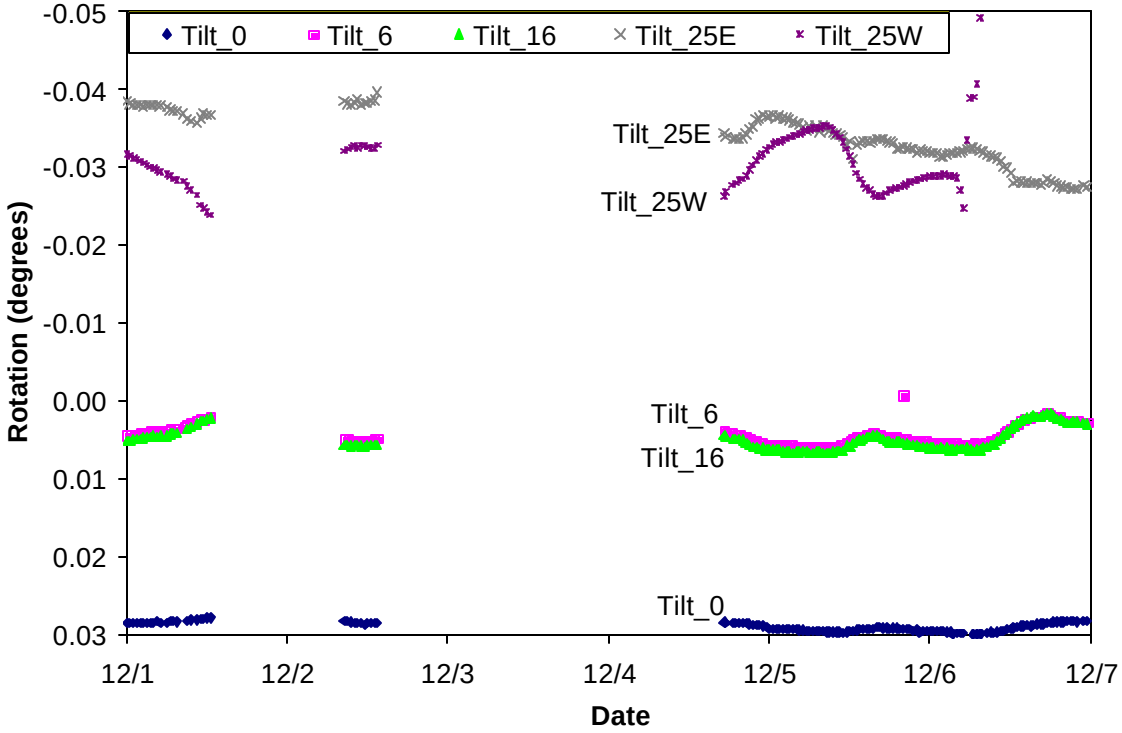

Figure E.20. Tiltmeter readings for December 1-7, 2002; the gaps are due to malfunctioning of the data acquisition system.

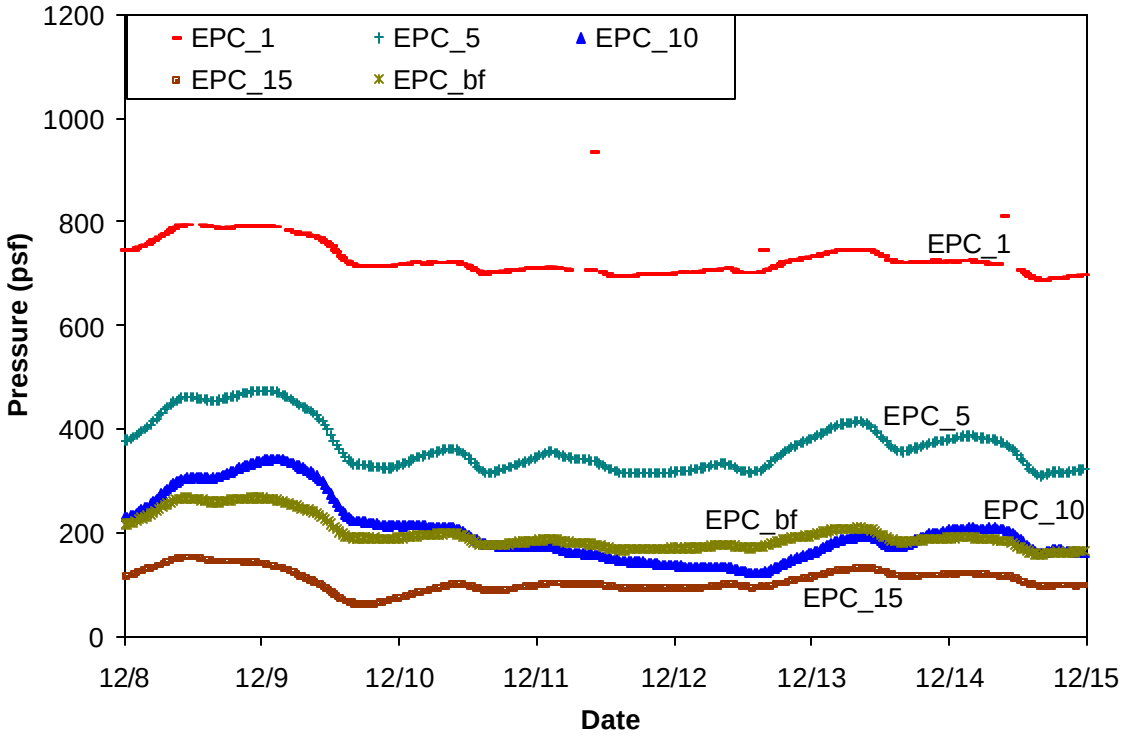

Figure E.21. Stem EPC readings for December 8-14, 2002.

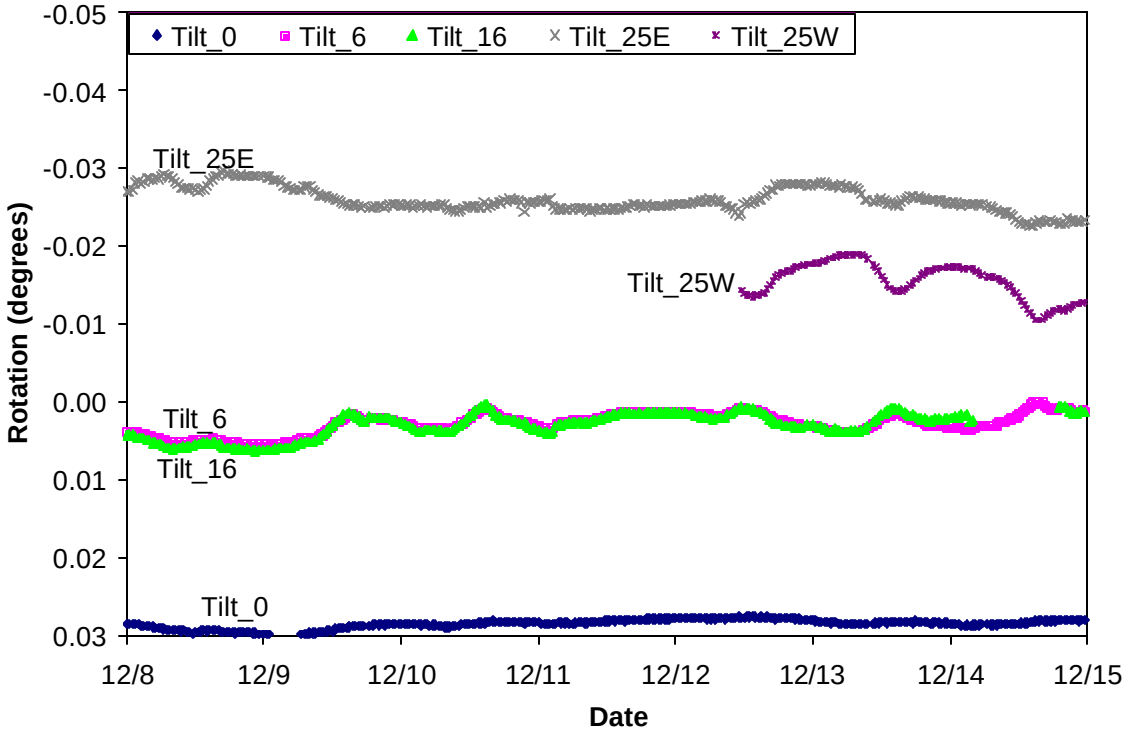

Figure E.22. Tiltmeter readings for December 8-14, 2002.

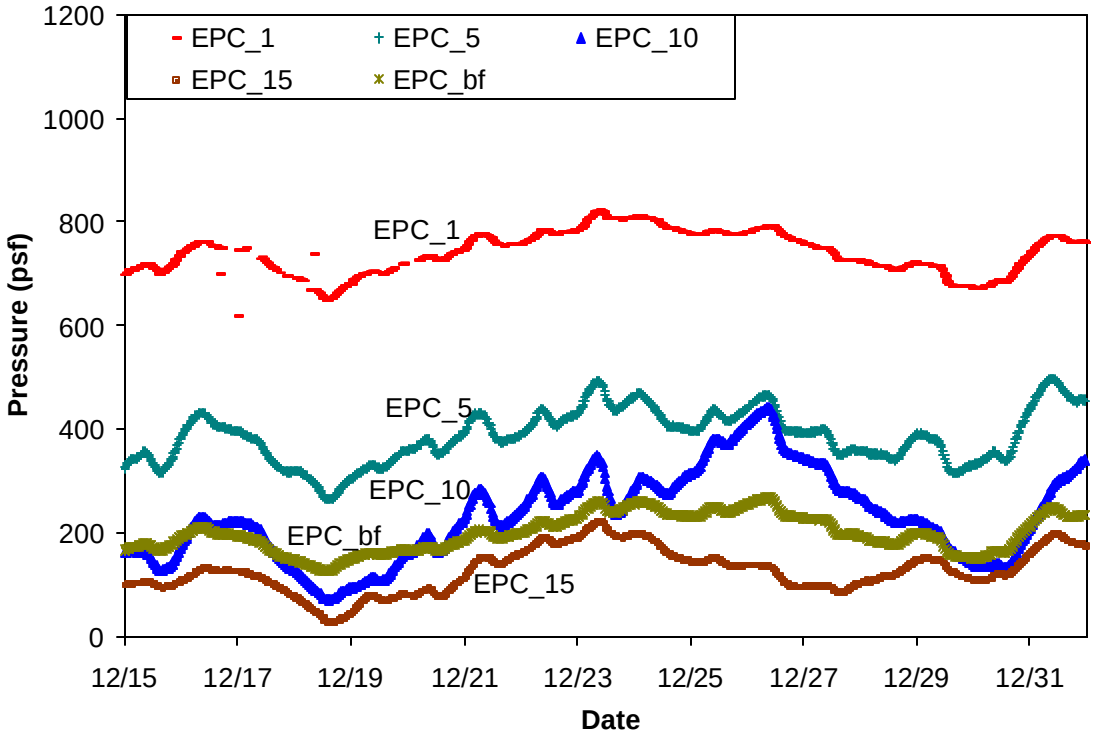

Figure E.23. Stem EPC readings for December 15-31, 2002.

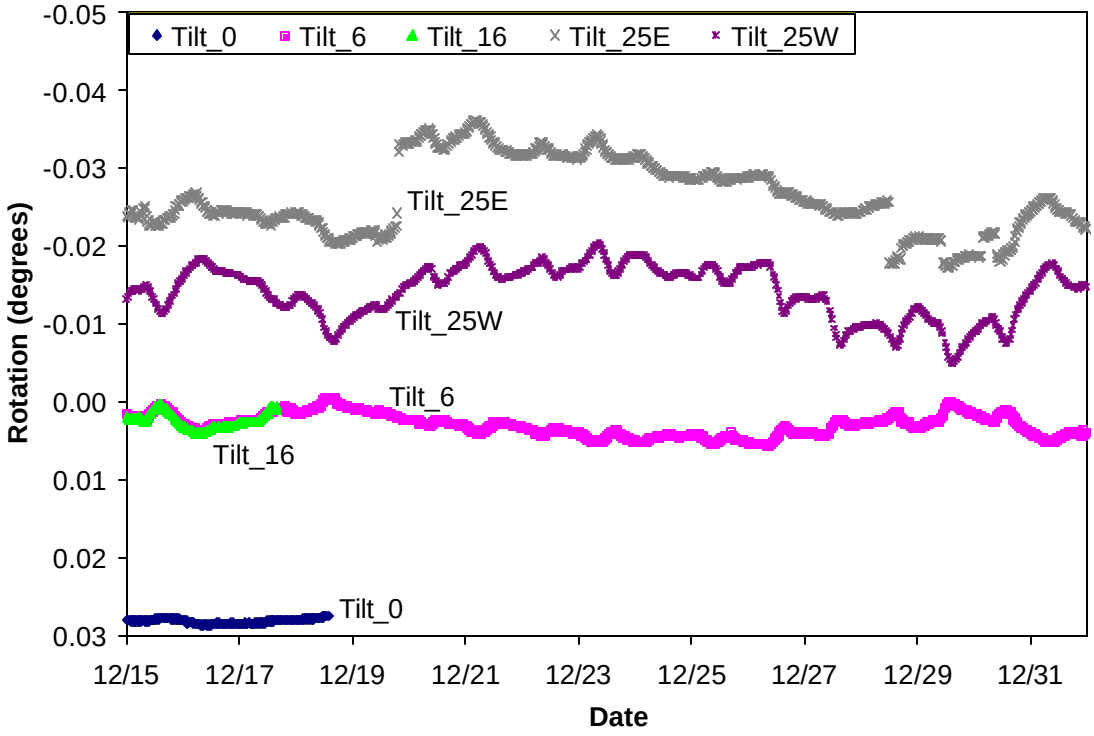

Figure E.24. Tiltmeter readings for December 15-31, 2002.

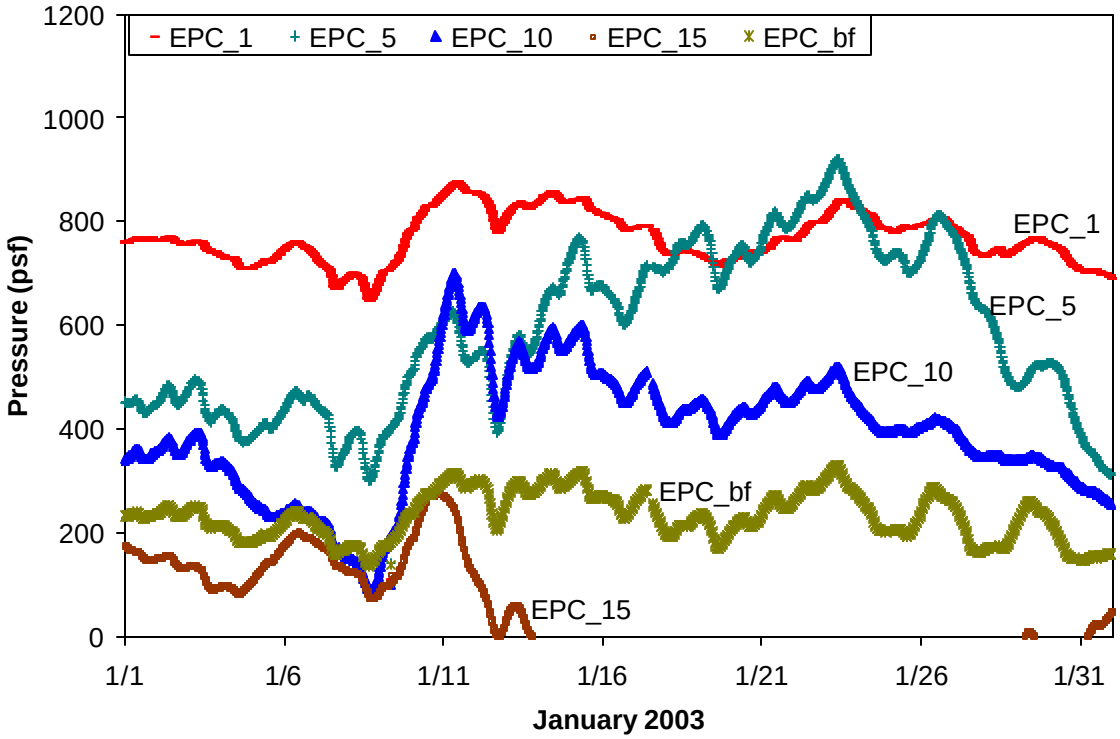

Figure E.25. Stem EPC readings for January 2003.

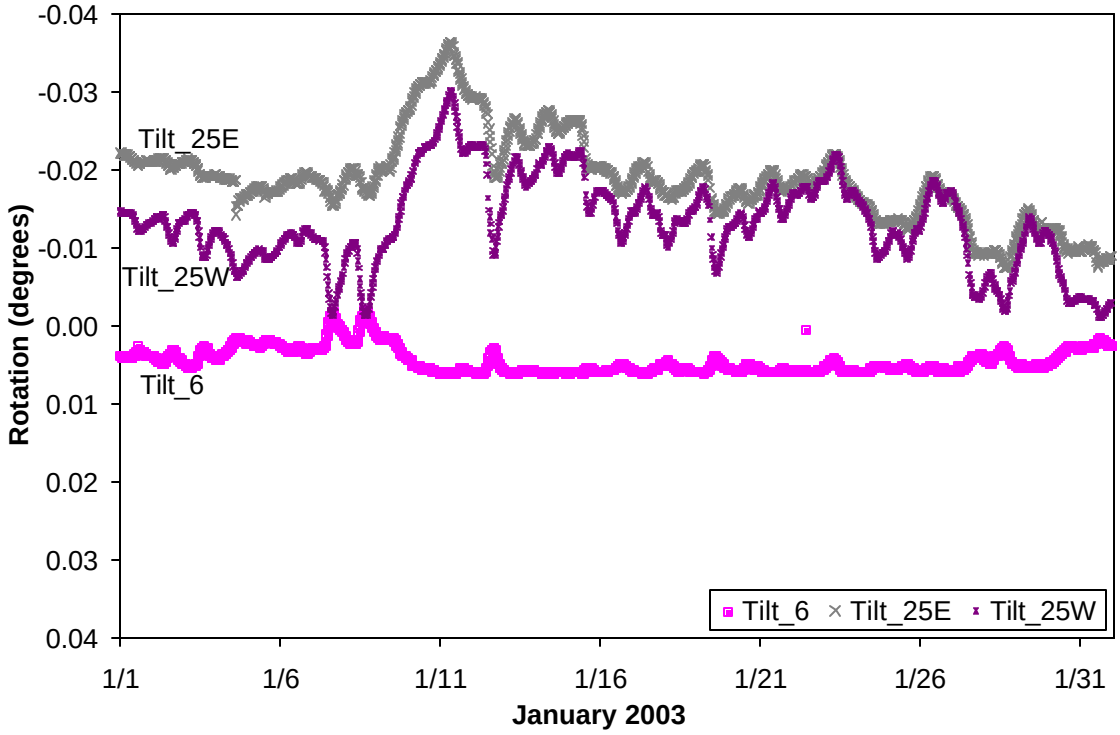

Figure E.26. Tiltmeter readings for January 2003.

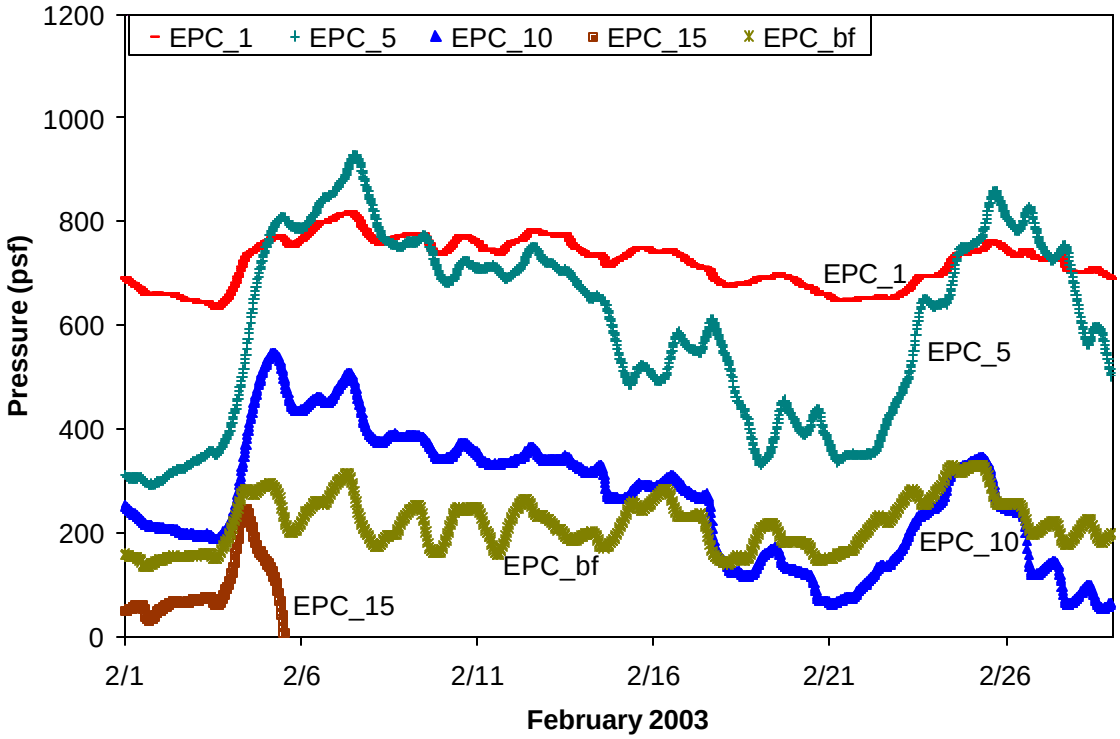

Figure E.27. Stem EPC readings for February 2003.

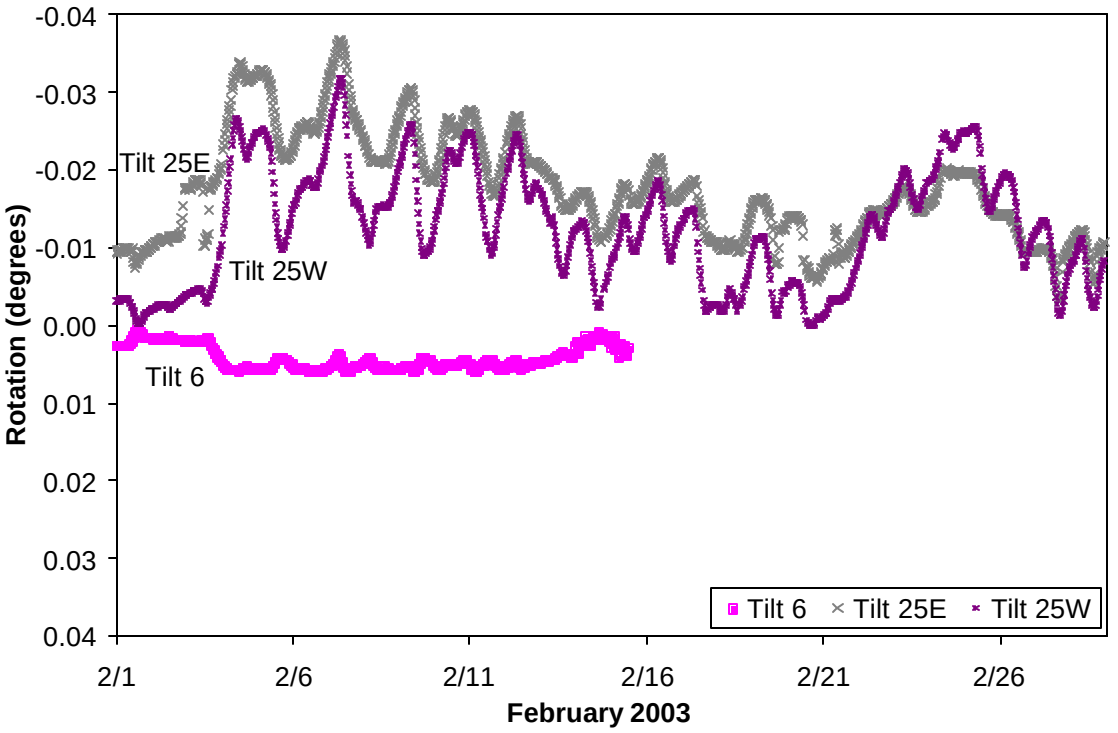

Figure E.28. Tiltmeter readings for February 2003.

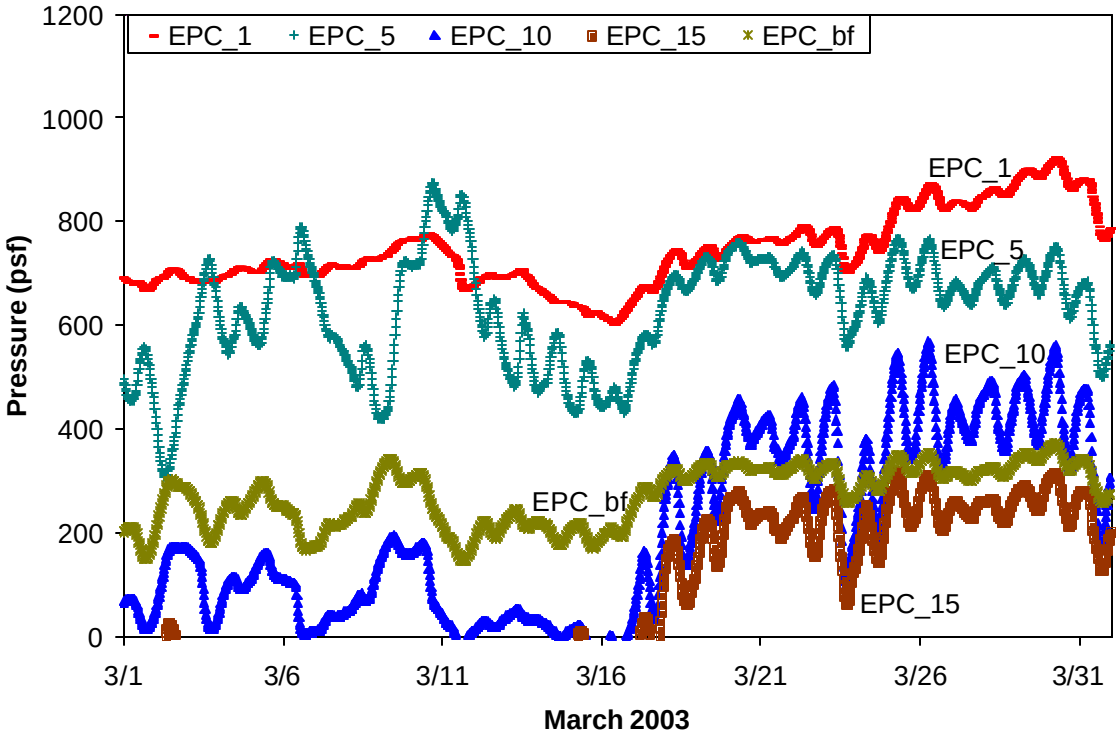

Figure E.29. Stem EPC readings for March 2003.

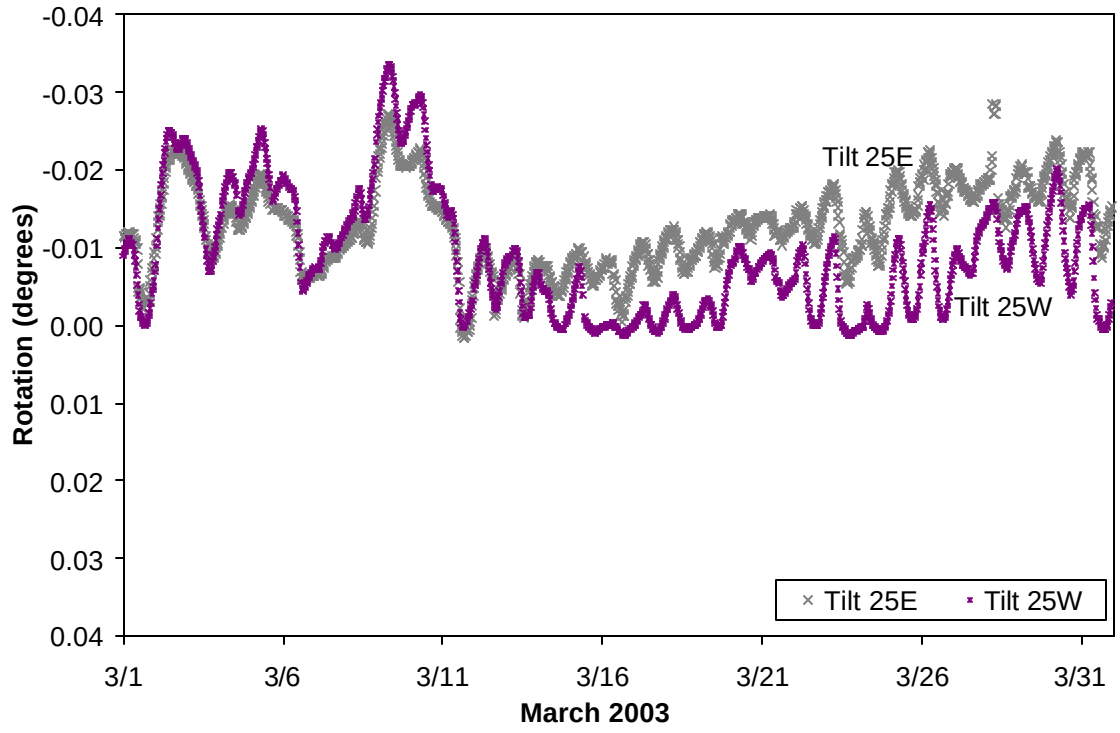

Figure E.30. Tiltmeter readings for March 2003.

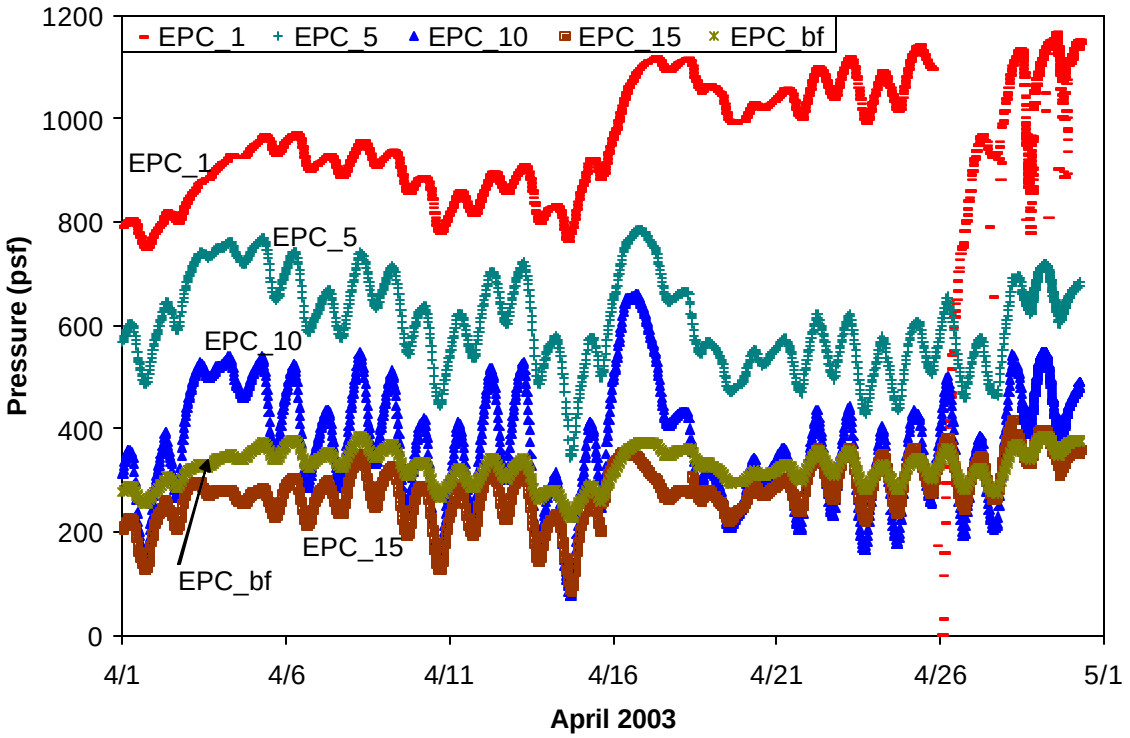

Figure E.31. Stem EPC readings for April 2003.

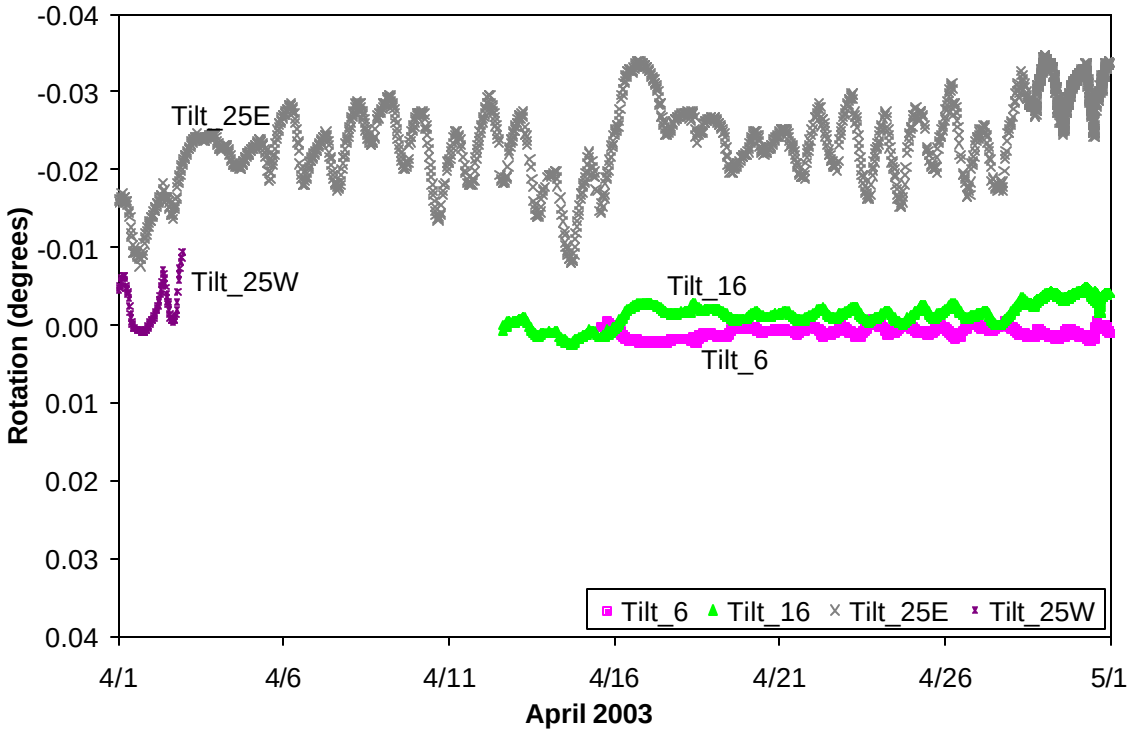

Figure E.32. Tiltmeter readings for April 2003.

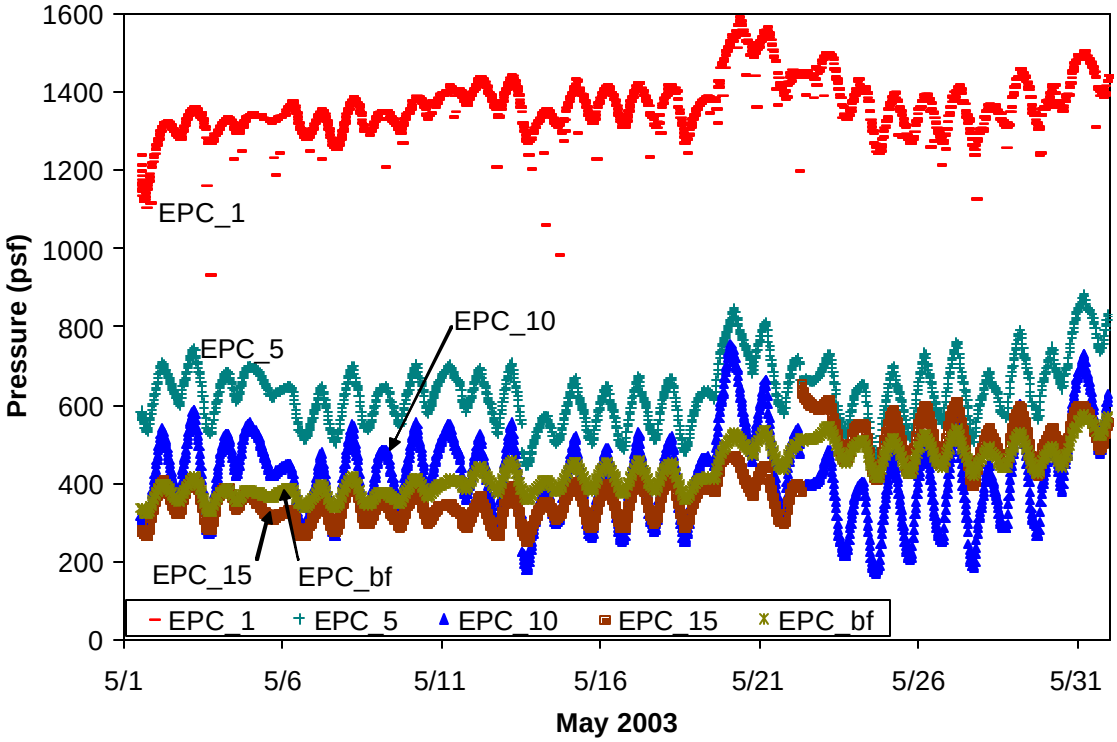

Figure E.33. Stem EPC readings for May 2003.

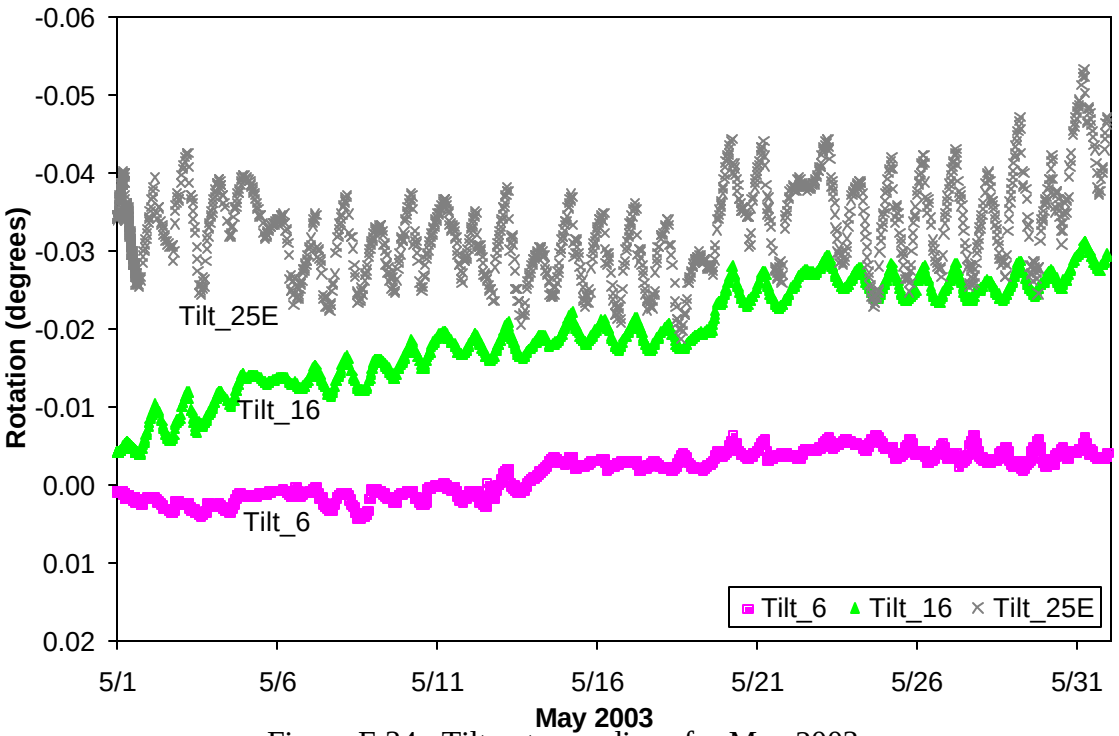

Figure E.34. Tiltmeter readings for May 2003.

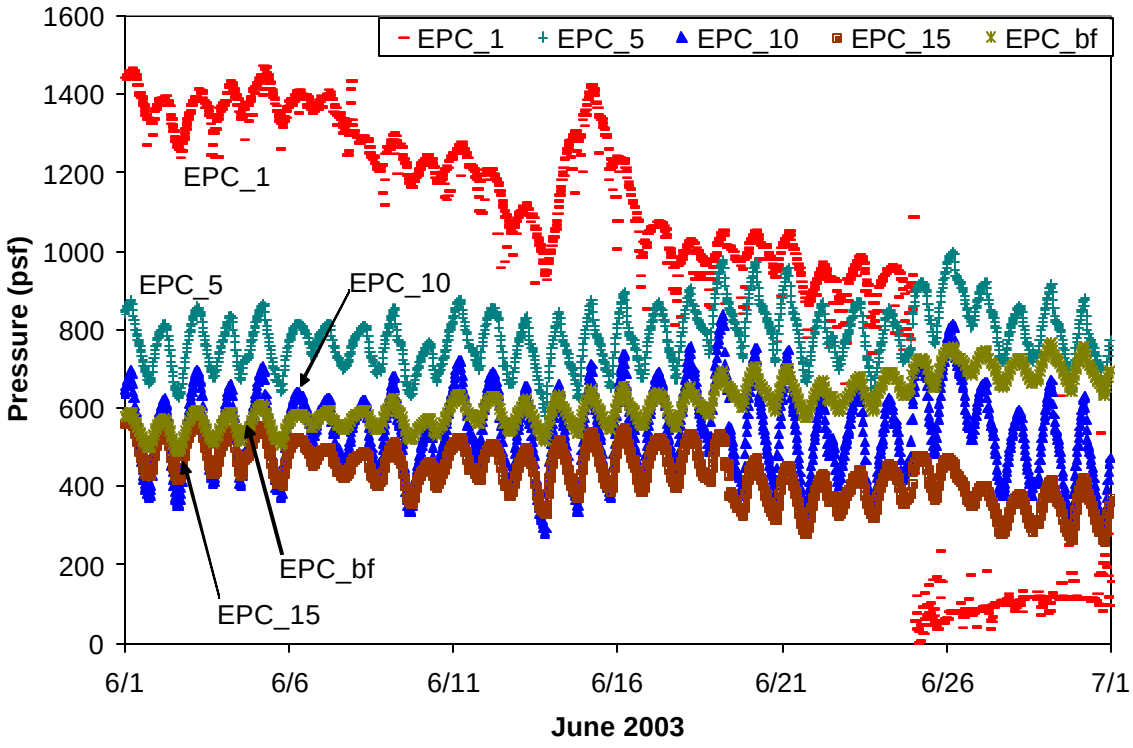

Figure E.35. Stem EPC readings for June 2003.

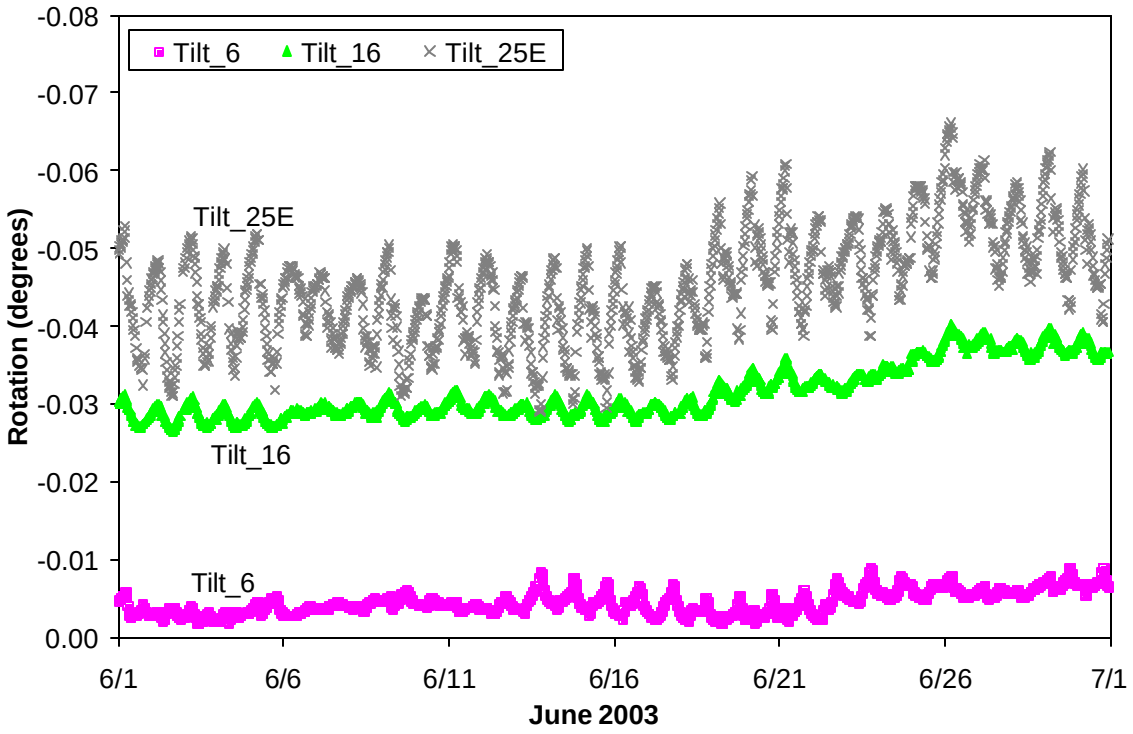

Figure E.36. Tiltmeter readings for June 2003.

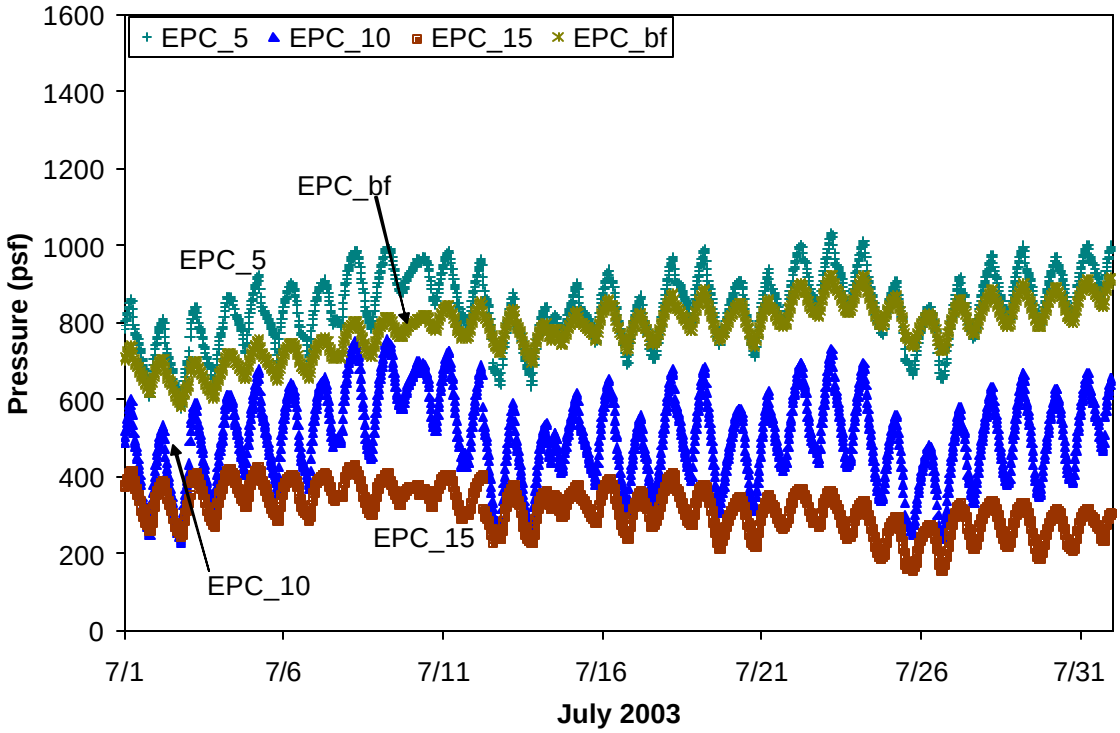

Figure E.37. Stem EPC readings for July 2003.

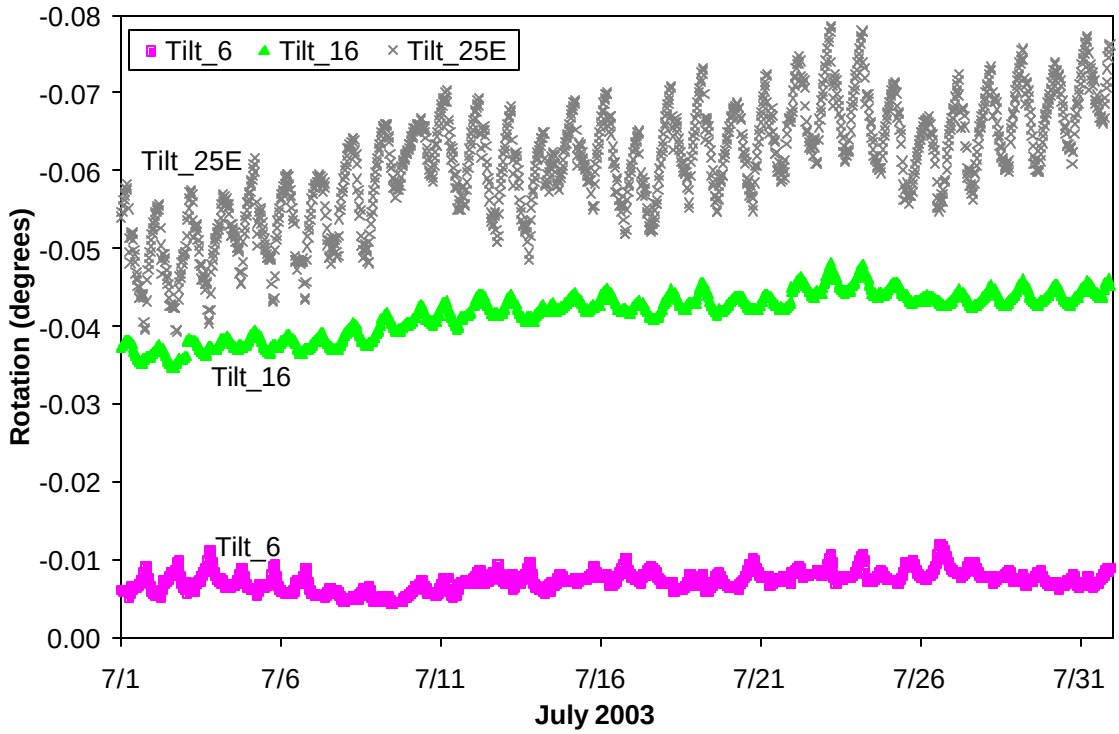

Figure E.38. Tiltmeter readings for July 2003.

Appendix F

Structural Analysis Parameter Study

Introduction

This appendix contains a parameter study of the internal forces that are typically obtained during the structural analysis of a cantilever retaining wall and used for designing the wall. The study focuses on the distribution and magnitude of the shear forces (*V*) and bending moments (*M*) in the stem of the wall. The influence of lateral earth pressure profile is evaluated by comparing two common theories, namely active and at-rest pressures, with pressure profiles that were measured for the instrumented retaining wall at six discrete times during the monitoring period. Design values for the internal forces are also evaluated according to the Mn/DOT Load Factor Design (LFD) and Load and Resistance Factor Design (LRFD) methods.

Two versions of the LFD procedure are considered, including the procedure as defined in the Mn/DOT standard, and a variation in which one of the load factors for the lateral earth pressure is reduced. Two versions of the LRFD procedure are also considered, one which utilizes active earth pressure theory and the other which uses at-rest pressure theory. The goal of these comparisons is to evaluate the safety margins in the internal forces (*V* and *M*) that are calculated according to the Mn/DOT LFD and LRFD procedures, so as to verify the adequacy of the load factors and load combinations in these two procedures.

Lateral Earth Pressure Distributions

Lateral earth pressures were measured in-situ for panel BJ of the retaining wall on the south side of Interstate 494 in Bloomington, MN between West Bush Lake Road and East Bush Lake Road. The panel is 26 ft high and was backfilled to an elevation of 25 ft above the base of the stem of the retaining wall. Details of the retaining wall, instrumented panel and monitoring procedure are given in Chapter 3. Chapters 4 and 5 present the earth pressure data and panel response that were measured during the 12-month monitoring period.

Six pressure profiles that were measured during the monitoring period were selected for the structural analysis parameter study included in this appendix. The pressure profiles are listed in Table F.1 and are shown in Figure F.1.

Table F.1. Measured earth pressure profiles.

Date	**Description**
Nov. 27, 2002	Pressure profile at the end of the backfilling process.
Dec. 20, 2002	Pressure profile prior to soil freezing.
Jan. 3, 2003	Pressure profile during sub-freezing temperatures (-10º to 20º F).
Feb. 15, 2003	Pressure profile when the top layer of soil (~ 10 ft.) was frozen.
Mar. 18, 2003	Profile after the effect of soil freezing dissipated.
April 24, 2003	Profile measured at 5:34 AM during the coldest portion of a daily cycle.

With the exception of the profile measured on April 24, 2003, all measured pressure distributions were approximately bilinear in shape, as mentioned earlier in the report, with the largest pressure occurring at the base of the stem. Unlike the other measured profiles, the one for April 24, 2004 was approximately linear, and the distribution for active pressure theory is seen to provide a reasonably good approximation of these measured pressures, except at the base of the stem. All other measured pressures have magnitudes that are smaller than those for active pressure. The active and at-rest pressure distributions shown in Fig. F.1 were obtained using pressure coefficients (K_a = 0.275, K_o = 0.4264) and soil unit weight (w_s = 120 pcf) that are described in the following section.

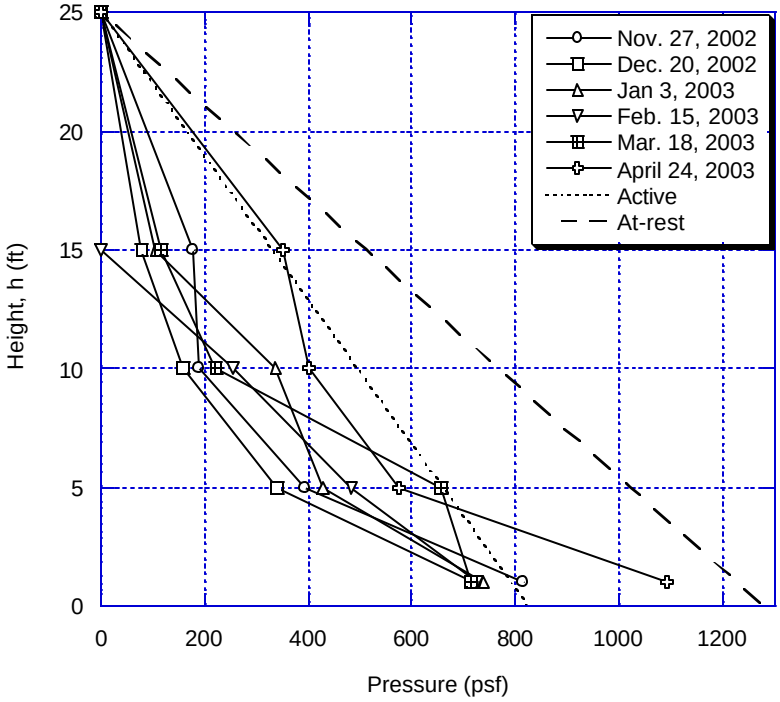

Figure F.1. Lateral earth pressure distributions.

The measured pressure profiles given in Fig. F.1 were integrated with respect to vertical distance along the stem of the wall to obtain shear forces, V

$$V = \int p dy \cong \sum \frac{1}{2}(p_i + p_{i+1})(y_{i+1} - y_i) \qquad \text{(F.1)}$$

where p_i is a pressure measured at a distance y_i from the base of the stem, and h is the height of the stem. The shear force profile corresponding to active and at-rest pressure theories is given by

$$V = \int p dy = \int K w_s (h - y) dy = \frac{1}{2} K w_s h^2 \left[2\left(\frac{y}{h}\right) - \left(\frac{y}{h}\right)^2 \right] \qquad \text{(F.2)}$$

where K is the coefficient corresponding to either active (K_a) or at-rest (K_o) pressure. Shear force distributions are shown in Fig. F.2 for all measured pressure profiles, as well as for the two pressure theories. Shear forces for all measured profiles except for one measured on April 24, 2003 have smaller magnitudes than either the active and at-rest

pressure theories. Moreover, the shear forces for active pressure theory agree well with the ones measured on April 24, 2003.

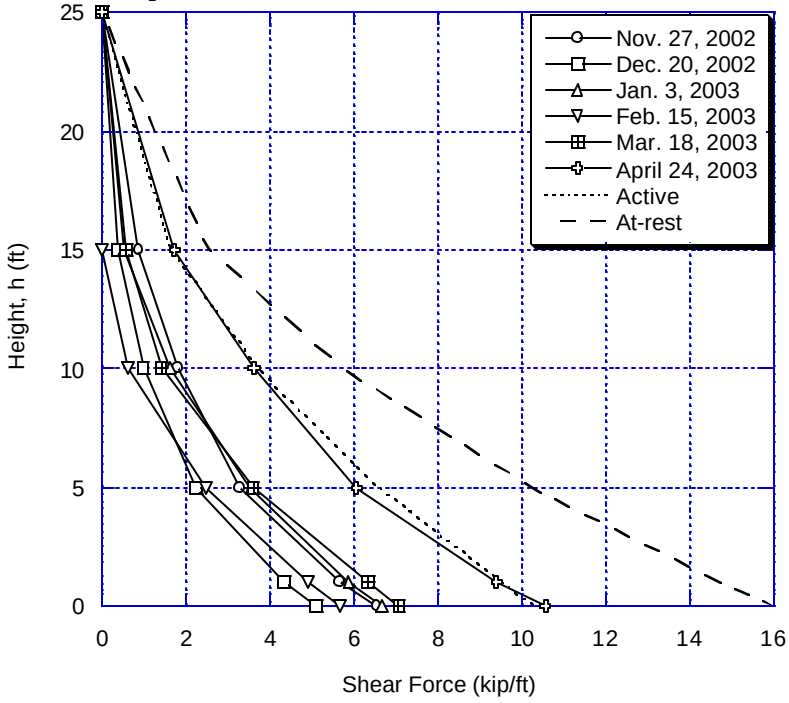

Figure F.2. Shear force distributions.

The first moment of the measured pressure profiles given in Fig. F.1 were integrated with respect to vertical distance along the stem of the wall to obtain bending moments, M

$$M = \int ypdy \cong \sum \frac{1}{2}(p_i + p_{i+1})(y_{i+1} - y_i)(y_i - y + y_c) \tag{F.3}$$

where y_c is the vertical centroidal distance from the base of each trapezoidal segment of the pressure distribution. The bending moment profiles corresponding to active and at-rest pressure theories are given by

$$M = \int ypdy = \int yKw_s(h-y)dy = \frac{1}{6}Kw_s h^3\left[3\left(\frac{y}{h}\right)^2 - 2\left(\frac{y}{h}\right)^3\right] \tag{F.4}$$

Bending moment distributions are shown in Fig. F.3 for all measured pressure profiles, as well as for the two pressure theories. Bending moments for all measured profiles except the one measured on April 24, 2003 have smaller magnitudes than either the active and at-rest pressure theories. Moreover, as for earth pressure and shear force, the bending moments corresponding to active pressure theory agree well with those for the pressure profile measured on April 24, 2003.

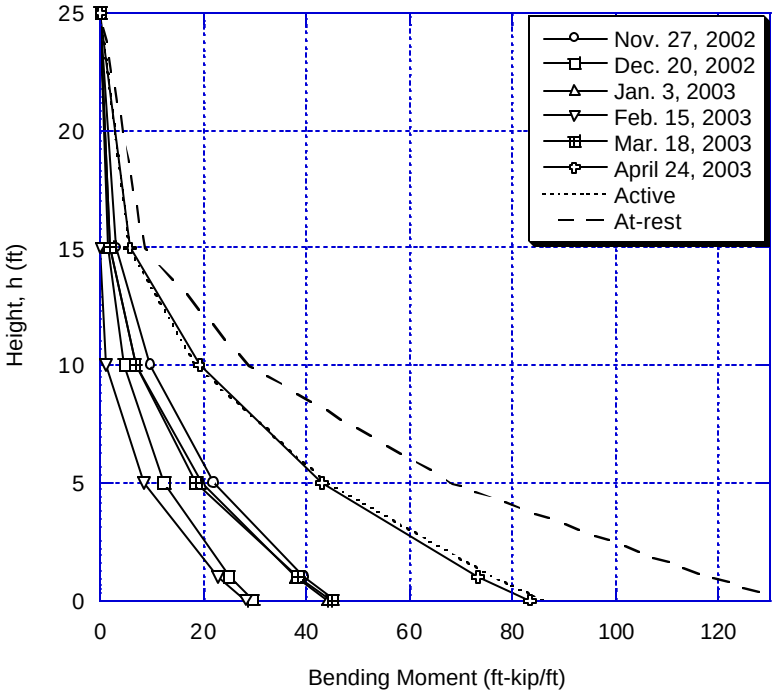

Figure F.3. Bending moment distributions.

Retaining Wall Design Procedures

The Mn/DOT LFD and LRFD Standards allow active earth pressures to be used for the design of retaining walls that have sufficient flexibility to permit movement of the retained soil. This movement mobilizes the active pressures, and for a level fill, the MnDOT Standards specify an equivalent fluid weight of 33 psf. For a unit soil weight (w_s) of 120 pcf, as specified in the fifteenth edition of the AASHTO Standard Specifications, the corresponding active soil pressure coefficient (K_a) is equal to 0.275. This coefficient corresponds to an angle of internal friction (f) equal to 34.7º that agrees well with the values that were determined by testing the fill material for the instrumented retaining wall (See Appendix C).

The Mn/DOT LFD and LRFD standards specify a unit soil weight of 125 pcf, instead of the magnitude of 120 pcf used in the present study. However, the smaller magnitude specified by AASHTO (120 psf) was used because it agrees more closely with soil properties determined as part of this study (See Chapter 6).
At-rest earth pressures are not required by either of the Mn/DOT Standards (i.e., LFD or LRFD) for the design of cantilever retaining walls if they are sufficiently flexible to permit movement of the retained soil. However, an LRFD load case is considered in the present study with at-rest pressures to allow comparison with field measurements. A pressure coefficient for at-rest conditions (K_o) equal to 0.426 was used for this case. This coefficient, coupled with a unit soil weight (w_s) equal to 120 pcf, provides an equivalent fluid weight (51 pcf) that is approximately equal to, but slightly smaller than, the value specified in the Mn/DOT standards (53 psf) for those soil retaining structures that are sufficiently rigid to require at-rest pressures.

The Mn/DOT LFD method utilizes the following factored load combination to satisfy safety under expected loads

$$fR_n \geq l\left[D + g(L+I)n + b_E E + W\right] \qquad \text{(F.5)}$$

where R_n is the nominal resistance, and f is the resistance factor. The right-hand side of equation (F.5) represents the factored load effect, where l, g, n, and b_E are load factors, and D, L, I, E and W are the load effects consistent with dead, live, impact, earth pressure and wind loading, respectively. The present study focuses on the treatment of earth pressure effects, consequently, the only component of the factored forces given by (F.5) that is needed is that produced by the lateral earth pressure. That is, no dead, live (surcharge), impact or wind loading effects (D, L, I or W, respectively) were present in the pressure measurements that were taken of the instrumented retaining wall panel. Thus, only the factored earth pressure, $l\,b_E E$, is needed.

The Mn/DOT LFD Standard specifies a value of 1.3 for l, and b_E, is defined as either 1.3 for active pressure conditions, or 1.0 for at-rest conditions. Unlike the Mn/DOT LFD Standard, AASHTO specifies 1.15 for this latter case. In the present study, only active pressure is considered relative to LFD, in which case b_E = 1.3. However, a second LFD case is considered in which b_E is taken equal to unity. It is noted that this load case is only applicable for Service Load Design (i.e., for checking cracking) and it is included in the present study to investigate of the effect of incorrectly selecting b_E, or as a way to determine if the value for the load factor b_E is too large for active pressure conditions. The Mn/DOT LRFD design procedure includes more load conditions than the LFD procedure, and multiple load combinations, each with different load factors, to define the factored effects. For the design of a retaining wall stem, the LRFD load combinations that are most likely to generate the largest forces and moments are referred to as Strength Combinations Ia and Ib in the Mn/DOT Standard, and they are given by

$$fR_n \geq h_i(0.9DC + 1.0EV + 1.5EH + 1.75LS) \qquad \text{(F.6)}$$

and

$$fR_n \geq h_i(1.25DC + 1.35EV + 1.5EH + 1.75LS) \qquad \text{(F.7)}$$

where DC, EV, EH and LS are the load effects corresponding to components and attachments, vertical earth pressure, lateral earth pressure and live surcharge, respectively, and the numerical coefficients are the load factors, g_i.
The partial factor h_i in equations (F.6) and (F.7) is equal to the product of h_D, h_R and h_I, where these factors, respectively, are related to ductility, redundancy and operational importance of the structure. The Mn/DOT LRFD Standard recommends a value of unity for all three factors for most bridges. So, in the present study, h_D and h_I were taken equal to 1.0. However, a value of 1.05 was assumed for h_R because a cantilever retaining wall is not a highly redundant structural system, even though an individual panel can shed some lateral load to adjacent panels by means of the panel connections. In summary, for the present study, both LRFD load combinations produce a factored lateral earth pressure effect given by $g_i h_i EH$, where g_i = 1.5 and h_i = 1.05.

Table F.2. Factored load cases.

Load Case	**Description**
LFD (β_E=1.3)	Mn/DOT LFD for Strength Design, w/ active pressures and λ=1.3, β_E=1.3
LFD (β_E=1.0)	Mn/DOT LFD for Service Load Design, w/ active pressures and λ=1.3, β_E=1
LRFD (active)	Mn/DOT LRFD w/ active pressures (K_o=0.275) and η_i=1.05, γ_i=1.5
LRFD (at-rest)	Mn/DOT LRFD w/ at-rest pressures (K_o=0.426) and η_i=1.05, γ_i=1.5

The factored earth pressures, shear forces and bending moments obtained using the LFD and LRFD design methods (Table F.2.) are given in Tables F.3 – F.5. The shear forces and bending moments are given per unit of wall length. The magnitudes of the factored pressures, shear forces and bending moments are largest for the LRFD procedure with at-rest earth pressure, and smallest for the LFD procedure with β_E=1.0. The factored forces for the other two load cases are approximately equal (~7% difference), namely the LFD procedure with β_E=1.3 and the LRFD procedure with η_i=1.05. The difference between the latter two methods increases to 13% if η_R is taken as unity as recommended in the Mn/DOT LRFD Standard.

Table F.3. LFD and LRFD Factored Lateral Earth Pressures (psf).

Height (ft)	**LFD** (β_E=1.3)	**LFD** (β_E=1.0)	**LRFD** (active)	**LRFD** (at-rest)
25	0	0	0	0
15	558	429	520	806
10	837	644	780	1,209
5	1,115	858	1,040	1,612
1	1,338	1,030	1,247	1,934

Table F.4. LFD and LRFD Factored Shear Forces (lb/ft).

Height (ft)	**LFD** (β_E=1.3)	**LFD** (β_E=1.0)	**LRFD** (active)	**LRFD** (at-rest)
25	0	0	0	0
15	2,789	2,145	2,599	4,029
10	6,274	4,826	5,847	9,066
5	11,154	8,580	10,395	16,118
1	16,062	12,355	14,969	23,210

Table F.5. LFD and LRFD Factored Bending Moments (ft-lb/ft).

Height (ft)	**LFD** (β_E=1.3)	**LFD** (β_E=1.0)	**LRFD** (active)	**LRFD** (at-rest)
25	0	0	0	0
15	9,295	7,150	8,663	13,432
10	31,371	24,131	29,233	45,332
5	74,360	57,200	69,300	107,453

1	128,494	98,842	119,750	185,678

Safety Margin in Retaining Wall Design Procedure

Load factors, in theory, should be defined in a probabilistic manner in conjunction with resistance factors in order to achieve a threshold reliability index. However, this procedure requires a large amount of experimental data, including structural tests to failure, and a complex computational procedure. In the present study, only one retaining wall panel was monitored, and all available data correspond to the service load range. As such, the load combinations described in the preceding section (Table F.2) had to be evaluated in a more simplistic manner.

In order to evaluate the safety provided to retaining walls designed with the previously defined factored forces, a parameter, referred to in this study as the "partial safety margin", c, is defined as follows

$$c = \frac{R_{max}}{R_{meas}} \tag{F.8}$$

where R_{max} is factored force (either V or M) obtained using one of the four load combinations described in the preceding section (Table F.2) , and R_{meas} is the factored force calculated using the measured pressure profiles (Table F.1). The partial safety margin, c, defined in (F.8) represents a "composite" load factor that includes the influence of the individual load factors for each load combination (i.e., l and b_E for LFD or h_i and g_i for LRFD), as well as the variations in assumed pressure profiles.

In general, the value for the partial safety margin (c) should equal or exceed 1.5, but it need not exceed a value of 2.25. The justification for these limits can be explained relative to the full (complete) safety margin, which is defined as the ratio of c and the resistance factor, f. According to equations (F.5), (F.6) or (F.7), the ratio c/f is ideally equal to the ratio of the factored load effect, R_n, and the earth pressure effect, E or EH. The latter ratio, (R_n/E or R_n/EH) is traditionally referred to as the Factor of Safety in the Allowable Stress and Working Stress Design methods.

Historically, a minimum value of 1.67 and a maximum value of 2.5 have been used for as Factors of Safety in these methods, depending upon the structural material and design code in use. The corresponding partial safety margins (c) are the product of these limits (i.e., 1.67 and 2.5) and the resistance factor (f). The f factor for flexure in both the LFD and LRFD Mn/DOT Standards is 0.9, and for shear it is either 0.9 (LRFD) or 0.85 (LFD). Assuming that f = 0.9, gives the previously mentioned limits of 1.5 and 2.25 for c.

Partial safety margins (c) were computed using the shear force (V) and bending moment (M) profiles for each of the four load combinations (Table F.2) to define R_{max}, and the shear force and bending moment profiles obtained from each of the six measured pressure profiles (Table F.1) to define R_{meas}. These partial safety margins are shown in Fig. F.4 – F.9 along the height of the retaining wall stem, with each of the plots corresponding to one of the six pressure profiles identified in Table F.1. No values for c are reported in the upper 10 ft of the wall stem because there were no pressure

measurements in this region, and since shear force and bending moment vanish at the top of the stem, the partial safety margins are indeterminate.

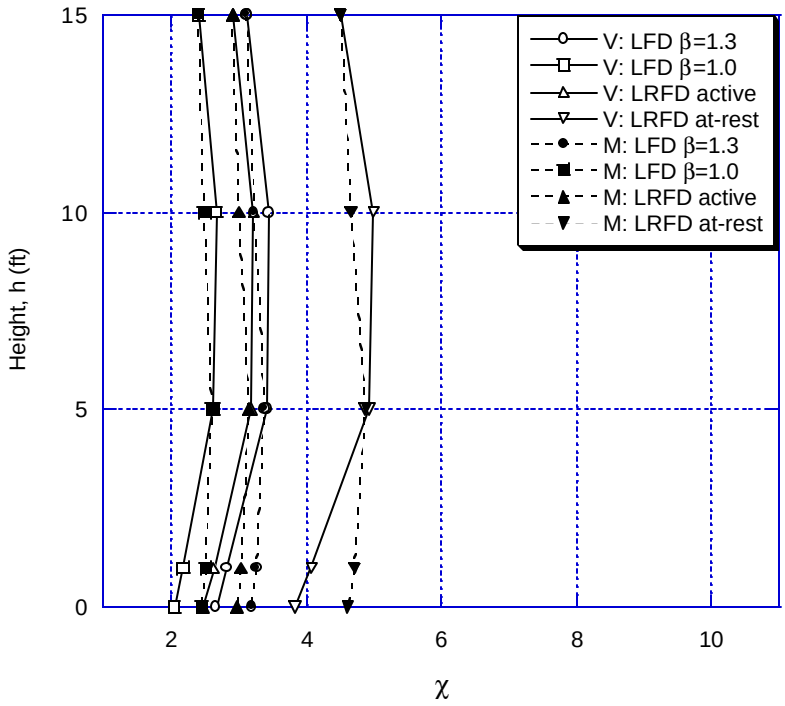

Figure F.4. Partial safety margins (c) for pressure profile measured on Nov. 27, 2002.

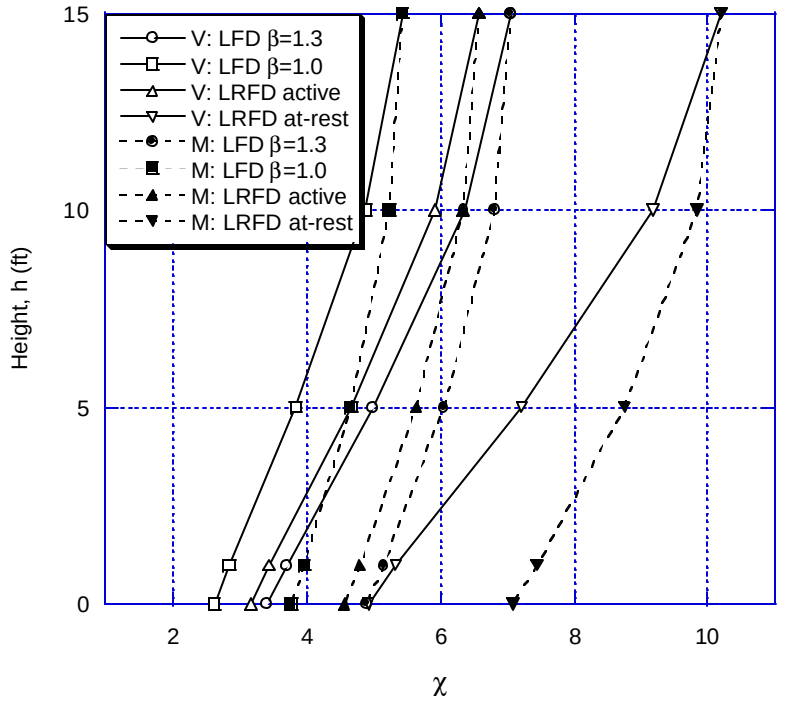

Figure F.5. Partial safety margins (c) for pressure profile measured on Dec. 20, 2002.

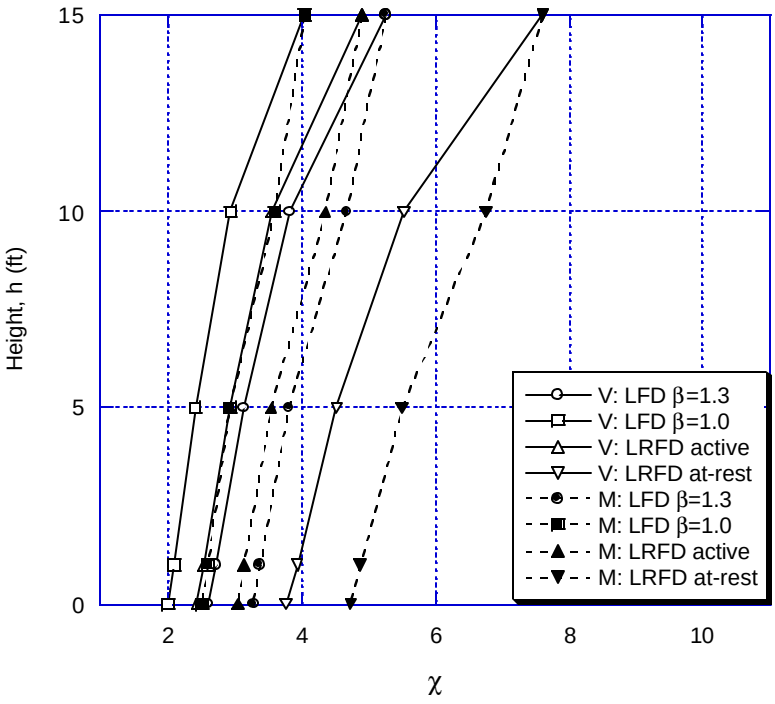

Figure F.6. Partial safety margins (c) for pressure profile measured on Jan. 3, 2003.

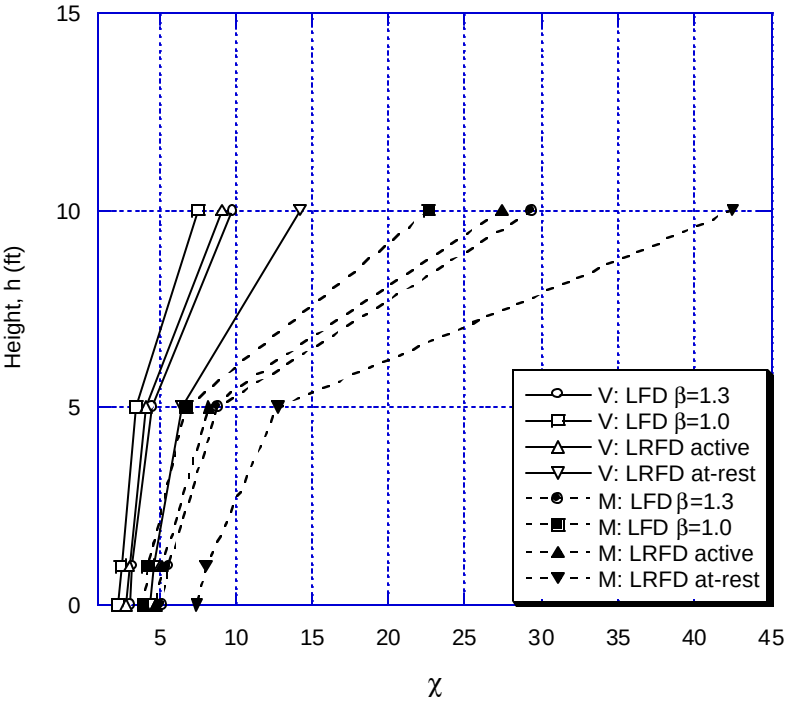

Figure F.7. Partial safety margins (c) for pressure profile measured on Feb. 15, 2003.

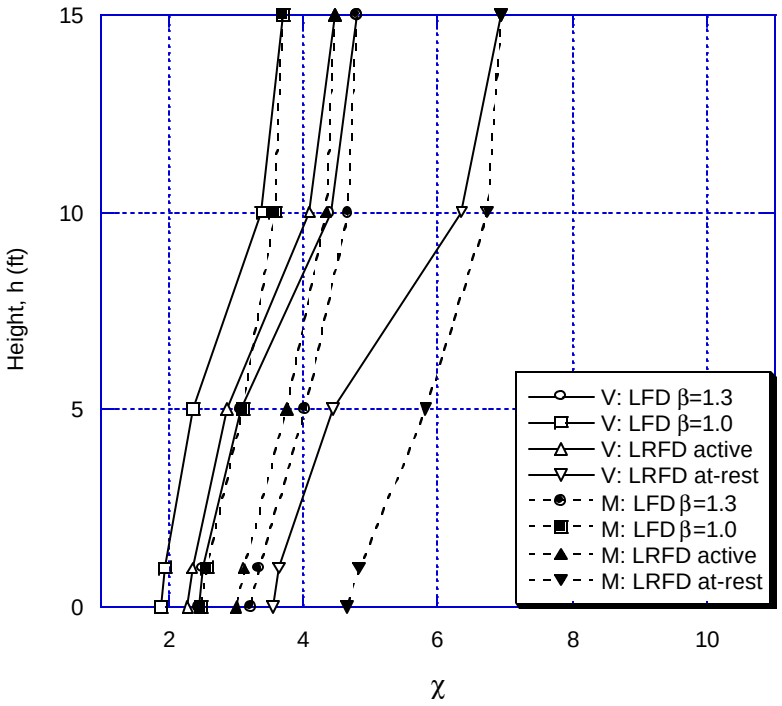

Figure F.8. Partial safety margins (c) for pressure profile measured on Mar. 18, 2003.

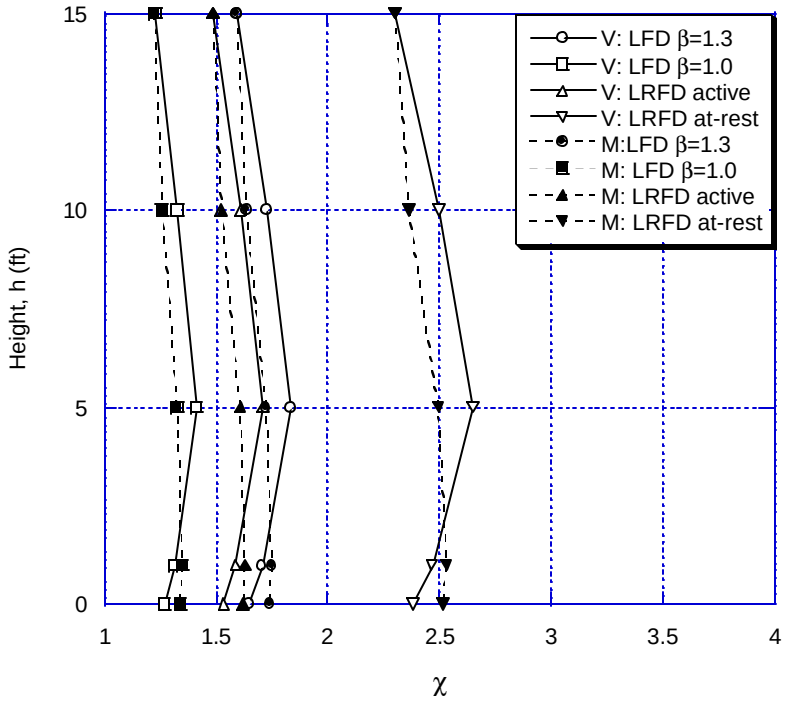

Figure F.9. Partial safety margins (c) for pressure profile measured on April 24, 2003.

Partial safety margins computed using the pressure profile measured on Nov. 27, 2002 (Fig. F.4) exhibit nearly vertical distributions along the height of the wall. The values for c were greater than or equal to 2 for all load cases (Fig. F.4), and the smallest values for c occurred at the base of the stem. The LFD load case with b_E=1.3 generated partial

safety factors that are approximately equal to, but slightly larger than, those for the LRFD case with active pressures, while the LFD case with β_E =1.0 generated the smallest values for γ. The LRFD load case with at-rest pressures generated the largest partial safety factors, with magnitudes that were unnecessarily large for the intended purpose (4 = γ = 5).

Partial safety margins computed using the pressure profiles measured on December 20, 2003 (Fig. F.5), January 3, 2003 (Fig. F.6) and March 18, 2003 (Fig. F.8) were of similar magnitude to those shown in Fig. F.4, especially at the base of the stem. However, values for γ computed at the top of the wall for pressures measured on those dates were considerably larger to than those for the base of the stem. This skewed vertical distribution of partial safety margins represents a departure from those for Nov. 27, 2002, and it is the result of changes in lateral earth pressure distribution over time, especially as the soil froze in response to winter temperatures. With decreasing winter temperatures, there was a trend for the pressures near the top of the stem to decrease, while pressures near the base remained approximately constant (Fig. F.1). Thus, the curvature of the upwardly concave distribution of pressures became more pronounced, and, the corresponding shear forces and bending moments decreased, in turn, leading to larger partial safety margins.

The trend described above culminated with the pressure profiles measured during the coldest period of the winter, which included the pressure profile measured on February 15, 2003 (Fig. F.1). The partial safety margins for this profile show very large values at a height of 10 ft. above the base of the stem (Fig. F.7). This feature is a direct outcome of a vanishing pressure profile in the top 10 ft of the wall, because the frozen soil in this region supported itself and applied no pressure to the wall. Since the pressure vanished above a height of 15 ft., shear force and bending moment also vanish above that elevation as well. Thus, partial safety factors (F.8) cannot be evaluated for the top 10 ft of the wall. By the time the soil had thawed and active pressures had been reestablished over the height of the wall, large fluctuations in lateral earth pressure were observed with the daily cycle of above-freezing temperatures. One of the pressure profiles with the largest such magnitudes was recorded on April 24, 2003 (Fig. F.1), and the partial safety margins computed for this profile (Fig. F.9) once again exhibit a nearly vertical distribution for γ, as was noted at the end of backfilling (Fig. F.4). Given the magnitude of the pressures measured during April 24, 2003, this profile produced the largest shear forces and bending moments in the retaining wall panel (Fig. F2. and F.3). Consequently, this profile produced the smallest partial safety margins calculated for all six pressure profiles. In fact, for the LFD load case with β_E=1.0, γ falls to values as small as 1.2, which is considerably below the proposed lower limit of 1.5. It is concluded, therefore, that the LFD load combination with β_E=1.0 is not adequate, especially since the unfactored pressures, shear forces and bending moments for this profile matched those for active pressure theory.

Discussion of Results

The largest and, therefore, most important shear forces and bending moments in a cantilever retaining wall are those at the base of the stem. Thus, the safety margin at this location is of interest in the present study. Partial safety margins for shear force and bending moment, respectively, at the base of the stem are shown in Figures F.10 and F.11 as a function of both load combination and the date when the earth pressures were sampled. Mean values for c, obtained by averaging all values in a given profile, are shown in Figures F.12 and F.13, respectively, for shear force and bending moment. The four plots described above are similar and, in general, exhibit the same trends with load combination and date of measurement. In most cases, the magnitude for c is acceptable (i.e., c = 1.5). The sole exception is for the LFD with b_E=1.0 on April 24, 2003, when c drops to values as low as 1.2 for both shear force and bending moment. Based on the data described above, the following conclusions can be drawn regarding the appropriateness of the various load combinations for the instrumented retaining wall.

1. The LFD (with b_E = 1.3) and LRFD methods based on active earth pressures give comparable results, with safety margins that are somewhat conservative in most cases (c = 2.2 for the LFD and c = 2.1 for the LRFD), and for the largest measured soil pressures both methods maintained partial safety margins that exceeded the lower limit of 1.5 (c = 1.6 for the LFD and c = 1.5 for the LRFD). The use of either of these methods for the design or cantilever retaining walls in Minnesota appears to be justified.
2. The LFD with active earth pressures and b_E = 1.0 gives the least conservative results, with the corresponding factored shear forces and bending moment providing adequate margins of safety in most cases (c = 1.7). However, the instance of largest soil pressures (April 24, 2003) generated unacceptably low safety margins (c = 1.2). On the basis of these calculations, the LFD method with β_E = 1.0 is not recommended for the design of retaining walls in Minnesota.
3. The LRFD method with at-rest earth pressures provides results that are grossly over conservative in most cases (c = 3.2). Even for the soil pressure profile measured on April 24, 2002, the margins of safety for this method exceed 2.3. Consequently, this method is deemed uneconomical and should not be used for calculating shear forces and bending moments for the design of cantilever retaining walls in Minnesota.

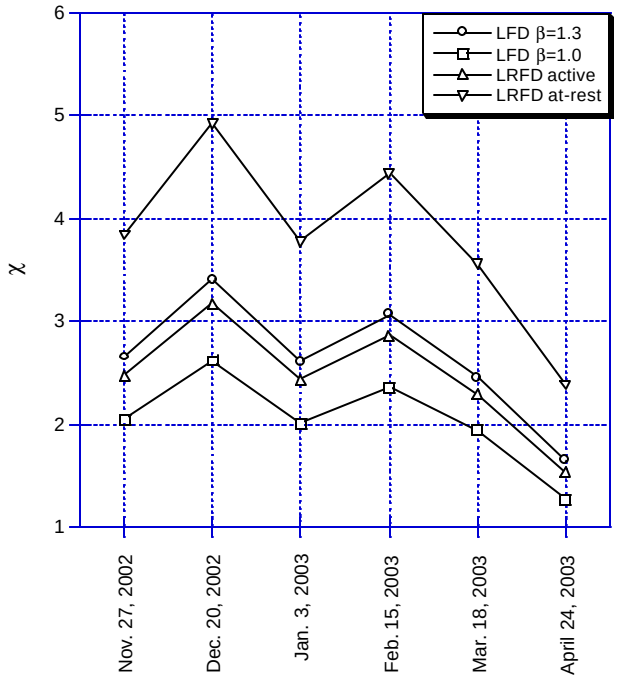

Figure F.10. Partial safety margins (c) for shear force (V) at base of stem.

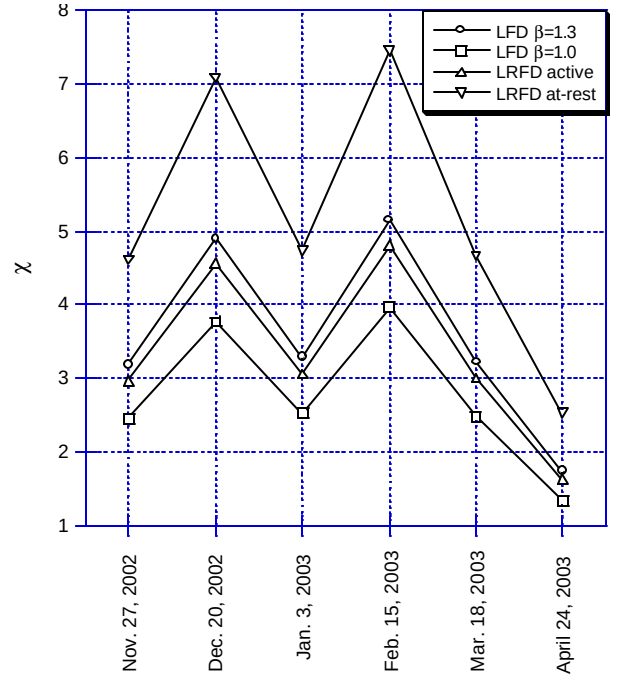

Figure F.11. Partial safety margins (c) for bending moment (M) at base of stem.

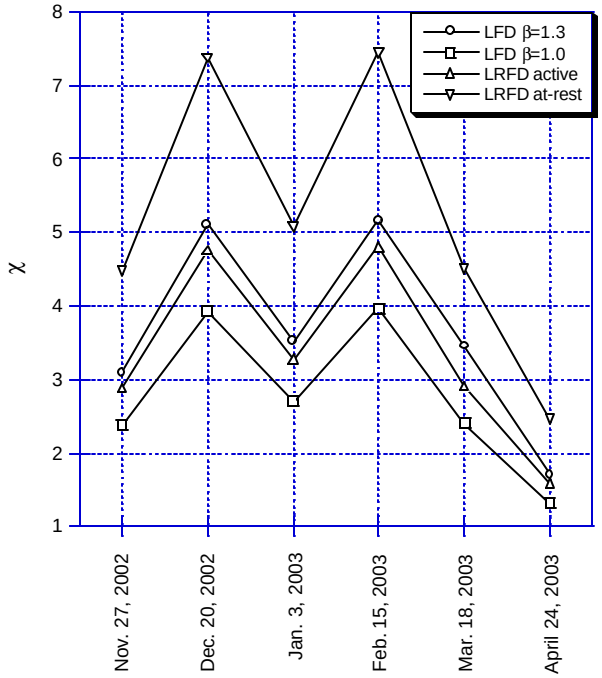

Figure F.12. Mean partial safety margins (c) for shear force (V).

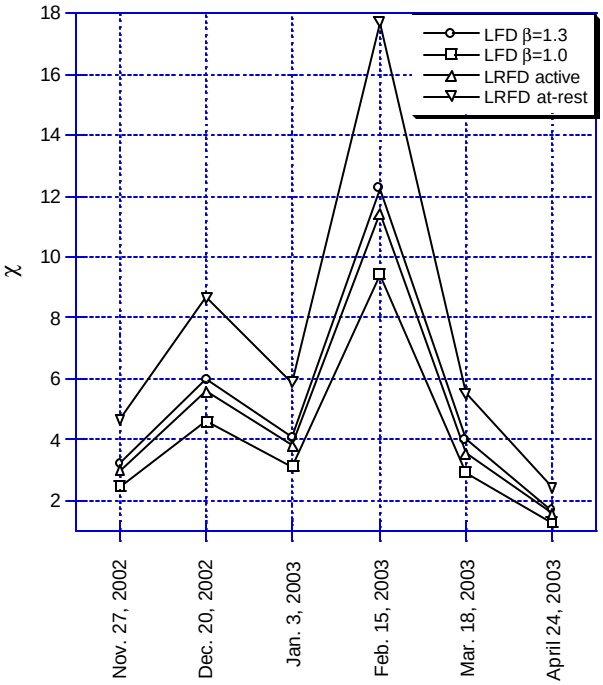

Figure F.13. Mean partial safety margins (c) for bending moment (M).